Classification:	**Unclassified**	**BM Code: 17.03.07.03**
Issue Purpose	**Approve for Use**	**May, 2011**

Sakhalin Energy Investment Company Ltd.

Acoustic & Hydrographic Studies on the North East Sakhalin Shelf 27th July to 5th October, 2010. Sakhalin Island, Russian Federation.

(Акустико-гидрофизические исследования на северо-восточном шельфе о. Сахалин с 27 июля по 5 октября 2010 г., о. Сахалин, Российская Федерация)

Document Number: 0000-S-90-04-T-0305-00-E
Revision 01

The copyright of this document is vested in Sakhalin Energy Investment Company Ltd. All rights reserved. Neither the whole nor any part of this document may be reproduced, stored in any retrieval system or transmitted in any form or by any means (electronic, mechanical, reprographic, recording or otherwise) without the prior written consent of the copyright owner. The contents of this controlled document shall not be altered without formal approval of the document Custodian.

Document History

Filename 0000-S-90-04-T-0305-00-E

Date	Issue	Custodian	Process Owner	Authoriser	Consulted	Distributed
May. 2011	01	Larin Roman	Richard Evans	Richard Evans	Koen Broker	
			RHSE 4/5/11	RHSE 4/5/11	P.P.	

Revision Details

Rev	Location of Change	Brief Description of Change
01		Approve for Use

V.I. Il`icev Pacific Oceanological Institute

Far East Branch, Academy of Sciences of Russia

Vladivostok, Russian Federation

Acoustic & Hydrographic Studies on the North East Sakhalin Shelf

27th July to 5th October, 2010

Sakhalin Island, Russian Federation

S.V. Borisov
D.I. Borovoy
V.A. Gritsenko
A.N. Rutenko
V.A. Sosnin
V.G. Ushipovsky

Prepared for

Exxon Neftegas Limited

&

Sakhalin Energy Investment Company,

Yuzhno-Sakhalinsk, Sakhalin,

Russian Federation

March 2011

V.I. Il`icev Pacific Oceanological Institute
Far East Branch, Academy of Sciences of Russia
Vladivostok, Russian Federation

'Approved'
POI FEB RAS Director
Academic V.A. Akulichev

Date: 24 February 2011

Acoustic & Hydrographic Studies on the North East Sakhalin Shelf

27th July to 5th October, 2010

Sakhalin Island, Russian Federation

S.V. Borisov
D.I. Borovoy
V.A. Gritsenko
A.N. Rutenko
V.A. Sosnin
V.G. Ushipovsky

Prepared for

Exxon Neftegas Limited
&
Sakhalin Energy Investment Company,

Yuzhno-Sakhalinsk, Sakhalin,
Russian Federation

March 2011

TABLE OF CONTENTS

Executive Summary 1

1 Introduction 2

1.1 Objectives of the acoustic program 9

1.2 Operational strategy and methodology 9

1.3 Ambient noise studies and Western gray whale core areas 11

1.3.1 Monitor, control and acoustic station locations 16

1.4 Data recorded on the NE Sakhalin shelf during the 2009 field season 18

1.5 Terminology and algorithms used in the report 22

1.6 Statistical analysis of acoustic data 24

1.6.1 Calculation of one-third octave power spectral density percentile plots 24

2 Acoustic recording and processing equipment 29

2.1 Autonomous Underwater Acoustic Recorder (AUAR) 29

2.1.1 AUAR instrument test analysis 34

2.1.2 AUAR internal noise 36

2.1.3 AUAR dynamic range 36

2.1.4 Analog channel system filter response of the AUAR 37

2.1.5 Results of the AUAR instrument tests 38

2.2 Low Frequency, High Frequency and autonomous transducers 41

2.3 Hydrologic and bathymetric measurements 44

2.3.1 Recording and archival of navigational and bathymetric information 47

2.4 Upgraded AUAR and Mini-AUAR Power Supplies 48

3 Ambient and anthropogenic acoustic noise on the NE Sakhalin shelf 53

3.1 Acoustic noise recorded in the North and the South of the study area 53

3.2 Measurements of sound generated by the Lebedinskoye seismic survey 57

3.3 Measurements of seismic sounds recorded in the Offshore Feeding Area 59

3.4 Anthropogenic acoustic measurements near the PA-B and Molikpaq platforms 66

4 Analysis of Transmission Loss TL(r,f) experiments on the Sakhalin shelf 70

4.1 Analysis of Transmission Loss TL(r,f) along profile TLP-5 71

4.2 Analysis of Transmission Loss TL(r,f) along profile TLP-7γ..... 75

4.3 Analysis of Transmission Loss TL(r,f) along profile TLP-22 82

4.4 Analysis of TL(r,f) along point profiles TLP-ADP-B-3 and TLP-ADP-A-5..... 89

5 Acoustic measurements of noise from the jet drive boat and Photo-ID zodiac 94

6 Analysis of Bathymetric and Hydrologic Studies on the NE Sakhalin Shelf 112

6.1 Meteorological conditions observed in the study area in 2010 114

6.2 Hydrological conditions observed over the study area in August 2010..... 118

6.3 Monitoring the inter-annual variation of hydrology in the feeding areas..... 130

6.4 Possible explanation for the stationary fresh water lens off Piltun Bay in 2010 133

6.5 The effect of shallow bays on inshore hydrological conditions 147

7 Main Results..... 156

8 Conclusions 157

9 Future plans..... 159

10 Acknowledgements..... 160

11 Authors 161

12 Bibliography..... 162

Appendix A - Daily Sonograms for AUAR Data 170

Appendix B - Calibration Certificates 172

Appendix C – Estimation of Western Gray Whale Core Areas 173

Appendix D - Cross-calibration Results 176

LIST OF TABLES

Table 1.1 - Numbers, names, locations and depths of the acoustic, monitoring and control stations. 17
Table 1.2(a) - Operational times, parameters and locations of AUARs at monitor stations 1 to 10. 26
Table 1.2(b) - Operational times, parameters and locations of AUARs at monitor stations 11 to 15, the control station. 27
Table 1.2(c) - Operational times, parameters and locations of AUARs at acoustic stations A9 & A10. 27
Table 1.3 – Plot showing the days when AUARs were active at each monitoring station (by station). 28
Table 2.1 – Performance of AUARs on the instrument tests. 41
Table 2.2 – Valeport MIDAS CTD+500 specifications 46
Table 6.1: Weather Conditions in the Survey Area 115
Table D.1 - Cross-calibration - statistical relative error analysis in the frequency bands 10-1000 Hz, 10 Hz to 15 kHz for AUARs No. 4, 7, 9 and the reference (mini-AUAR No. 24) 185
Table D.2 - Cross-calibration - statistical relative error analysis in the frequency bands 10-1000 Hz, 10-15 kHz for AUARs No. 2, 3, 5, 8, and the reference (mini-AUAR No. 24). 185
Table D.3 - Cross-calibration - statistical relative error analysis in the frequency bands 10-1000 Hz, 10-15 kHz for AUARs No. 16, 17, 26, 27, and the reference (mini-AUAR No. 24) 185
Table D.4 - Cross-calibration - statistical relative error analysis in the frequency bands 10-1000 Hz, 10-15 kHz for AUARs No. 6, 11, 13, 19, 21 and the reference (mini-AUAR No. 24). .. 186
Table D.5 - Cross-calibration - statistical relative error analysis in the frequency bands 10-1000 Hz, 10-15 kHz for mini-AUARs No. 15, 18, 23, 25 and the reference (mini-AUAR No. 24) 186
Table D.6 - Cross-calibration - statistical relative error analysis in the frequency bands 10-1000 Hz, 10-15 kHz for AUARs No. 14, 23, transducer reference hydrophones GI50-48 and GI50-27 and the reference (mini-AUAR No. 24). 186
Table D.7 - Cross-calibration - statistical relative error analysis in the frequency bands 10-1000 Hz, 10-15 kHz for AUARs No. 3, 9, 18 and the reference (mini-AUAR No. 24). 187

LIST OF FIGURES

Figure 1.1 – Autonomous Underwater acoustic recorder (AUAR). 4
Figure 1.2 – AUAR power supply modules using non-rechargeable batteries 5
Figure 1.3 – Mini-AUAR used for short-term source or TL measurements. 6
Figure 1.4 - Research vessel *Akademik Oparin*..... 7
Figure 1.5 - Map of the NE Sakhalin Shelf showing the locations of the LUN-A, Molikpaq, Orlan and PA-B platforms as well as the AUAR deployment locations. 8
Figure 1.6 - Map of the NE Sakhalin Shelf showing (a) the 2004 to 2010 bathymetric grids and (b) the locations where vertical hydrologic profiles were acquired in 2004 to 2010. 10
Figure 1.7 – Deploying an AUAR from the *Akademik Oparin.* 12
Figure 1.8 – Rigid hull zodiac with the electric winch used to raise the AUARs. 13
Figure 1.9 – Raising an AUAR using the stern crane of the *Akademik Oparin.* 14
Figure 1.10 - Map showing the AUAR locations and cumulative probability contours showing the density distributions of western gray whales from the 2001 to 2005 aerial surveys, 2002 to 2006 vessel based surveys, 2001 to 2006 shore-based behavior scan surveys and the 2004 to 2006 shore-based vehicle scan surveys. 19
Figure 1.11 - Sonogram *G(f,t)* with plots of sound pressure level *D(Δf,t)* of acoustic energy recorded at the Molikpaq acoustic station on 8th August 2010. 21
Figure 1.12 –Fouling of the hydrophone by algae. 23
Figure 1.13 - Percentile plots of one-third octave power spectral density estimated at the Lunskoye monitor station for August and September, 2010. 25
Figure 2.1 – Internal noise spectra of an AUAR recorded using a flash drive (black) and a continuously operational hard drive (no gaps) (red) with an analog channel gain of (a) 2; (b) 38..... 30
Figure 2.2 - (a) Charging AUAR batteries; (b) Hydrophone used in AUAR & mini- AUAR..... 31
Figure 2.3 – Deployment schematics for (a) AUAR; (b) Mini-AUAR. 33
Figure 2.4 – Acoustic release and buoy. 34
Figure 2.5 - Spectral characteristics of the Cylindrical (GI-50) hydrophones used during the 2010 field season. 35
Figure 2.6 - Spectra showing the internal noise of the AUAR recording system: 37
(a) 0-15 kHz and (b) 0-350 Hz. 37
Figure 2.7 - Spectrum showing the internal noise and dynamic range of the AUAR recording

system. 38
Figure 2.8 - Amplitude-frequency characteristics of an AUAR analog channel normalized to a gain K=1 at 1 kHz for AUARs and mini-AUARs used during the 2010 field season: AUAR analog frequency response (a) 2 Hz to 20 kHz; (b) 2 to 120 Hz. 39
Figure 2.9 - Amplitude-frequency characteristics of an AUAR analog channel normalized to a gain K=1 at 1 kHz for AUARs and mini-AUARs used during the 2010 field season: AUAR analog frequency response (a) 2 Hz to 20 kHz; (b) 2 to 120 Hz. 40
Figure 2.10 - Low frequency resonance transducer and calibrated monitor hydrophone. 42
Figure 2.11 - High frequency broadband piezoelectric transducer and calibrated monitor hydrophone mounted on a frame to the right of the transducer. 43
Figure 2.12 – Equipment for acoustic signal generation and reference signal recording. 44
Figure 2.13 - MIDAS CTD+500 profiler and sensors. 45
Figure 2.14 – Computer display showing the navigation data for the vessel. 48
Figure 2.15 – Charging AUAR batteries with CTEK M200 chargers. 49
Figure 2.16 – Using a Kulon-12fu indicator to check battery capacity. 50
Figure 2.17 – General purpose power supply modules, containing *Duracell D* batteries for the AUAR and mini-AUAR units. 51
Figure 3.1 - Sonogram *G(f,t)* of acoustic data recorded at the Control (6th August to 27th September) and Piltun monitor stations (9th August to 27th September). 55
Figure 3.2 – Power spectral density percentile plots of sound pressure level of acoustic data recorded at the Control and Piltun monitor stations. 57
Figure 3.3 – Map showing the acoustic monitoring stations used during the summer-fall period under the joint Gray Whale monitoring program. 58
Figure 3.4 – Sample sound pressure traces *p(t)* (top panels), peak amplitudes, and SPL_{rms} levels (bottom panels) for acoustic pulses recorded at monitoring stations A10 and Odoptu-S-10 during offshore seismic operations in the southern part of the Lebedinskoye field. 59
Figure 3.5 - Sonogram *G(f,t)* and plots of sound pressure level of acoustic data recorded at the A10, Odoptu-N-20 and Odoptu-S-20 monitor stations in 2010. 60
Figure 3.6 - Sonogram *G(f,t)* and plots of sound pressure level of acoustic data recorded at the Odoptu-N-10 monitor station in 2010. 61
Figure 3.7 - Sonogram *G(f,t)* and plots of sound pressure level of acoustic data recorded at the Lunskoye, OFA and Orlan monitor stations in 2010. 62
Figure 3.8 – One-third octave power spectral density percentile plots of acoustic data recorded

at the Orlan monitor stations in 2010: (a) for data with seismic impulses; and (b) without seismic impulses.....63
Figure 3.9 - Sonogram *G(f,t)* and plots of sound pressure level of acoustic data recorded at the Arkutun-Dagi monitor station. 64
Figure 3.10 - Plots of acoustic impulses recorded at the Arkutun-Dagi monitor station during a seismic survey 65
Figure 3.11 - Plots of peak, SPL_{rms} and SEL for acoustic impulses recorded at the Arkutun-Dagi monitor station during a seismic survey east of the offshore feeding area. 65
Figure 3.12 – Map showing the PA-B and Molikpaq (PA-A) platforms and acoustic monitoring stations and acoustic monitoring stations PA-B-10, PA-B-20 and Molikpaq. 66
Figure 3.13 – Platform PA-B. 67
Figure 3.14 – Platform *Molikpaq.* 67
Figure 3.15- Sonogram *G(f,t)* and plots of sound pressure level of acoustic data recorded at the PA-B-20 and Molikpaq monitor stations.....68
Figure 3.16 – One-third octave power spectral density percentile plots of acoustic data recorded at the Molikpaq monitor station in (a) 2009; and (b) 2010.....69
Figure 4.1 - Map of the study area showing the major facilities as well as the profiles along which frequency dependent TL studies were conducted in 2010.....70
Figure 4.2 - Map of the study area showing the major facilities as well as the AUAR deployment locations for TLP-5 on which frequency dependent TL studies were conducted on 17th-18th September, 2010. 71
Figure 4.3 - TLP-5: Bathymetry and hydrologic parameters (velocity *C(r,z)*, temperature *T(r,z)*, and salinity *S(r,z)* acquired on 18th September, 2010. 72
Figure 4.4 - TLP-5: Frequency dependent TL plot showing data for source locations A-E and the distance from the source locations to the Arkutun-Dagi location. 73
Figure 4.5 - TLP-5: One third octave averaged frequency dependent TL plot showing the results for all the source locations and data in Figure 4.4. 74
Figure 4.6 - TLP-5: Range dependent one third octave averaged frequency dependent TL plot showing the results for four one third octave frequency bands for the Arkutun-Dagi station. 74
Figure 4.7 - Map of the study area showing the major facilities as well as the AUAR deployment locations for TLP-7γ along which frequency dependent TL studies were conducted on 29th-30th August, 2010.....75

Figure 4.8 - TLP-7γ: Bathymetry and hydrologic parameters (velocity *C(r,z)*, temperature *T(r,z)*, and salinity *S(r,z)* acquired on 30th August, 2010. 76
Figure 4.9 - TLP-7γ: Frequency dependent TL plot showing data for all the source locations and the distance from the source locations to the A8 location. 77
Figure 4.10 - TLP-7γ: One-third octave averaged frequency dependent TL plot showing the results for all the source locations and data in Figure 4.9. 78
Figure 4.11 - TLP-7γ: Range dependent one third octave averaged frequency dependent TL plot showing the results for four one third octave frequency bands for the A8 station. 78
Figure 4.12 - TLP-7γ: Frequency dependent TL plot showing data for source locations E-I and the distance from the source locations to the PA-B-20 location. 79
Figure 4.13 - TLP-7γ: One-third octave averaged frequency dependent TL plot showing the results for source locations E-I and data in Figure 4.12. 79
Figure 4.14 - TLP-7γ: Range dependent one third octave averaged frequency dependent TL plot showing the results for four one third octave frequency bands for the PA-B-20 station. 80
Figure 4.15 - TLP-7γ: Frequency dependent TL plot showing data for source locations A, B and the distance from the source locations to the PA-B-20 location. 80
Figure 4.16 - TLP-7γ: One-third octave averaged frequency dependent TL plot showing the results for source locations A-B and data in Figure 4.15. 81
Figure 4.17 - TLP-7γ: Range dependent one third octave averaged frequency dependent TL plot showing the results for four one third octave frequency bands for the PA-B-20 station. 81
Figure 4.18 - Map of the study area showing the major facilities as well as the AUAR deployment locations for TLP-22 along which frequency dependent TL studies were conducted on 10th-12th August, 2010. 82
Figure 4.19 - TLP-22: Bathymetry and hydrologic parameters (velocity *C(r,z)*, temperature *T(r,z)*, and salinity *S(r,z)* acquired on 12th September, 2010. 83
Figure 4.20 - TLP-22: Frequency dependent TL plot showing data for source locations A-H and the distance from the source locations to the PA-B-20 location. 84
Figure 4.21 - TLP-22: One-third octave averaged frequency dependent TL plot showing the results for source locations A-H and data in Figure 4.20. 85
Figure 4.22 - TLP-22: Range dependent one third octave averaged frequency dependent TL plot showing the results for four one third octave frequency bands for the PA-B-20 station. 85
Figure 4.23 - TLP-22: Frequency dependent TL plot showing data for source locations E-H and the distance from the source locations to the Piltun location. 86

Figure 4.24 - TLP-22: One-third octave averaged frequency dependent TL plot showing the results for source locations E-H and data in Figure 4.23. 86
Figure 4.25 - TLP-22: Range dependent one third octave averaged frequency dependent TL plot showing the results for four one third octave frequency bands for the Piltun station. 87
Figure 4.26 - TLP-22: Frequency dependent TL plot showing data for source locations A-D and the distance from the source locations to the Piltun location. 87
Figure 4.27 - TLP-22: One-third octave averaged frequency dependent TL plot showing the results for source locations A-D and data in Figure 4.26. 88
Figure 4.28 - TLP-22: Range dependent one third octave averaged frequency dependent TL plot showing the results for four one third octave frequency bands for the Piltun station. 88
Figure 4.29 - Map of the study area showing the major facilities as well as the AUAR deployment locations for TLP-ADP-B-3 and TLP-ADP-A-5 along which frequency dependent TL studies were conducted on 21st August and 8th September, 2010. 89
Figure 4.30 - TLP-ADP-B3: Bathymetry and hydrologic parameters (velocity *C(r,z)*, temperature *T(r,z)*, and salinity *S(r,z)* acquired on 21st August, 2010. 91
Figure 4.31 - TLP-ADP-A5: Bathymetry and hydrologic parameters (velocity *C(r,z)*, temperature *T(r,z)*, and salinity *S(r,z)* acquired on 9th September, 2010. 92
Figure 4.32 - TLP-ADP-A5: Frequency dependent TL plot showing data for source location A and the distance from the source locations to the Arkutun-Dagi location. 93
Figure 4.33 - TLP-22: One-third octave averaged frequency dependent TL plot showing the results for source location A and data in Figure 4.32. 93
Figure 5.1 – Picture of the jet-drive RHIB used by the satellite-tagging team. 94
Figure 5.2 – Picture of zodiac used by the Photo-ID team. 95
Figure 5.3 - Map of the study area with the locations where the acoustic output of the satellite tagging jet-drive boat and Photo-ID zodiac were measured. 96
Figure 5.4 - Sonogram *G(f,t)* and of acoustic signals recorded by mini-AUAR#23 (left) and mini-AUAR#14 (right) when the jet-drive boat sailed the first track. The letters designate moments in time when the jet-drive boat passed the points shown in Figure 5.6. 97
Figure 5.5 - Sonogram G(f,t) and of acoustic signals recorded by mini-AUAR#23 (left) and mini-AUAR#14 (right) 99
Figure 5.6(a) – First track of the jet-drive boat (uniform speed of 2-3 knots). Spectra are calculated for points 2 & T. 100
Figure 5.6(b) – First track of the Photo-ID zodiac (uniform speed of 2-3 knots). Spectra are

calculated for points 2, 3 & T. 100
Figure 5.7(a) – Second track of the jet-drive boat (uniform speed of 6-7 knots). Spectra are calculated for points 1 & T. 101
Figure 5.7(b) – Second track of the Photo-ID zodiac (uniform speed of 18-20 knots). Spectra are calculated for point T. 101
Figure 5.8(a) – Third track of the jet-drive boat (uniform speed of 13-15 knots). Spectra are calculated for points 1 & T. 102
Figure 5.8(b) – Third track of the jet-drive boat and Photo-ID zodiac (uniform speed of 13-15 knots). Spectra are calculated for point T. 102
Figure 5.9(a) – Acceleration track of the jet-drive boat. Spectra are calculated for points A1, A2 and A3. 103
Figure 5.9(b) – Acceleration track of the Photo-ID zodiac. Spectra are calculated for point A1. 103
Figure 5.9(c) – Fifth acceleration track of the Photo-ID zodiac. Spectra are calculated for point A2. 104
Figure 5.10 - Sonogram *G(f,t)* and of acoustic signals recorded by mini-AUAR#23 (left) and mini-AUAR#14 (right) when the Photo-ID zodiac sailed the first and second tracks. The letters designate moments in time when the jet-drive boat passed the points shown in Figure 5.6 and 5.7. 105
Figure 5.11 - Sonogram *G(f,t)* and of acoustic signals recorded by mini-AUAR#23 (left) and mini-AUAR#14 (right) when the Photo-ID zodiac sailed the third, fourth, and fifth tracks. The letters designate moments in time when the jet-drive boat passed the points shown in Figure 5.6 and 5.7. 106
Figure 5.12 – Power spectral density levels *G(f)* of acoustic signals recorded when the Photo-ID zodiac and the jet-drive boat sailed at 2 knots towards mini-AUAR#14 at a range of 50 m. 107
Figure 5.13 – Power spectral density levels *G(f)* of acoustic signals recorded when the Photo-ID zodiac and the jet-drive boat sailed perpendicular to the A-B line at 2 knots while mini-AUAR#23 located 250-300 m abeam recorded the data. 107
Figure 5.14 – Power spectral density levels *G(f)* of acoustic signals recorded when the Photo-ID zodiac and the jet-drive boat sailed towards mini-AUAR#23 at 2 different speeds. 108
Figure 5.15 – Power spectral density levels *G(f)* of acoustic signals recorded when the Photo-ID zodiac and the jet-drive boat sailed at 15 knots while mini-AUAR#23 located 260 m abeam

on the port side recorded the data. 109
Figure 5.16 – Power spectral density levels *G(f)* of acoustic signals recorded when the jet-drive boat sailed at different speeds while mini-AUAR#23 located 250-300 m abeam on the port side recorded the data (spectra are for location T). 109
Figure 5.17 – Power spectral density levels *G(f)* of acoustic signals recorded when the jet-drive boat sailed at different acceleration rates. The spectrum for a uniform speed of 2 knots is provided for comparison. 110
Figure 5.18 – Power spectral density levels *G(f)* of acoustic signals recorded when the Photo-ID zodiac sailed at different acceleration rates. The spectrum for a uniform speed of 2 knots is provided for comparison. 111
Figure 6.1 - Map of the NE Sakhalin Shelf showing the bathymetry of the study area and the locations where vertical hydrologic profiles were acquired as of September 2010. 113
Figure 6.2 – Average daily wind directions and wind speeds for the summer months of 2010. The red line is the average for each month. 116
Figure 6.3 – Average daily wind directions and wind speeds for the summer months of 2009. The red line is the average for each month. 117
Figure 6.4 - Spatial distribution of water temperature and salinity near the sea surface in August 2010 (constructed from vertical hydrologic profiles acquired between 3rd and 10th August, 2010). 118
Figure 6.5 - Distribution of Temperature *T(r,z)* and salinity *S(r,z)* and the location of the sampling stations for a hydrologic transect in the offshore feeding area acquired on 3rd August 2010. 119
Figure 6.6 - Distribution of Temperature *T(r,z)* and salinity *S(r,z)* and the location of the sampling stations for a hydrologic transect near Piltun Bay acquired on 8th August, 2010. 120
Figure 6.7 - Spatial distribution of water temperature and salinity near the sea floor in August 2010 (constructed from vertical hydrologic profiles acquired between 3rd and 10th August, 2010). 121
Figure 6.8 – Spatial distribution of water temperature near the sea floor in August 2004, 2005, 2006, 2007, 2008 and 2009. 122
Figure 6.9 - Distribution of Temperature *T(r,z)* and salinity *S(r,z)* and the location of the sampling stations for a hydrologic transect adjacent to Chayvo Bay acquired on 25th-26th August, 2010. 123
Figure 6.10 - Distribution of Temperature *T(r,z)* and salinity *S(r,z)* and the location of the

sampling stations for a hydrologic transect adjacent to Chayvo Bay acquired on 2nd September, 2010. 124
Figure 6.11 - Distribution of Temperature *T(r,z)* and salinity *S(r,z)* and the location of the sampling stations for a hydrologic transect adjacent to Chayvo Bay acquired on 6th September, 2009. 125
Figure 6.12 - Distribution of Temperature *T(r,z)* and salinity *S(r,z)* and the location of the sampling stations for a hydrologic transect in the offshore area acquired on 9th September, 2010. 126
Figure 6.13 - Spatial distribution of near-surface water temperature and salinity in September 2010 (constructed from vertical hydrologic profiles acquired between 4th and 20th September, 2010). 127
Figure 6.14 - Spatial distribution of near-surface water temperature and salinity for the southern section of the offshore area in September-October 2008 (constructed from vertical hydrologic profiles acquired between 28th September and 4th October, 2008). 128
Figure 6.15 - Spatial distribution of near-surface water temperature and salinity during September, 2010 (constructed from vertical hydrologic profiles acquired between 4th and 20th September, 2010). 129
Figure 6.16 - Spatial distribution of near-surface water temperature and salinity for the offshore area in September-October 2008 (constructed from vertical hydrologic profiles acquired between 28th September and 4th October, 2008). 130
Figure 6.17 – Inter-annual water temperature and salinity variations in the waters adjacent to Piltun Bay for August. 132
Figure 6.18 – Inter-annual water temperature and salinity variations in the waters adjacent to Piltun Bay for September. 132
Figure 6.19 – Inter-annual water temperature and salinity variations in the offshore feeding area for August. 134
Figure 6.20 – Inter-annual water temperature and salinity variations in the offshore feeding area for September. 134
Figure 6.21 – Map of the survey area showing the hydrological station locations in June/early July 2010. Different symbols indicate profiles taken at different times. 135
Figure 6.22 - Distribution of Temperature *T(r,z)* and salinity *S(r,z)* and the location of the sampling stations for a hydrologic transect in the offshore area acquired on 6th June, 2010. 136

Figure 6.23 - Distribution of Temperature *T(r,z)* and salinity *S(r,z)* and the location of the sampling stations for a hydrologic transect in the area adjacent to Piltun Bay acquired on 12th June, 2010. 137
Figure 6.24 - Distribution of Temperature *T(r,z)* and salinity *S(r,z)* and the location of the sampling stations for a hydrologic transect in the area adjacent to Piltun Bay acquired on 18th June, 2010. 138
Figure 6.25 - Distribution of Temperature *T(r,z)* and salinity *S(r,z)* and the location of the sampling stations for a hydrologic transect in the area adjacent to Piltun Bay acquired on 22nd June, 2010. 139
Figure 6.26 - Distribution of Temperature *T(r,z)* and salinity *S(r,z)* and the location of the sampling stations near the mouth of Piltun Bay acquired on 26th June, 2010, during the passing of the fresh water boundary. 140
Figure 6.27 - Distribution of Temperature *T(r,z)* and salinity *S(r,z)* and the location of the sampling stations near Piltun Bay acquired on 26th June, 2010. 141
Figure 6.28 - Distribution of Temperature *T(r,z)* and salinity *S(r,z)* and the location of the sampling stations near Piltun Bay acquired on 27th June, 2010. 142
Figure 6.29 - Distribution of Temperature *T(r,z)* and salinity *S(r,z)* and the location of the sampling stations near Piltun Bay acquired on 28th June, 2010. 143
Figure 6.30 - Distribution of Temperature *T(r,z)* and salinity *S(r,z)* and the location of the sampling stations near Piltun Bay acquired on 2nd July, 2010. 144
Figure 6.31 - Distribution of Temperature *T(r,z)* and salinity *S(r,z)* and the location of the sampling stations in the inshore and offshore areas acquired on 28th June, 2010. 145
Figure 6.32 – Map of the survey area showing the boundaries of the fresher water and the hydrological station locations from 26th June to 7th July 2010. Different symbols indicate profiles taken at different times. The blue line represents the probable eastern boundary of the fresher water slug. 146
Figure 6.33 – Satellite images of the out flow of water from: (Top) Piltun Bay; and (Bottom) Chayvo Bay. 148
Figure 6.34 – Out flow of water from Piltun Bay on 4th August, 2010. 149
Figure 6.35 - Vertical distribution of sound velocity, turbidity, dissolved oxygen, temperature, pH and salinity in the patch of water outflowing from Piltun Bay, compared to background water. 150
Figure 6.36 – Out flow of water from Piltun Bay in early September, 2010. 151

Figure 6.37 - Spatial distribution of turbidity in: (Left) near-surface and (Right) near-bottom water turbidity for August 2010. 152
Figure 6.38 - Spatial distribution of turbidity in: (Left) near-surface and (Right) near-bottom water turbidity for September, 2010. 152
Figure 6.39 - Vertical distribution of sound velocity, turbidity, dissolved oxygen, temperature, pH and salinity in the offshore area on 5th August, 2010. 153
Figure 6.40 - Spatial distribution of dissolved oxygen (mL/L) in: (Left) near-surface and (Right) near-bottom for August 2010. 154
Figure 6.41 - Spatial distribution of dissolved oxygen (mL/L) in: (Left) near-surface and (Right) near-bottom for September, 2010. 154
Figure D.1 – Cross-calibration of the AUARs and sonobuoys on the *Akademik Oparin.* 177
Figure D.2 - Spectra of acoustic signals synchronously measured by AUARs No. 2, 3, 5, 8, and the reference mini-AUAR No. 24 (after instrument response [amplitude-frequency] correction). (a) 10 Hz-15 kHz; (b) 10 Hz-1 kHz; (c) 1-15 kHz. 178
Figure D.3 - Spectra of acoustic signals synchronously measured by AUAR No. 4, 7, 9, and the reference mini-AUAR No. 24 (after instrument response [amplitude-frequency] correction). 179
Figure D.4 - Spectra of acoustic signals synchronously measured by AUARs No. 6, 11, 13, 19, and 21, and the reference mini-AUAR No. 24 180
Figure D.5 - Spectra of acoustic signals synchronously measured by mini-AUARs No. 14 and 23, transducer reference hydrophones GI50-48 and GI50-27 and the reference mini-AUAR No. 24 181
Figure D.6 - Spectra of acoustic signals synchronously measured by mini-AUARs No. 15, 18, 23 and 25, and the reference mini-AUAR No. 24 182
Figure D.7 - Spectra of acoustic signals synchronously measured by AUARs No. 16, 17, 26 and 27, and the reference mini-AUAR No. 24 183
Figure D.8 - Spectra of acoustic signals synchronously measured by AUARs No. 3, 9 and 18, and the reference mini-AUAR No. 24 184

Executive Summary

In 2010 the Pacific Oceanological Institute (POI) deployed 24 Autonomous Underwater Acoustic Recorders (AUARs) to conduct acoustic studies on the NE Sakhalin shelf. The goal of the program was to measure key acoustic and hydrologic data, and to estimate sound propagation to the feeding areas of the Korean-Okhotsk gray whale (*Eschrichtius robustus*)[1].

The 2010 acoustic program measured anthropogenic and ambient noise levels, conducted bathymetric and hydrologic surveys and made Transmission Loss (TL) measurements along acoustic profiles from potential sources of anthropogenic noise to the edge of the offshore and Piltun feeding areas. These TL measurements have been and will be used to calibrate acoustic models that, in conjunction with the recorded spectra of noise sources have been and will be used to predict the sound levels received in the gray whale feeding areas. The model predictions of the acoustic footprint have been and will be used to plan construction and development operations and will aid in determining the appropriate mitigation measures to be applied. These measurements showed that for a profile the bathymetry and velocity field significantly affects the received acoustic field. The spatial and temporal parameters of the sound velocity field vary significantly over the summer-fall season and under the influence of wind generated currents.

Hydrologic studies were conducted in parallel with acoustic measurements, and during the expedition 372 vertical hydrologic profiles were acquired. The hydrologic surveys and individual transects were acquired to obtain hydrological data for different meteorological conditions during the summer and fall seasons. Six thousand five hundred and sixty (6,560) km of bathymetry data were acquired in 2010; this data were used to study the spatial and temporal variation of hydro-physical parameters under the influence of winds, tides and storms. The relationship between benthos development and the hydrology of the area was also analyzed.

[1] The Korean Okhotsk (western) gray whale population is listed as endangered in the Russian Red Book and critically endangered by the International Union for the Conservation of Nature (IUCN).

1 Introduction

The shallow water (6 - 15 m) part of the NE Sakhalin shelf, starting south of the mouth of Piltun Bay and extending northwards up the Sakhalin coast, is the most important known summer and fall feeding area for Korean-Okhotsk (western) gray whales. Mother-calf pairs are usually seen in water depths of less than 10 m in the Piltun feeding area. Acoustic studies have been conducted in the region since 1999 since some of the planned oil and gas developments are near the Piltun feeding area. In 2001 a second gray whale feeding area (the offshore feeding area) was discovered in deeper water (30-60 m), approximately 20 km South East of the mouth of Chayvo Bay.

The acoustic program conducted on the NE shelf of Sakhalin Island in 2010 had the following objectives:

- An extension to the long-term acoustic monitoring program initiated in 2003. This acoustic program was designed to study temporal and spatial variations in the amplitude and frequency characteristics of ambient and anthropogenic sound at the edges of the Piltun and offshore gray whale feeding areas.
- In addition to the program monitoring the background acoustic environment, detailed studies of sound propagation characteristics and Transmission Loss (TL) (at frequencies between 15 Hz and 15 kHz) were conducted between current and proposed ENL and SEIC facilities, both onshore and offshore, and defined locations at the edge of the gray whale feeding areas.
- Experimental studies of the acoustic signature of a jet-drive boat used for satellite tagging studies were also conducted.
- In addition to the acoustic studies ENL and SEIC acquired a comprehensive grid of bathymetric and hydrologic data across the study area. This data were also used to investigate the spatial and temporal variations in the hydrology due to weather events (e.g. typhoons).
- Two joint studies were initiated in 2005 in conjunction with the behavioral and benthic teams; these studies were continued in 2009. The first study analyzed the data recorded near the behavioral monitoring stations; the spectral density of the data in the frequency range from 20 Hz to 15 kHz was analyzed in 1-minute windows and converted to one-third octave bands. The second, conducted jointly with the benthic team, investigated the relationship between the distribution of benthos and the bathymetry and hydrology of the study area [Fadeev, 2010].

This report describes the objectives of the 2010 program, the operational strategy and methodology; the equipment used during the 2010 field season (both new and upgraded [Borisov et. al. 2006, 2007, 2008]), its testing and calibration as well as the data processing and

analysis methodology. This report also includes a listing of the data acquired during the 2010 field season and a DVD containing the sonograms in 24-hour segments for all the acoustic data recorded in 2010 as well as the bathymetric and hydrologic data acquired during the 2004 to 2010 field seasons.

This report is mainly dedicated to analysis of the data, and includes conclusions and recommendations for future work. This data analysis includes the following components:

Western gray whale research program – Acoustic studies

1. Quantitative spectral analysis of the variation in the ambient acoustic noise level with weather conditions (including cyclones).
2. A temporal, spectral and spectral-temporal analysis of the acoustic data recorded at different locations on the Sakhalin shelf[2].
3. A temporal analysis of the variation of the spectral density (one-third octave bands) of acoustic data recorded at monitoring stations inside and at the edge of the Piltun and offshore feeding areas.
4. Analysis of the hydrologic data (sound velocity, temperature, and salinity) recorded between 2004 and 2010.
5. An experimental study of the relationship between the distribution of benthos and the hydrology and bathymetry of the study area, conducted jointly with the benthic team, [Fadeev 2010].

The acoustic measurements were conducted using 18 digital Autonomous Underwater Acoustic Recorders (AUARs) developed at POI FEB RAS[3] (POI) (Figure 1.1 and 1.2) with 27 day endurance; six smaller mini-AUARs with reduced (160 hours) endurance were used for short term TL and source level measurements (Figure 1.3). The AUARs were designed to accurately record frequencies between 2-15,000 Hz and enable accurate, concurrent acoustic measurements over a broad range of frequencies (including infrasounds[4]).

[2] The use of Autonomous Underwater Acoustic recorders (AUARs) for the 2010 program allowed an unprecedented characterization of the ambient sound levels at the Sakhalin monitoring stations. However, since the vessels used to house the scientists (*Academik Oparin*) was often a significant distance from the AUAR the identification and specific location of any transient anthropogenic sound source is generally unknown.
[3] POI FEB RAS – V.I Il`ichev Pacific Oceanological Institute, Far East Branch of the Russian Academy of Sciences.
[4] Infrasounds are sounds with a frequency of less than 20 Hz.

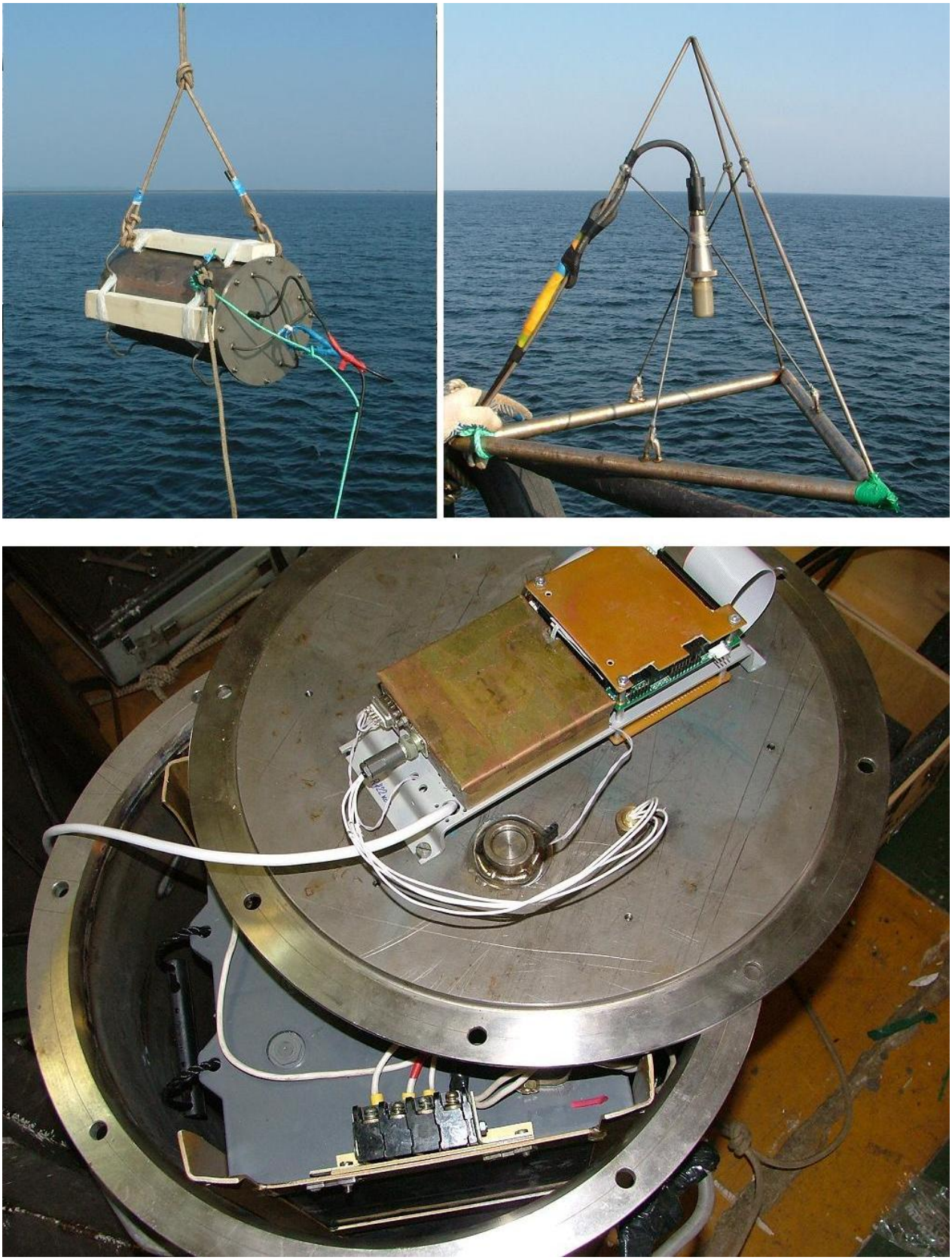

Figure 1.1 – Autonomous Underwater acoustic recorder (AUAR).

Figure 1.2 – AUAR power supply modules using non-rechargeable batteries

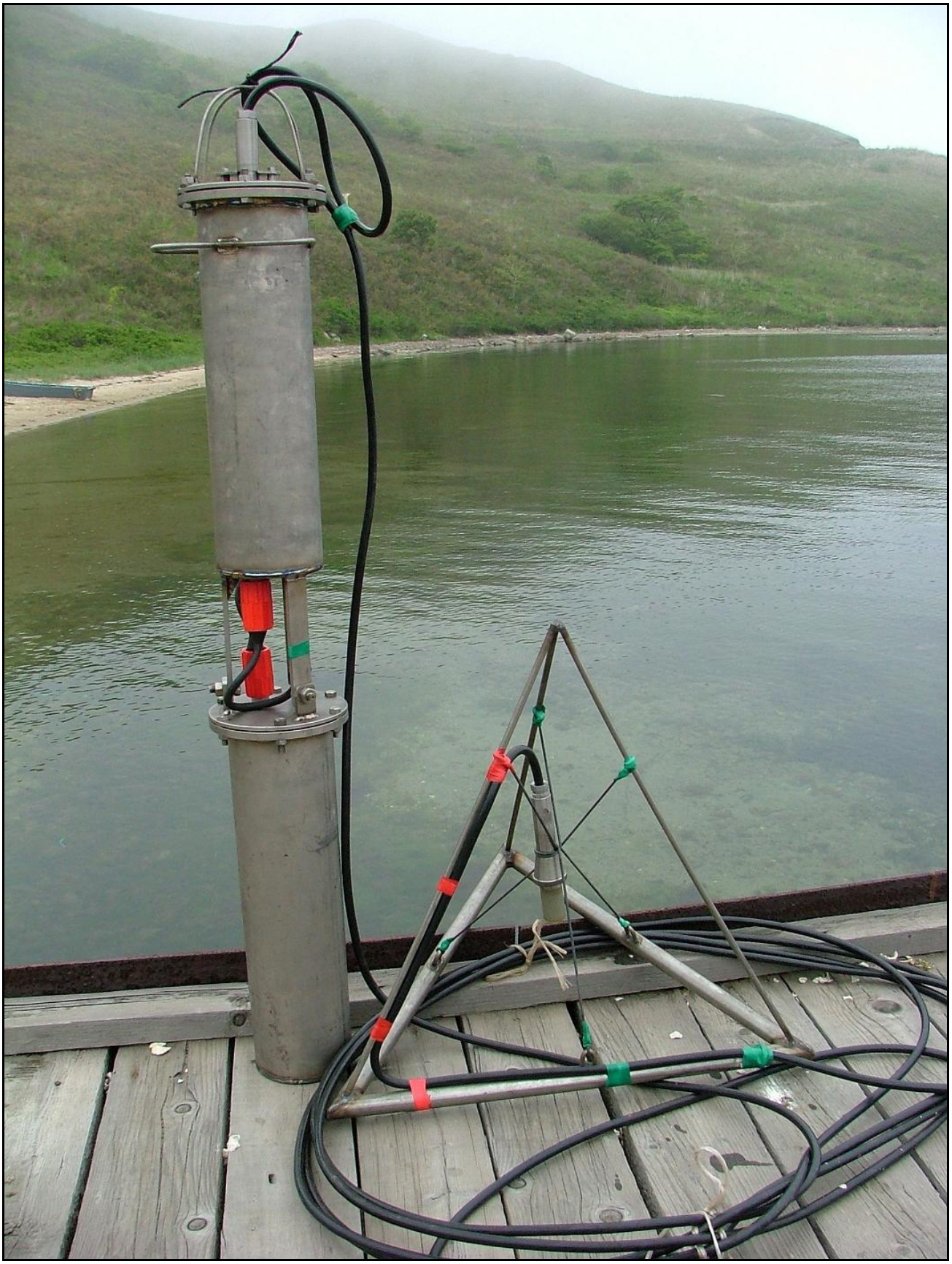

Figure 1.3 – Mini-AUAR used for short-term source or TL measurements.

All AUARs and mini-AUARs were deployed and retrieved by the *Akademik Oparin* (Figure 1.4). Simultaneous acoustic measurements were made at stations ranging from north of the Odoptu license area to the southern edge of the offshore feeding area (Figure 1.5), area monitoring region whose western edge extends 180 km along the NE Sakhalin shelf.

Figure 1.4 - Research vessel *Akademik Oparin*.

Previous work has shown that the results from acoustic modeling are very sensitive to the hydrologic, bathymetric and elastic properties of the sea bottom along the profile of interest. A comprehensive suite of bathymetric and hydrologic measurements were therefore acquired using the sonar on the *Akademik Oparin* and a hydrologic sonde. During the expedition 372 vertical hydrologic profiles (comprising sound velocity, temperature, salinity, turbidity, oxygen concentration and pH), and approximately 6,560 km of bathymetry data were acquired by the *Akademik Oparin*[5].

[5] Of the 372 vertical hydrologic profiles acquired in 2010, 168 were acquired in August, and 204 in September.

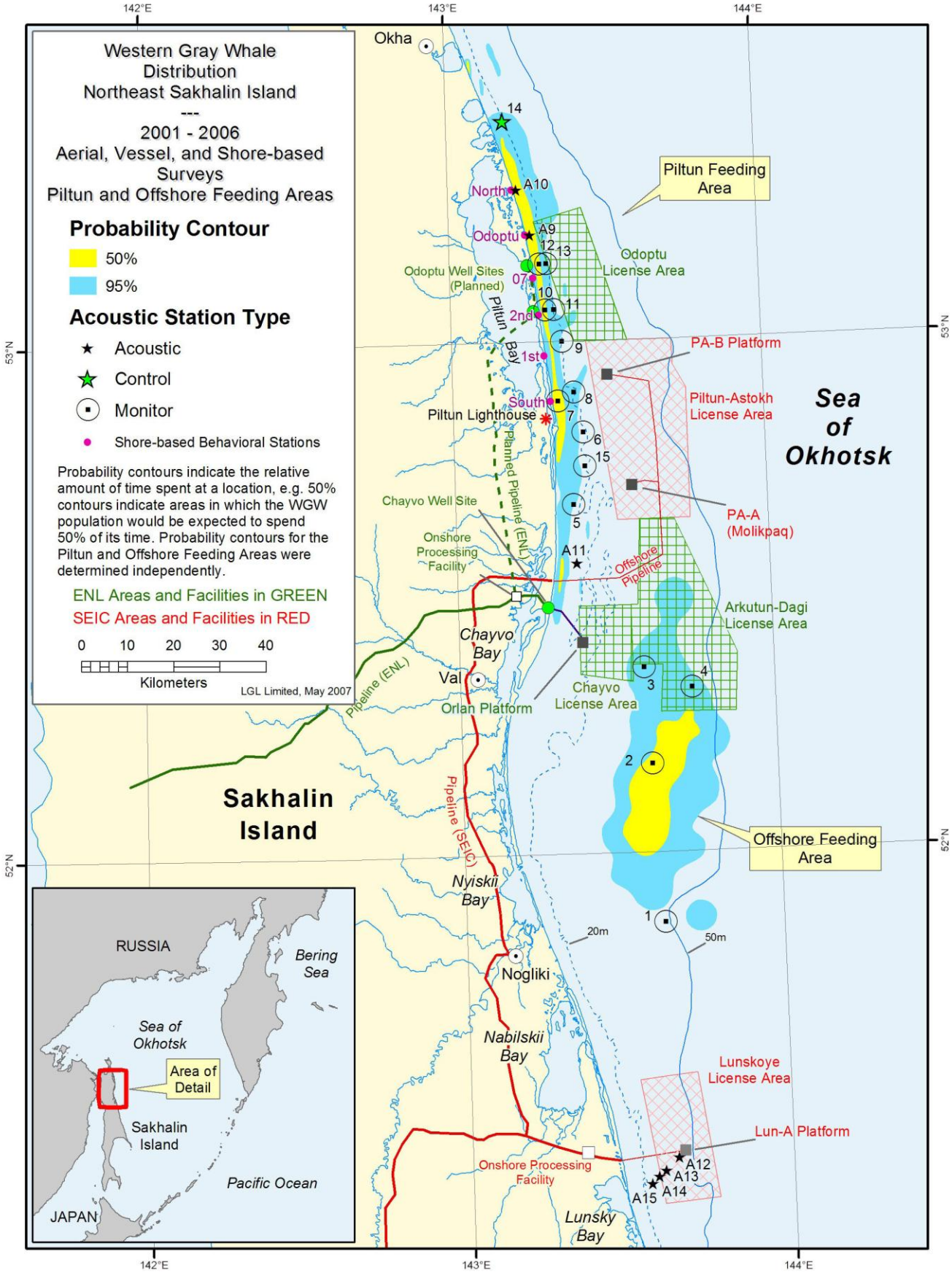

Figure 1.5 - Map of the NE Sakhalin Shelf showing the locations of the LUN-A, Molikpaq, Orlan and PA-B platforms as well as the AUAR deployment locations.

Figure 1.6 includes two maps showing the extent of the bathymetric grid and the points at which vertical hydrologic profiles were acquired. This plot shows the combined 2004 (323 vertical hydrologic profiles and 8,400 km of bathymetry data), 2005 (354 profiles and 7,788 km), 2006 (372 profiles and 12,147 km), 2007 (634 profiles and 7,200 km), 2008 (198 profiles and 8,260 km), 2009 (220 profiles and 9,260 km) and 2010 data.

1.1 Objectives of the acoustic program

The acoustic program conducted on the NE shelf of Sakhalin Island in 2010 had five main objectives:

1. The first objective was to study both temporal and spatial variations in the amplitude and frequency characteristics of ambient and anthropogenic sound at a series of monitoring stations located throughout the development area. These monitoring stations were positioned to be at the nearest outside edge of a gray whale feeding area to a proposed facility. The goal of this annual acoustic monitoring program is to estimate any change in the acoustic levels in the gray whale feeding areas due to the oil development and production activities.
2. The second objective was to study sound propagation characteristics and transmission loss (TL) along profiles between current and proposed ENL and SEIC facilities, both onshore and offshore, and defined locations at the edge of the gray whale feeding areas. These studies can be used to predict the potential acoustic impact if a facility with a known acoustic signature is installed at the proposed site.
3. The third objective was to acquire a comprehensive grid of bathymetric and hydrologic data across the study area, and to investigate the spatial and temporal variations in the hydrology due to weather events (e.g. typhoons). This data will be integrated with the 2,101 vertical hydrologic profiles and 63,055 km of bathymetry data acquired between 2004 & 2009.
4. The fourth objective was to estimate the one-third octave spectral density over the frequency range from 20 Hz to 15 kHz in 1-minute windows for all the behavioral monitoring AUARs in the Piltun feeding area.
5. The final objective was to study the relationship between the distribution and development of benthos and the hydrology and bathymetry of the study area [Fadeev, 2010].

1.2 Operational strategy and methodology

The shallow water (5 - 15 m) part of the NE Sakhalin shelf starting south of the mouth of Piltun Bay and extending northwards up the Sakhalin coast is one of the most important summer feeding areas for western gray whales. For this reason acoustic studies have been conducted in the area since 1999.

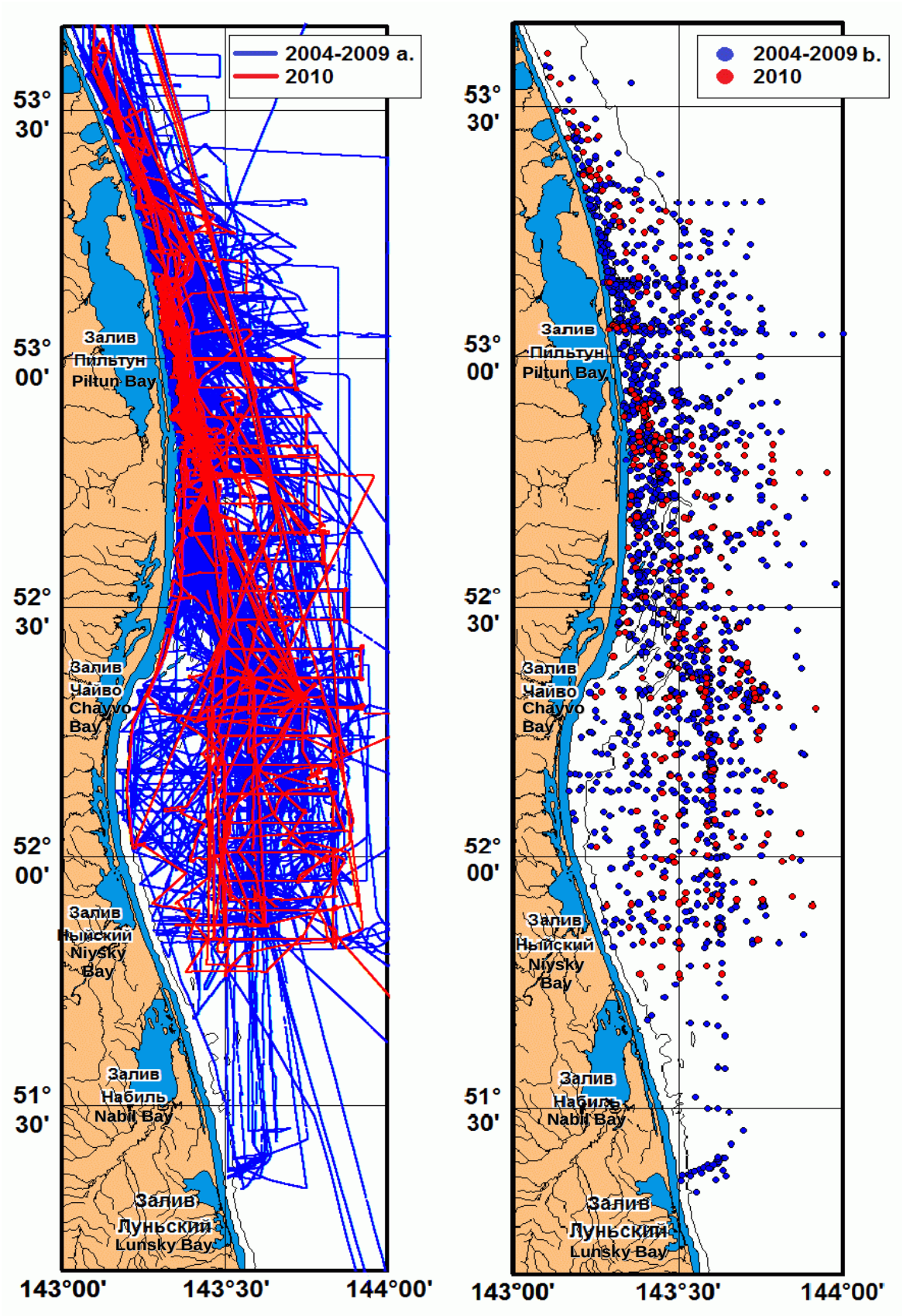

Figure 1.6 - Map of the NE Sakhalin Shelf showing (a) the 2004 to 2010 bathymetric grids and (b) the locations where vertical hydrologic profiles were acquired in 2004 to 2010.

In 2010, the main acoustic program was operated from a vessel and was led by Dr. Alexander Rutenko, who was based onshore, and Viktor Ushipovsky, field team manager onboard the *Akademik Oparin*. The plan was that both the acoustics and biology (distribution, benthic and Photo-ID studies) programs would be operated from the *Akademik Oparin* with Dr. Alexander Kalachev as the expedition leader for all activities aboard the vessel.

.

In 2010 18 AUARs designed and developed by POI were used to allow concurrent acoustic measurements to be acquired over a greatly enlarged spatial area. These AUARs could be deployed at depths up to 50 m (two are rated to 100 m), could record continuously for greater than 27 days and could measure the absolute acoustic amplitude of a signal over a frequency band from 2-15000 Hz. The expedition also had 6 mini-AUARs with similar recording characteristics, but only five days recording duration. A detailed description of this equipment was given in [Borisov et. al. 2006].

The *Akademik Oparin* can operate in water depths as shallow as 10 m. The AUARs were deployed from the stern of the *Akademik Oparin* as the vessel sailed slowly along its course. AUARs were retrieved manually using a zodiac deployed from the *Akademik Oparin* (Figure 1.7). After each AUAR was pulled to the surface it was towed to the vessel by a zodiac and transferred to the *Akademik Oparin* using its crane (Figures 1.8 & 1.9).

1.3 Ambient noise studies and Western gray whale core areas[6]

One of the key goals of the acoustic studies in the western gray whale research program is to measure and characterize the ambient noise field on the NE Sakhalin shelf. This long-term program commenced in 2003, and is currently ongoing. These data, in conjunction with the measurement of the acoustic signature of present and future facilities will allow the change in the acoustic environment due to the effect of oil development and production operations in the area, as well as on the gray whale population, to be more effectively estimated.

[6] This section is based on work performed by LGL Limited (Robin Tamasi, Peter Wainwright, Judy Muir, Sergei Yazvenko, Sonya Meier, and Steve Johnson).

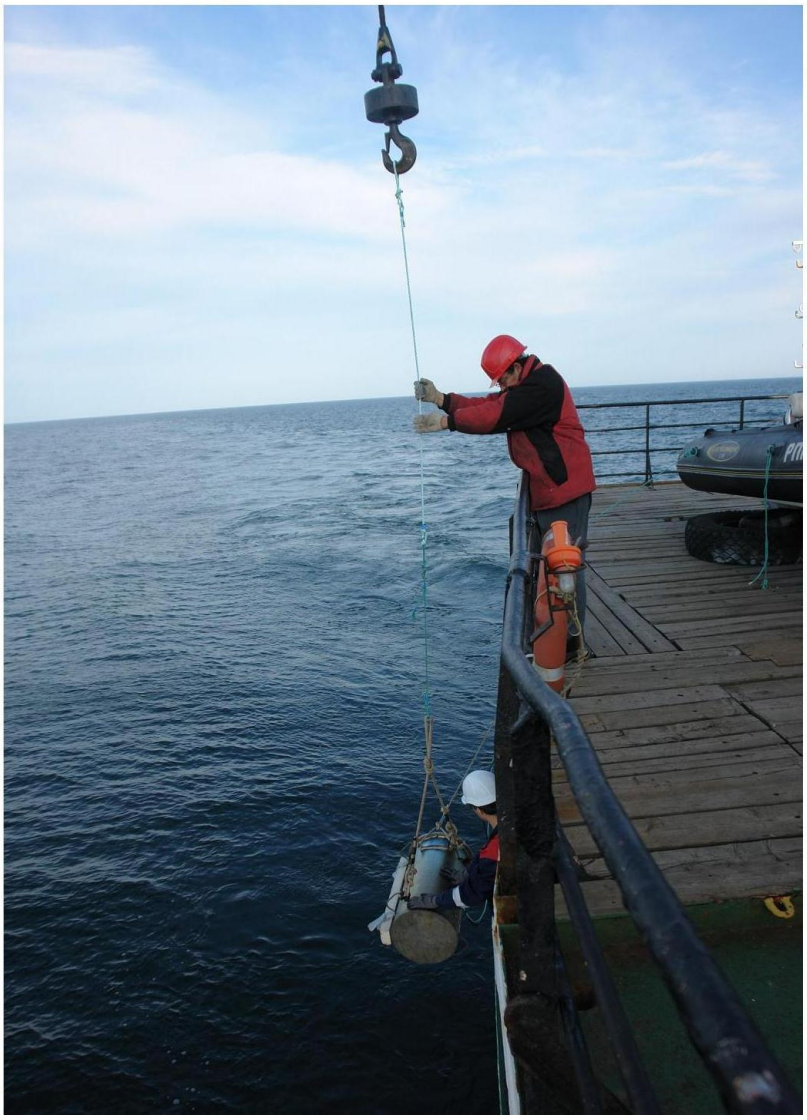

Figure 1.7 – Deploying an AUAR from the *Akademik Oparin.*

Figure 1.8 – Rigid hull zodiac with the electric winch used to raise the AUARs.

Figure 1.9 – Raising an AUAR using the stern crane of the *Akademik Oparin.*

In order to strategically plan the location of the monitoring stations for the 2003 to 2010 and future programs it was critical to estimate the core areas for the gray whales on the NE Sakhalin shelf. In 2003 the core areas were estimated and the acoustic monitoring locations selected using the sightings from all of the 2001 and 2002 aerial surveys [Borisov et. al. 2004], however in 2001 many more aerial surveys were acquired and they were concentrated in a reduced seasonal range. Further, no correction was made for survey effort. For 2004 the core areas were determined using whale densities estimated from the 2003 and 2004 aerial survey data taking the survey effort into account[7].

kernel density analyses, were used to generate probability contours. These contours are used to show the areas with the greatest likelihood of encountering gray whales, and to examine shifts in the 'centers of activity' of gray whales over time[8]. Cumulative probability contours of 50% and 95% were generated to visualize the distribution of gray whales. The 50% contour represents the area within which 50% of the whales sighted are expected to be found. In 2003 the probability contours were estimated using a conventional kernel density method[9]. This kernel density method employed a square-gridding process, which is robust for small sample sizes unless the variances of the north-south and east-west components of the distribution are very different, which is the case for the Piltun feeding area.

For the Piltun feeding area the distribution of whale sightings is oriented parallel to the coast with significantly greater variance in the along-shore direction than in the perpendicular-to-shore direction. For this reason, in 2004, a spatial grid was constructed for the Piltun feeding area that was oriented along-shore and with an along-shore grid cell dimension greater than the perpendicular-to-shore dimension, (i.e. each cell was 4 km by 0.5 km). Density was then computed for each cell as the number of observed whales normalized by the cumulative area surveyed within the cell. The same methodology was employed for the offshore feeding area except that, in this case, the conventional assumptions about distribution were satisfied and a spatial grid of 1 km by 1 km cells was employed.

---

[7] Density is the number of whales per unit area; multiple surveys over a grid cell result in larger densities within that cell if densities are not compensated for survey effort and average densities computed.
[8] Cumulative probability contours were computed independently for the Piltun and offshore feeding areas.
[9] The kernel density contours were mapped using the ArcView© 3.1 extension Animal Movement 2.04 [Hooge et. al., 1997]. Kernel density contours are an estimator that assesses an animal's probability of occurrence at each point in space based on a

There was significant variation among the 2003, 2004, 2005, and 2006 western gray whale core area estimates. Consequently, this analysis was updated in 2007 using all available systematic survey data. These included systematic sighting data from the 2001 to 2005 aerial surveys, 2002 to 2006 vessel-based surveys, 2001 to 2006 shore-based behavior scan surveys, and the 2004 to 2006 shore-based vehicle scan surveys. Appendix C gives details of this analysis.

1.3.1 Monitor, control and acoustic station locations

A systematic acoustic monitoring framework was developed in 2003 and extended from 2004 to 2006. The goal is to monitor changes in the acoustic field on the NE Sakhalin shelf and most importantly those changes in the anthropogenic sound level that could cause a significant increase in the Received Level (RL) in either the Piltun or offshore feeding areas.

Three types of stations for recording acoustic data were designated:

- **Monitor stations** - These are locations that are systematically monitored to gain an understanding of the changes in the acoustic field over time. They are reoccupied multiple times in a season and over multiple seasons. The monitor stations are generally located at the edge of a gray whale feeding area nearest to a proposed facility or in a location where the greatest cumulative impact from multiple facilities could be expected.
- **Control station(s)** - Dr. John Richardson (LGL Limited) recommended that a control station or stations be set up far enough away from the proposed development operations that the anthropogenic acoustic field would not be expected to increase. This station would reflect any changes to the ambient noise field unrelated to the oil development activities.
- **Acoustic stations** - These locations are infrequently monitored; their purpose is to gain an understanding of the anthropogenic sound field from a known location at a specific time related to development activities or to conduct TL experiments.

Eleven stations were designated prior to the start of the 2003 field season; seven were monitor stations, three were acoustic stations and one was a control station. For the 2004 season a further six monitor stations and seven acoustic stations were designated. In 2005 one additional acoustic station was designated. In 2006 one additional monitor station and four acoustic stations were designated. No new stations were designated between 2007 and 2009. Table 1.1 gives the names, identification numbers and locations of these stations[10].

---

utilization distribution.

[10] Where possible in order to facilitate long term monitoring the numbers and names of the monitor stations will be maintained year to year.

Table 1.1 - Numbers, names, locations and depths of the acoustic, monitoring and control stations.

#	Station		Latitude	Longitude	Depth
Monitor Stations:					
1	Lunskoye	Лунское	51° 51' 45" N	143° 37' 27.3" E	48 m
2	OFA (Offshore Feeding area)	ГЗК (Глубоководная зона кормления)	52° 10' 18" N	143° 36' 1.8" E	40 m
3	Orlan	Орлан	52° 21.6' N	143° 35.0' E	32 m
4	Arkutun-Dagi	Аркутун-Даги	52° 19' 9.6" N	143° 44' 4.6" E	40 m
5	Piltun-S	Пильтун-Ю	52° 40' 51" N	143° 22' 34" E	10 m
6	Piltun	Пильтун	52° 49.3' N	143° 24.9' E	20 m
7	PA-B-10	ПА-Б-10	52° 53' 2.1" N	143° 20' 10.6" E	10 m
8	PA-B-20	ПА-Б-20	52° 54' 00" N	143° 23' 20.5" E	20 m
9	Odoptu-PA-B	Одопту-ПА-Б	53° 00' 00" N	143° 21' 18" E	20 m
10	Odoptu-S-10	Одопту-Ю-10	53° 03.7' N	143° 18.3' E	10 m
11	Odoptu-S-20	Одопту-Ю-20	53° 03' 42" N	143° 19' 58" E	20 m
12	Odoptu-N-10	Одопту-С-10	53° 09.1' N	143° 17.4' E	10 m
13	Odoptu-N-20	Одопту-С-20	53° 09' 6" N	143° 18' 42' E	20 m
14	**Control**	**Контрольная**	**53° 25' 57' N**	**143° 11' 06' E**	**20 m**
15	Molikpaq	Моликпак	52° 45' 52" N	143° 26' 38" E	24 m
Acoustic Stations:					
A1	#1 (Chayvo-1)	#1 (Чайво-1)	52° 27.8' N	143° 19.0' E	11 m
A2	#2 (Chayvo-2)	#2 (Чайво-2)	52° 25.9' N	143° 20.6' E	11 m
A3	#3 (Chayvo-3)	#3 (Чайво-3)	52° 26.8' N	143° 24.6' E	17 m
A4	#4 (Piltun-1)	#4 (Пильтун-1)	52° 43' 14.4" N	143° 22' 26.7" E	10 m
A5	#5 (Piltun-2)	#5 (Пильтун-2)	52° 43' 48" N	143° 25' 49" E	20 m
A6	#6 (Piltun-3)	#6 (Пильтун-3)	52° 49.3' N	143° 24.9' E	20 m
A7	#7 (PA-B-1)	#7 (ПА-Б-1)	52° 55' 54" N	143° 19' 39" E	10 m
A8	#8 (PA-B-2)	#8 (ПА-Б-2)	52° 55' 54" N	143° 21' 42.4" E	20 m
A9	#9 (BEH-Odoptu)	#9 (Одопту (Пов))	53° 12' 33.1" N	143° 15' 51" E	10 m
A10	#10 (BEH-north)	#10 (Пов-север)	53° 17' 52.4" N	143° 13' 25.4" E	10 m
A11	#11 (Chayvo-4)	#11 (Чайво-4)	52° 34' 00" N	143° 23' 00" E	~18 m
A12	#12 (Lunskoye-1)	#12 (Лунское-1)	51° 24' 12" N	143° 38' 30" E	47 m
A13	#13 (Lunskoye-2)	#13 (Лунское-2)	51° 22' 42" N	143° 36' 00" E	37 m
A14	#14 (Lunskoye-3)	#14 (Лунское-3)	51° 22' 00" N	143° 34' 42" E	31 m
A15	#15 (Lunskoye-4)	#15 (Лунское-4)	51° 21' 12" N	143° 33' 24" E	24 m

The locations of the monitor stations were determined with reference to the major gray whale concentrations in the area (Figure 1.10)[11]. For the offshore feeding area, the locations of the stations (except the OFA station) were chosen to be on the 95% probability contour at the point closest to a current or proposed facility. The location of the monitor stations remained constant between 2004 and 2010[12]. The western gray whale distribution in the Piltun feeding area varies with bathymetry, with most whales feeding in water depths between ~8-12 m. Mother-calf pairs have been seen in the Piltun feeding area, often in water depths of 5-10 m, and fewer whales have been seen outside the 20 m contour. Thus, the two key acoustic monitoring points in the Piltun feeding area are the 20 m and the 10 m bathymetry contour (regarded as the edge and center of the whale distribution).

The control station location has remained the same since 2003[13]. This location has a similar hydrology and bathymetric character to the Piltun feeding area, is far enough away to serve as an acoustic control point, but close enough for effective operational support. Stations A1 to A8 and A11 to A15 were not occupied in 2010. All the unused acoustic stations were previously used for TL experiments.

1.4 Data recorded on the NE Sakhalin shelf during the 2009 field season

During the 2010 expedition, as in previous seasons, AUARs were used to make simultaneously acoustic measurements over a shelf area extending about 180 km from the northern boundary of the Odoptu license area to the southern edge of the offshore feeding area (Figure 1.10). In previous years monitoring of acoustic noise in the Offshore Feeding Area had to be abandoned in September to prevent the possible loss of an AUAR due to fishing activity in the area. However, in 2010 Gazprom were acquiring a 3D seismic survey in the area and the area was

[11] Various vessel-based (MMO, Photo-ID, Benthic) and land based (vehicle surveys, behavioral) biology programs were being conducted over the same seasonal range, so an evaluation of the effect of any changes in the acoustic field on the behavior or distribution of gray whales could be evaluated.

[12] 2004: The Orlan station is on the 95% cumulative probability contour (from 2003) closest to the proposed location of the Orlan platform, the Lunskoye station is at the southern edge of the offshore feeding area, the OFA (Offshore Feeding Area) station is approximately in the center of the offshore feeding area and the Arkutun-Dagi station is at the North Eastern edge of the offshore feeding area. 2005: The Odoptu-S-10, Odoptu-N-10, Odoptu-N-10 and Odoptu-S-10 stations were at the 10 m and 20 m bathymetry contours off the coast from the two proposed Odoptu well pads. The Piltun station is at the 20 m bathymetry contour between the Molikpaq platform and the major gray whale concentration off Piltun lighthouse. The PA-B stations were at the 10 m (PA-B-10) and 20 m (PA-B-20) bathymetry contours closest to the proposed PA-B location. The Piltun-S station is on the 95% cumulative probability contour at the southern bathymetry contour of the Piltun feeding area and the Odoptu-PA-B station at the 20 m bathymetry contour between the proposed locations of the Odoptu-S well pad and the PA-B platform. 2006: The Molikpaq station is at the 20 m bathymetry contour between the Molikpaq platform and the major gray whale concentration off Piltun lighthouse.

closed to fishing, the AUARs were therefore deployed.

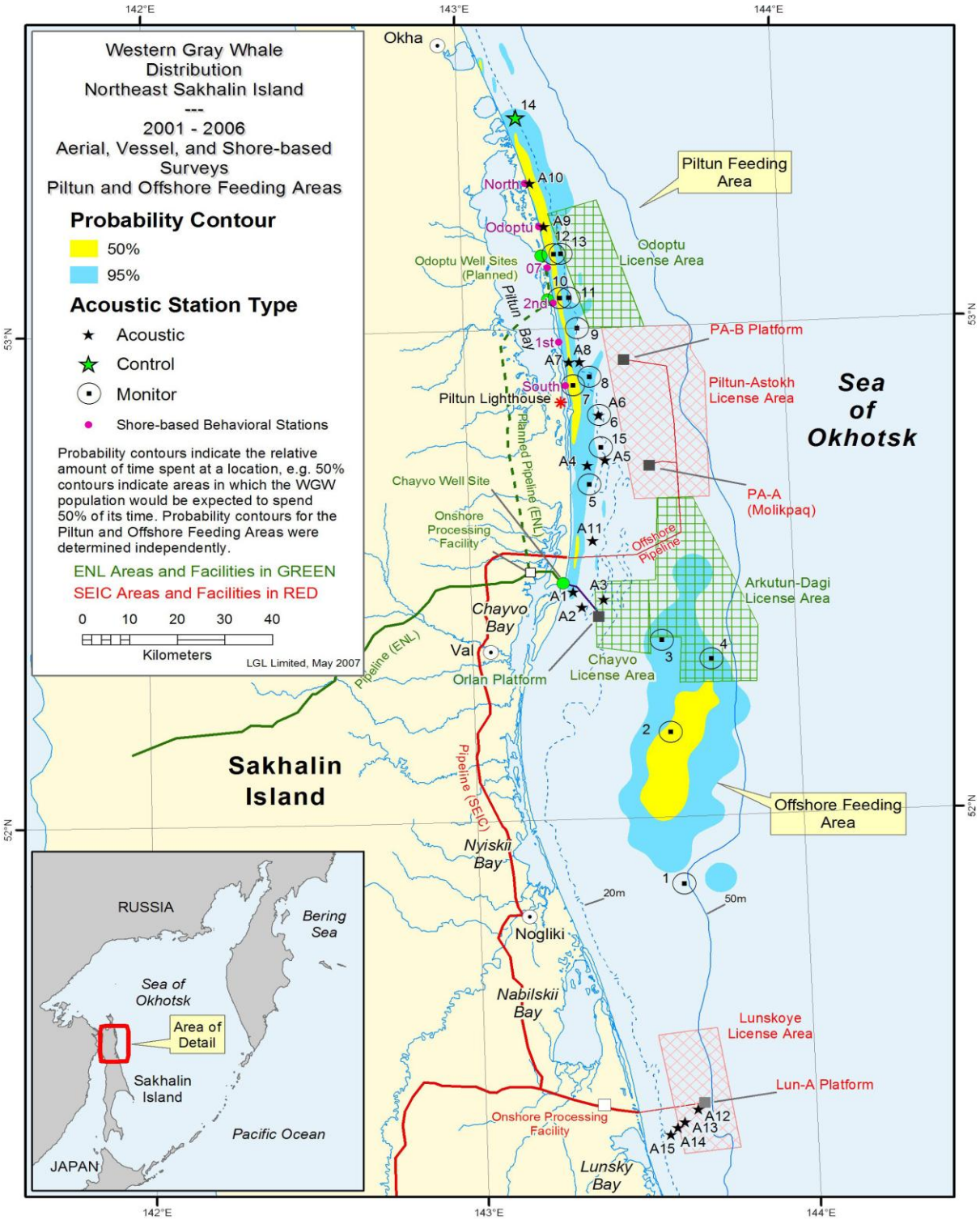

Figure 1.10 - Map showing the AUAR locations and cumulative probability contours showing the density distributions of western gray whales from the 2001 to 2005 aerial surveys, 2002 to 2006 vessel based surveys, 2001 to 2006 shore-based behavior scan surveys and the 2004 to 2006 shore-based vehicle scan surveys.

[13] The control station was located on the 20 m bathymetry contour approximately 40 km north of the Odoptu North pad site.

This section discusses the data recorded on the NE Sakhalin shelf during the 2010 field season. It describes the deployment dates, recording times, hydrophone depths and locations of the AUARs as well as their operational characteristics. Tables 1.2 and 1.3 give these details for the 16 AUARs used in the study.

All the acoustic data from the 2010 field program will be presented as sonograms[14], where the spectral density values *G(f,t)* are represented by different colors[15], one sonogram representing the acoustic data for one AUAR for one day. Included on the plots along with these daily sonograms, on a common time axis, are plots of the variation in sound pressure level $D(\Delta f,t)$ with time over the annotated bandwidth. The sonograms *G(f,t)* cover a broad frequency band (2 Hz to 15 kHz) and are plotted with a logarithmic frequency axis to aid in the visual analysis of the data (e.g. Figure 1.11). The logarithmic scale on the frequency axis clearly shows the pseudo-noise signals below 20 Hz. This is flow noise caused by a tidal current with a velocity exceeding 1 m/s and is recorded twice a day. The acoustic data for the infrasonic band should therefore be analyzed during slack tide periods when flow noise is absent (approximately 4 hours). These sonograms *G(f,t)* show the variation in the spectral levels of ambient and anthropogenic sound with frequency and time due to changing meteorological conditions, vessel movements and industrial activity. All sonograms *G(f,t)* will be in absolute amplitude (dB re 1 $\mu Pa^2/Hz$), all instrument and sensor corrections having been applied to the data. Appendix A shows the days on which data were acquired at each station, and sonograms for all the data are available on a DVD accompanying this report.

It was expected that Rosneft would acquire a seismic survey in the Lebedinskoye area using air guns during the 2010 field season. Therefore, when the AUARs were deployed at the annual monitoring stations the gain in the analog channel of each AUAR was set to reduce likelihood of overload (clipping) of the recorded acoustic signal, even during seismic exploration. A seismic survey conducted by Gazprom to the east of the Offshore feeding area was not expected. As a consequence the AUAR gains were therefore too high and the hydrophones too sensitiveThis led to signal clipping during the first deployment and the gains had to be changed for the second deployment of the stations in the Offshore feeding area.

[14] A sonogram is a plot showing the variation in acoustic power spectral density level with frequency and time *G(f,t)*.
[15] The scale of the sonograms varies from 37 to 120 dB re 1 $\mu Pa^2/Hz$ in 3 dB increments.

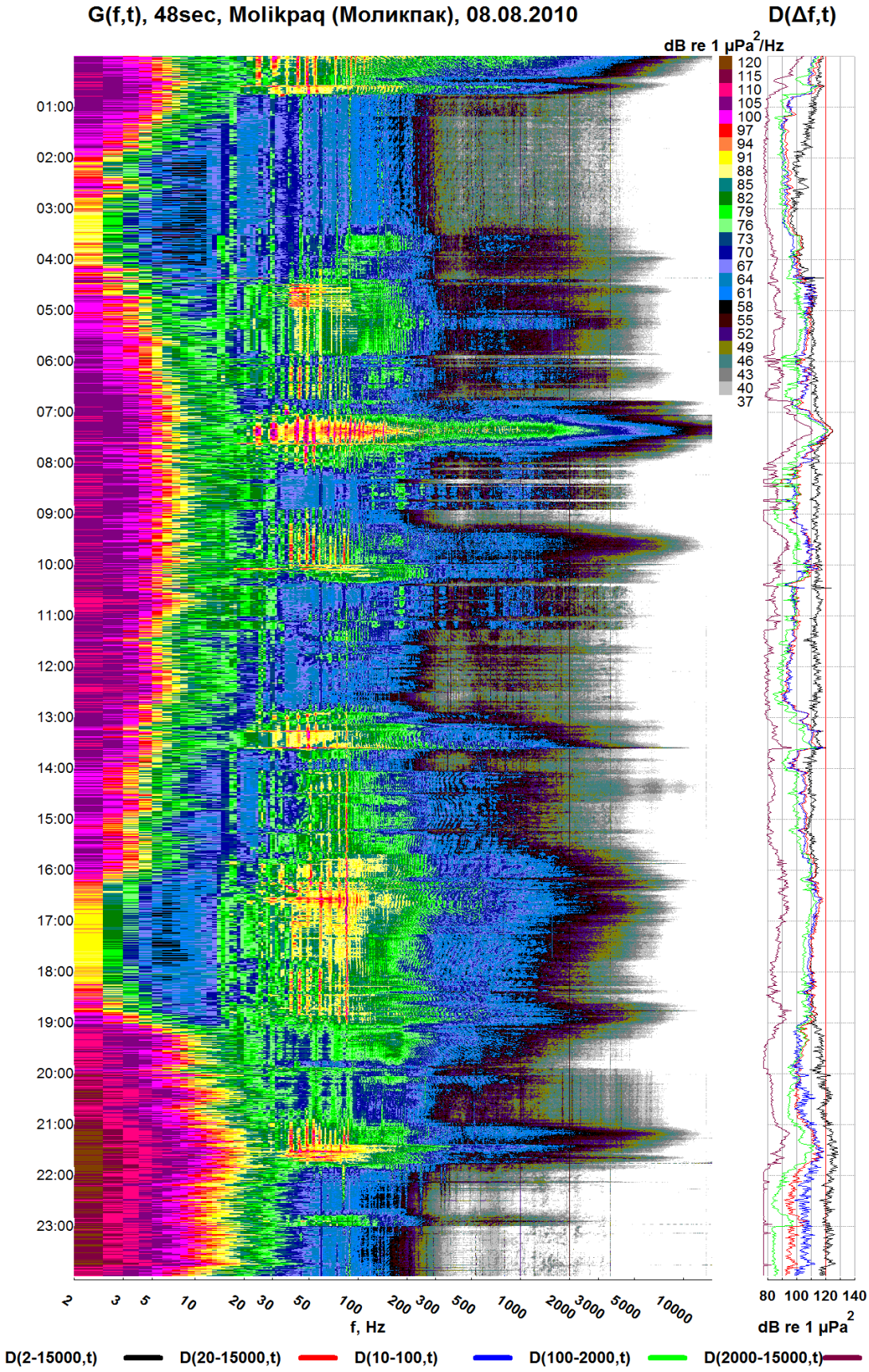
G(f,t), 48sec, Molikpaq (Моликпак), 08.08.2010
D(Δf,t)
dB re 1 μPa²/Hz
120
115
110
105
100
97
94
91
88
85
82
79
76
73
70
67
64
61
58
55
52
49
46
43
40
37
01:00
02:00
03:00
04:00
05:00
06:00
07:00
08:00
09:00
10:00
11:00
12:00
13:00
14:00
15:00
16:00
17:00
18:00
19:00
20:00
21:00
22:00
23:00
2
3
5
10
20
30
50
100
200
300
500
1000
2000
3000
5000
10000
f, Hz
80
100
120
140
dB re 1 μPa²
D(2-15000,t)
D(20-15000,t)
D(10-100,t)
D(100-2000,t)
D(2000-15000,t)

Fi **energy**

As discussed earlier, the retrograde motion of water particles in propagating surface waves with wave heights greater than 1 m causes intense, low-frequency, flow noise (pseudo-noise), which could also overdrive the analog channel of the AUAR. The magnitude of this effect is dependent on water depth and is at a maximum for AUARs deployed at the 10 m bathymetry contour. Turbulent bottom currents (due to the orbital motion of water particles in propagating surface waves) trap and transport sand, altering the sea floor topography, and carry polychaetes from the sea floor. In 2009, massive biofouling by polychaetes and their shells of the pyramids and rubber straps used to deploy the measuring hydrophones on the bottom was encountered at annual acoustic monitoring stations. Hydrophones were deployed in larger pyramids on rubber straps in 2010 to try and reduce this effect and the low-frequency pseudo-noise that was added to the acoustic signal.However, this approach was not very effective.

Alkaline cell battery packs were used for the first time as a power source for two AUARs in 2010. An AUAR with such a battery pack (Figure 1.2) was installed at the *Control* station, and operated for its total service life of 52 days, turning itself off after its hard drives were full. Figure 1.12 shows its hydrophone, which was covered by small algae during this extended deployment.

1.5 Terminology and algorithms used in the report

Ambient and anthropogenic acoustic data recorded by an AUAR was written to the AUAR disc in a raw format and converted to microPascals (μPa)[16] after downloading to the computer on the *Akademik Oparin* (or during analysis). Acoustic spectra in decibels were used to describe the variation in acoustic power as a function of frequency. In this report sound pressure power density spectra $G(f)$ ($\mu Pa^2/Hz$)[17] will be used when spectral data are plotted. The sonograms $G(f,t)$ are plots of power spectral density vs. frequency and time and also include the variation in sound pressure level $D(\Delta f,t)$ (dB re 1 μPa) with time over the annotated bandwidth[18]. Figure 1.11 shows a sonogram; the color scales generally run from 37 to 120 dB re 1 $\mu Pa^2/Hz$ and the frequency range from 2 Hz to 15 kHz.

[16] The data were scaled (after incorporating hydrophone sensitivity, system instrument response and system gain (at 1 kHz), to convert the data to standard units of pressure (measured through an omni-directional hydrophone).
[17] Energy and power spectra are scaled to 1 Hz whatever the analysis length.
[18] Sound pressure level is the integral of the acoustic energy over the specified frequency band.

Figure 1.12 –Fouling of the hydrophone by algae.

The ***Spectral level*** of an acoustic signal relates to the level of acoustic power in a 1 Hz band. This term is generally only applied to sounds with continuous frequency spectra[19]. These spectra are often averaged over a number of one-second windows[20] to improve the statistical stability of the ambient noise data[21]; the number of one-second windows used in the averaging is given at the top of each plot (if the data is averaged over multiple windows).

A detailed description of the methodology and algorithms used to normalize acoustic data and calculate spectral estimates is given in [Borisov et.al., 2006].

[19] A continuous frequency spectrum is a spectrum with signal present at all sampled frequencies.
[20] Average of X 1-second spectral estimates.

1.6 Statistical analysis of acoustic data

The sonograms *G(f,t)* described in the previous sections illustrate the variation in the power spectral density level in the 2–15,000 Hz frequency range due to changes in the ambient and anthropogenic noise levels generated by weather conditions, vessel movements, and industrial activity. The calibrated power spectral density levels in the sonograms represent 1-minute spectral averages $\hat{G}(f, \Delta t = 1\text{min})$ of adjacent 1-second spectral estimates computed by fast Fourier transform (FFT, Δf=1 min). Additional averaging was conducted during this analysis; the estimated 1-second spectral estimates computed by the FFT (Δf = 1 Hz) were averaged to generate 1-minute spectral averages $\hat{G}(f, \Delta t = 1\text{min})$. These one-minute spectral averages were also averaged across frequency to generate one-minute one-third octave spectral estimates at the specified central frequencies[22].

During the 2010 season all systems recorded data continuously, unlike in previous years when gaps of about 20 minutes occurred every 4 hours and 40 minutes due to disk transfer overhead. Acoustic data may also have been distorted by amplitude overloads, and spurious values caused by movement of the hydrophone, or equipment malfunction or overload. This spurious data must be removed or compensated when analyzing long term changes in the data at monitoring stations.

1.6.1 Calculation of one-third octave power spectral density percentile plots

To statistically estimate the variation in the one-third octave power spectral density estimates with time and amount of construction work, percentile distribution plots were generated for the analysis period specified. The following procedure is used to construct these percentile plots for constructing such estimates. One-third octave spectral values $\hat{G}_{1/3oct}(f = f_i, \Delta t = 30\text{min})$ for the central frequency f_i for a given time period are analyzed independently of other frequencies. The series of one-third octave spectral values for a given central frequency are arranged in a one-dimensional matrix and are sorted to determine the maximum and minimum levels as well as the level corresponding to 10%, 25%, 50%, 75%, and 90% (in 0.1 dB increments). For

[21] Spectral averaging is used to obtain a lower variance spectral estimate.
[22] Central frequencies were 5, 6, 8, 10, 13, 16, 20, 25, 32, 40, 50, 63, 79, 100, 126, 158, 200, 251, 316, 398, 501, 631, 794, 1,000, 1,259, 1,585, 1,995, 2,512, 3,162, 3,981, 5,012, 6,310, 7,943, and 10,000 Hz

example, if exactly half of all the measured spectral values for central frequency $f_i \leq$ 95 re 1μPa^2, then the 50% percentile level will be set as 95 dB.

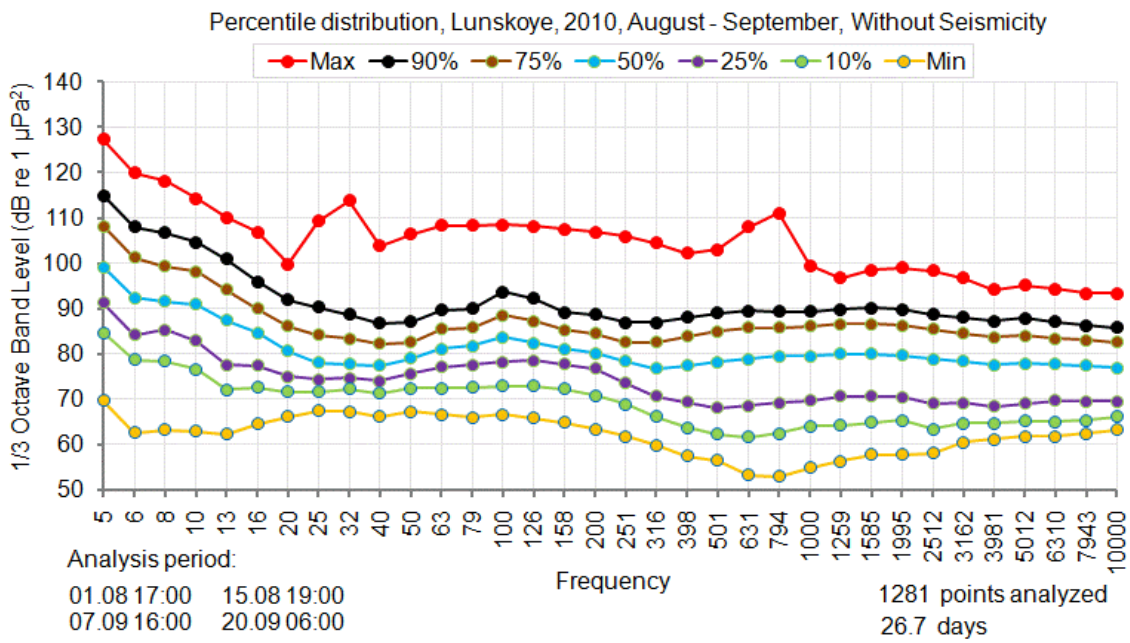

Figure 1.13 - Percentile plots of one-third octave power spectral density estimated at the Lunskoye monitor station for August and September, 2010.

Figure 1.13 gives an example of the results of this procedure performed on one-third octave power spectral density estimates $\hat{G}_{1/3oct}(f = f_i, \Delta t = 30\text{min})$ of acoustic signals measured by an AUAR deployed at the Lunskoye acoustic monitoring station. The start and end times for the continuous measurements is indicated below the graph. In this case the acoustic data were acquired from 17:00 on 1st August to 19:00 on 15th August, and from 16:00 on 7th September to 06:00 on 20th September. The break in the data is due to interference from a Gazprom seismic survey in the area from 16th August to 6th September that clipped the acoustic data. Statistical analysis was conducted on 1281 30-minute power spectral density estimates and corresponds to a 26.7 day data series.

Figure 1.13 shows the characteristic features in the percentile distribution plots. At frequencies less than 20 Hz, the difference between the minimum and maximum values is greater than 60 dB, which is due to flow noise (Figure 1.11). The 15-20 dB difference between the maximum and 90% percentile plots is explained by the passage of a vessel near the monitoring station. The divergence of the curves at frequencies greater than 200 Hz is possibly due to sounds from distant vessels (for example, from the vessel supporting work at the Lunskoye platform), and variations in the noise generated by surface waves and wind.

Table 1.2(a) - Operational times, parameters and locations of AUARs at monitor stations 1 to 10.

Station		Date		Time		Time	AUAR	Location		Depth	Gain	Sens.
Name	#	Start	End	Start	End	(hr)	#	Latitude	Longitude	(m)		(mV/Pa)
Lunskoye	1	1-Aug	25-Aug	14:21	19:01	**581**	№ 9	51°51.763	143°37.415	46	8	49.5
Lunskoye	1	26-Aug	20-Sep	8:33	10:30	**602**	№ 5	51°51.720	143°37.438	46	1	49.0
OFA	2	1-Aug	25-Aug	16:51	14:43	**574**	№ 16	52°10.295	143°36.067	42	8	52.1
OFA	2	26-Aug	20-Sep	14:53	14:37	**600**	№ 9	52°10.270	143°36.073	41	1	10.4
Orlan	3	2-Aug	25-Aug	10:53	09:51	**551**	№ 5	52°21.560	143°34.982	33	8	49.0
Orlan	3	26-Aug	25-Sep	20:49	19:23	**719**	№ 16	52°21.632	143°34.992	33	1	52.1
Arkutun-Dagi	4	1-Aug	26-Aug	20:33	19:30	**599**	№ 3	52°19.252	143°44.080	41.8	8	46.4
Arkutun-Dagi	4	24-Aug	19-Sep	17:50	05:50	**612**	№ 18	52°19.080	143°43.990	46	1	5.5
Piltun-S	5	8-Aug	3-Sep	19:59	09:38	**614**	№ 19	52°40.825	143°22.572	17	8	48.5
Piltun-S	5	5-Sep	25-Sep	18:23	16:33	**478**	№ 4	52°40.830	143°22.583	18	8	49.4
Piltun	6	9-Aug	25-Sep	12:56	14:16	**1129**	№ 26	52°49.328	143°24.890	20	8	50.0
PA-B-10	7	7-Aug	29-Aug	21:04	16:18	**523**	№ 11	52°52.963	143°20.033	9	8	49.5
PA-B-10	7	1-Sep	25-Sep	07:05	13:23	**582**	№ 11	52°52.978	143°20.433	10	8	49.5
PA-B-20	8	6-Aug	3- Sep	19:05	13:54	**667**	№ 17	52°53.982	143°23.332	19	8	49.6
PA-B-20	8	5-Sep	24-Sep	13:48	13:57	**456**	№ 21	52°54.022	143°23.355	20	8	49.7
Odoptu-PA-B	9	6-Aug	14-Aug	17:46	19:16	**194**	№ 21	52°59.975	143°21.285	22	8	49.7
Odoptu-PA-B	9	4-Sep	27-Sep	14:43	08:58	**546**	№ 17	52°59.980	143°21.312	22	8	49.6
Odoptu-S-10	10	7-Aug	3-Sep	09:53	19:36	**658**	№ 27	53°03.745	143°18.325	10	8	50.25
Odoptu-S-10	10	4-Sep	24-Sep	16:01	12:03	**476**	№ 19	53°03.690	143°18.280	11	8	48.5
Odoptu-S-20	11	7-Aug	17-Aug	17:31	13:12	**980**	№ 13	53°03.680	143°19.970	20	8	49.5
Odoptu-S-20	11	9-Sep	24-Sep	20:56	11:08	**350**	№ 7	53°03.680	143°20.153	21	8	49.2

Table 1.2(b) - Operational times, parameters and locations of AUARs at monitor stations 11 to 15, the control station.

Station		Date		Time		Time	AUAR	Location		Depth	Gain	Sens.
Name	#	Start	End	Start	End	(hr)	#	Latitude	Longitude	(m)		(mV/Pa)
Odoptu-N-10	12	7-Aug	4-Sep	12:40	17:49	**677**	№ 4	53°09.128	143°17.428	10	1	49.4
Odoptu-N-10	12	5-Sep	27-Sep	08:20	18:14	**538**	№ 27	53°09.088	143°17.360	11	1	50.25
Odoptu-N-20	13	6-Aug	29-Aug	14:41	12:58	**550**	№ 6	53°09.072	143°18.725	20	1	49.9
Odoptu-N-20	13	29-Aug	27-Sep	13:36	17:45	**700**	№ 3	53°09.142	143°18.798	22	1	9.3
Molikpaq	15	5-Aug	3-Sep	20:23	10:49	**687**	№ 8	52°45.813	143°26.637	24	8	44.5
Molikpaq	15	1-Sep	25-Sep	20:36	15:09	**571**	№ 6	52°45.922	143°26.647	24	8	49.9
Control	14	6-Aug	27-Sep	08:58	14:39	**1254**	№ 2	53°25.982	143°11.108	20	8	49.0
BEH-north	A.10	6-Aug	4-Sep	10:15	08:27	**694**	№ 7	53°18.363	143°13.823	10	1	49.2
BEH-north	A.10	4-Sep	27-Sep	09:01	16:03	**559**	№ 8	53°18.367	143°13.765	11	1	44.5

Table 1.2(c) - Operational times, parameters and locations of AUARs at acoustic stations A9 & A10.

Station		Date		Time		Time	AUAR	Location		Depth	Gain	Sens.
Name	#	Start	End	Start	End	(hr)	#	Latitude	Longitude	(m)		(mV/Pa)
BEH-Odoptu	A.9	14-Jun	7-Jul	19:10	15:00	548	№ 4	53°12.785	143°15.847	12	38	49.4
BEH-Odoptu	A.9	7-Jul	25-Jul	16:15	16:45	433	№ 3	53°12.505	143°16.072	10	2	46.4
BEH-Odoptu	A.9	8-Aug	6-Sep	13:50	19:00	701	№ 3	53°12.527	143°16.042	11	2	46.4
BEH-Odoptu	A.9	13-Sep	23-Sep	15:30	03:00	238	№ 9	53°12.522	143°16.082	11	2	46.4
BEH-north	A.10	9-Aug	3-Sep	08:45	18:15	597	№ 17	53°17.867	143°13.940	10	2	49.6
BEH-north	A.10	11-Sep	23-Sep	10:45	11:00	288	№ 21	53°17.845	143°13.967	11	2	49.7

Table 1.3 – Plot showing the days when AUARs were active at each monitoring station (by station).

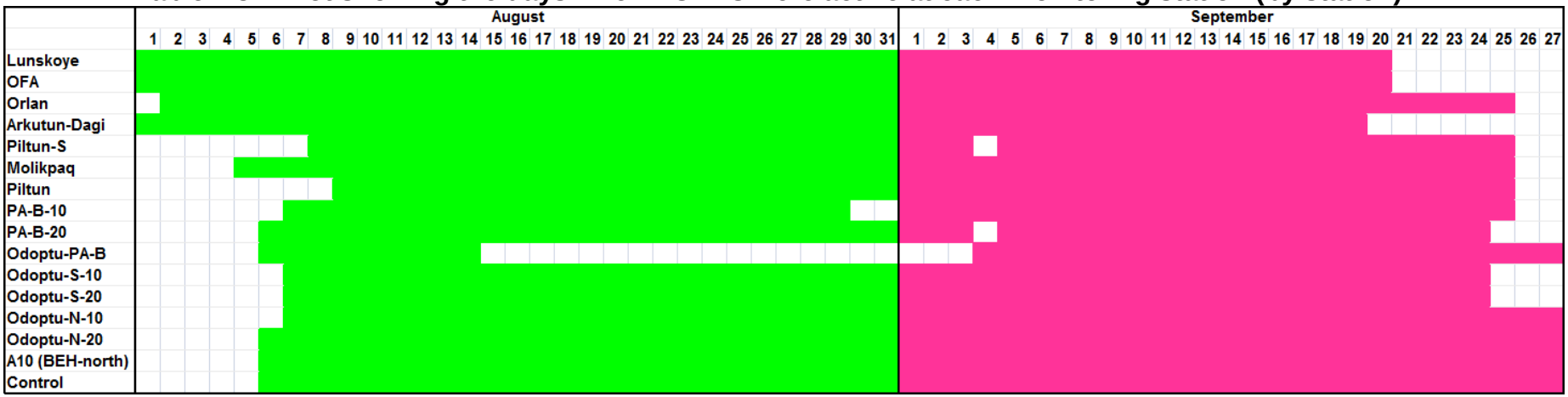

2 Acoustic recording and processing equipment

The acoustic measurements were conducted using 18 digital AUARs (Figure 1.1) developed at POI. Between 2005 and 2007 an additional six mini-AUARs (Figure 1.2) were constructed; these were smaller with a reduced (72 hours) record time and were used for TL and source level measurements. Non-rechargeable alkaline batteries were used in specially constructed battery packs as a power supply for the mini AUARs in 2010, increasing their operational time to 160 hours. The AUARs (all variants), were designed to enable accurate, autonomous, synchronous acoustic measurements over a broad range of frequencies (2 Hz to 15 kHz) to be recorded. A detailed description of this equipment has been provided by Borisov [Borisov et. al. 2006]. The hydrological studies were conducted on vertical profiles using a Valeport MIDAS-CTD+500 multi-parameter autonomous combination sonde, which measures hydrostatic pressure (depth), sound velocity, temperature, conductivity (salinity), oxygen concentration, pH and turbidity.

2.1 Autonomous Underwater Acoustic Recorder (AUAR)

The AUARs[23] are made of welded titanium alloy and are rated to depths of up to 50 m (two are rated to 100 m). Signals from two external sensors (hydrophones, accelerometers or hydrologic measuring equipment) can be input to the AUAR electronics. Inside the AUAR there are three sealed 115 ampere-hour batteries secured in a titanium frame and the AUAR electronics and power handling circuitry is attached to the lid. After successful testing during the 2009 expedition all of the AUARs and all six mini-AUARs were modified to enable continuous recording of acoustic signals; thus the units did not have the 22-minute gaps required to write data from the flash drive to the hard disk that characterized earlier versions.

The AUAR digital recorder is based on the Prometheus single board computer, which has an integrated 16 bit analog to digital converter (ADC). The AUAR uses two 160 GB hard drives for primary data storage, mounted on a rubber cushion to isolate them mechanically from the AUAR housing. While one of the drives records data, the other remains in standby mode with its motor off. Figure 2.1 gives plots of the internal noise of AUARs with a flash drive and with direct recording to the hard drive for analog channel gains of 2 and 38.

[23] 2003/2005/2006/2007/2008/2009 AUAR dimensions are length 0.8 m, diameter 0.38 m, weight in air ~155 kg.

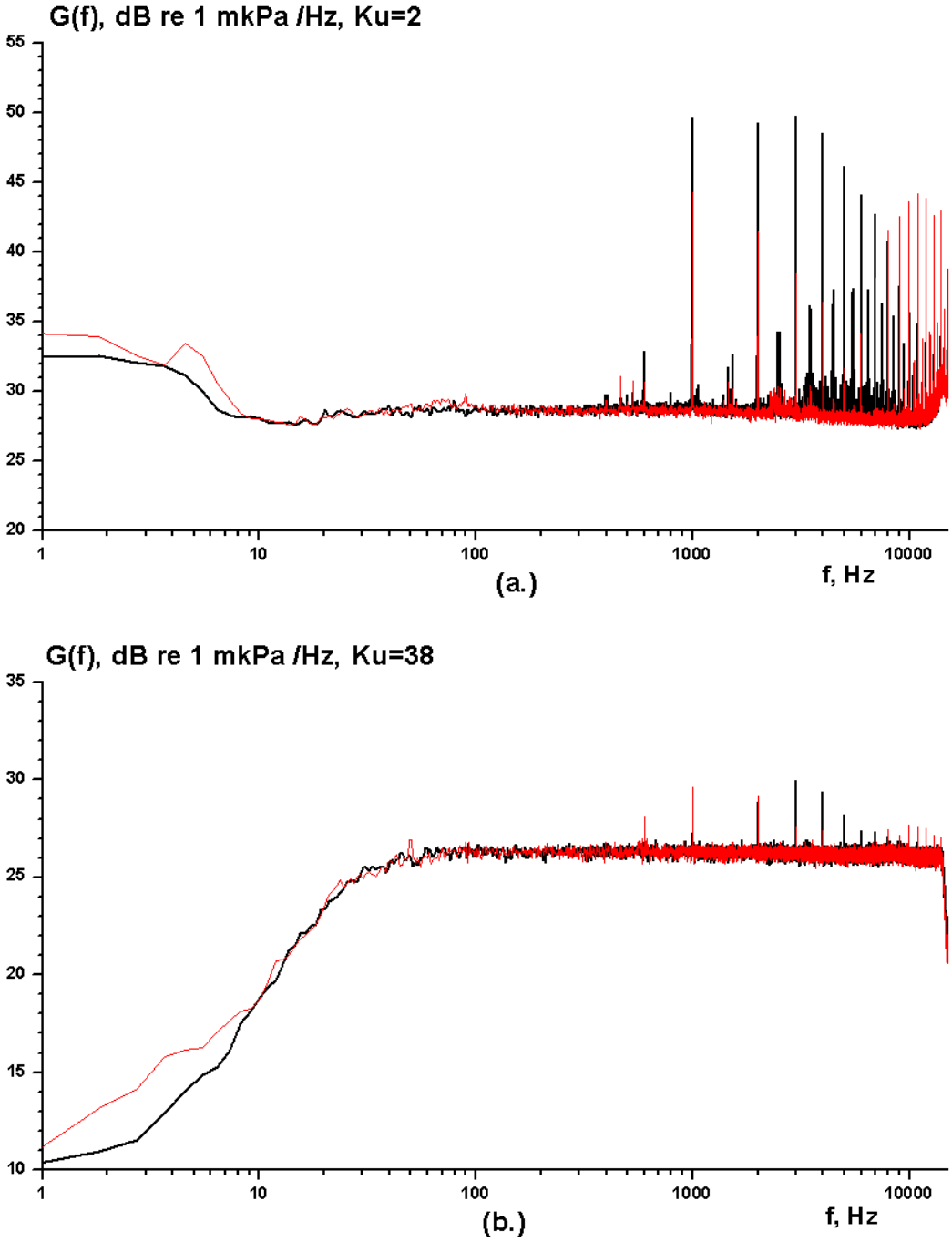

Figure 2.1 – Internal noise spectra of an AUAR recorded using a flash drive (black) and a continuously operational hard drive (no gaps) (red) with an analog channel gain of (a) 2; (b) 38.

The Prometheus computer can address 137 GB on a single drive; paired drives are therefore used to increase the recording capacity to 274 GB leading to a maximum AUAR operational time of 52 days. However, three 115 ampere-hour rechargeable batteries only provide sufficient power for 30 days of operational time; using non-rechargeable batteries allows an operational period of greater than the 52 day disk limit, thus data storage is the limiting factor.

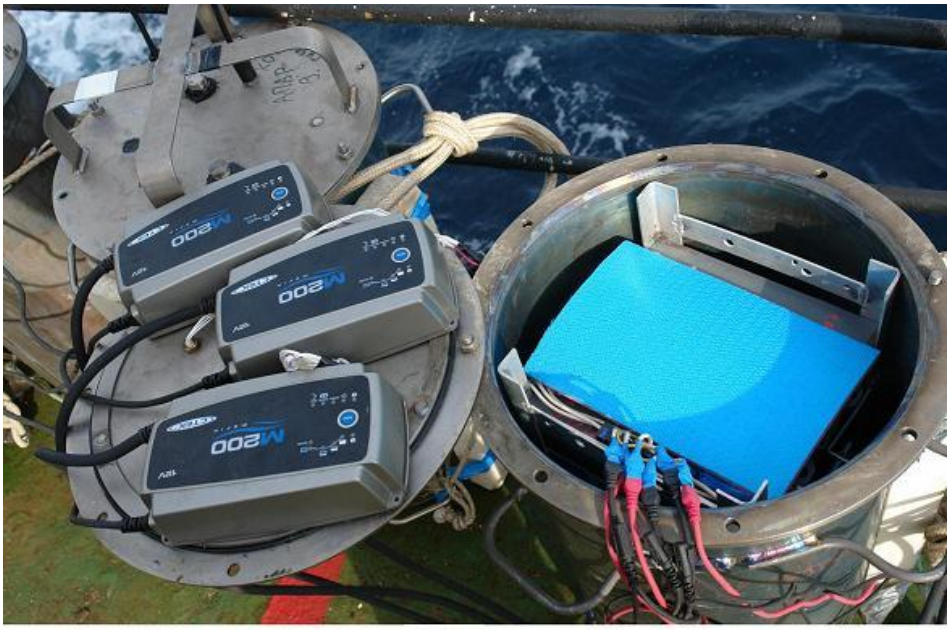

(a.)

(b.)

Figure 2.2 - (a) Charging AUAR batteries; (b) Hydrophone used in AUAR & mini- AUAR.

All of the AUARs and mini-AUARs use cylindrical hydrophones (model # GI-50 (ГИ-50)) (Figure 2.2(b)) with integrated pre-amplifiers designed specifically for use with the AUARs. Figure 2.2(a) shows the parallel charging of three AUAR batteries on the *Akademik Oparin.*

In order to optimize the dynamic range of the 16 bit ADC the signal amplitudes should be approximately equal across the entire frequency range. However, ambient noise generally has an amplitude maximum at low frequencies and drops off with higher frequencies. The ADC does not always have the dynamic range required to record ambient and anthropogenic noise at frequencies from 1 Hz to 15 kHz. Therefore, for all hydrophones, low-frequency amplitude correction is effected in the hydrophone preamplifier. These amplitude corrections ensure a consistent signal level across the entire frequency band for the analog channel of the AUARs with these hydrophones. An inverse correction is applied during spectral estimation.

In 2006, the resolution of the system timer in the QNX operating system was increased and periodic software corrections of the hardware clock were made to reduce the clock drift to less than seven seconds in a 52 day AUAR deployment. A tone was used to confirm that the AUAR computer was operating correctly prior to deployment. Prior to deployment of an AUAR a standard test signal was recorded; this signal is used to verify the AUAR gain and any other scaling factors.

Figure 2.3 shows the deployment configuration of the two types of AUAR and how the AUAR and its hydrophone are anchored when deployed. Practical experience has shown that at shallow deployment depths (10-30 m), movement of any surface buoy due to wave action can be mechanically conducted down the rope or cable to the hydrophone, where this mechanical movement can be recorded as acoustic noise. Therefore the mini-AUAR surface buoys (Figure 2.3(b)) are deployed so as to reduce this noise by isolating the hydrophone from the surface buoy with an anchor, thus reducing the mechanical coupling between the surface buoy and the hydrophone. The hydrophone is also deployed 15 m from the AUAR to prevent distortion of the acoustic field by scattering or masking by the AUAR container at high frequencies. The hydrophone is deployed inside a pyramid shaped metal frame to which it is attached by rubber straps, isolating it to the best extent possible from the sea floor. In 2010, acoustic releases were used in all AUAR deployments (Figure 2.4). Using acoustic releases (Figure 2.3(a)) virtually eliminates the possibility of unauthorized retrieval of the AUAR and ‘isolates’ the hydrophone as much as possible from surface waves.

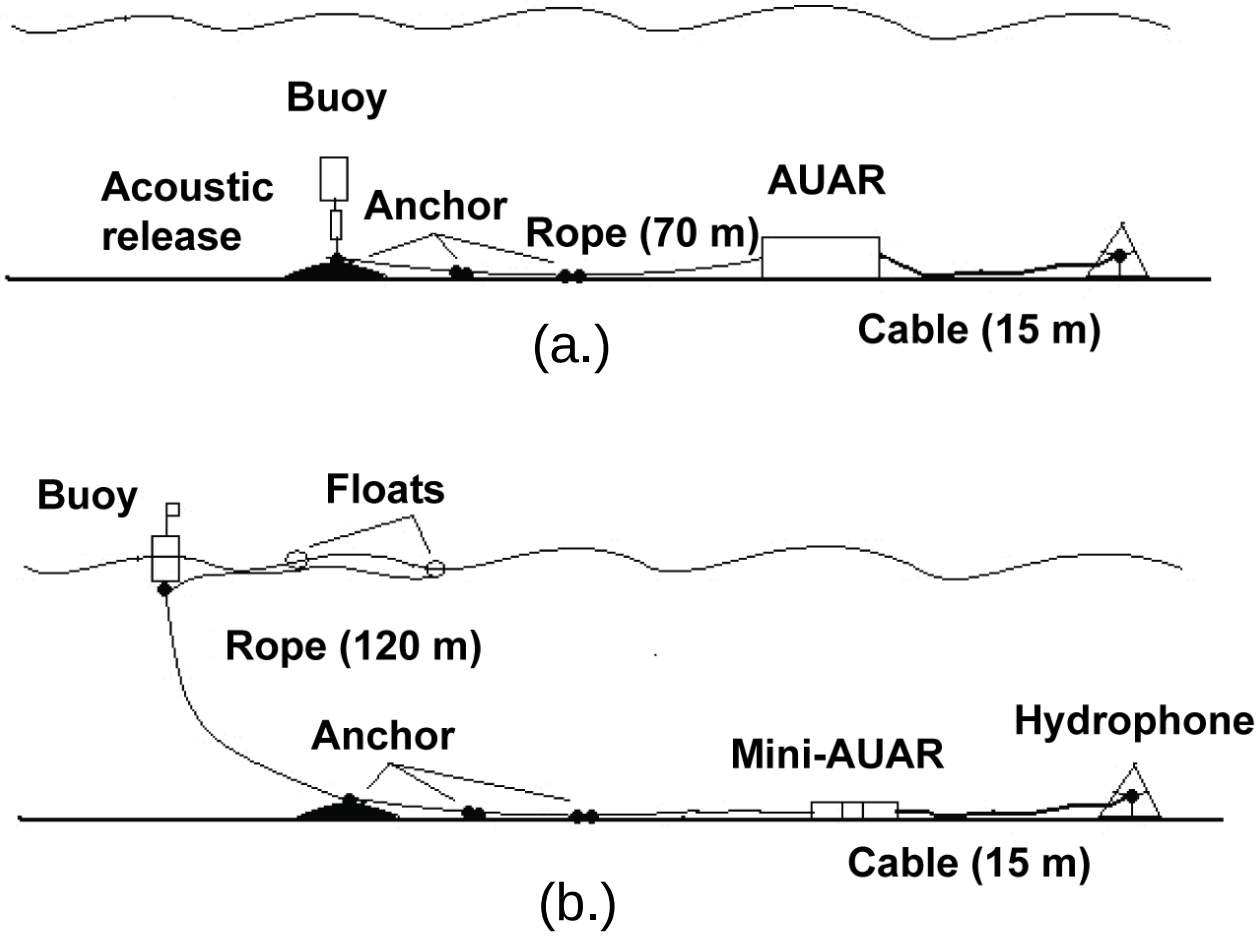

Figure 2.3 – Deployment schematics for (a) AUAR; (b) Mini-AUAR.

The AUARs and mini-AUARs employed during the 2010 field season utilized GI-50 hydrophones. The frequency response of these hydrophones is shown in Figure 2.5. All of these hydrophones have a low-frequency amplitude correction accomplished by the hydrophone preamplifier. This correction is in addition to the low-frequency gain correction in the AUAR analog channel [Borisov et. al. 2006]. Calibration certificates for all the hydrophones used in the 2010 expedition are listed in Appendix B and available in a file on the DVD available with the report.

To compute TL from acoustic measurements made by different AUARs, and to compare acoustic data over time, the data has to be calibrated to an absolute pressure standard. The hydrophones were manufactured with nominal sensitivities and the gains were set in the field.

Field cross-calibrations confirmed the absolute calibration of the data. Further details of the AUARs used in 2010, their location, deployment depth and recording settings can be found in Table 1.2. A detailed description of the testing of the recording equipment is given in [Borisov et al., 2007].

Figure 2.4 – Acoustic release and buoy.

2.1.1 AUAR instrument test analysis

In order to ensure that all of the AUARs adhered to the design specifications, and that the AUARs recorded accurate absolute acoustic measurements, a set of instrument tests was created (internal noise, dynamic range and frequency response). These tests were designed to ensure that all the AUARs were operating within specifications and to generate an instrument response filter for the analog component of each AUAR.

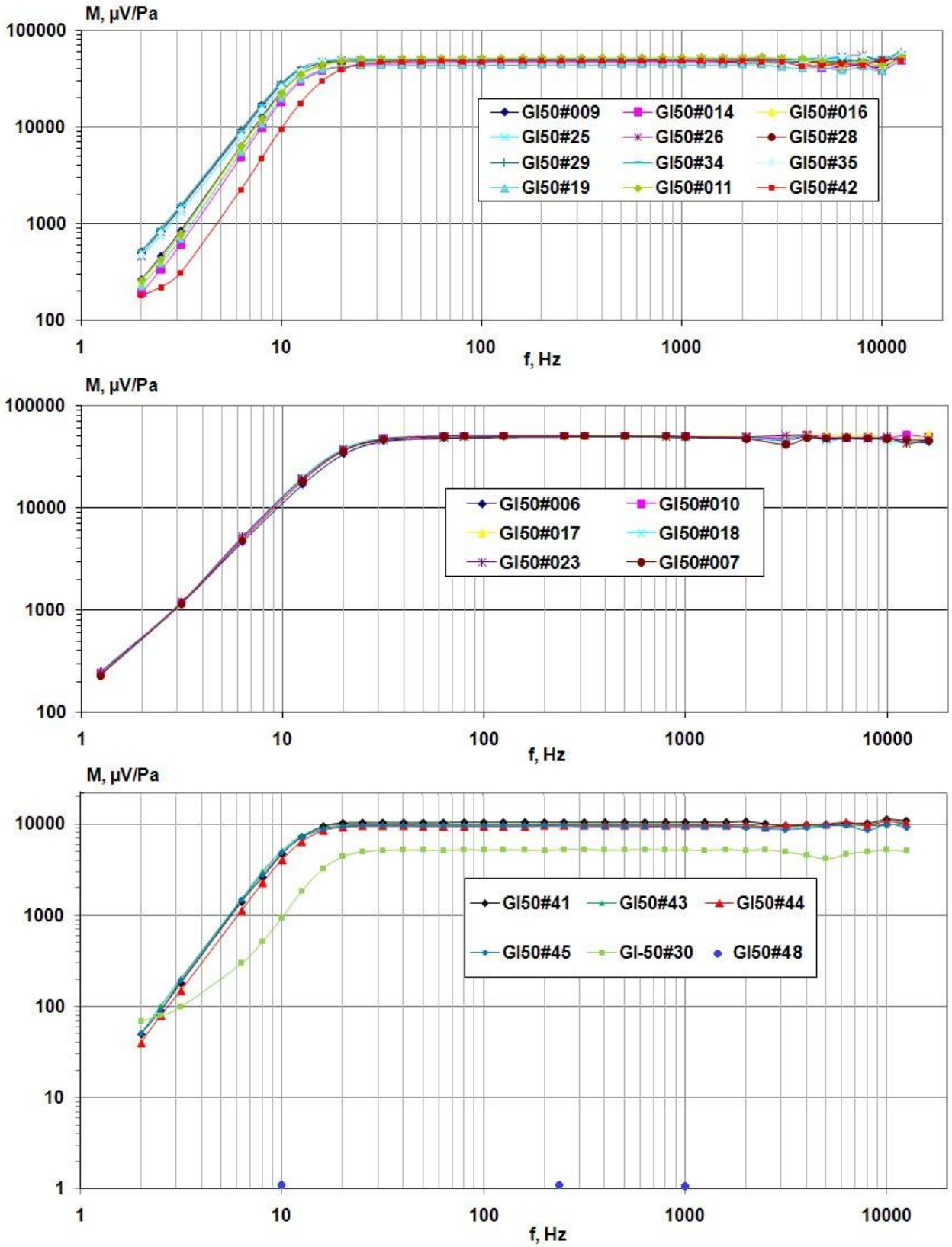

Figure 2.5 - Spectral characteristics of the Cylindrical (GI-50) hydrophones used during the 2010 field season.

Estimates of the AUAR analog instrument response, measured in the laboratory prior to the field season *K(f)* and the hydrophone sensitivity *M(f)* was used to generate an inverse filter; this filter was subsequently applied to the analog voltage measurements to back out the system instrument response and generate absolute acoustic measurements. These frequency dependent responses correct the acoustic data over the range from 2 Hz - 15 kHz.

In 2010, measurements of the internal noise, dynamic range and analog channel system filter response of each AUAR were made using the procedure described by Borisov [Borisov et.al. 2007]. The following results quantitatively characterize the performance of the AUARs used during the 2010 field season.

2.1.2 AUAR internal noise

The AUAR internal noise was measured using a dummy GI-50 equivalent hydrophone constructed in 2005. The preamplifier electronics in the shielded housing of the equivalent hydrophone is identical to that of the corresponding hydrophone except that a ceramic capacitor with the same capacitance as the hydrophone ceramics is connected to its input. The internal noise measurements were performed using the procedure approved in 2006 and described in Borisov [Borisov et.al. 2007]. Figure 2.6 displays a spectral analysis of the results, showing the internal noise of the AUAR analog channels with a GI-50 hydrophone over the frequency ranges 0-15 kHz (top) and 0-350 Hz (bottom)[24].

2.1.3 AUAR dynamic range

Figure 2.7 displays spectra of the tonal signals recorded by an AUAR during the dynamic range measurements, with the gain factor set to its maximum value of 38. When the sound pressure level is close to the maximum input acoustic pressure level, the dynamic range is limited by non-linear harmonic distortion and is 60 dB (Figure 2.7 – Blue curve). If the input signal level is decreased by 10 dB (Figure 2.7 – Green curve), the dynamic range of the AUAR increases to 75 dB and is limited by the second and fourth harmonics. The red curve on Figure 2.7 shows that the internal instrument noise level of the AUAR recording channel with an equivalent GI-50 is approximately 27 dB re 1 $\mu Pa^2/Hz$ in the frequency band from 50 Hz to 15 kHz, increasing to a

[24] The results were not corrected for the amplitude-frequency response of the analog channel.

maximum of 35 dB re 1 $\mu Pa^2/Hz$ at a frequency between 12-30 Hz. Since the instrument noise is below the harmonic distortion for most of the recorded frequency range, harmonic distortion limits the dynamic range of the AUAR.

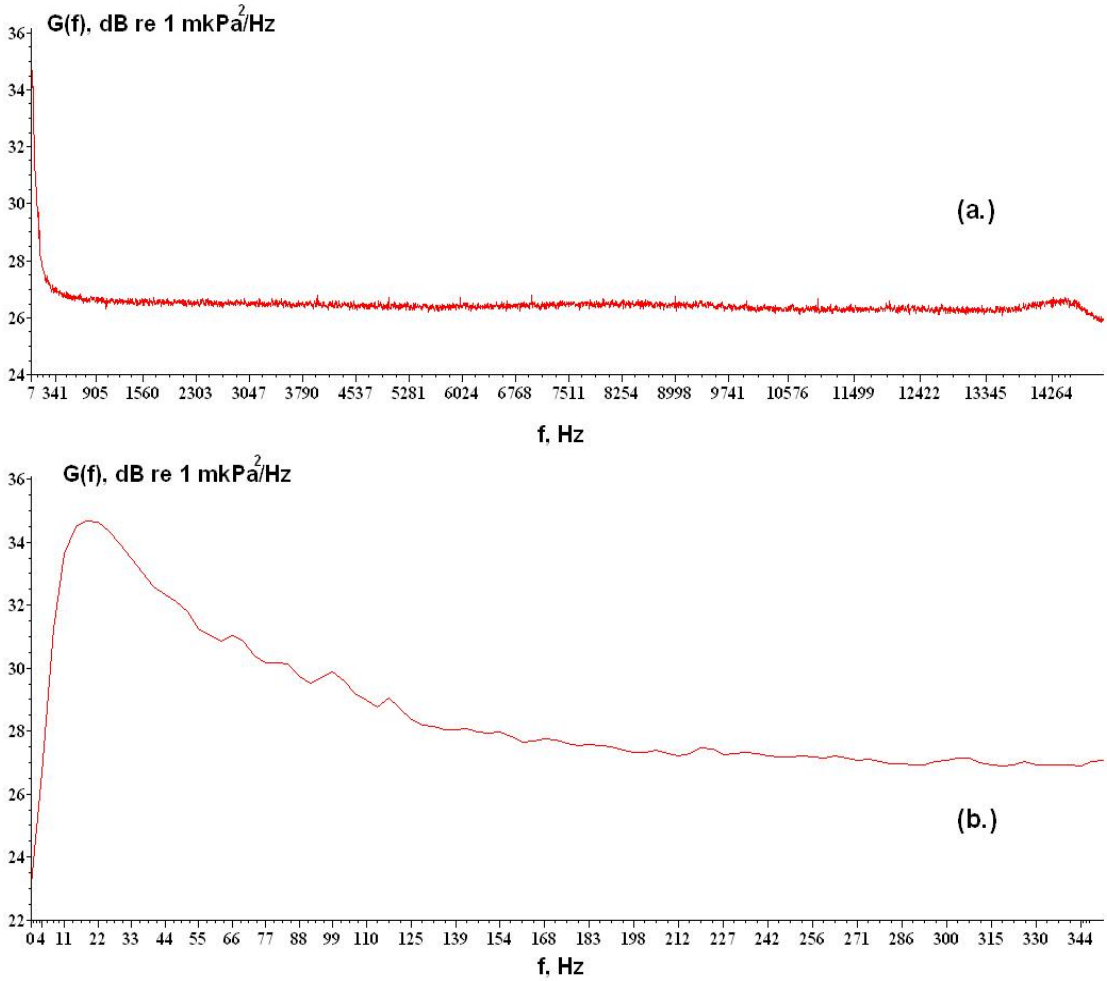

Figure 2.6 - Spectra showing the internal noise of the AUAR recording system: (a) 0-15 kHz and (b) 0-350 Hz.

2.1.4 *Analog channel system filter response of the AUAR*

The filter response of each AUAR analog channel was measured under laboratory conditions using a broadband white noise signal (*K(f)*), the results are used to estimate an analog instrument filter response for each AUAR, normalized to the gain at 1 kHz (Figures 2.8 and 2.9). The measurements were made for two scaling factors: 1 and 8. Figure 2.8 shows that *K(f)* decreases with an increase in the gain factor at frequencies below 15 Hz, due to the presence of a 1μF separating capacitor at the output of the hydrophone preamplifier causing a corresponding decrease in the input resistance of the scale amplifier with an increase in gain.

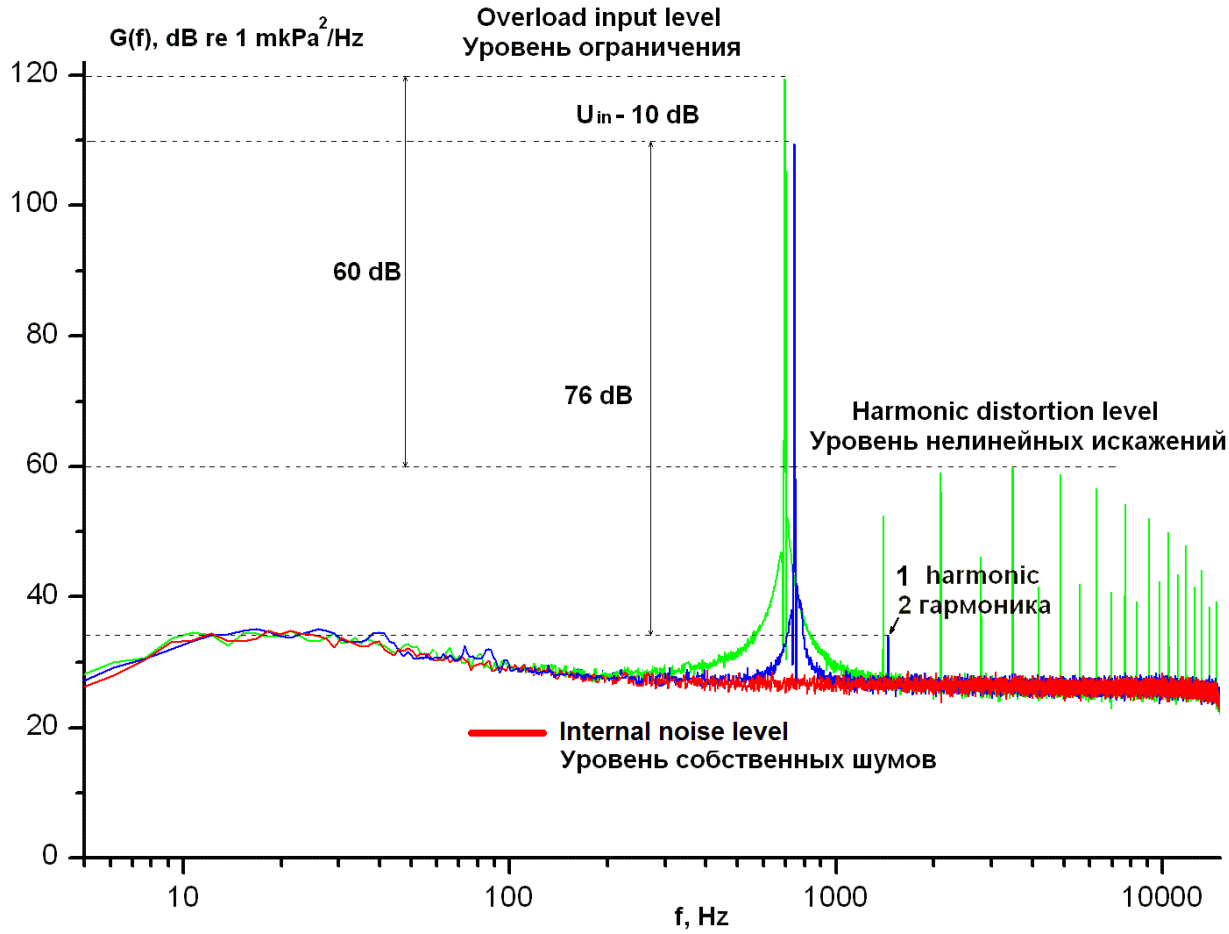

Figure 2.7 - Spectrum showing the internal noise and dynamic range of the AUAR recording system.

This filter response, together with the frequency response of the hydrophone (*M(f)*) used in a given AUAR (Figure 2.5), is used to construct a system filter response. This is used to correct the data as it is processed, reducing the analog voltage measurements to absolute acoustic pressure for the frequency band from 2 Hz to 15 kHz.

2.1.5 Results of the AUAR instrument tests

The unit to unit performance of all the AUARs was confirmed by regular testing. All the AUARs were subject to the tests listed in Borisov [Borisov et.al. 2007]; Table 2.1 gives the individual test results for all eighteen AUARs and six mini-AUARs performed in the laboratory. All AUARs performed within specifications.

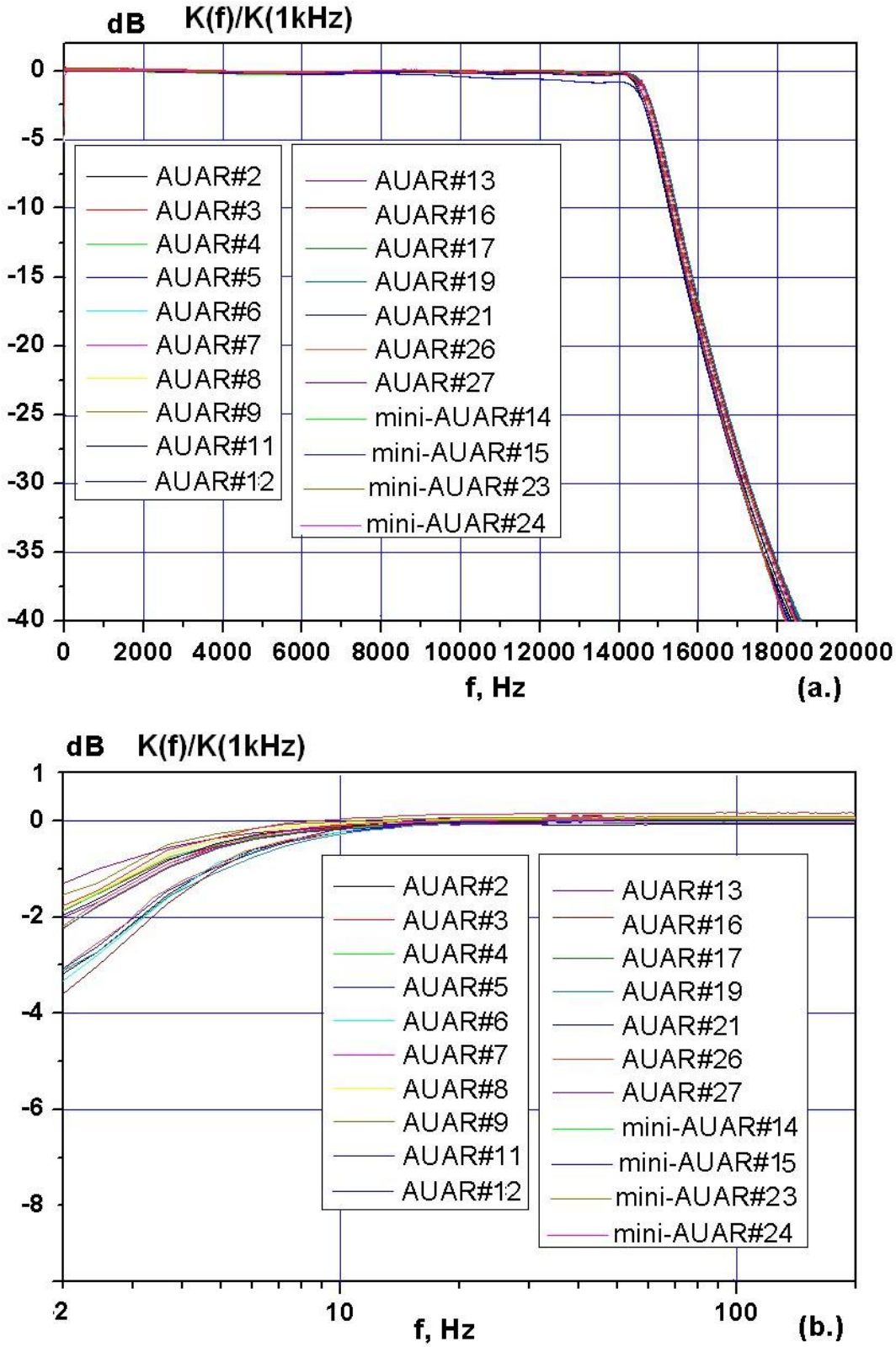

Figure 2.8 - Amplitude-frequency characteristics of an AUAR analog channel normalized to a gain K=1 at 1 kHz for AUARs and mini-AUARs used during the 2010 field season: AUAR analog frequency response (a) 2 Hz to 20 kHz; (b) 2 to 120 Hz.

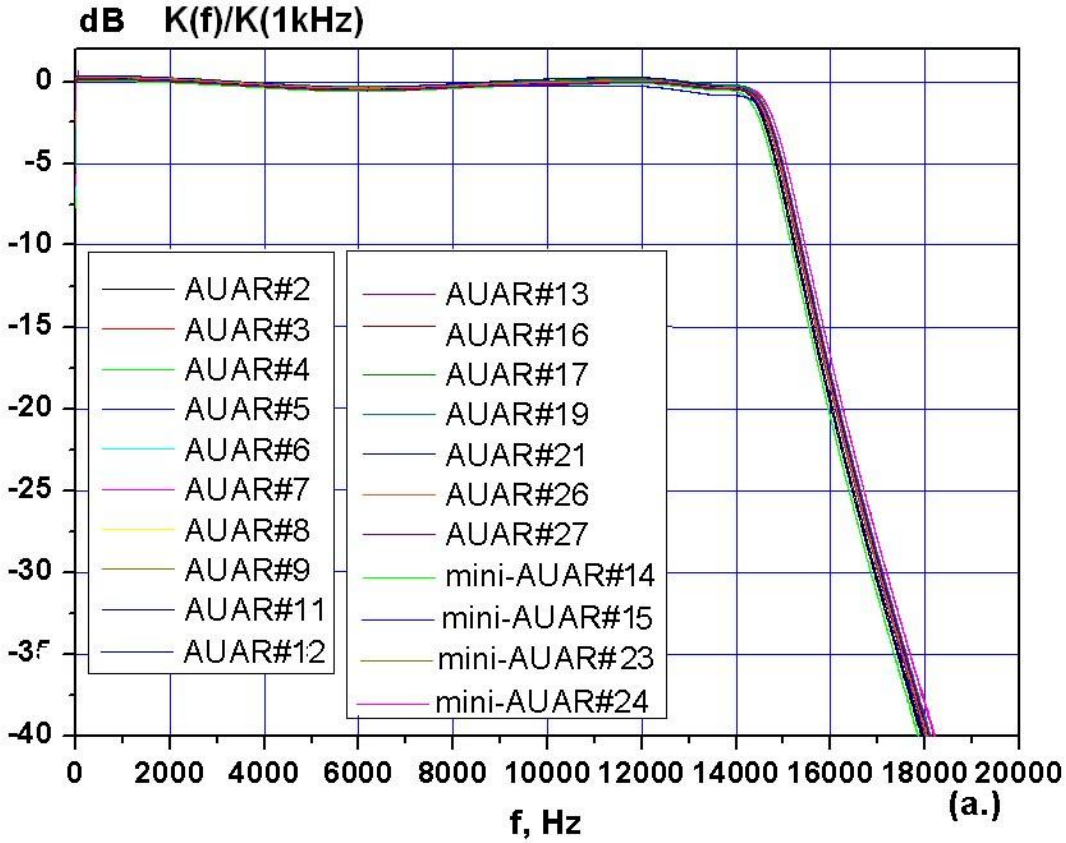

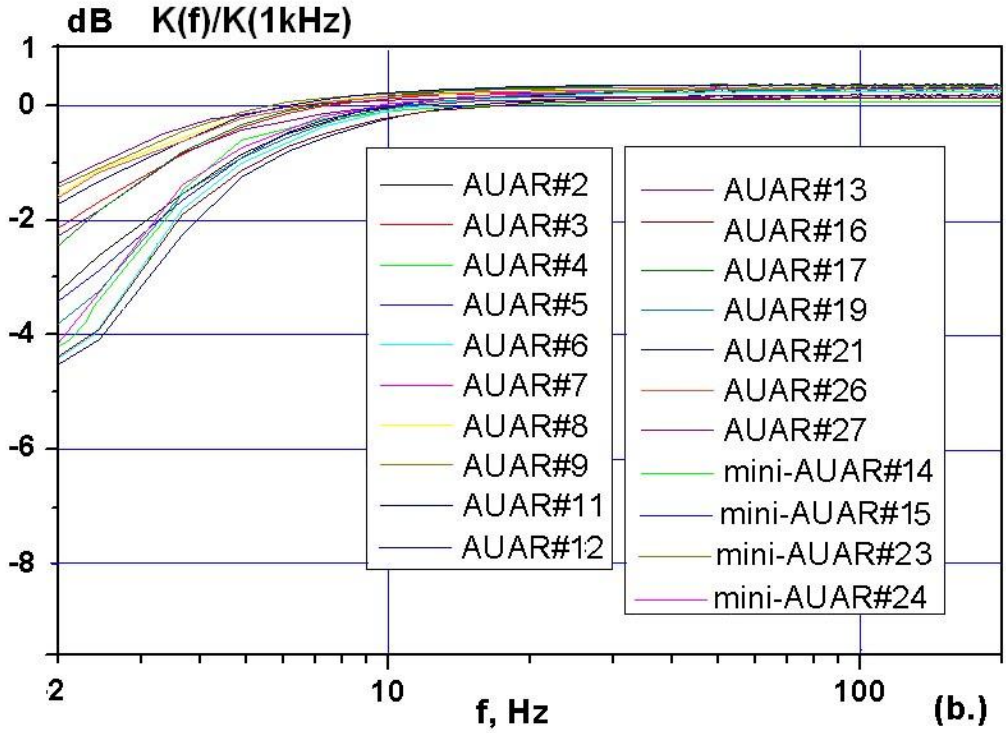

Figure 2) a gain K=1 at 1 kHz for AUARs and mini-AUARs used during the 2010 field season: AUAR analog frequency response (a) 2 Hz to 20 kHz; (b) 2 to 120 Hz.

Table 2.1 – Performance of AUARs on the instrument tests.

AUAR serial number										
02	**03**	**04**	**05**	**06**	**07**	**08**	**09**	**11**	**12**	**13**
Internal noise (dB re 1 μPa²/Hz) *(5-200 Hz)*										
38.1	38.4	40.0	36.5	41.6	40.5	36.0	35.9	35.5	36.6	23.7
Internal noise (dB re 1 μPa²/Hz) *(200 Hz - 15 kHz)*										
26.7	28.0	37.3	26.5	31.1	29.1	27.1	26.3	26.5	27.7	14.5
Dynamic range , dB										
76	76	77	76	75	75	76	75	77	76	78
AUAR serial number										
14	**15**	**16**	**17**	**18**	**19**	**23**	**24**	**26**	**27**	
Internal noise (dB re 1 μPa²/Hz) *(5-200 Hz)*										
41.0	40.0	37.6	35.7	39.0	24.0	40.5	38.0	44.0	38.8	
Internal noise (dB re 1 μPa²/Hz) *(200 Hz - 15 kHz)*										
29.6	30.0	26.4	27.0	32.1	13.6	32.5	33.5	27.6	36.8	
Dynamic range , dB										
76	76	76	75,8	76	77	76	77	75	76	

2.2 Low Frequency, High Frequency and autonomous transducers

A low frequency (LF) resonant electromagnetic transducer (Figure 2.10) and high frequency (HF) piezoelectric broadband transducer (Figure 2.11) deployed from the *Akademik Oparin* were used for sound propagation and TL studies at frequencies from 15 Hz -15 kHz. The acoustic level of signals generated by these transducers was monitored using two calibrated hydrophones and recorded on the *Akademik Oparin*[25].

Field tests have shown that when the LF resonance transducer was deployed at a depth of 10 m from the anchored *Akademik Oparin* in water 25 m deep, the level of the 27 Hz acoustic signal generated by the transducer was ~180 dB re 1 μPa^2/Hz at a distance of 1 m from the transducer.

The 2010 expedition used a HF broadband piezoelectric (ceramic) transducer, this transducer is

[25] While the transducers were operating the acoustic signal levels were measured using a calibrated hydrophone located 1 m away from the transducer.

cylindrical[26] and consists of eight piezoelectric rings connected in parallel coated with a composite material and sealed at the ends with metal flanges (Figure 2.11).

Figure 2.10 - Low frequency resonance transducer and calibrated monitor hydrophone.

To prevent possible damage to the transducer from impacts against the side of the vessel while being deployed and recovered, a reinforced cage was manufactured around the transducer. A calibrated reference hydrophone was suspended by rubber straps from a frame attached to the cage at a distance 1 m from the surface of the transducer. This attachment method controls the

[26] Dimensions are diameter 60 cm, height 150 cm, weight ~100 kg in air, and ~15 kg in water.

position of the reference hydrophone relative to the transducer in currents and as the ship rolls, significantly improving the accuracy of reference measurements of the source level of the transducer.

Figure 2.11 - High frequency broadband piezoelectric transducer and calibrated monitor hydrophone mounted on a frame to the right of the transducer.

A Eurosound PWR-2000 power amplifier was used to drive the broadband transducer. The amplifier has an output voltage of 300 V, and a maximum power output of 5 kW. Tonal and swept FM signals were generated by an Istek GFG-3015 signal generator. This signal generator has an external control function through a standard RS-232 interface, allowing its operation to be programmed from a computer. This enabled the concurrent operation, of both the LF and HF transducers, and synchronous recording of signals from their integrated reference hydrophones through an integrated shipboard system (Figures 2.11 and 2.12). The program can automatically control the operation of the generator without an operator, changing the frequency, amplitude and signal type according to a pre-programmed schedule.

Simultaneous operation of the two transducers when deployed from two different cranes and automation of the operation of the signal generator and power amplifier significantly reduced the time taken on a source location when acquiring acoustic TL profiles.

Figure 2.12 – Equipment for acoustic signal generation and reference signal recording.

2.3 Hydrologic and bathymetric measurements

Calibration with empirical TL data is used to enhance numerical modeling along the TL profiles. To calibrate the model along an acoustic profile, the bathymetry and sound velocity of the water layer along the profile must be known. The hydrological characteristics (sound velocity, temperature and salinity), however, are constantly changing. Thus, to complement the TL measurements, the bathymetric profile was obtained using the ship's echo sounder and hydrological data were acquired using a hydrological sonde (Figure 2.13).

The sonde is also used to measure the hydrology in the two gray whale feeding areas on the NE Sakhalin shelf; annual hydrological observations are conducted on planned transects using this profiler. These measurements are used to assess the temporal variation in the hydrological

characteristics of the feeding areas, and the effects of meteorological conditions, tidal currents, coastal upwelling, and the water inflow from the Amur estuary and Piltun Bay.

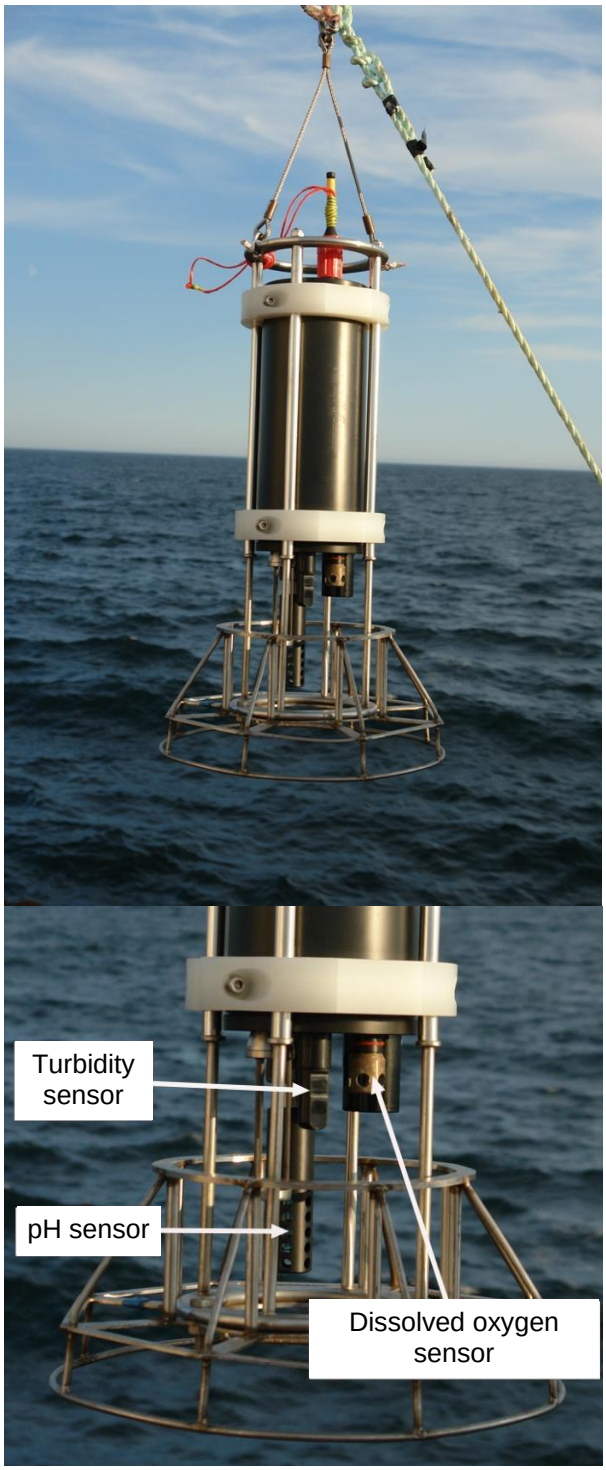

Figure 2.13 - MIDAS CTD+500 profiler and sensors.

A MIDAS CTD+500 multi-parameter profiler, manufactured by Valeport Limited, England, was the hydrological sonde used during the 2010 field season. The profiler can measure hydrological

parameters such as temperature, conductivity, sound velocity, and pressure. It is also equipped with dissolved oxygen, turbidity and pH sensors, see Table 2.2 for the profiler specifications. Appendix A gives the calibration certificates for the sonde sensors. The DataLog-Pro and DataLog-400 software included with the profiler is used to adjust measurement modes, transfer data to a computer, visualize data, and calculate salinity and relative density from measured parameters.

Table 2.2 – Valeport MIDAS CTD+500 specifications

Sensor	Type	Range	Accuracy	Resolution
Conductivity	Pressure balanced inductive coils	0,1-80 mS/cm	±0.01 mS/cm	0.004 mS/cm
Sound velocity	Travel time	1400-1600 m/sec	±0.005 m/sec	0.001 m/sec
Temperature	Fast response PRT	-5°C to +35°C	± 0.01°C	0.002°C
Pressure	Strain gauge	200 bar	± 0.1 % of full range	± 0.005 % of full range
Turbidity	Seapoint	0–2000 FTU (max)	± <2 % up to 750 FTU	0.005 % of full range
Dissolved oxygen	Oxyguard	0–200 %	± 1 % of readings	0.005 % of saturation
pH	Pressure-balanced electrode	2–12	± 0.1	0.001

The MIDAS CTD+500 multi-parameter profiler operates in three selectable modes: continuous, burst and profiling. Continuous recording requires a wired connection.

For these studies the sonde was used in profile mode, which allows independent operation and provides vertical profiles for the required parameters at 8 Hz base sampling rate. In this mode the profiler remains active and operates continuously on battery power until a selected parameter, e.g., conductivity, reaches a set value. The profiler must remain activated and operates continuously, consuming power. Vertical profiling requires setting two pressure parameters: initial recording depth and the depth interval between readings. When the profiler operates in this mode it compares the measured pressure with the next preset reading along the profile as the sonde is lowered through the water column. If the pressure is equal to the preset value the measured readings are recorded, otherwise they are ignored.

All parameters are measured at precisely the same instant and recorded on the internal 16 MB flash drive (which could be upgraded to 32 MB). Once the measurements are complete the data

can be transferred to a computer via a RS-232 port. The profiler is independently powered by eight 1.5 V batteries.

2.3.1 Recording and archival of navigational and bathymetric information

NMEA standard format messages from the depth profiler[27] and GPS receiver[28] on the *Academik Oparin* were input into a computer. Signals from the GPS were relayed to the computer through a COM port, and a COM to USB converter and COM port emulator software was used to input signals from the depth sounder. The computer was running the ECS dKart Navigator[29] that can process and store data in NMEA format, and computes and plots the vessel's course (Figure 2.14). Navigation information (time, coordinates, depth, speed, and heading (from compass)) was recorded every 10 seconds. The depth below keel estimates were corrected for the vessel draft (approximately 4.5 m). These data were periodically copied to another computer, where they were archived and corrections were applied. Inaccurate or invalid values from the depth sounder and GPS were deleted and data corresponding to times when the vessel was at anchor were also deleted. Depth sounder values were tidally adjusted using POI's Bathymet program. The tidal height was estimated from comprehensive observations in the area of Piltun Bay. This theoretical estimate was subtracted from the measured depth (plus the vessel draft) to give a tide-corrected depth.

In standard practice (for marine navigation), tides are calculated relative to the lowest low water low tide (chart datum), and chart depth is displayed relative to this datum. Common practice is to tide correct the depths by adding the tidal values (from tide tables) to the chart depths. Since the tidal corrections are identical to those from tide tables the correction procedure can be considered as the adjustment of the bathymetry data to the chart datum using generally accepted navigational practice. It is therefore possible to tide-correct the bathymetric measurements by subtracting the theoretical tidal values from real measurements. This correction was applied to all bathymetry data acquired on expeditions between 2004 and 2010. The archive contains both the original and corrected data. In addition, the bathymetric data acquired using a portable depth sounder operated from a Zodiac operating at depths less than 10 m were also added to the archive.

---

[27] Wesmar, operating frequency 20 kHz, beam width 7°.
[28] Furuno SPR-1400.
[29] dKart Navigator (version 6.32, SP10) is a professional navigation solution for communication with navigation equipment such

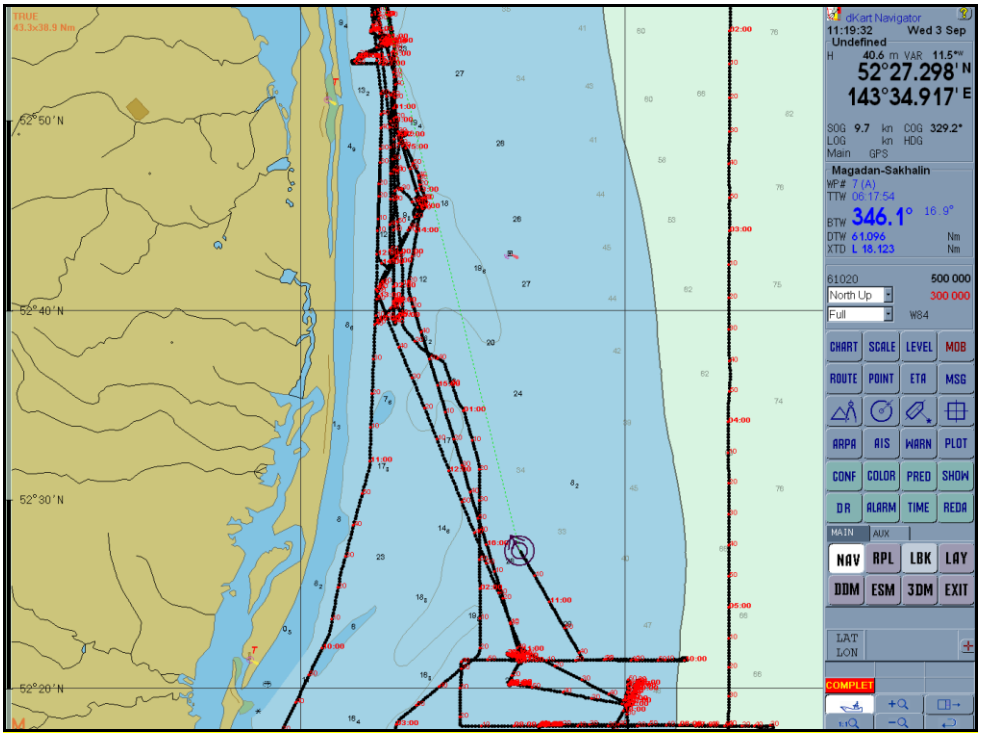

Figure 2.14 – Computer display showing the navigation data for the vessel.

Bathymetry data also has errors due to surface waves and other stochastic effects. The magnitude of surface waves can be comparable to those of tides, but surface waves fluctuate much more rapidly. This effect can therefore be compensated for by averaging inside a spatial grid (i.e. all the data is divided into spatial groups and averaged). This excludes the effects of surface waves from the data as every cell of the grid contains data from different times and also compensates the bathymetry data for wind driven currents. This procedure will be applied to bathymetric data acquired in the field. Further data processing and visualization will be performed using MATLAB. If uncorrected bathymetry is required for a specified time a back correction can be applied (i.e. theoretical tidal value can be added to the corrected data).

2.4 Upgraded AUAR and Mini-AUAR Power Supplies

The use of 115 Ah sealed gel rechargeable batteries in AUARs over many years has shown that these batteries have a high probability of losing charge over time. Nine M200 automatic chargers manufactured by CTEK SWEDEN AB, Sweden (Figure 2.15) were used to charge the AUAR batteries during the 2010 field season

as GPS, sonar, AIS, radar, compass, log etc.

Figure 2.15 – Charging AUAR batteries with CTEK M200 chargers.

The chargers are designed to operate on the open deck of a marine vessel in any weather. These chargers are characterized by a multi-stage charging algorithm that includes pulse removal of charge memory and continuous monitoring of the battery during charging. The chargers are also equipped with temperature sensors that automatically adjust charging voltage when the battery temperature differs from the nominal value of +25°C.

AUAR batteries were checked after charging using a Kulon-12fu lead-acid battery capacity indicator (Figure 2.16). The Kulon-12fu indicator allows battery wear to be estimated based on residual capacity.

The upgrade to the AUAR disk storage architecture allows 52 days of continuous acoustic recording; however, the re-chargeable battery capacity can only support 27–29 days of operation. In order to improve the operational longevity the team members developed and successfully tested non-rechargeable battery pack modules in 2010 (Figure 2.17).

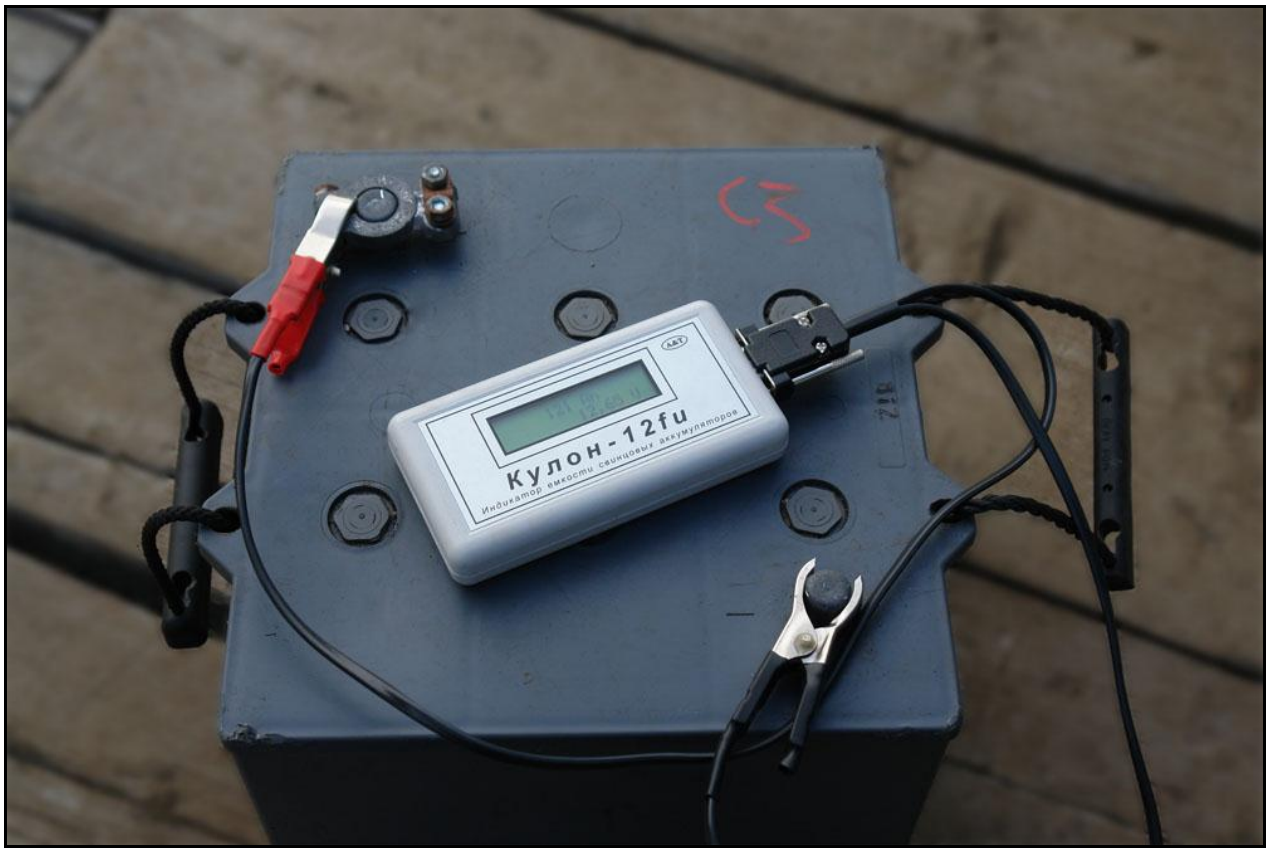

Figure 2.16 – Using a Kulon-12fu indicator to check battery capacity.

The battery pack module is a cylinder consisting of two metal plates connected by seven 10 mm poles. A 33 mm plastic tube runs through the centerline of the module. The top and bottom plates are covered by round fiberglass boards with conical spring terminals. The springs were manufactured from heat-treated stainless steel by POI and are coated to ensure stable contact with the battery terminals. A column of batteries is packed between the springs. The centerline tube and poles are used as guides for battery installation.

The field team used Duracell NM1200 type D batteries with an initial voltage of 1.65 V and a manufacturers rated capacity of 15 Ah. The AUAR battery pack modules are 112 mm in diameter, 330 mm in height, and contain 40 individual batteries. Each battery pack module includes 4 packs of 10 batteries connected in series. These packs are connected in parallel with galvanic protection achieved using Schottky diodes with a low forward voltage drop, resulting in a single battery pack module with an initial closed-circuit voltage of 16 V and a capacity of 60 Ah. All packs can also be connected in series to form a 60 V and 15 Ah battery pack module.

Figure 2.17 – General purpose power supply modules, containing *Duracell D* batteries for the AUAR and mini-AUAR units.

A standard AUAR container, which is 330 mm in diameter, can accommodate up to 16 battery pack modules. An AUAR with 10 battery pack modules (400 individual batteries) installed at the Piltun monitoring station operated for 47 days. After the AUAR was recovered by the *Akademik Oparin* and all data were retrieved, the AUAR electronics were again programmed for a standard

data gathering mode and turned on with the same set of batteries to determine the full uninterrupted operating period. The AUAR operated for another 9 days on the *Akademik Oparin*. An AUAR with 10 battery pack modules is therefore expected to have an unattended operating time of 56 days.

Battery pack modules for mini-AUARs have the same design, but a different height (Figure 2.17). They include 48 individual batteries, and have an output voltage of 19.1 V. A total of 6 modules were manufactured. After the end of experiments using the mini-AUARs they were also tested for the full uninterrupted operating time. A mini-AUAR with a battery pack module is expected to have an unattended operating time of 160 hours (6.5 days).

3 Ambient and anthropogenic acoustic noise on the NE Sakhalin shelf

This section analyzes the ambient noise measurements recorded on the NE Sakhalin shelf in 2010 and discusses the temporal and spectral variation in ambient noise with meteorological conditions and sea state. The ambient sound levels are also compared with those generated by anthropogenic activities. In 2010, as in the previous years, acoustic data were recorded using AUARs, and ambient noise data were acquired at monitoring stations across the area (Table 1.1 and Figure 1.5).

3.1 Acoustic noise recorded in the North and the South of the study area

Previous reports have discussed the variation in ambient noise due to wind, surface waves and rain. For example, the broadband noise level near Chayvo rose by 12 dB when the sea state increased from 1 (calm) to 4 (moderate) [Borisov et. al. 2003]. A rainstorm with strong wind squalls pushed the ambient noise level an additional 16-18 dB higher. For frequencies above 2.5 kHz the spectral level of ambient noise recorded during a storm had a peak value of ~64 dB re 1 $\mu Pa^2/Hz$ (56 dB re 1 $\mu Pa^2/Hz$ for a storm without rain). Spectral analysis of the data acquired in 2003 showed that the sound field in the frequency band from 200-800 Hz generated by an approaching storm had the clear interference structure resulting from waveguide propagation on the shelf [Borisov et. al. 2004]. The data showed that noise produced by wind and surface waves is much lower for shallow water (10 m) than for areas outside the 20 m contour. The highest ambient sound level was recorded in the frequency band from 200-1000 Hz. The ambient noise in this frequency band had a peak value of 71 dB re 1 $\mu Pa^2/Hz$ during a storm and 46 dB re 1 $\mu Pa^2/Hz$ in calm weather (no rain).

Meteorological conditions in the summer and fall of 2010 were stable in contrast to 2009. Figure 3.1 shows a sonogram of acoustic data recorded in August-September 2010 at the Control monitoring station (reference station, 20 m depth - located significantly to the North of the Sakhalin-1 and Sakhalin-2 projects) and the Piltun monitoring station (also at 20 m depth - between the Molikpaq and PA-B platforms on the eastern margin of the Piltun feeding area).

Figure 3.1 shows that during the period from 6th August to 27th September, 2010, this area was hit by two powerful atmospheric cyclones, 10-15th August and 21st-22nd September, which

caused storm driven waves and swells. Wind gusts, rain and storm-induced surface waves caused broad-band acoustic noise up to 15 kHz, and orbital motion of the water particles; this caused flow noise at, and physical movement of the hydrophone. During these periods as can be seen on the sonogram of Figure 3.1 the power spectral density level for frequencies below 20 Hz exceeded 115 dB re 1 $\mu Pa^2/Hz$ and sound pressure levels as high as 140 dB re 1 $\mu Pa^2/Hz$ in the 10-100 Hz frequency range. Additionally, low-frequency (20-30 Hz) narrow band components are present in the spectra due to resonant vibrations of, for example, the hydrophone suspension. These noises are also well defined during tidal currents and can be used to isolate the time periods corresponding to the phases of strong tidal currents, cyclones and the large Sea-of-Okhotsk dead swell on the spectrogram (see sonogram *G(f,t)* of 17th August).

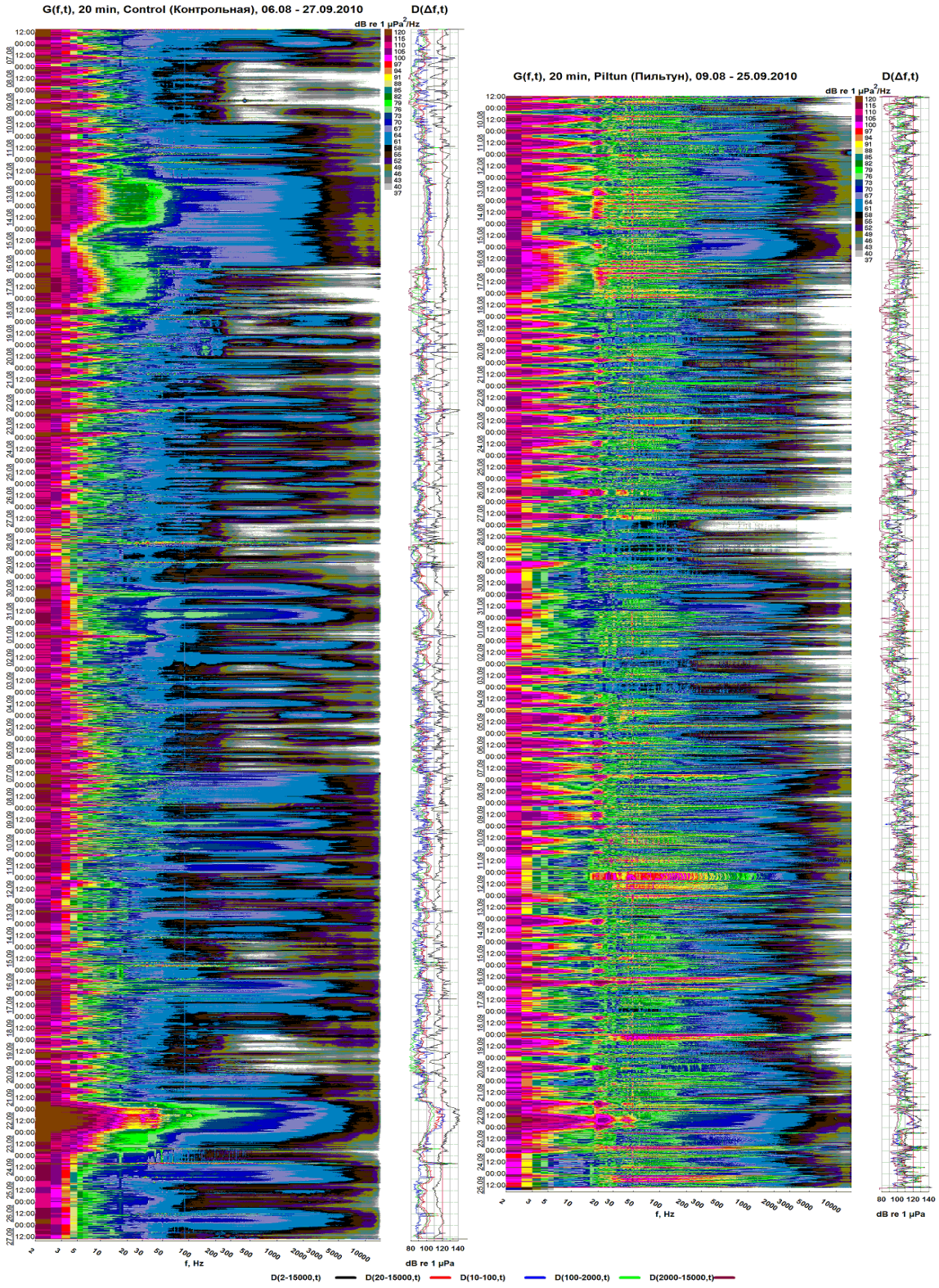

Figure 3.1 - Sonogram *G(f,t)* of acoustic data recorded at the Control (6th August to 27th September) and Piltun monitor stations (9th August to 27th September).

The sonograms *G(f,t)* shown in Figure 3.1 allow us to visualize and assess anthropogenic sound

levels over time at the Piltun monitoring station vs. the ambient noise measured at the Control station. It is likely that the 20-300 Hz acoustic noise recorded almost continuously at the Piltun station was generated by *Smit Sibu* the standby vessel for the Molikpaq and PA-B platforms, which was stationed between these platforms, across from the Piltun acoustic monitoring station.

Figure 3.2 gives the results of a statistical analysis of the data from these stations in August and September. These results show that even with simultaneous Sakhalin-5 seismic survey at the Lebedinskoye field, the 90% power spectral density percentile level at 15 Hz was no greater than 94 dB re 1 μPa^2 at the Control station, which is the most northerly acoustic monitoring station.

At the Piltun station, the 90% power spectral density percentile level at frequencies above 15 Hz is significantly larger with well defined peaks of 113 dB re 1 μPa^2 and 110 dB re 1 μPa^2 at 20 Hz and 50 Hz, respectively. These plots are characterized by a high in the 16-300 Hz frequency band, in contrast to the relative low at the same frequencies at the Control station. Figure 3.1 shows that strong anthropogenic noise is in fact observed at these frequencies.

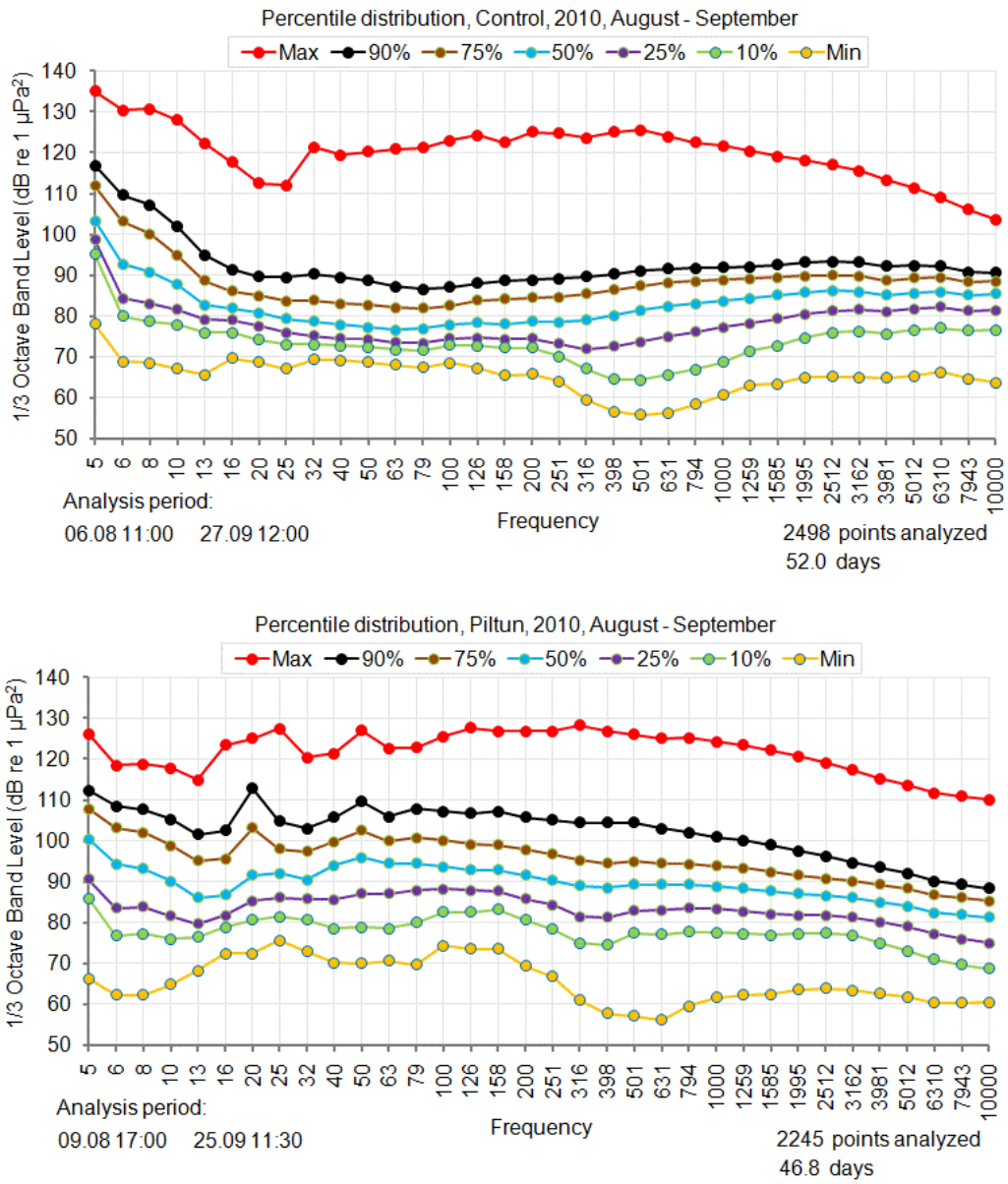

Figure 3.2 – Power spectral density percentile plots of sound pressure level of acoustic data recorded at the Control and Piltun monitor stations.

3.2 Measurements of sound generated by the Lebedinskoye seismic survey

Rosneft conducted a seismic survey over the Sakhalin-5 Lebedinskoye field. Figure 3.3 is a map showing the locations of acoustic stations A10, Odoptu-N-10, Odoptu-N-20, Odoptu-S-10, Odoptu-S-20, and Odoptu-PA-B for the joint Gray Whale monitoring program (which recorded the impulses from the survey in August and September), and sites G.1, G.2, and G.3 where POI used cabled digital acoustic stations to continuously monitor the seismic pulses emitted both onshore and offshore from August-November, 2010

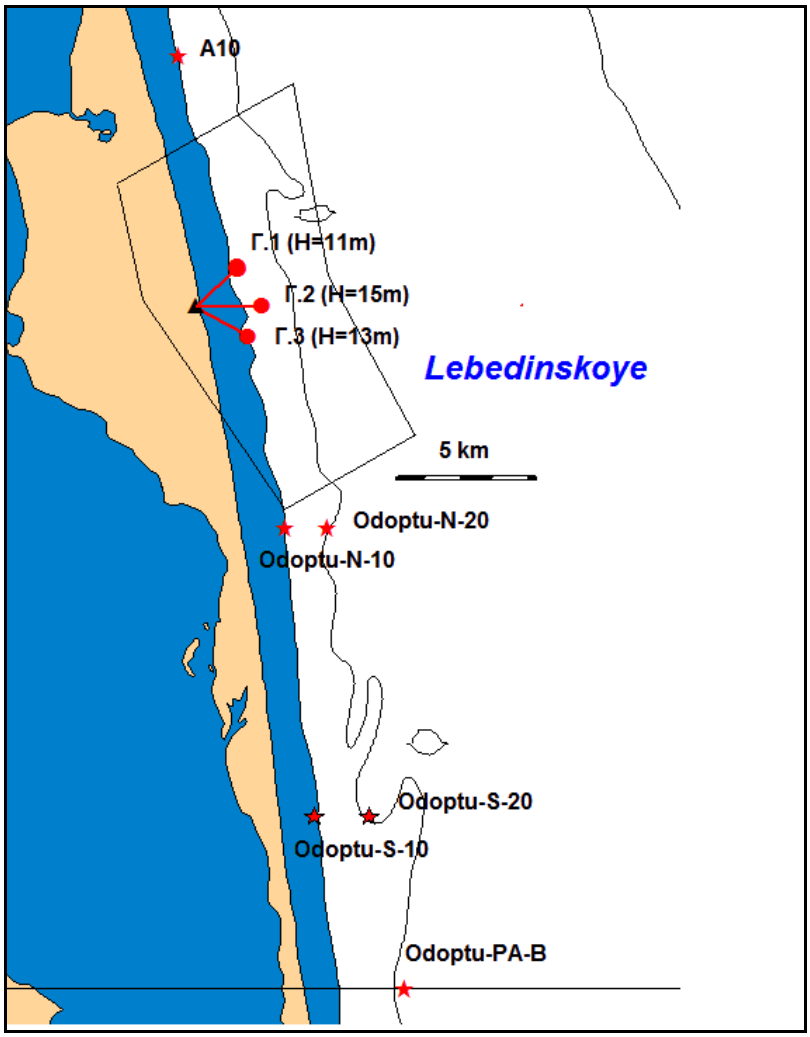

Figure 3.3 – Map showing the acoustic monitoring stations used during the summer-fall period under the joint Gray Whale monitoring program. Also shown are hydrophones deployed at the G.1, G.2, and G.3 stations in 2010 and connected to an onshore recording station by cables. These hydrophones recorded and monitored in real-time seismic pulses generated offshore and onshore during seismic operations at the Lebedinskoye field (see boundaries on the figure).

The upper panels of Figure 3.4 show examples of the acoustic pulses *p(t)*, measured at acoustic monitoring stations A10 and Odoptu-S-10 during the offshore seismic survey in the southern part of Lebedinskoye field (see Figure 3.3). This plot shows that the peak variations of *p(t)*, in the measured pulses reached 17 and 8 Pa, and the SPL_{rms} values were as high as 135 dB re 1 μPa and 130 dB re 1 μPa at stations A10 and Odoptu-S-10, respectively.

The peak *p(t)* values observed at monitoring stations Odoptu-N-10 and Odoptu-N-20 during the Lebedinskoye seismic survey exceeded 350 Pa, which is the maximum value that can be correctly measured by hydrophones with 10 mV/Pa sensitivity.

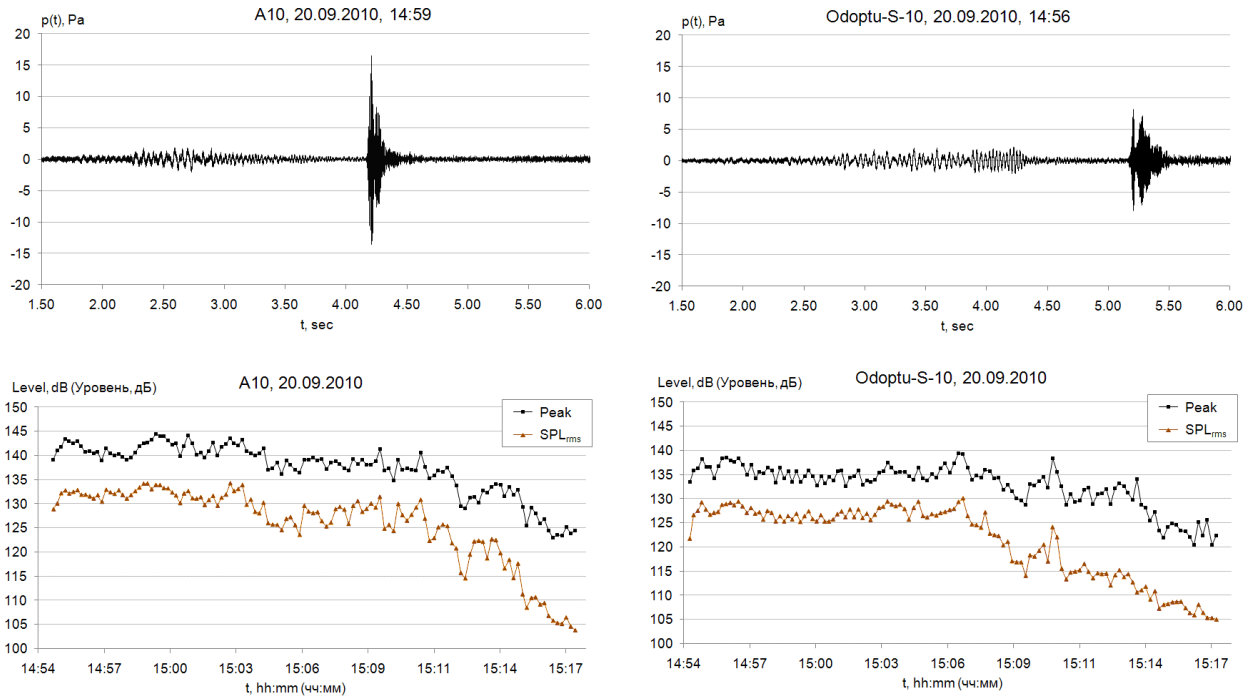

Figure 3.4 – Sample sound pressure traces *p(t)* (top panels), peak amplitudes, and *SPL_{rms}* levels (bottom panels) for acoustic pulses recorded at monitoring stations A10 and Odoptu-S-10 during offshore seismic operations in the southern part of the Lebedinskoye field.

Figure 3.5 presents a sonogram *G(f,t)* of acoustic data recorded simultaneously by AUARs deployed at acoustic monitoring stations A10, Odoptu-N-20 and Odoptu-S-20. It can be seen from Figure 3.5 that the survey began on 18th August in the southern part of the Lebedinskoye field. Figure 3.6 presents sonograms *G(f,t)* for acoustic noise measured at the Odoptu-N-10 acoustic monitoring station on the 10 m bathymetric contour.

3.3 Measurements of seismic sounds recorded in the Offshore Feeding Area

A Sakhalin-3 seismic survey was carried out near the offshore gray whale feeding area in August-September 2010. Figure 3.7 presents sonograms of acoustic signals measured in 2010 at three annual acoustic monitoring stations: Lunskoye, OFA and Orlan. It can be seen from this figure that between 15th August and 7th September the entire offshore feeding area was exposed to impulsive seismic signals. Figure 3.7 indicates that the Orlan monitoring station was located further from the seismic survey area than the other stations as the spectral.levels from seismic survey activity appear weaker at this station It can also be seen from this figure that by seismo-acoustic pulses in the 6-30 and 50-300 Hz frequency ranges most effectively propagated into the offshore feeding area; and the one-third octave power spectral density percentile plots of

Orlan data shown in Figure 3.8: . During the seismic survey (Figure 3.8(a)) the 50%, 75% and 90% percentile plots have well defined highs in these frequency ranges, which are lacking during periodswithout seismic activity (Figure 3.8(b)).

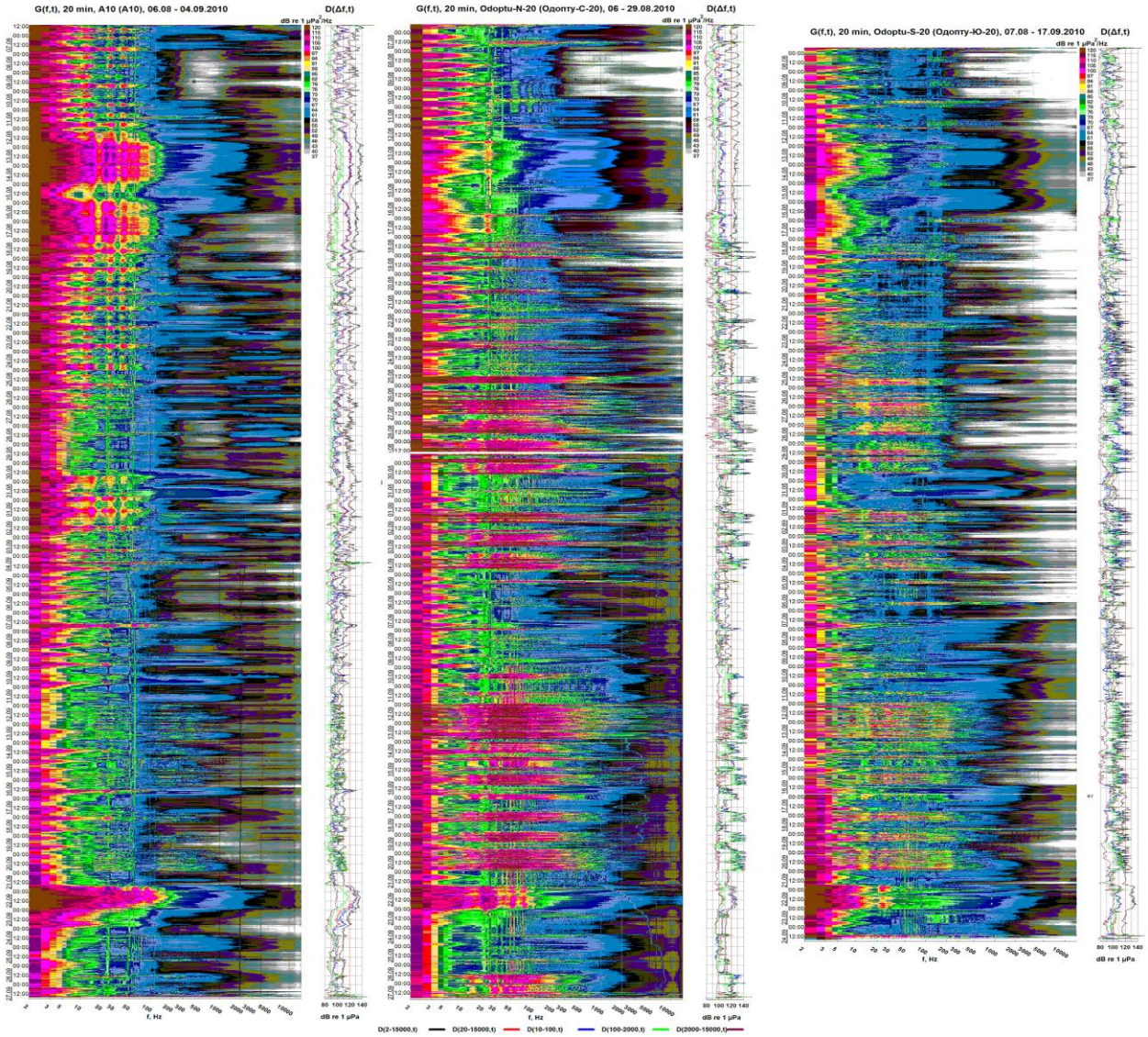

Figure 3.5 - Sonogram *G(f,t)* and plots of sound pressure level of acoustic data recorded at the A10, Odoptu-N-20 and Odoptu-S-20 monitor stations in 2010.

Figure 3.9 presents a sonogram *G(f,t)* of acoustic data recorded at the Arkutun-Dagi acoustic monitoring station. During the first AUAR deployment (1-26 August, 2010) the hydrophone had a sensitivity of 50 mV/Pa and the gain factor was 8; analysis of this deployment showed that the amplitude of the seismic impulses was limited by saturation of the system input. When the AUAR was re-deployed (26th August to 20th September, 2010), a 5 mV/Pa hydrophone was used with a gain factor of 1. Figure 3.10 illustrates an acoustic impulse with an amplitude *p(t)* of up to 370 Pa, as recorded with these settings.

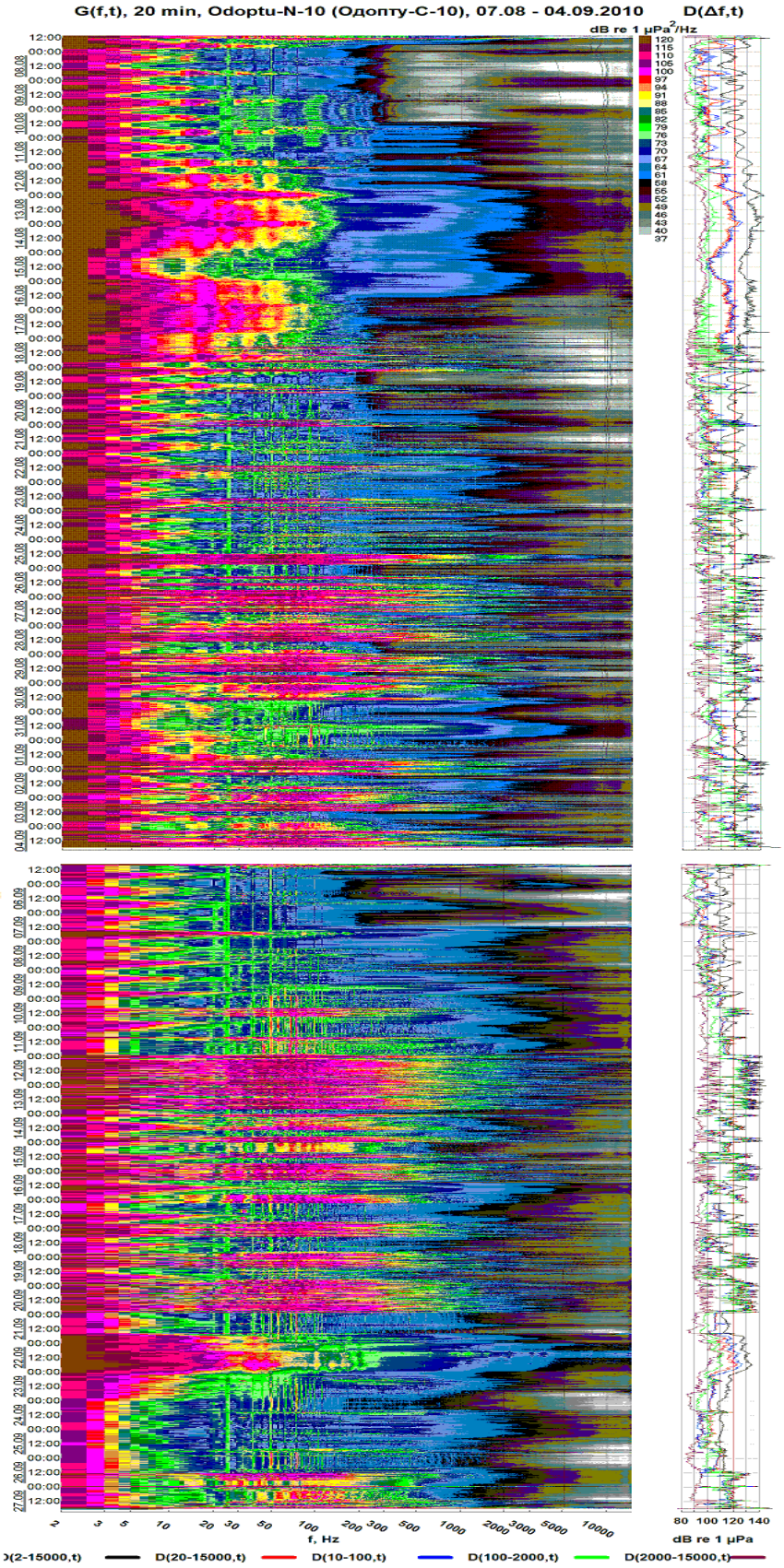

Figure 3.6 - Sonogram *G(f,t)* and plots of sound pressure level of acoustic data recorded at the Odoptu-N-10 monitor station in 2010.

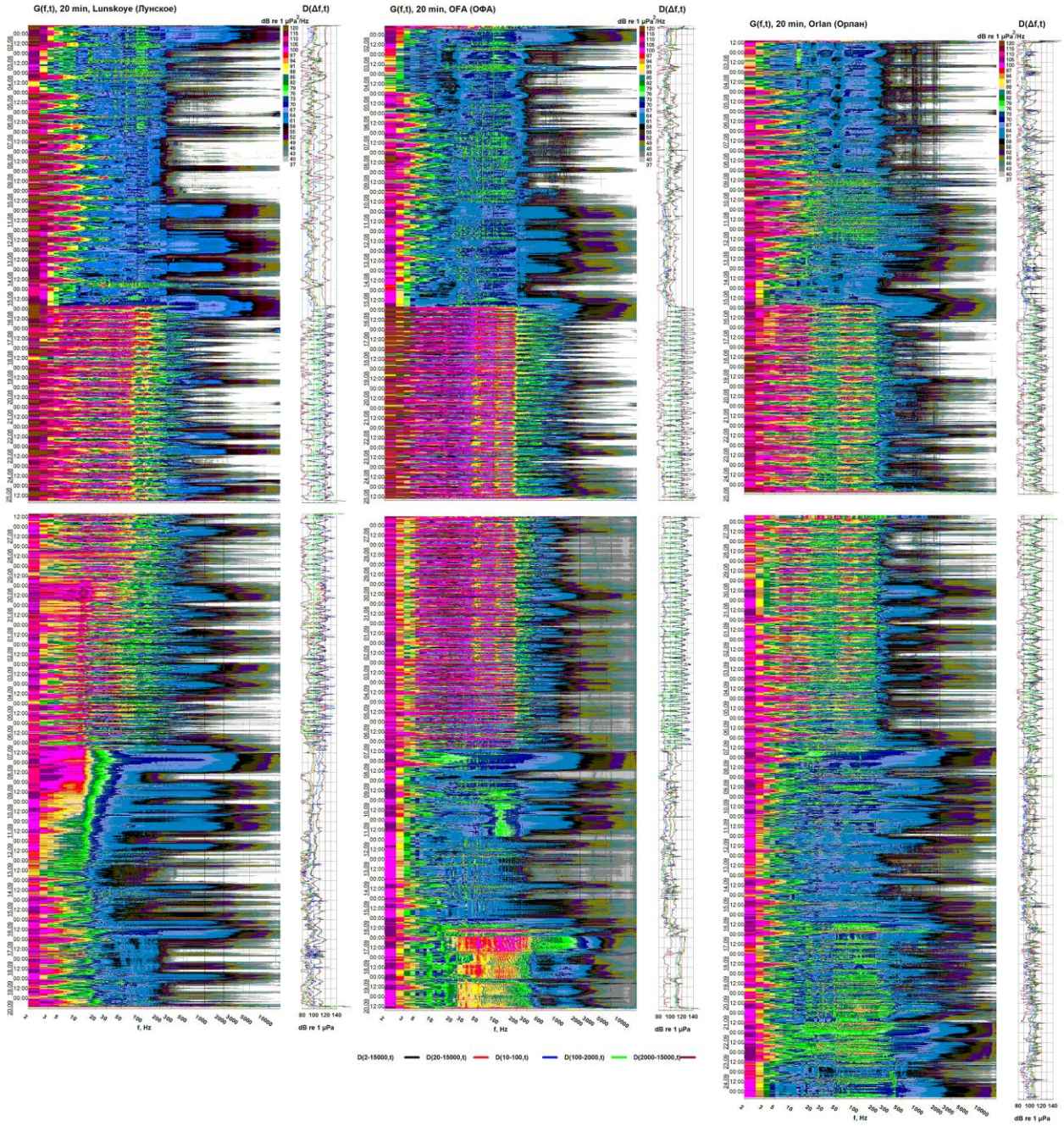

Figure 3.7 - Sonogram *G(f,t)* and plots of sound pressure level of acoustic data recorded at the Lunskoye, OFA and Orlan monitor stations in 2010.

Figure 3.11 shows plots of various sound level metrics for impulses recorded at the Arkutun-Dagi acoustic monitor station from a seismic survey acquired along an unknown profile to the east of the offshore feeding area. These plots show that the peak values *p(t)* of the recorded impulses reached 172 dB re 1 μPa, the values of SPL_{rms} reached 162 dB re 1 μPa, and the values of SEL reached 156 dB re 1 $\mu Pa^2 \cdot s$.

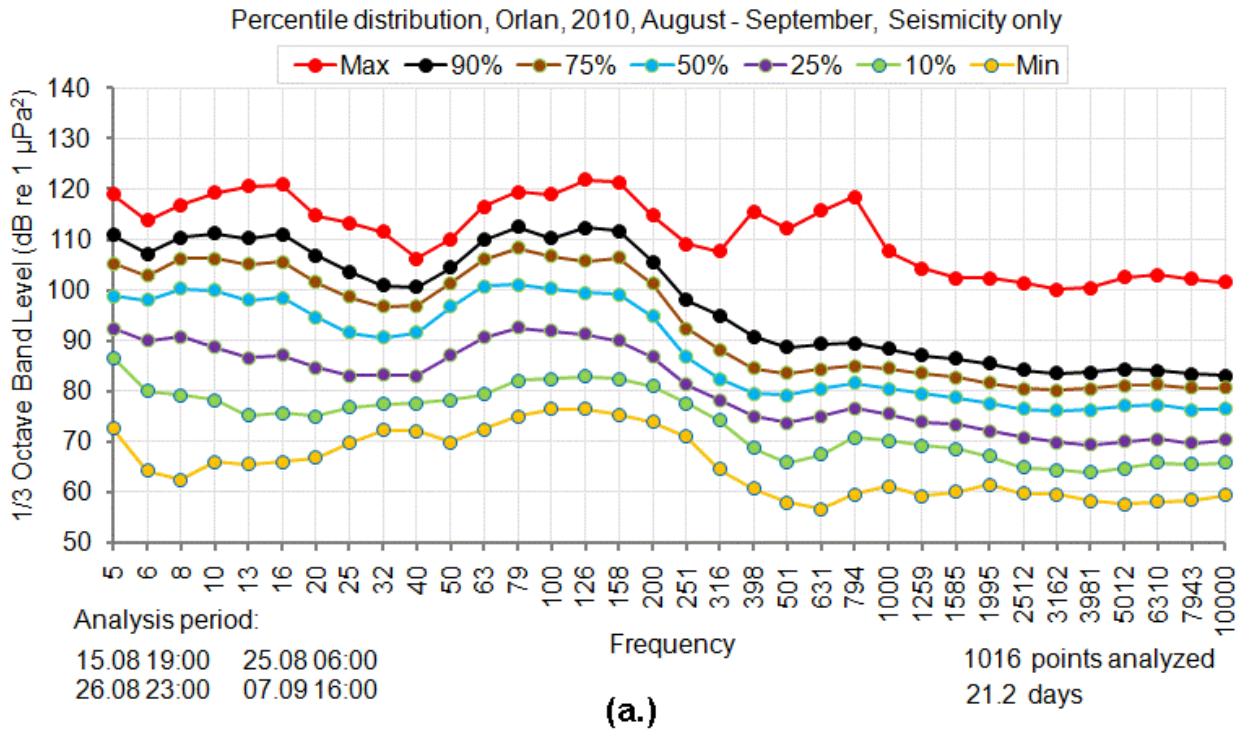

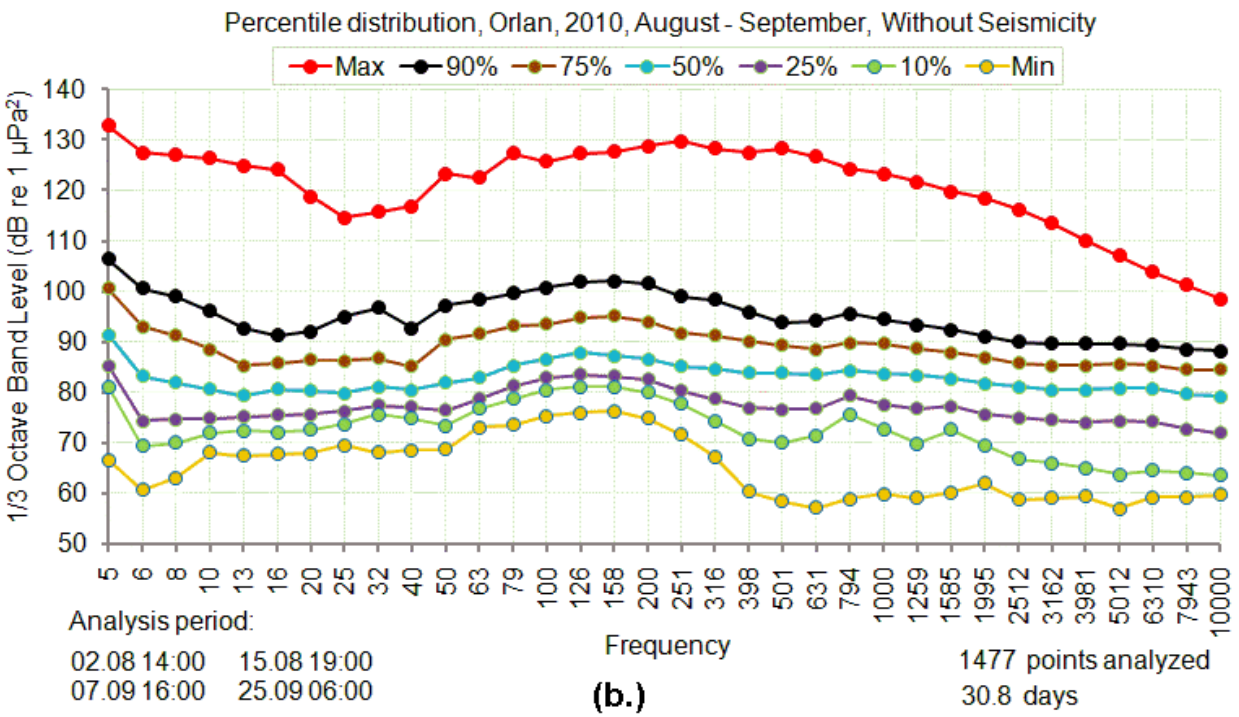

Figure 3.8 – One-third octave power spectral density percentile plots of acoustic data recorded at the Orlan monitor stations in 2010: (a) for data with seismic impulses; and (b) without seismic impulses.

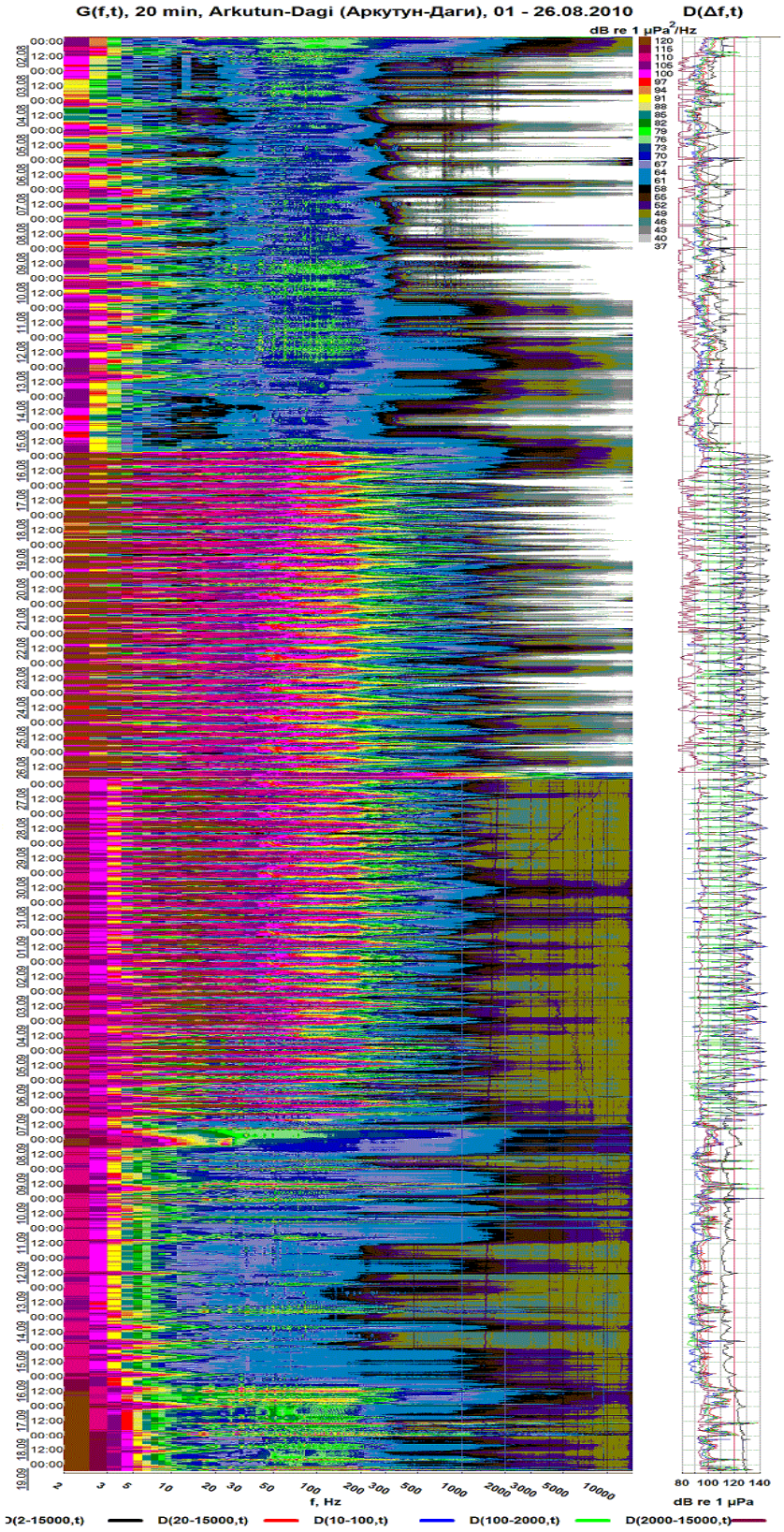

Figure 3.9 - Sonogram *G(f,t)* and plots of sound pressure level of acoustic data recorded at the Arkutun-Dagi monitor station.

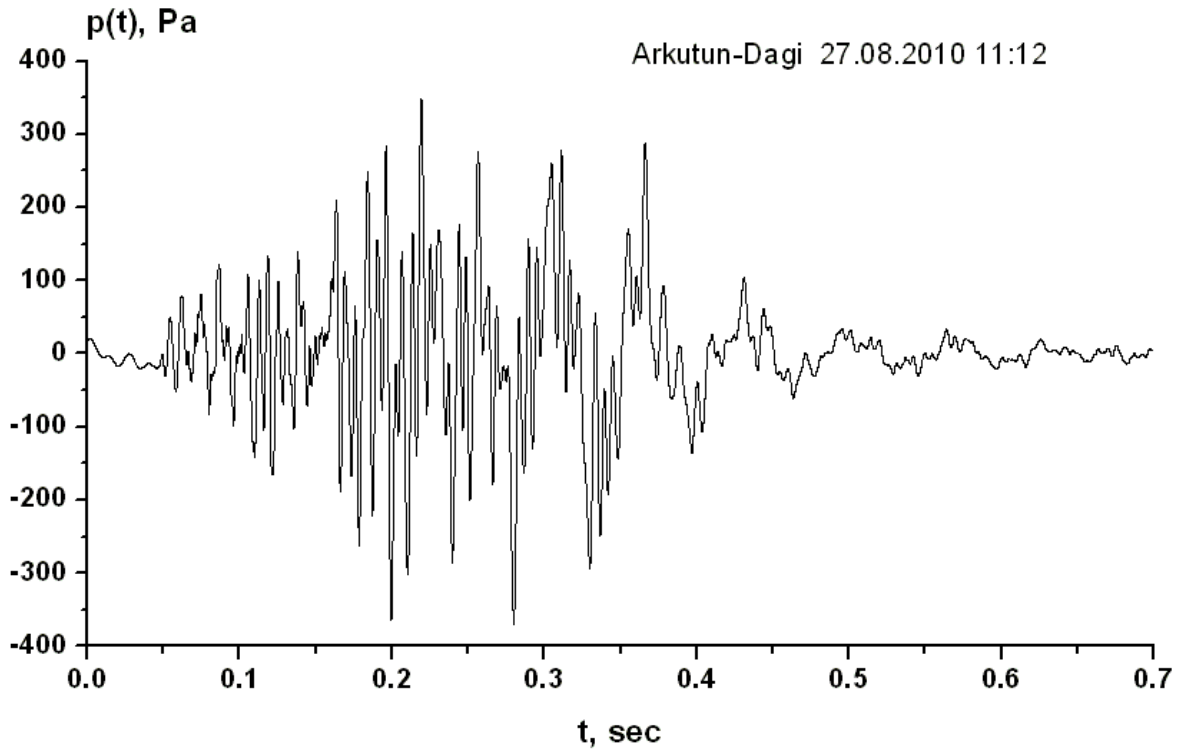

Figure 3.10 - Plots of acoustic impulses recorded at the Arkutun-Dagi monitor station during a seismic survey

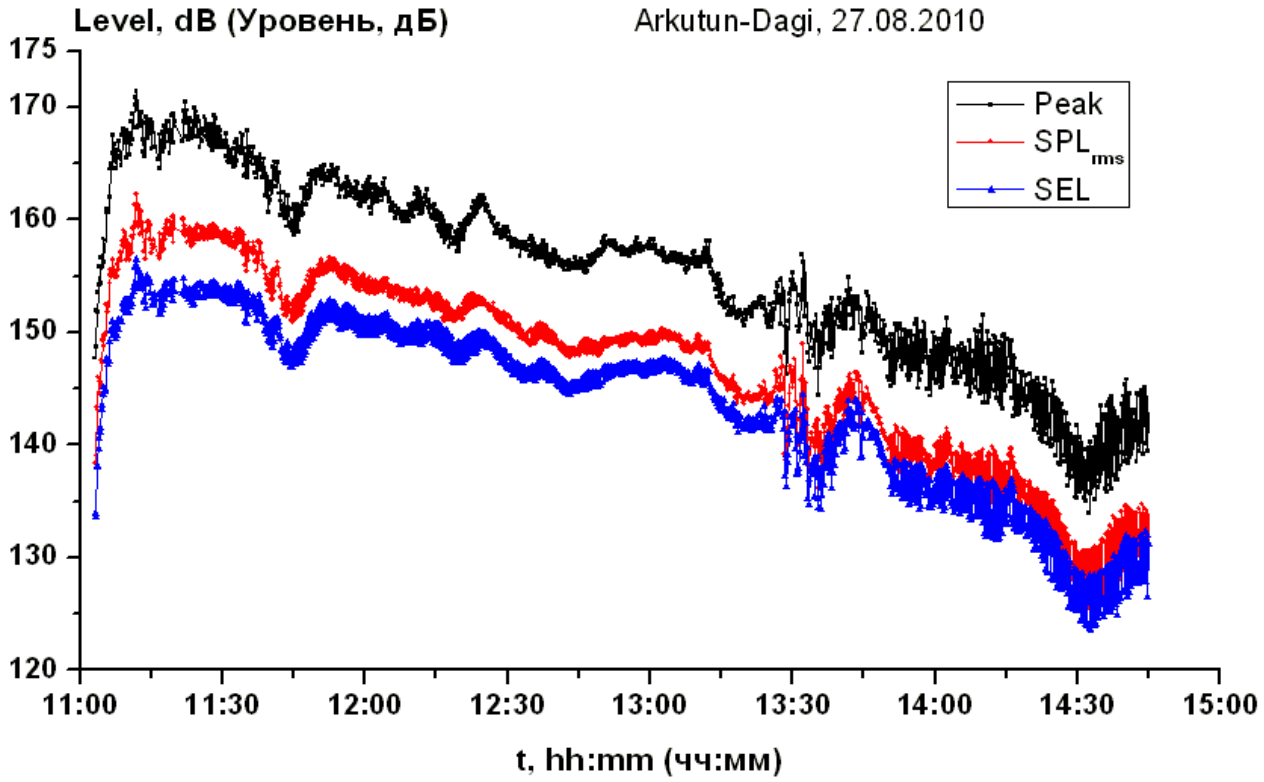

Figure 3.11 - Plots of peak, SPL_{rms} and SEL for acoustic impulses recorded at the Arkutun-Dagi monitor station during a seismic survey east of the offshore feeding area.

3.4 Anthropogenic acoustic measurements near the PA-B and Molikpaq platforms

Figure 3.12 is a map showing the locations of the acoustic stations where the acoustic measurements were made, and the profiles along which anthropogenic sound generated by the platform and its supply vessels propagated. It can be seen that stations PA-B-20 and PA-B-10 located at the eastern border and inside the Piltun feeding area respectively, recorded anthropogenic acoustic data generated near the PA-B platform (Figure 3.13) and the Molikpaq station recorded anthropogenic acoustic data generated near the Molikpaq platform (Figure 3.14). Figure 3.15 shows sonograms which provide a quantitative estimate of variations in ambient and anthropogenic acoustic levels as measured at similar ranges and water depth conditions for sound from the *PA-B* and *Molikpaq* platforms. It is clear from Figure 3.15 that the anthropogenic noise recorded at PA-B-20 possesses continuous narrow-band low-frequency quasi-harmonic components alternating with more intense and broader-band noises that are probably generated by support vessels. The spectrum of acoustic noise measured at the Molikpaq monitoring station does not exhibit any distinguishable quasi-harmonic components, and more importantly, is devoid of the powerful 50 Hz tonal signals which caused concern in 2009.

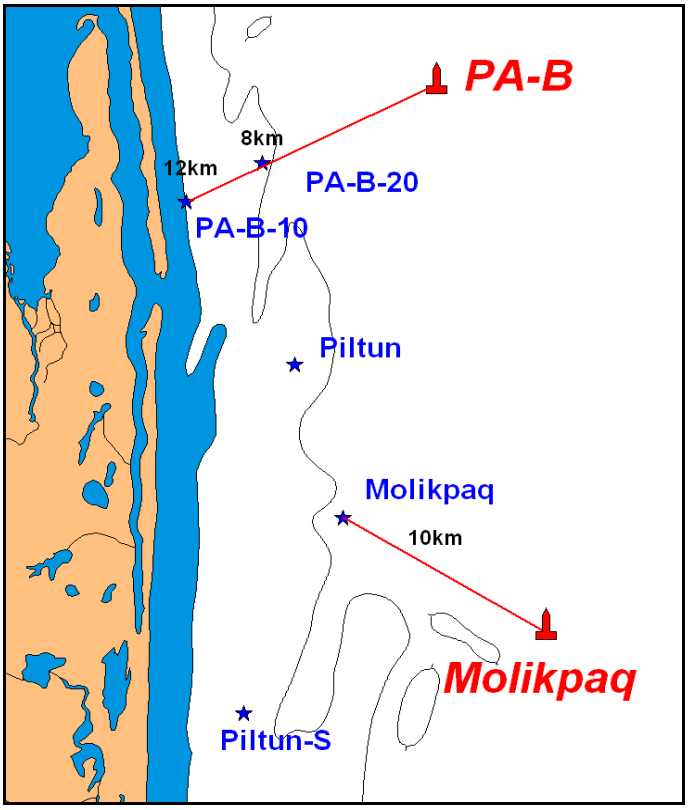

Figure 3.12 – Map showing the PA-B and Molikpaq (PA-A) platforms and acoustic monitoring stations and acoustic monitoring stations PA-B-10, PA-B-20 and Molikpaq.

Figure 3.13 – Platform PA-B.

Figure 3.14 – Platform *Molikpaq.*

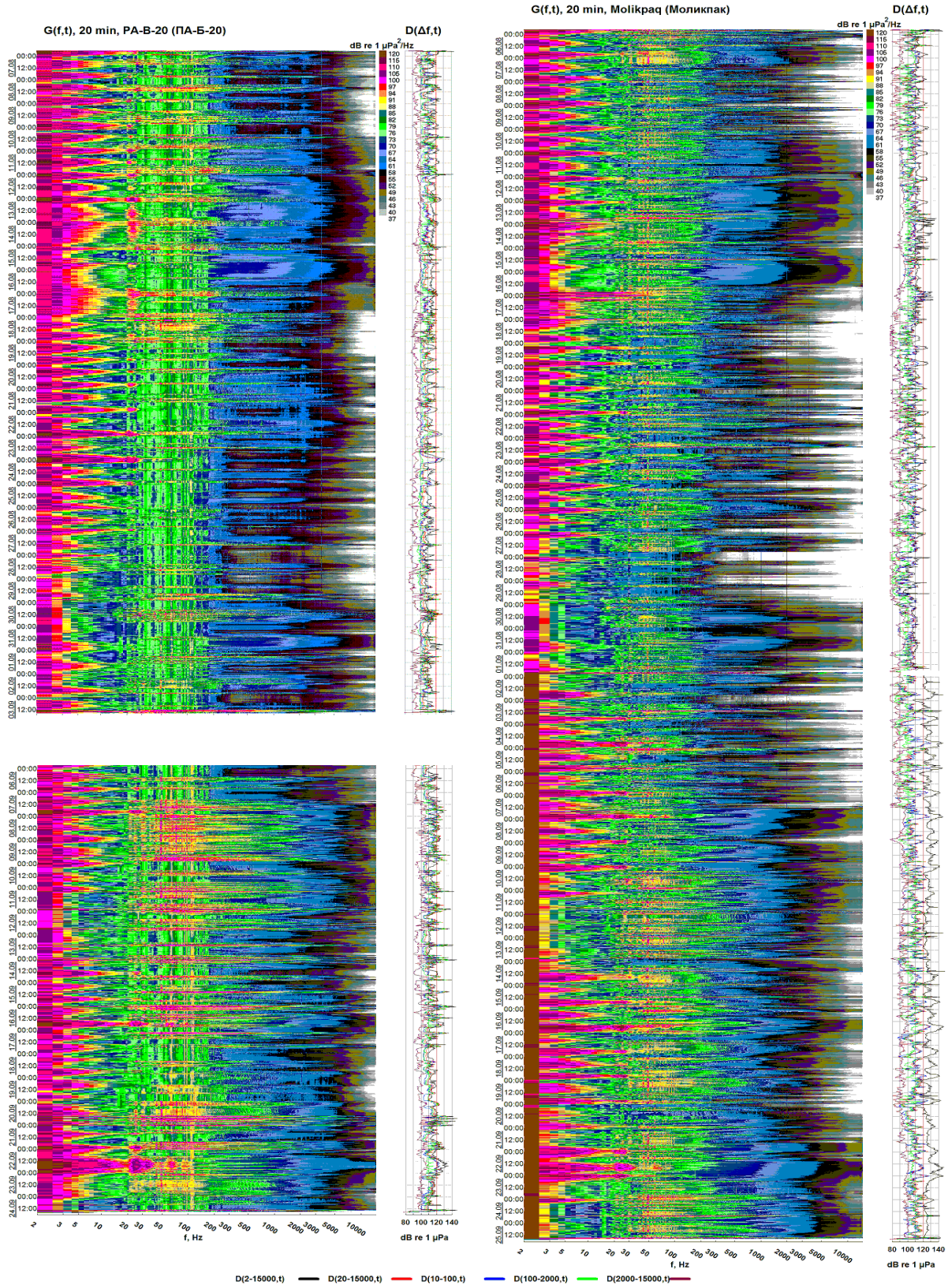

Figure 3.15- Sonogram *G(f,t)* and plots of sound pressure level of acoustic data recorded at the PA-B-20 and Molikpaq monitor stations.

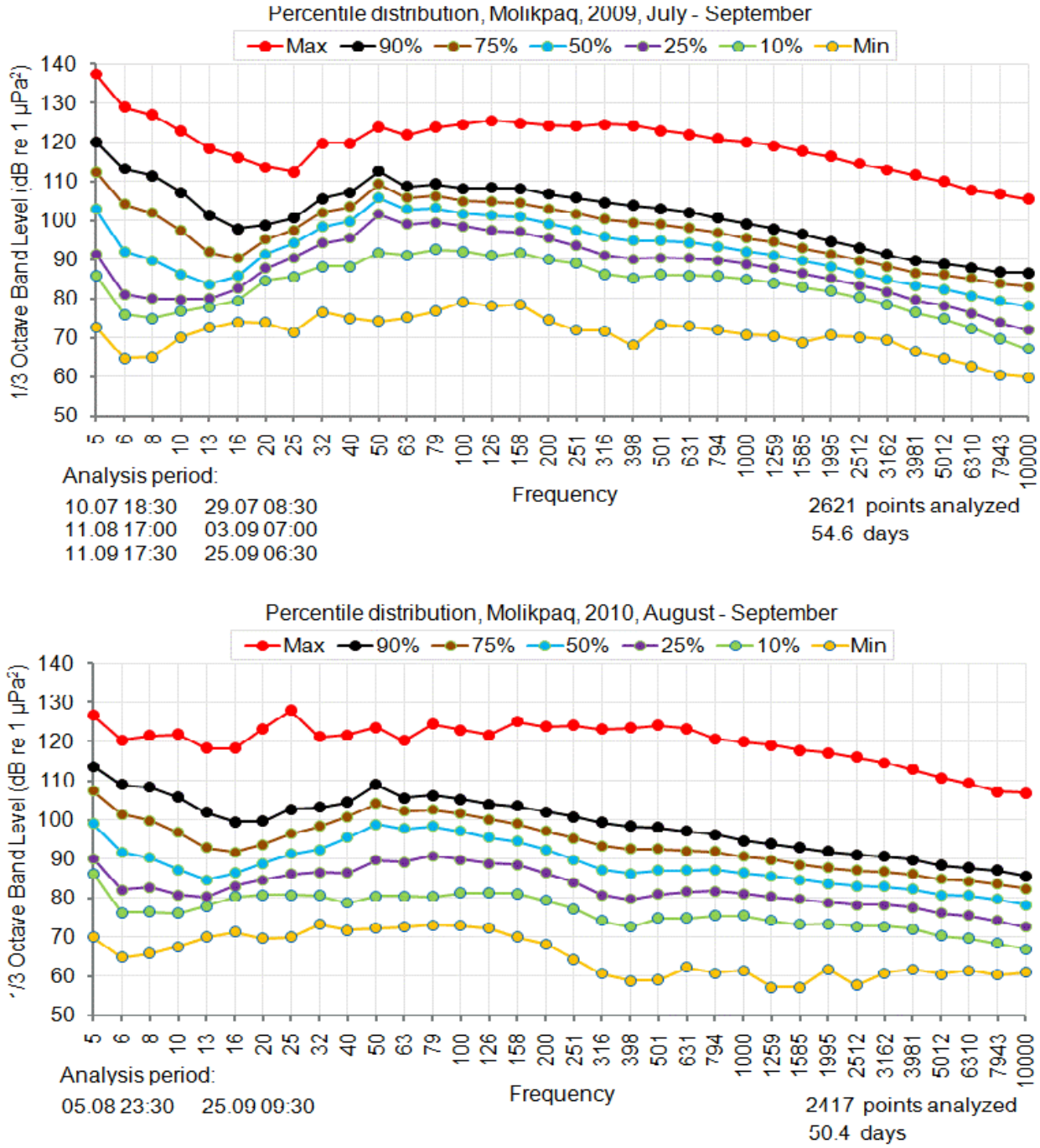

Figure 3.16 – One-third octave power spectral density percentile plots of acoustic data recorded at the Molikpaq monitor station in (a) 2009; and (b) 2010.

Figure 3.16 gives the results of the statistical analysis of acoustic signals measured at the Molikpaq acoustic monitoring station in 2009 and 2010. This figure shows that the 25% one-third octave power spectral density percentile plot for 2010 has no peak at 50 Hz, although it reached 101 dB re 1 µPa^2 in 2009. The 50%, 75% and 90% percentile plots for 2010 show a noticeable power peak at 50 Hz, although this is approximately 6 dB lower than in 2009.

4 Analysis of Transmission Loss *TL(r,f)* experiments on the Sakhalin shelf

Figure 4.1 presents a map showing the Transmission Loss (TL) profiles acquired in 2010; these experimental measurements are used to estimate the propagation losses for different frequencies generated and received at defined locations along the specified profiles (TLP-ADP-B-3, TLP-ADP-A-5, TLP-5, TLP-7γ, TLP-22). The procedure for estimating TL from experimental data was described in greater detail in [Borisov et al, 2007].

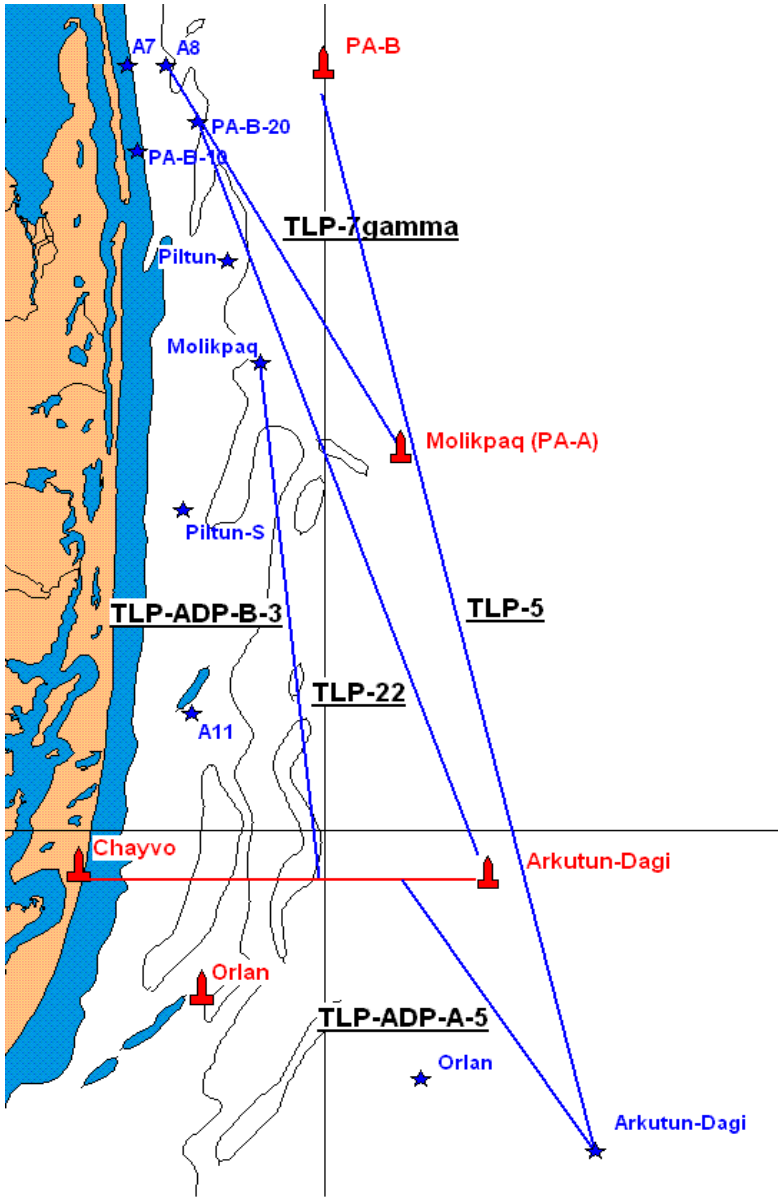

Figure 4.1 - Map of the study area showing the major facilities as well as the profiles along which frequency dependent TL studies were conducted in 2010.

4.1 Analysis of Transmission Loss *TL(r,f)* along profile TLP-5

Figure 4.2 is a map of the study area showing TL profile TLP-5. Experimental TL profile TLP-5 is 69 km long starting at the PA-B platform location and ending at the Arkutun-Dagi monitoring station at the northern edge of the offshore feeding area. The hydrological conditions along the profile were monitored at all the source locations and at intermediate hydrology points Z1, Z2, Z3, and Z4, where the source points were greater than 7 km apart. Figure 4.3 shows the bathymetry and the spatial distribution of hydrology along the profile during the acoustic measurements.

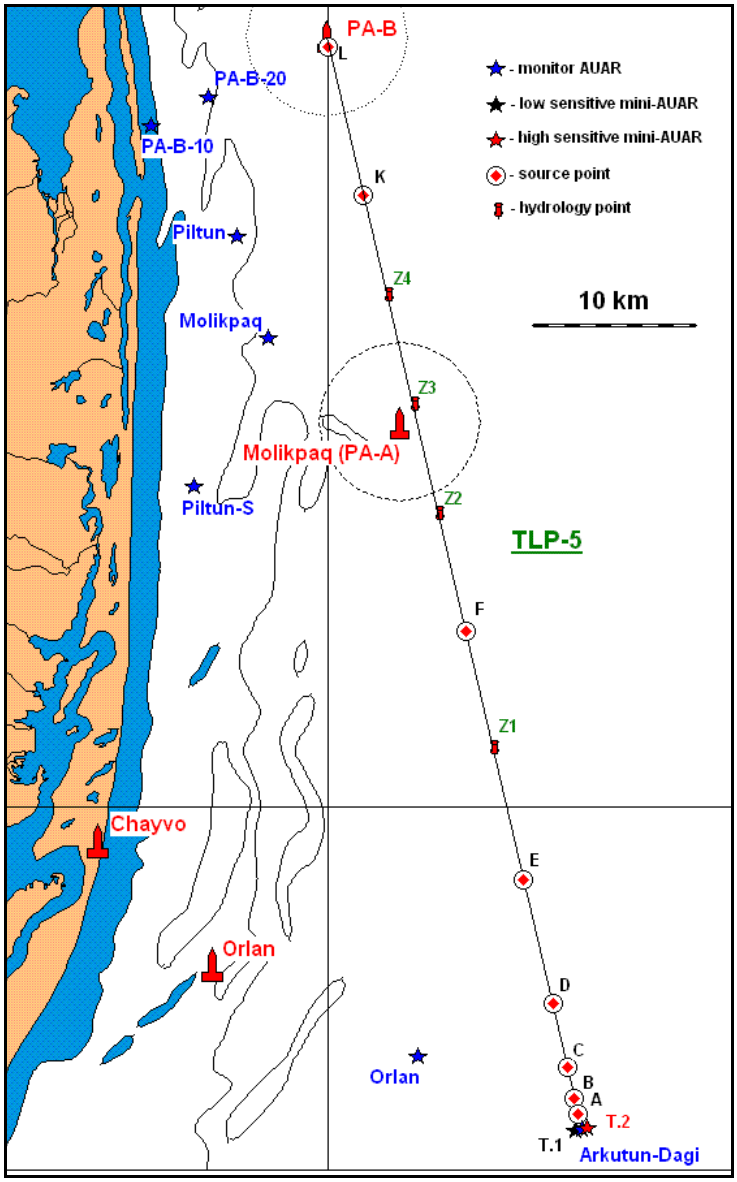

Figure 4.2 - Map of the study area showing the major facilities as well as the AUAR deployment locations for TLP-5 on which frequency dependent TL studies were conducted on 17th-18th September, 2010.

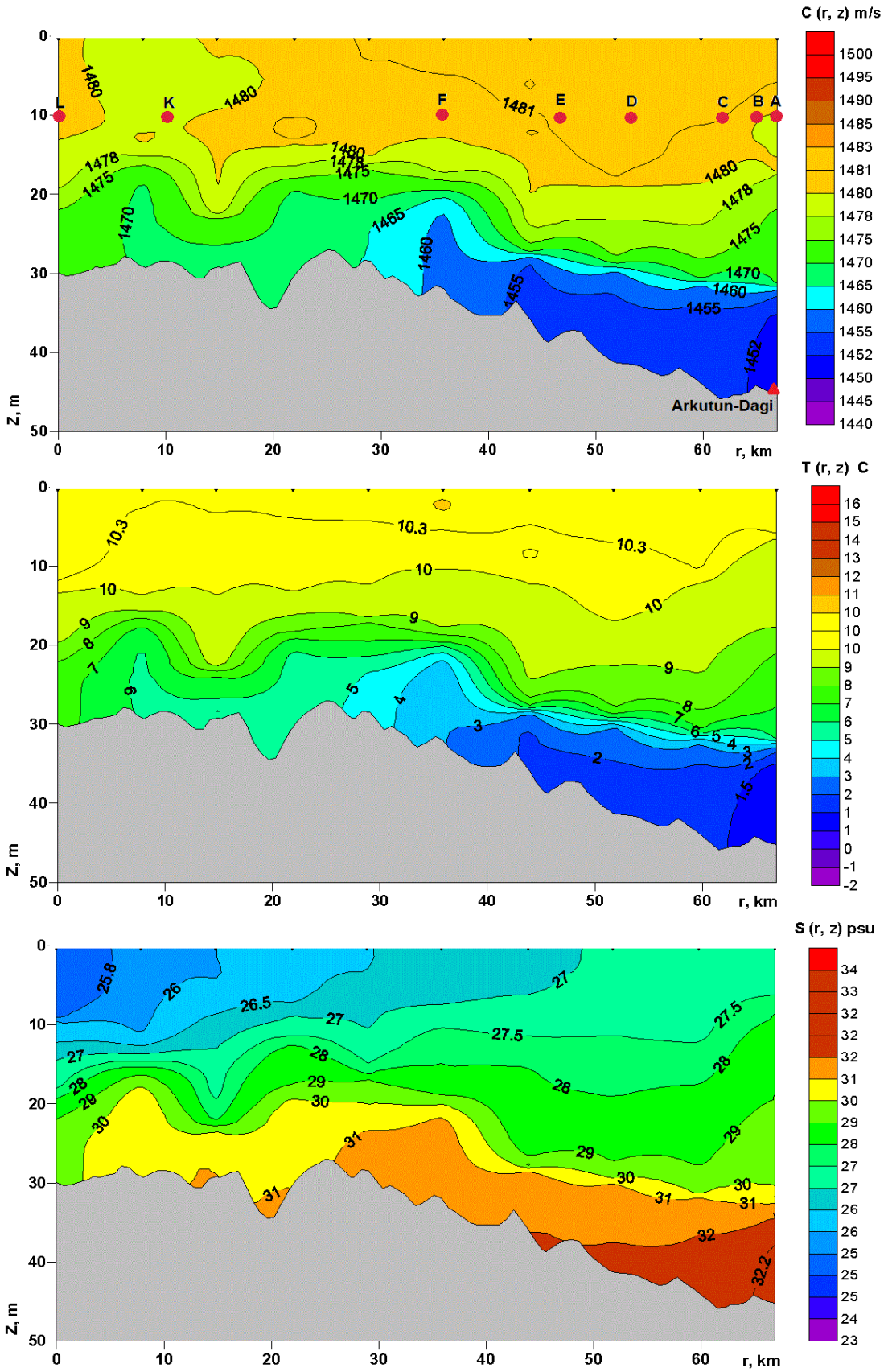

Figure 4.3 - TLP-5: Bathymetry and hydrologic parameters (velocity *C(r,z)*, temperature *T(r,z)*, and salinity *S(r,z)* acquired on 18th September, 2010.

There are twelve source locations (A, B, C, D, E, F, G, H, I, J, K and L (1.5 km from the Orlan platform)) along the profile. The source locations are 1 km, 2 km, 4 km, 5 km, 8 km, 16 km, 32 km, 60 km, and 69 km respectively from the Arkutun-Dagi location. Both an AUAR and two mini-AUARs were deployed at the Arkutun-Dagi location, recording while signals were transmitted at the twelve source locations. Figures 4.4 to 4.6 presents the TL results obtained from the analysis of the data, acquired using the procedure described previously [Borisov et.al., 2006] over the frequency range from 10 Hz to 15 kHz.

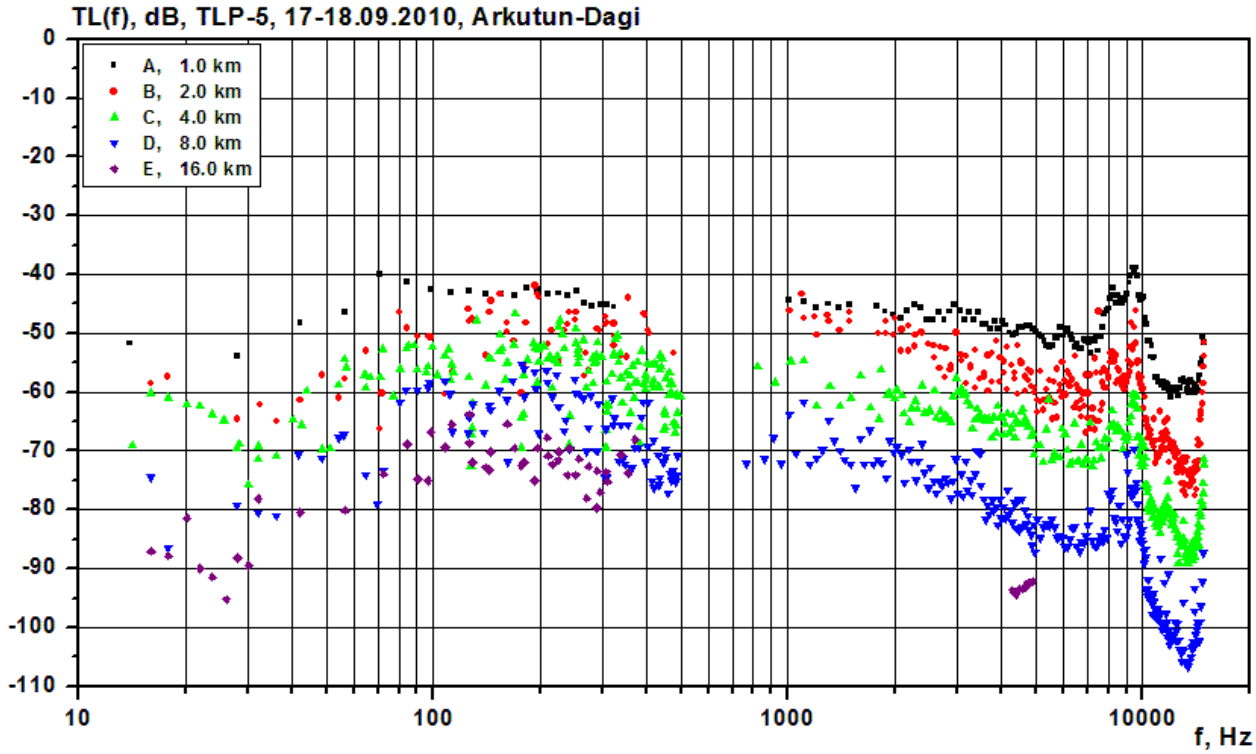

Figure 4.4 - TLP-5: Frequency dependent TL plot showing data for source locations A-E and the distance from the source locations to the Arkutun-Dagi location.

The absence of experimental data for source locations I, J, K and L is explained by the relatively high level of ambient acoustic noise and the low signal levels of LF and HF signals generated at the longest ranges. Further analysis will be attempted in a reduced frequency bin size.

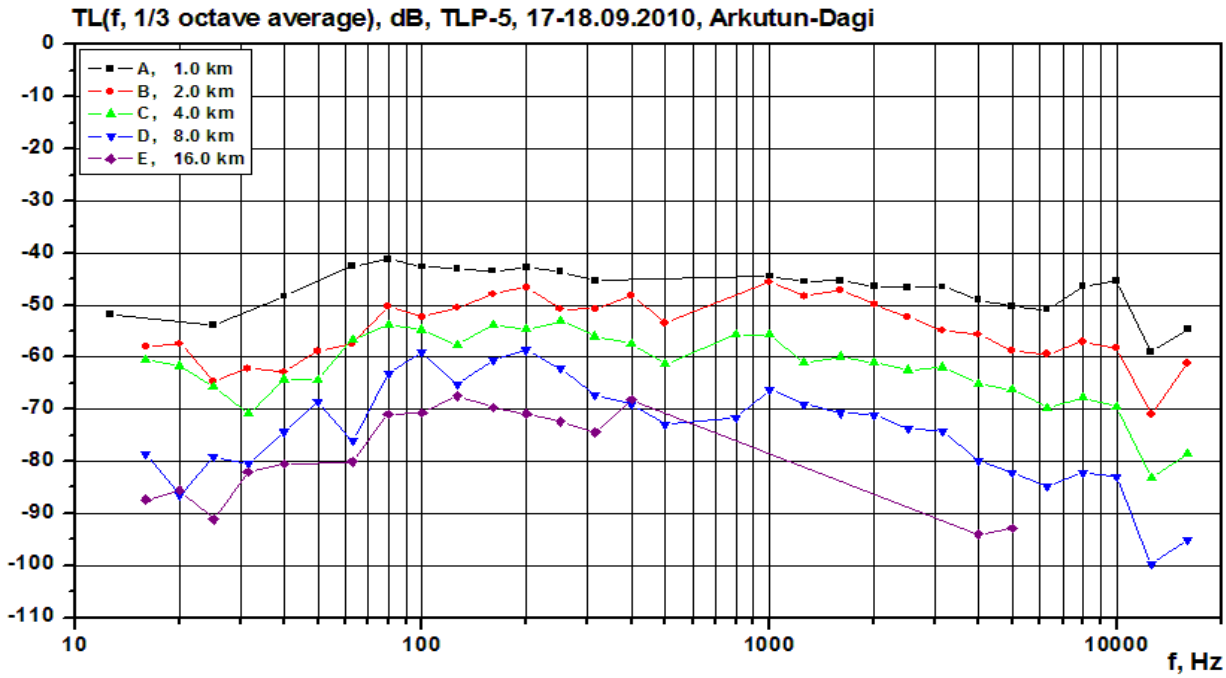

Figure 4.5 - TLP-5: One third octave averaged frequency dependent TL plot showing the results for all the source locations and data in Figure 4.4.

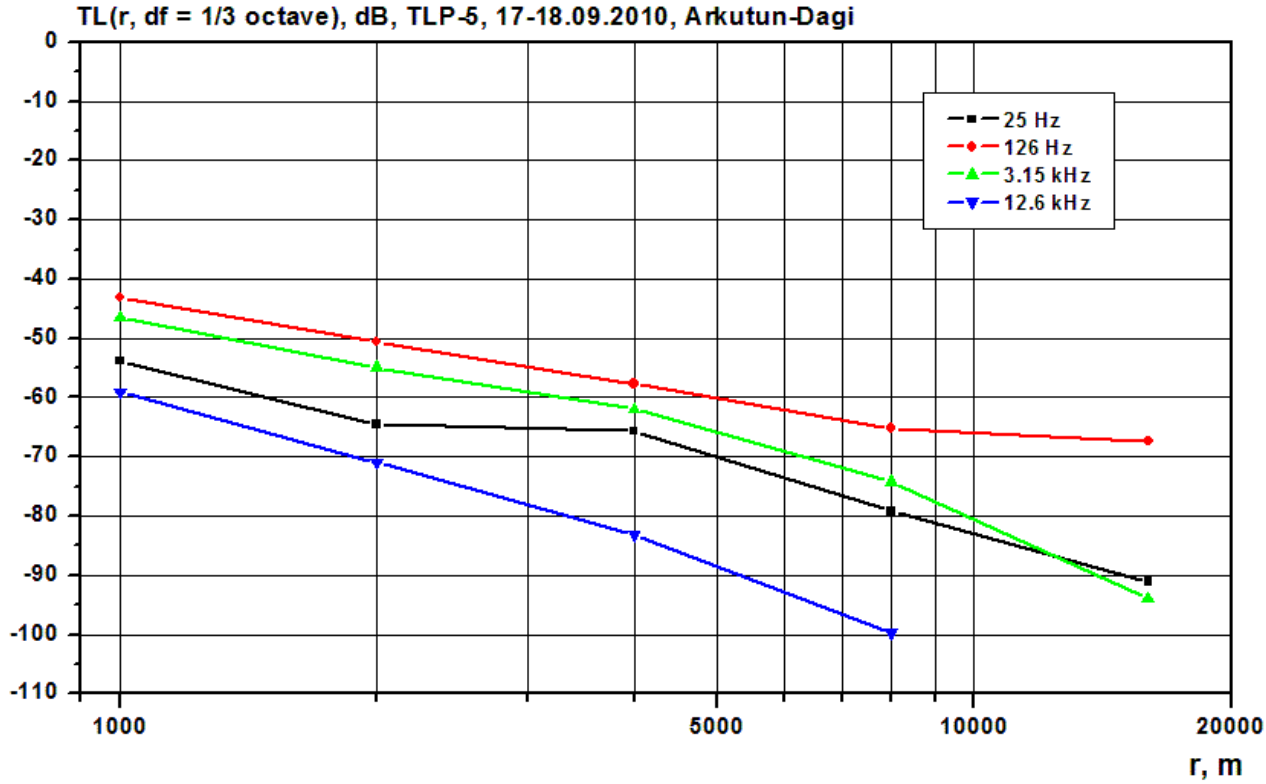

Figure 4.6 - TLP-5: Range dependent one third octave averaged frequency dependent TL plot showing the results for four one third octave frequency bands for the Arkutun-Dagi station.

4.2 Analysis of Transmission Loss *TL(r,f)* along profile TLP-7γ

Figure 4.7 is a map of the study area showing TL profile TLP-7γ. Experimental TL profile TLP-7γ is 27 km long starting at the Molikpaq platform location, passing through the PA-B-20 station and ending at the A8 acoustic station at the eastern edge of the Piltun feeding area. The hydrological conditions along the profile were monitored at all the source locations.

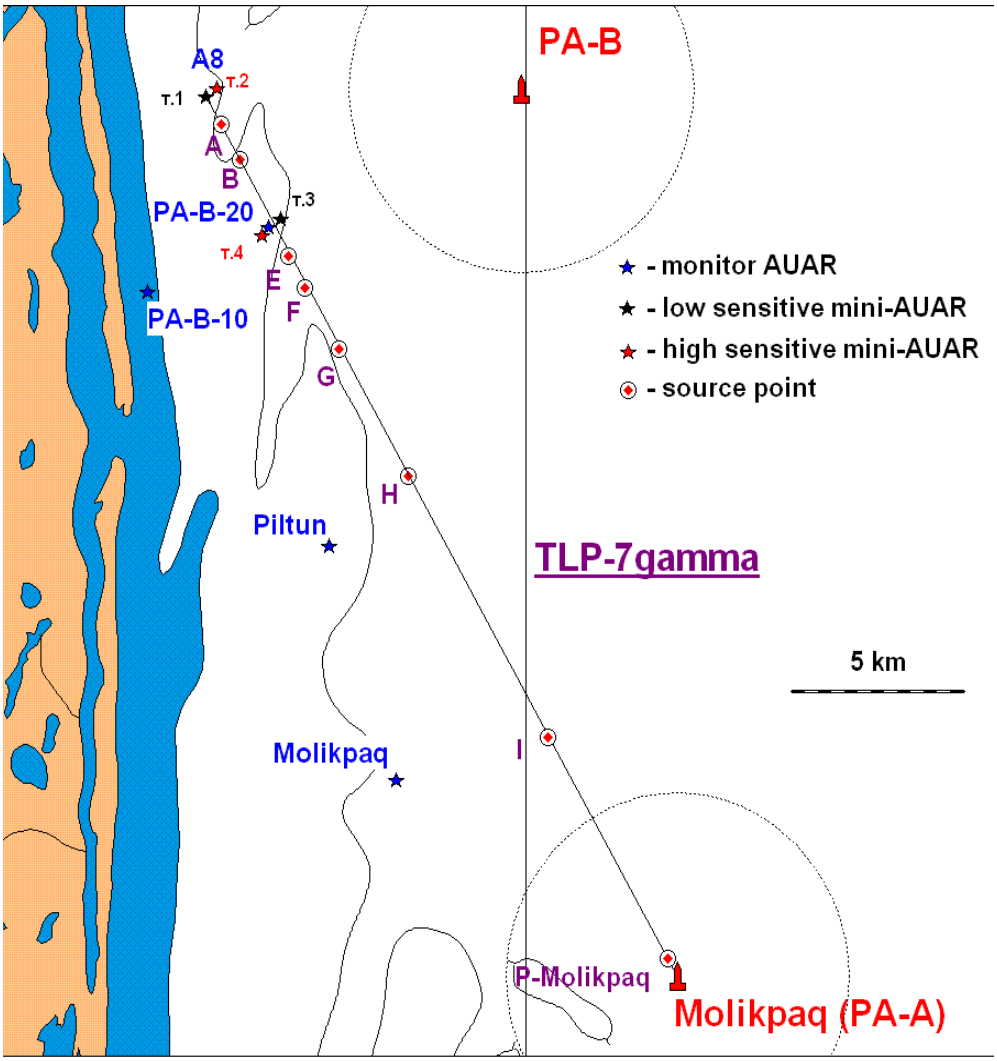

Figure 4.7 - Map of the study area showing the major facilities as well as the AUAR deployment locations for TLP-7γ along which frequency dependent TL studies were conducted on 29th-30th August, 2010.

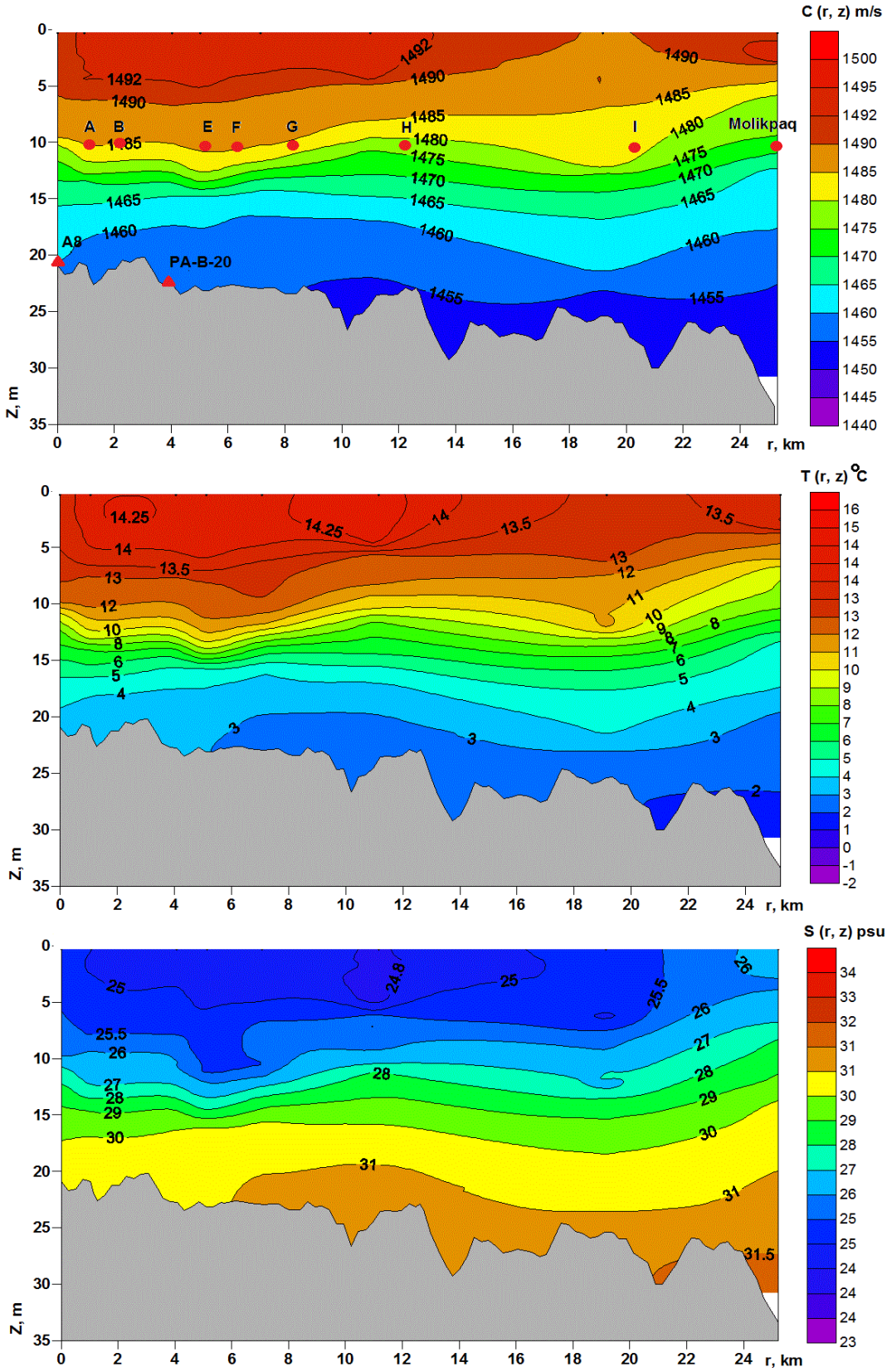

Figure 4.8 - TLP-7γ: Bathymetry and hydrologic parameters (velocity *C(r,z)*, temperature *T(r,z)*, and salinity *S(r,z)* acquired on 30th August, 2010.

Figure 4.8 shows the bathymetry and the spatial distribution of hydrology along the profile during the acoustic measurements. There are eight source locations (A, B, E, F, G, H, I and J (P-Molikpak, 500 m from the Molikpaq platform)) along the profile. The source locations are 3 km, 2 km, 1 km, 2 km, 4 km, 8 km, 16 km, and 23 km respectively from the A8 location and 1 km, 2 km, 5 km, 6 km, 8 km, 12 km, 20 km, and 27 km respectively from the PA-B-20 location. Two mini-AUARs were deployed at the A8 location and both an AUAR and two mini-AUARs were deployed at the PA-B-20 location, recording while signals were transmitted at the source locations. Figures 4.9 to 4.17 present the TL results obtained from the analysis of the data, acquired over the frequency range from 10 Hz to 15 kHz.

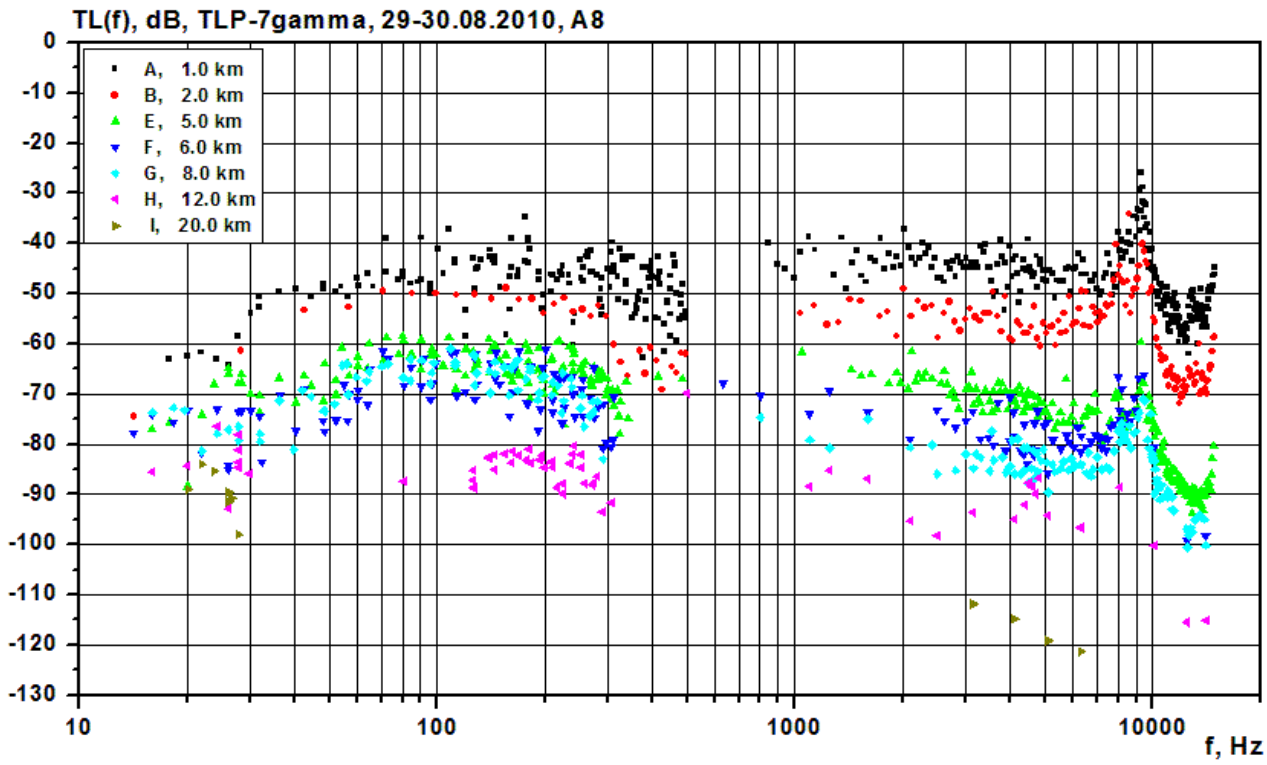

Figure 4.9 - TLP-7γ: Frequency dependent TL plot showing data for all the source locations and the distance from the source locations to the A8 location.

The absence of experimental data for source location J is explained by the relatively high level of ambient acoustic noise (due to a vessel anchored nearby) and the low signal levels of HF signals generated at the longest ranges. Further analysis will be attempted in a reduced frequency bin size.

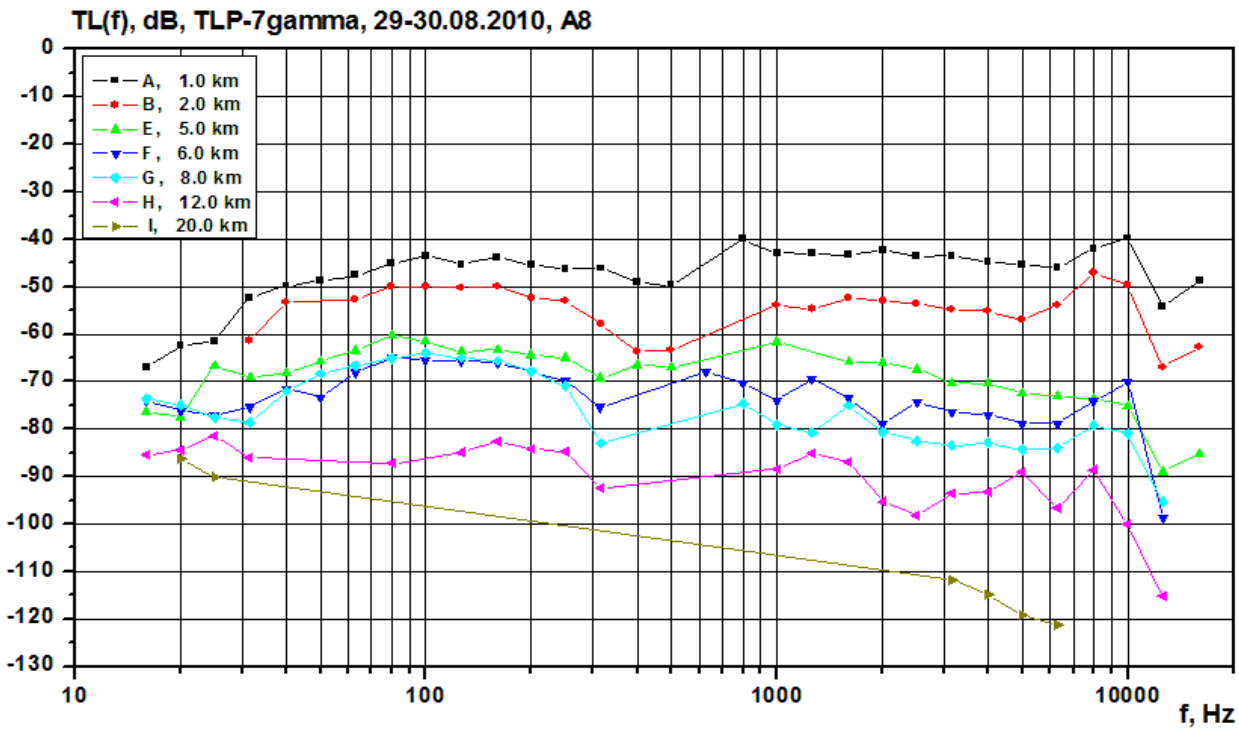

Figure 4.10 - TLP-7γ: One-third octave averaged frequency dependent TL plot showing the results for all the source locations and data in Figure 4.9.

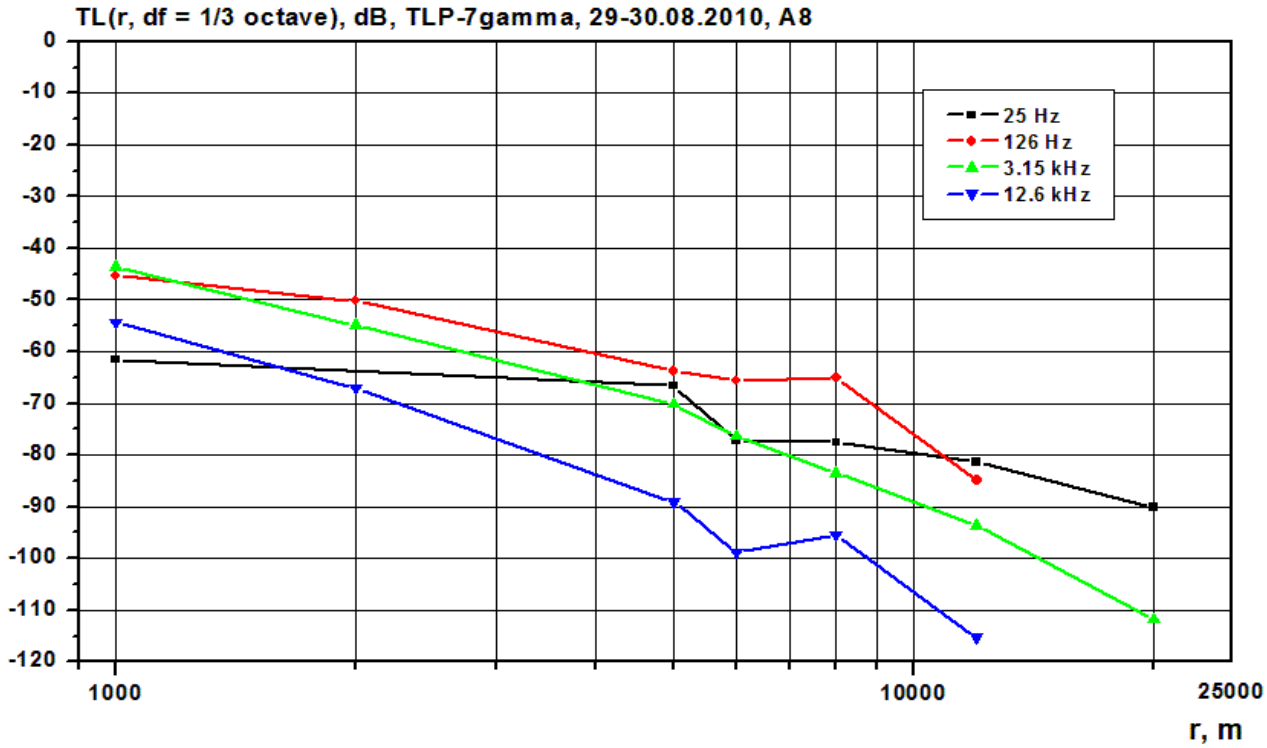

Figure 4.11 - TLP-7γ: Range dependent one third octave averaged frequency dependent TL plot showing the results for four one third octave frequency bands for the A8 station.

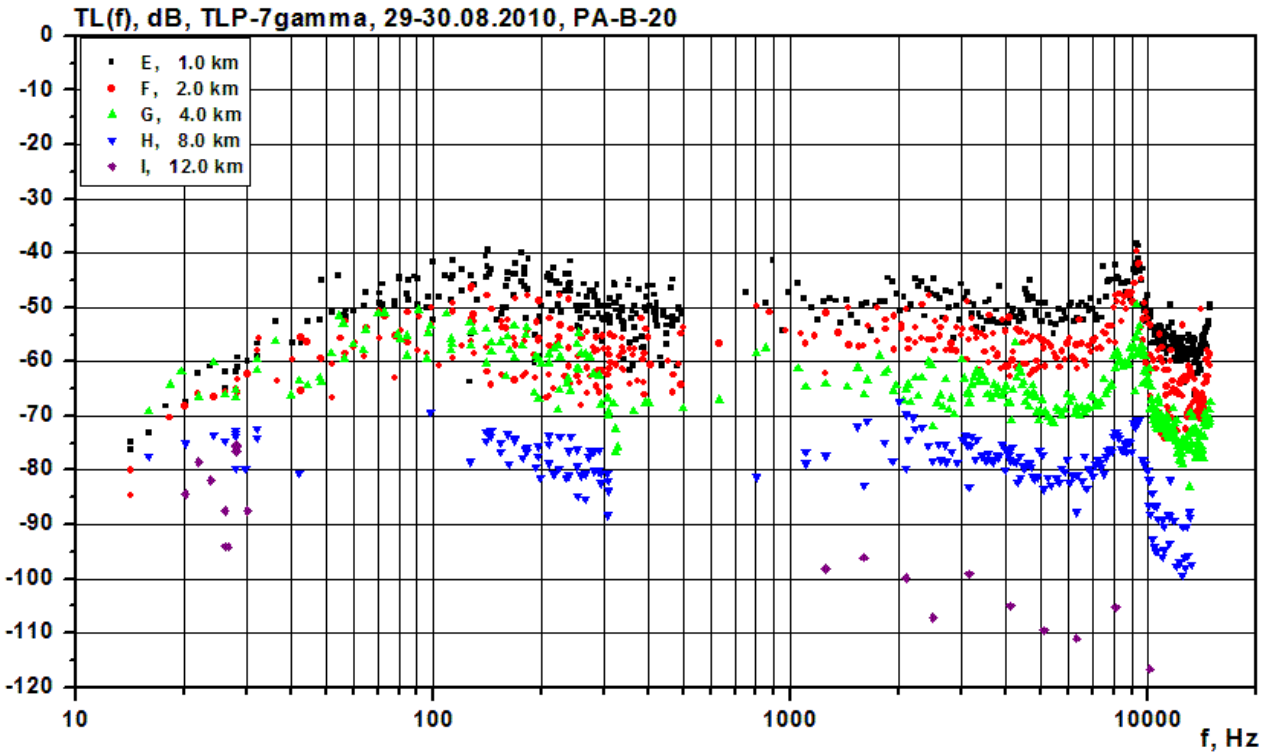

Figure 4.12 - TLP-7γ: Frequency dependent TL plot showing data for source locations E-I and the distance from the source locations to the PA-B-20 location.

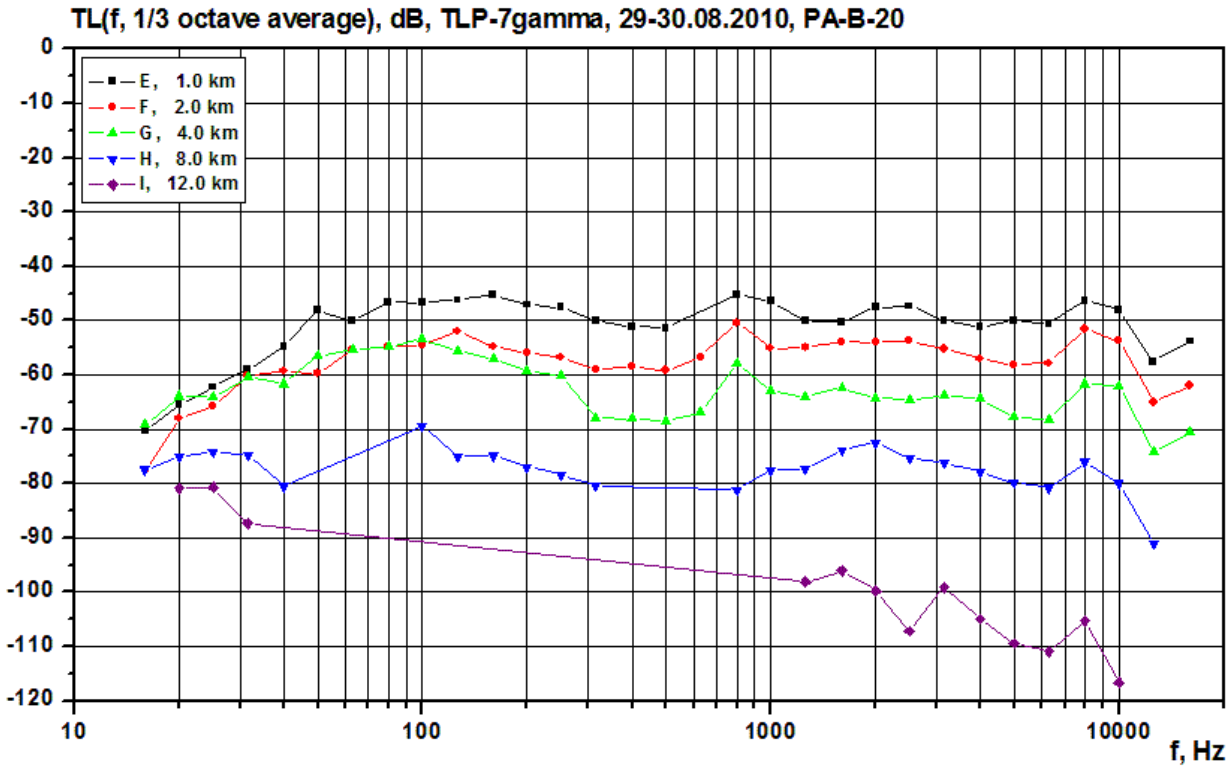

Figure 4.13 - TLP-7γ: One-third octave averaged frequency dependent TL plot showing the results for source locations E-I and data in Figure 4.12.

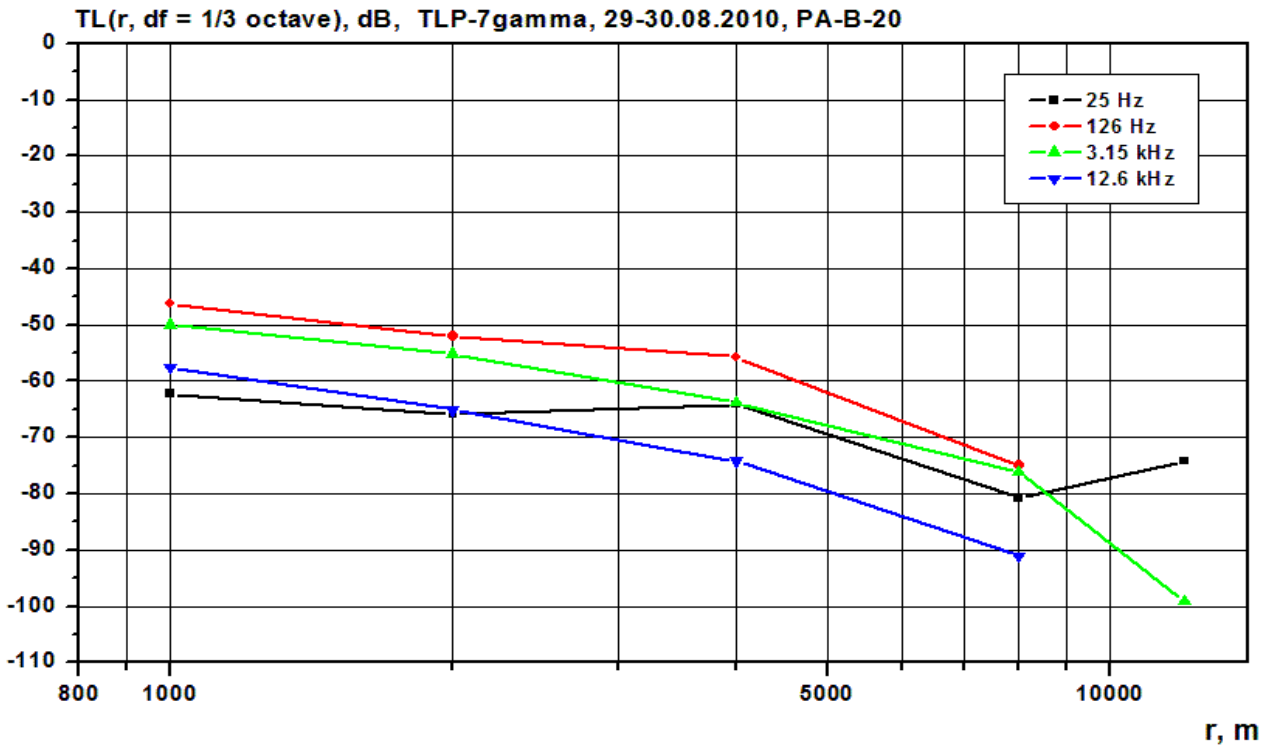

Figure 4.14 - TLP-7γ: Range dependent one third octave averaged frequency dependent TL plot showing the results for four one third octave frequency bands for the PA-B-20 station.

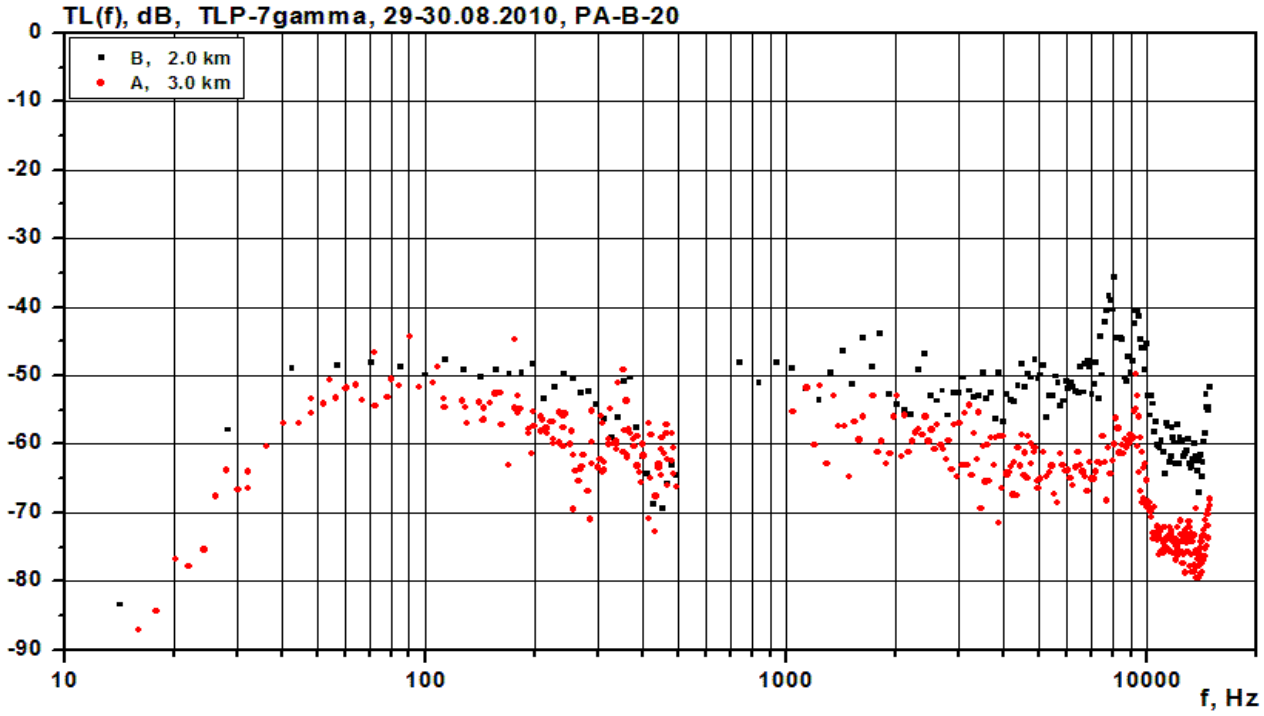

Figure 4.15 - TLP-7γ: Frequency dependent TL plot showing data for source locations A, B and the distance from the source locations to the PA-B-20 location.

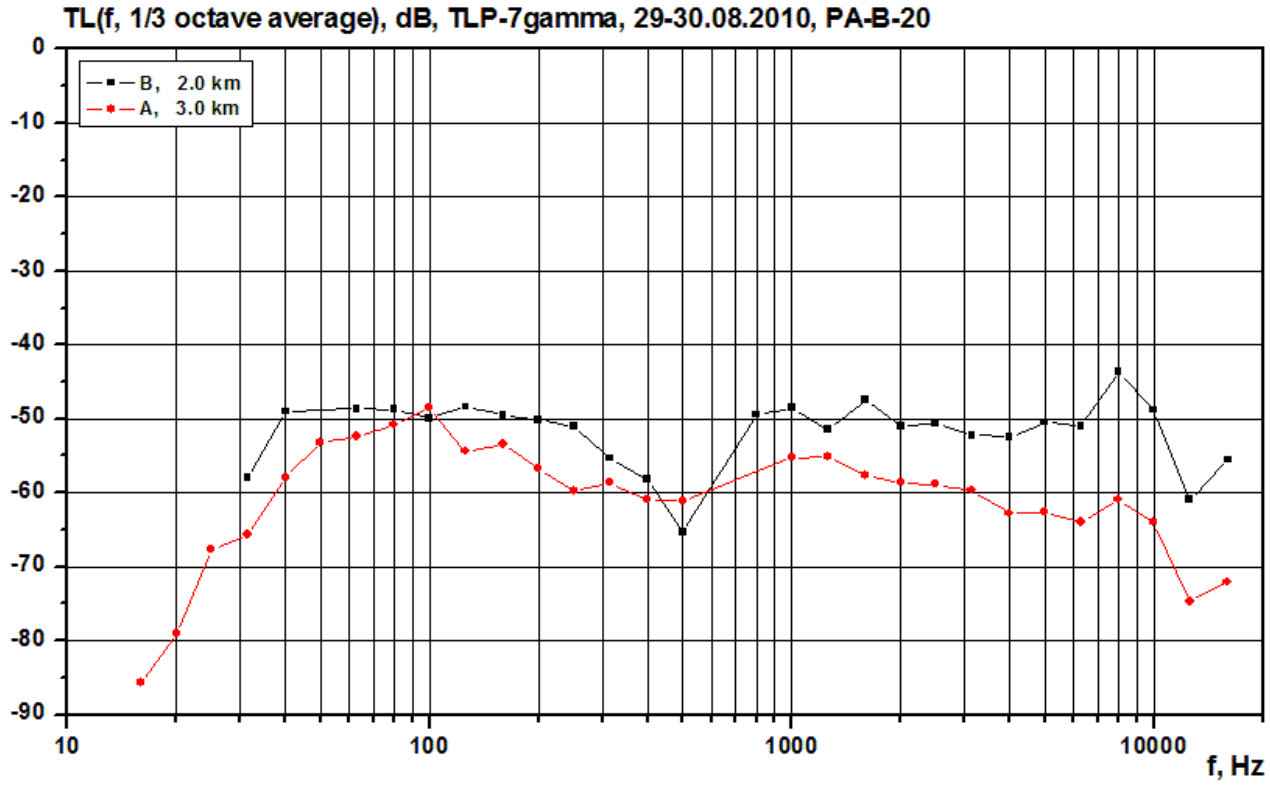

Figure 4.16 - TLP-7γ: One-third octave averaged frequency dependent TL plot showing the results for source locations A-B and data in Figure 4.15.

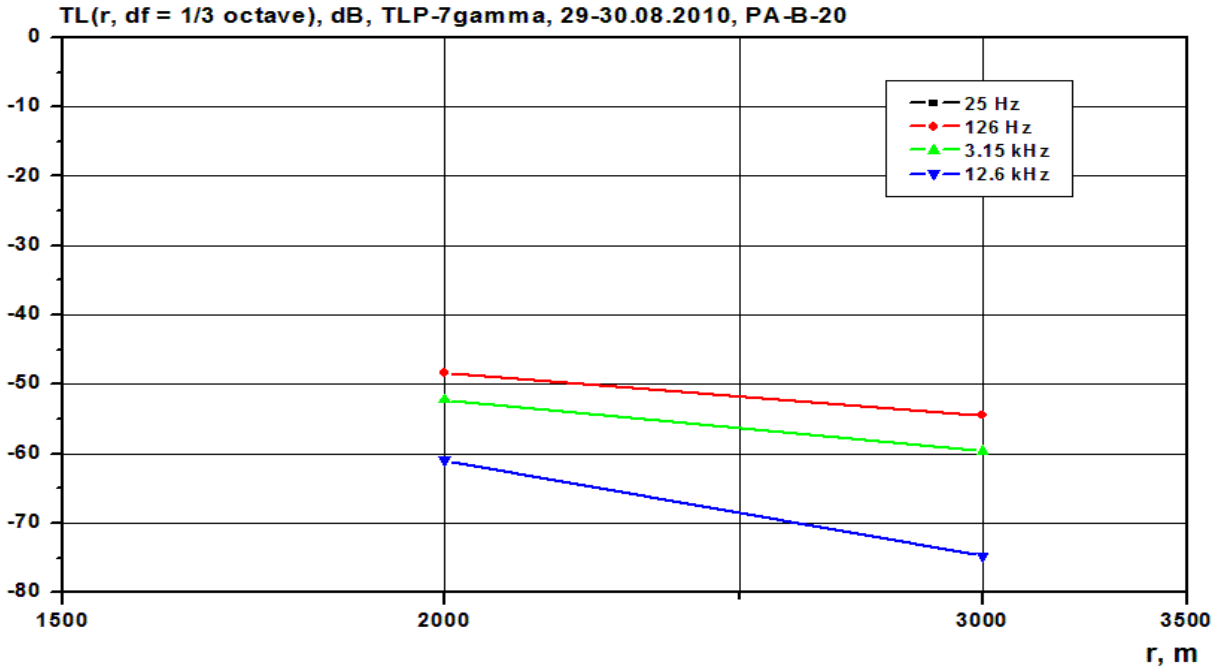

Figure 4.17 - TLP-7γ: Range dependent one third octave averaged frequency dependent TL plot showing the results for four one third octave frequency bands for the PA-B-20 station.

4.3 Analysis of Transmission Loss *TL(r,f)* along profile TLP-22

Figure 4.18 is a map of the study area showing TL profile TLP-22. Experimental TL profile TLP-22 is 49 km long starting at the future Arkutun-Dagi platform location, passing through the Piltun station and ending at the PA-B-20 acoustic station at the eastern edge of the Piltun feeding area. The hydrological conditions along the profile were monitored at all the source locations.

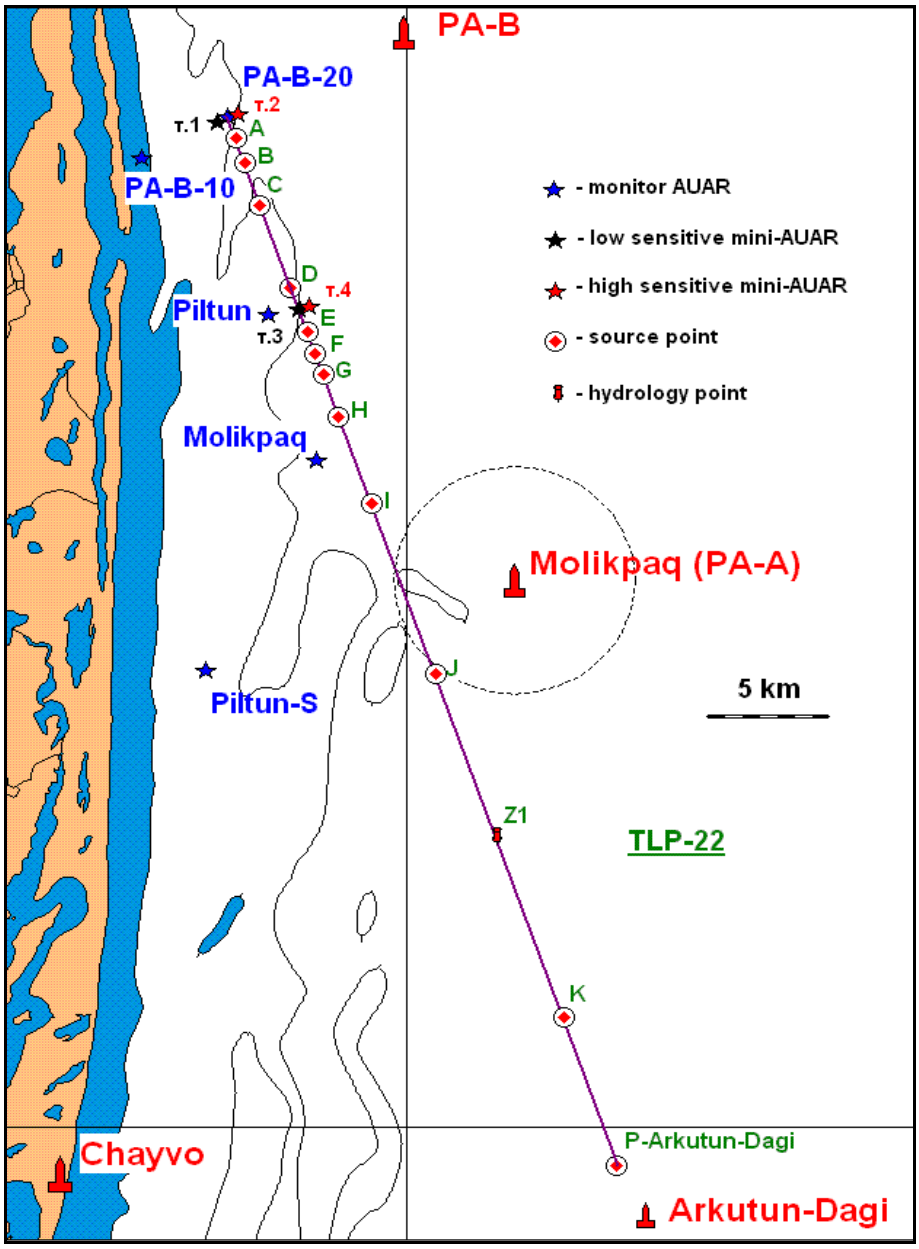

Figure 4.18 - Map of the study area showing the major facilities as well as the AUAR deployment locations for TLP-22 along which frequency dependent TL studies were conducted on 10th-12th August, 2010.

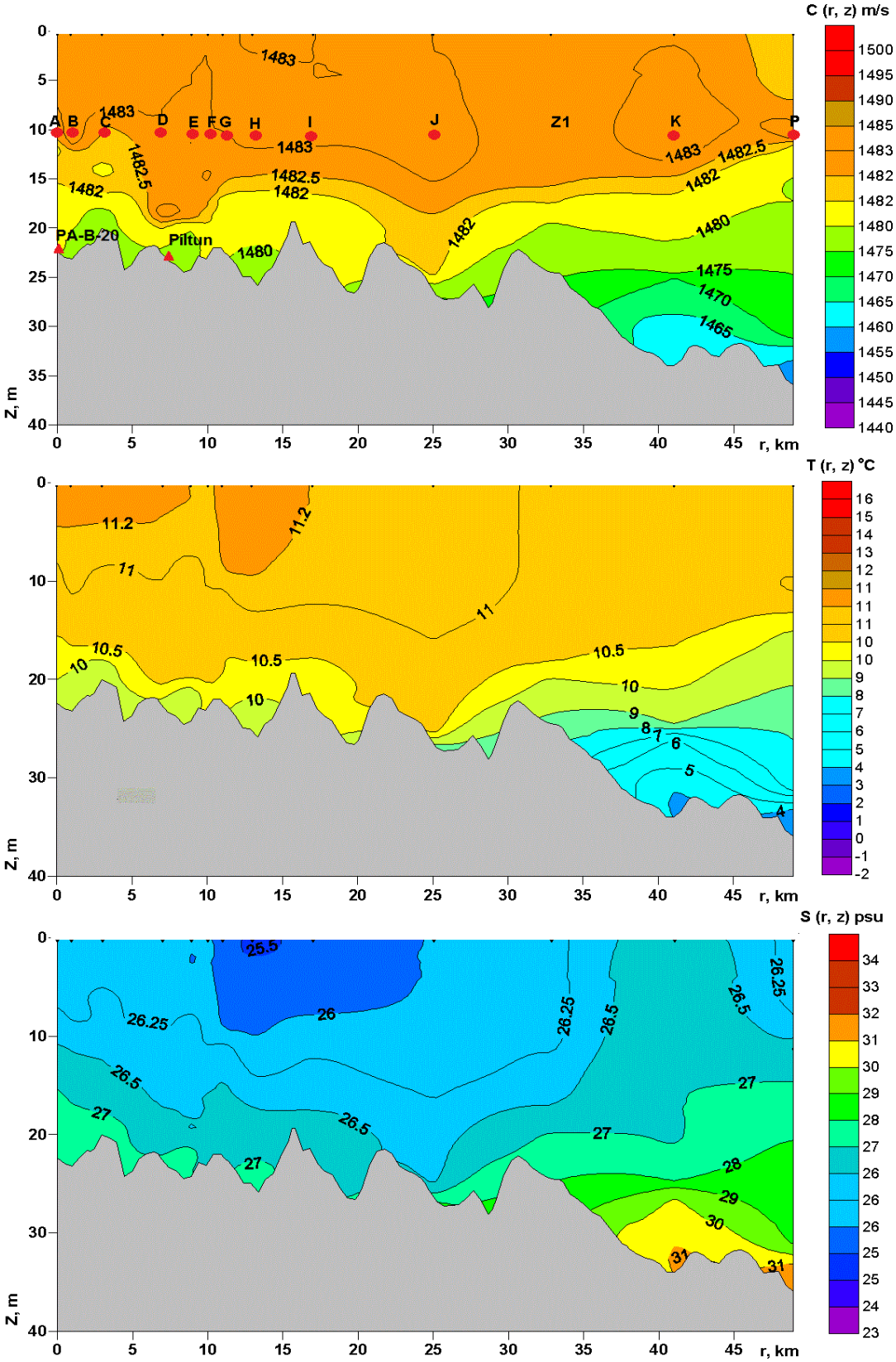

Figure 4.19 - TLP-22: Bathymetry and hydrologic parameters (velocity *C(r,z)*, temperature *T(r,z)*, and salinity *S(r,z)* acquired on 12th September, 2010.

Figure 4.19 shows the bathymetry and the spatial distribution of hydrology along the profile during the acoustic measurements. There are twelve source locations (A, B, C, D, E, F, G, H, I, J, K and L (P-Arkutun-Dagi, 3.5 km from the future Arkutun-Dagi platform location)) along the profile. The source locations are 1 km, 2 km, 4 km, 8 km, 10 km, 11 km, 12 km, 14 km, 18 km, 26 km, 42 km and 49 km respectively from the PA-B-20 location and 3 km, 2 km, 1 km, 2 km, 5 km, 6 km, 8 km, 12 km, 20 km, and 27 km respectively from the Piltun location. Both an AUAR and two mini-AUARs were deployed at the PA-B-20 and Piltun locations, recording while signals were transmitted at the source locations. Figures 4.20 to 4.28 present the TL results obtained from the analysis of the data, acquired over the frequency range from 10 Hz to 15 kHz.

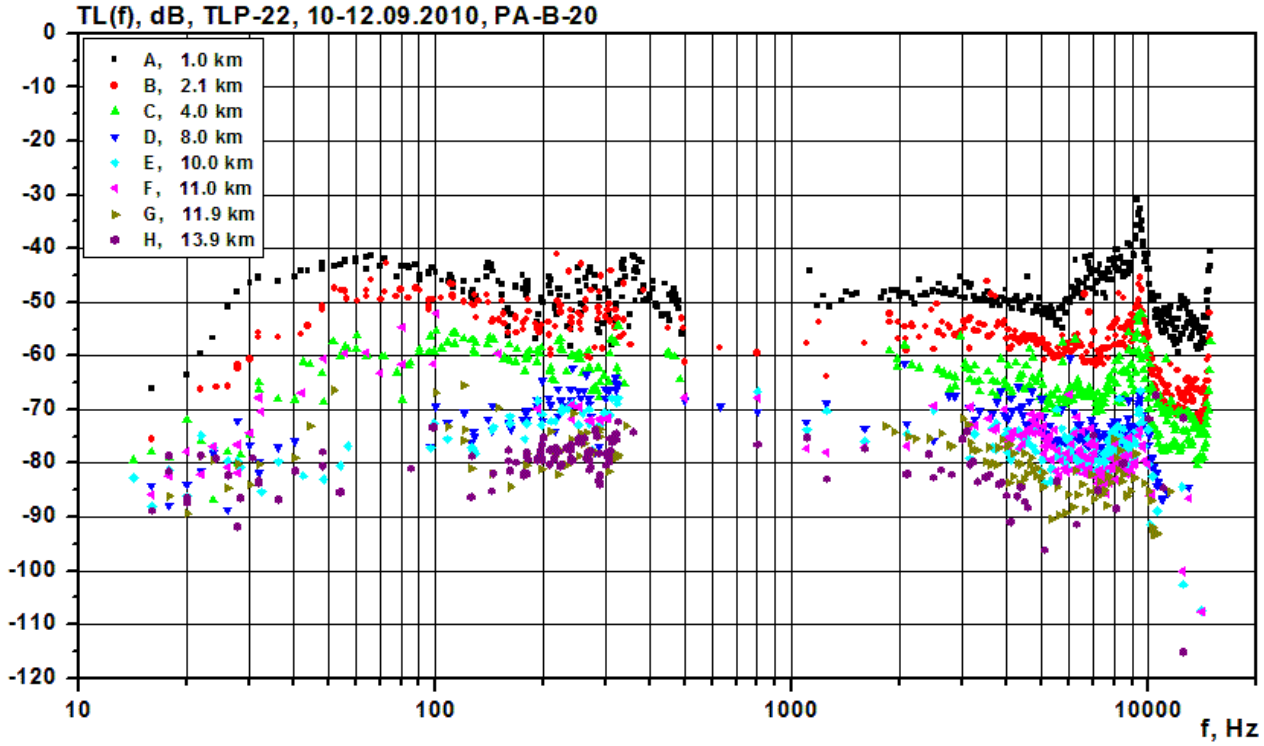

Figure 4.20 - TLP-22: Frequency dependent TL plot showing data for source locations A-H and the distance from the source locations to the PA-B-20 location.

The absence of experimental data for source locations I, J, K and L is explained by the relatively high level of ambient acoustic noise and the low signal levels of HF signals generated at the longest ranges. Further analysis will be attempted in a reduced frequency bin size.

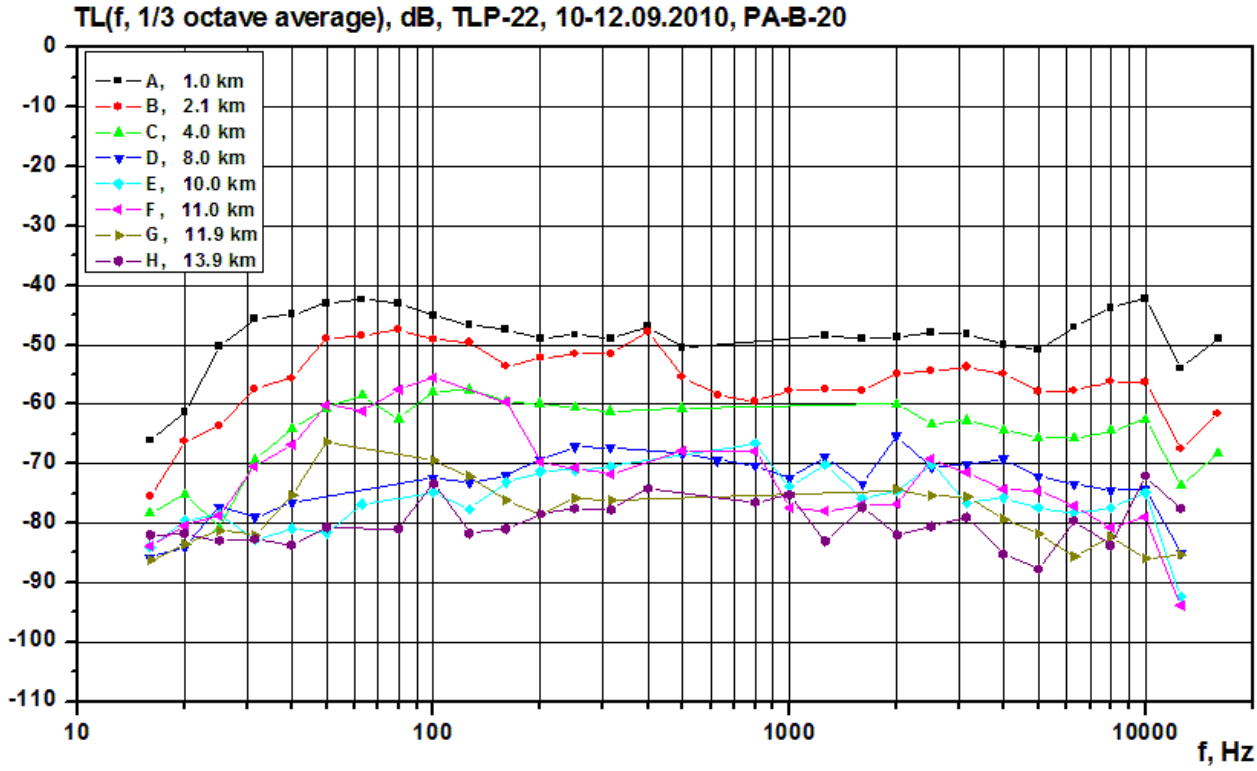

Figure 4.21 - TLP-22: One-third octave averaged frequency dependent TL plot showing the results for source locations A-H and data in Figure 4.20.

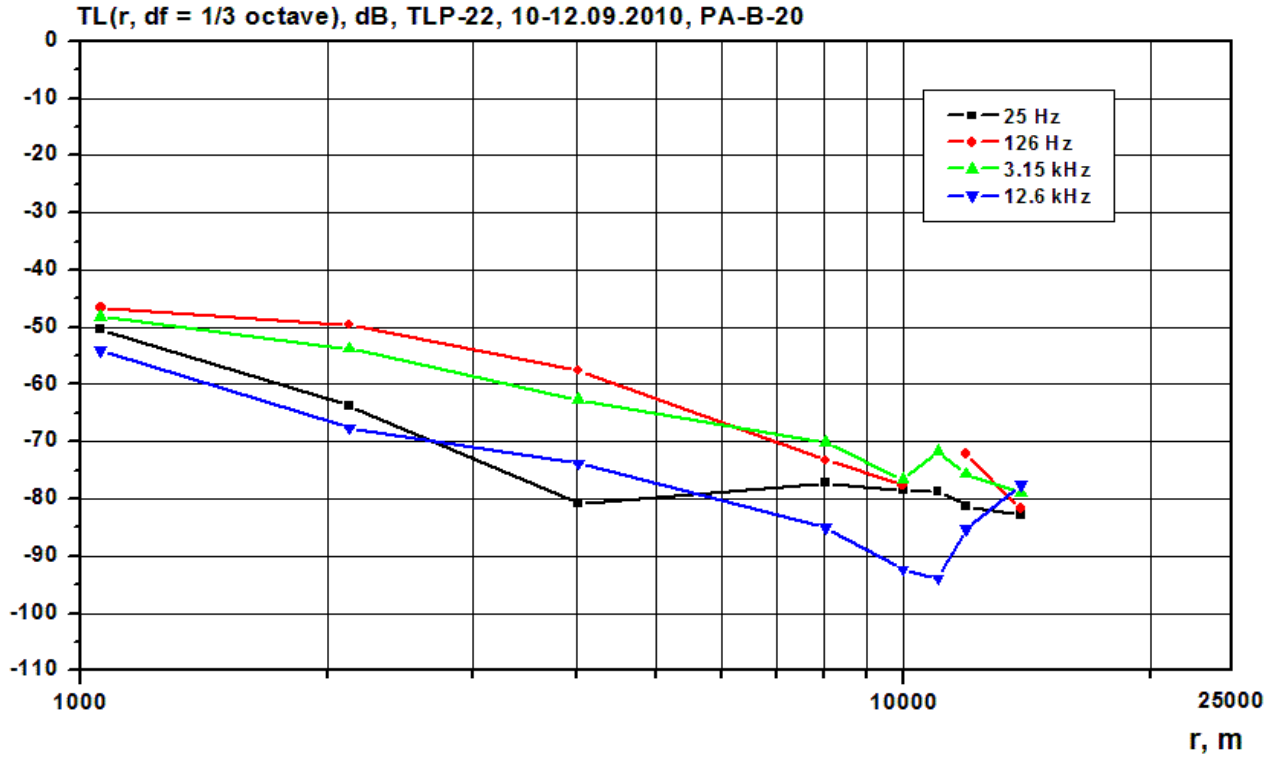

Figure 4.22 - TLP-22: Range dependent one third octave averaged frequency dependent TL plot showing the results for four one third octave frequency bands for the PA-B-20 station.

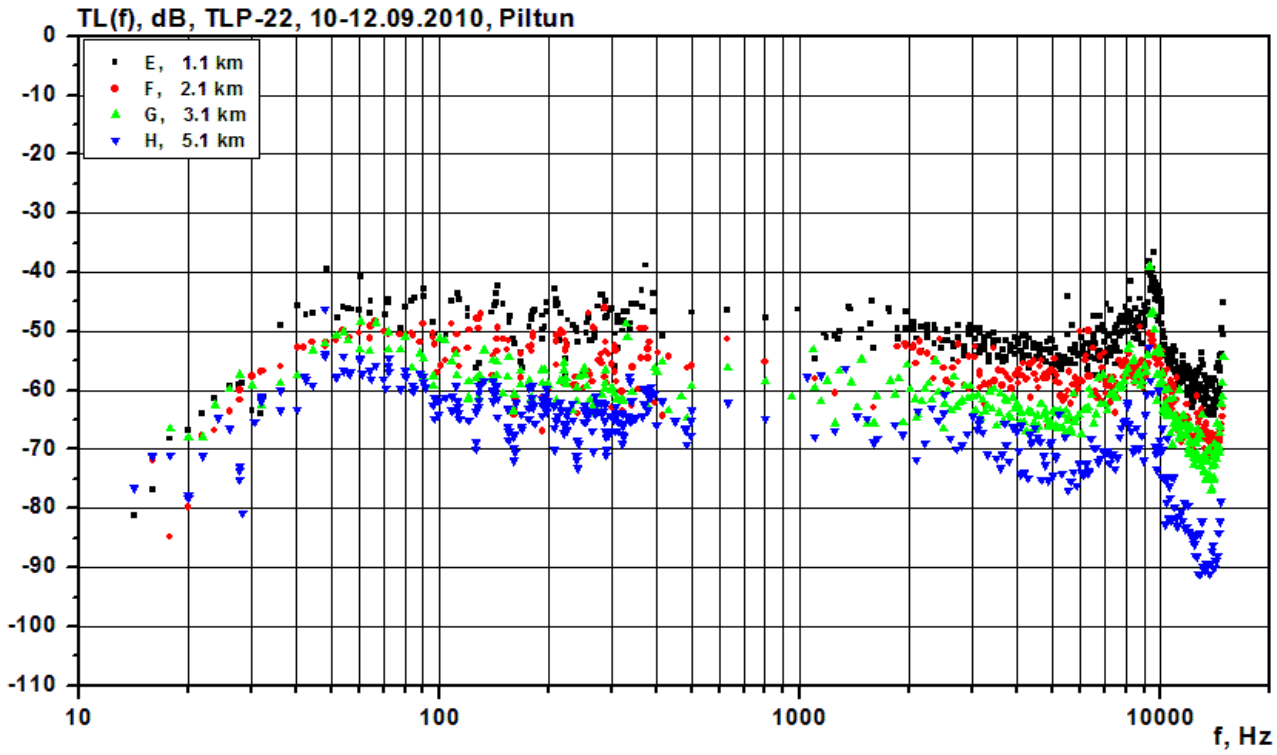

Figure 4.23 - TLP-22: Frequency dependent TL plot showing data for source locations E-H and the distance from the source locations to the Piltun location.

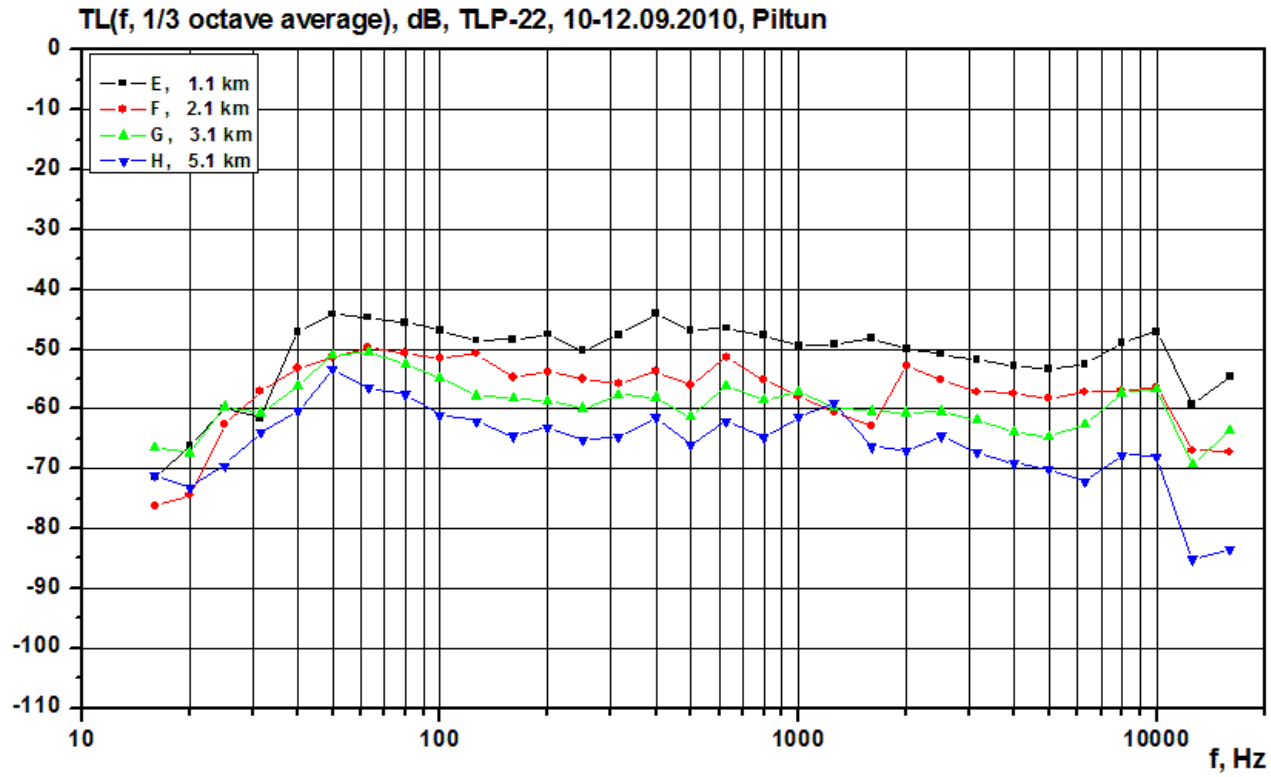

Figure 4.24 - TLP-22: One-third octave averaged frequency dependent TL plot showing the results for source locations E-H and data in Figure 4.23.

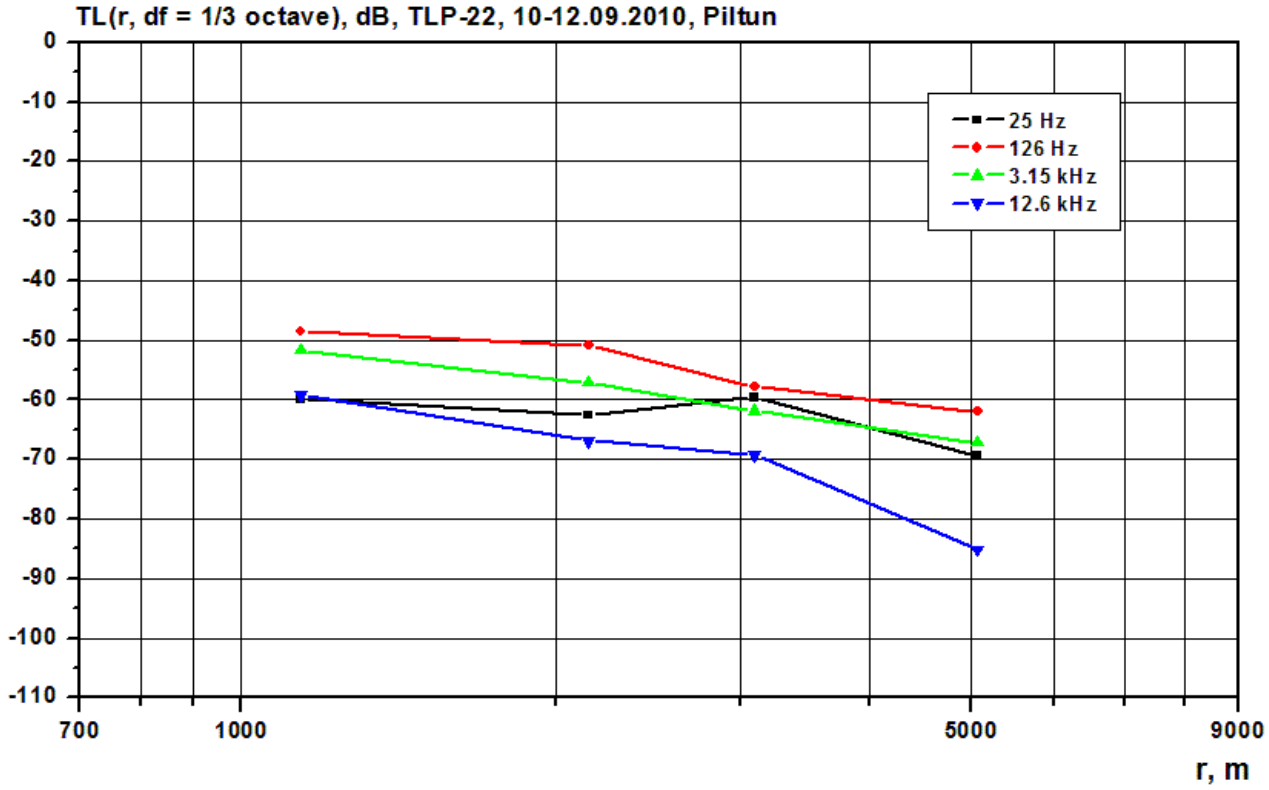

Figure 4.25 - TLP-22: Range dependent one third octave averaged frequency dependent TL plot showing the results for four one third octave frequency bands for the Piltun station.

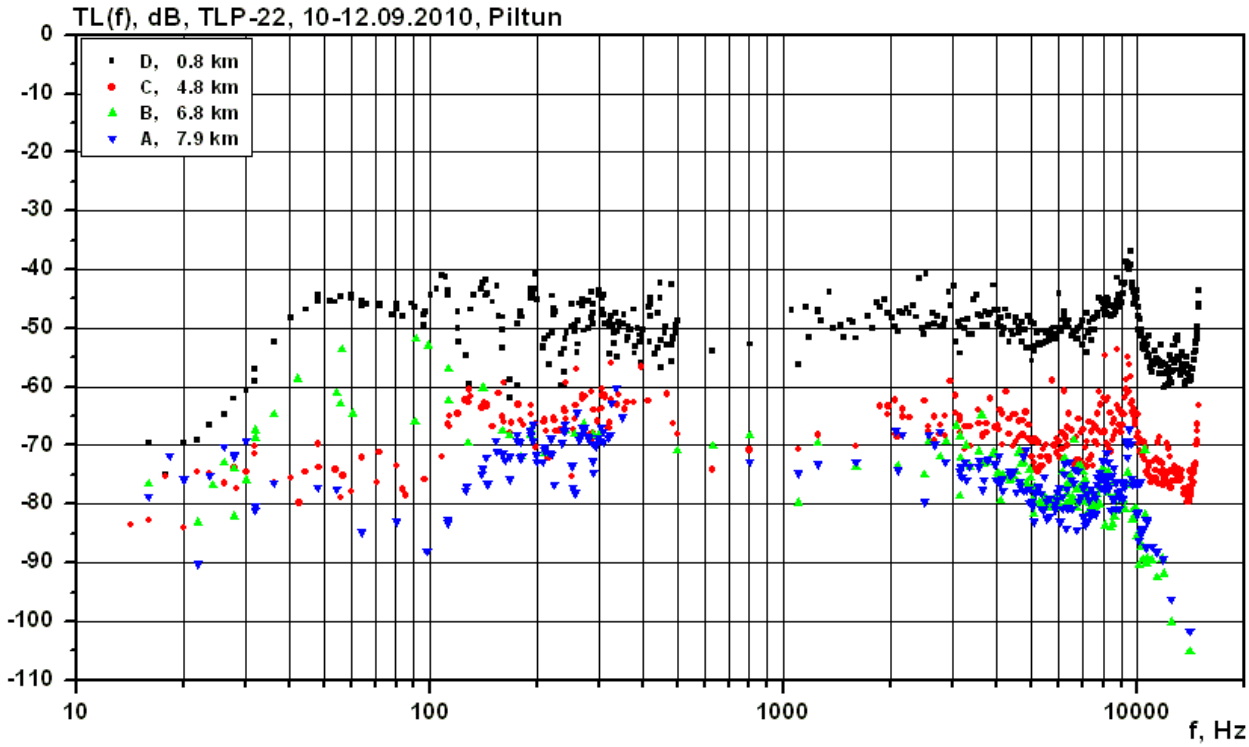

Figure 4.26 - TLP-22: Frequency dependent TL plot showing data for source locations A-D and the distance from the source locations to the Piltun location.

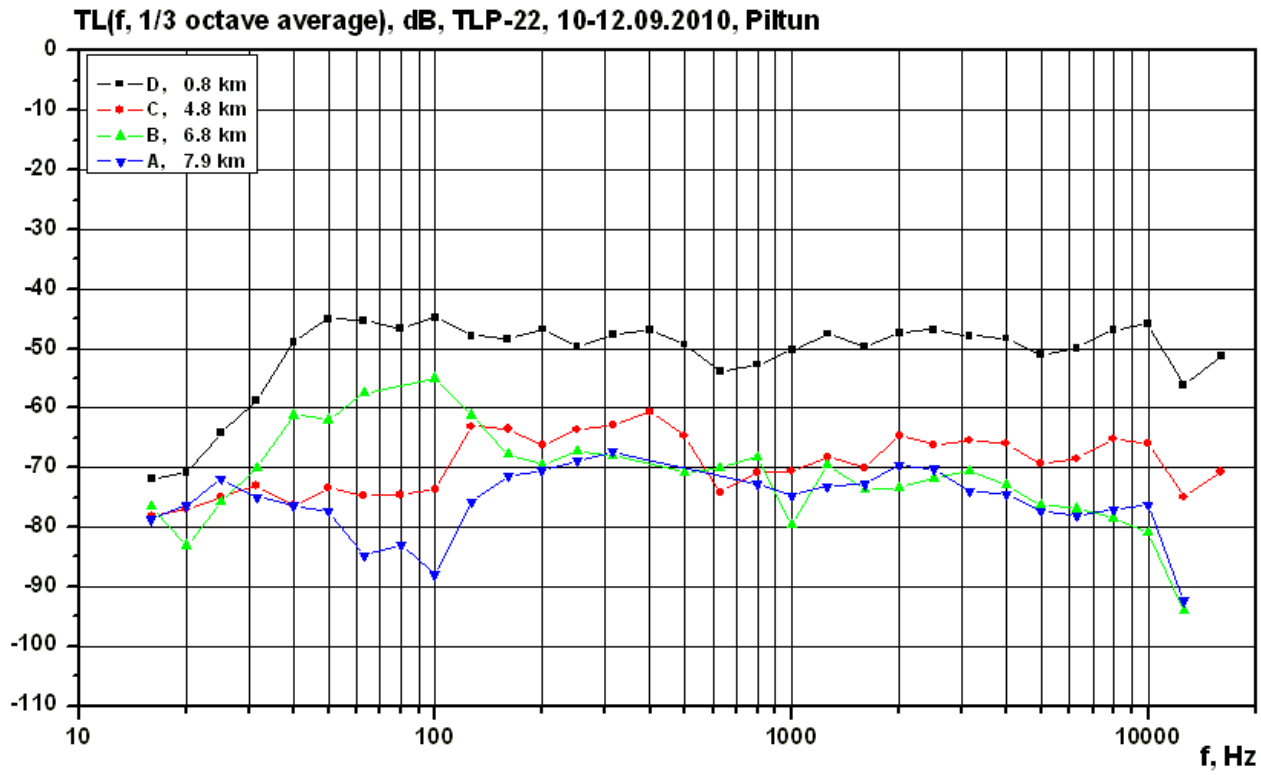

Figure 4.27 - TLP-22: One-third octave averaged frequency dependent TL plot showing the results for source locations A-D and data in Figure 4.26.

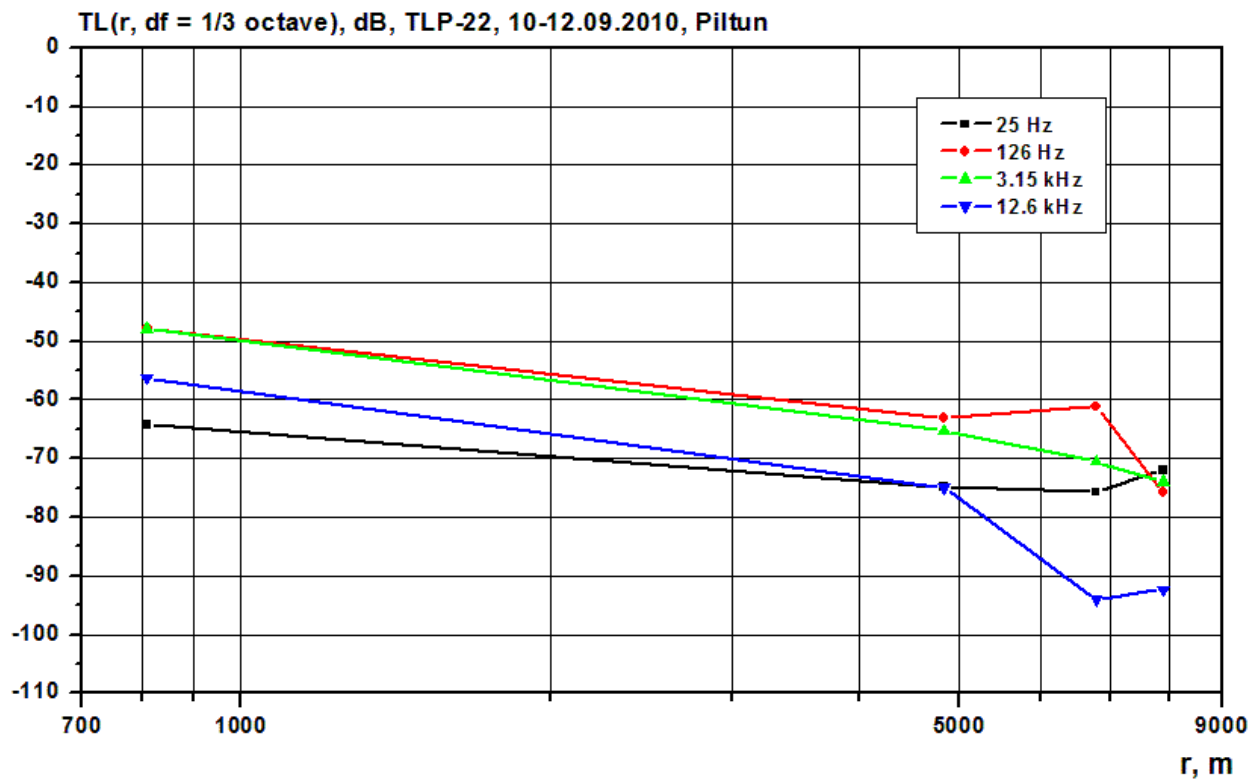

Figure 4.28 - TLP-22: Range dependent one third octave averaged frequency dependent TL plot showing the results for four one third octave frequency bands for the Piltun station.

4.4 Analysis of *TL(r,f)* along point profiles TLP-ADP-B-3 and TLP-ADP-A-5

Figure 4.29 is a map of the study area showing TL profiles TLP-ADP-B-3 and TLP-ADP-A-5. Experimental TL profile TLP-ADP-B3 is 33.3 km long starting at location B along the future Arkutun-Dagi pipeline, and ending at the Molikpaq acoustic station at the eastern edge of the Piltun feeding area. The profile was acquired on 21st August 2010.

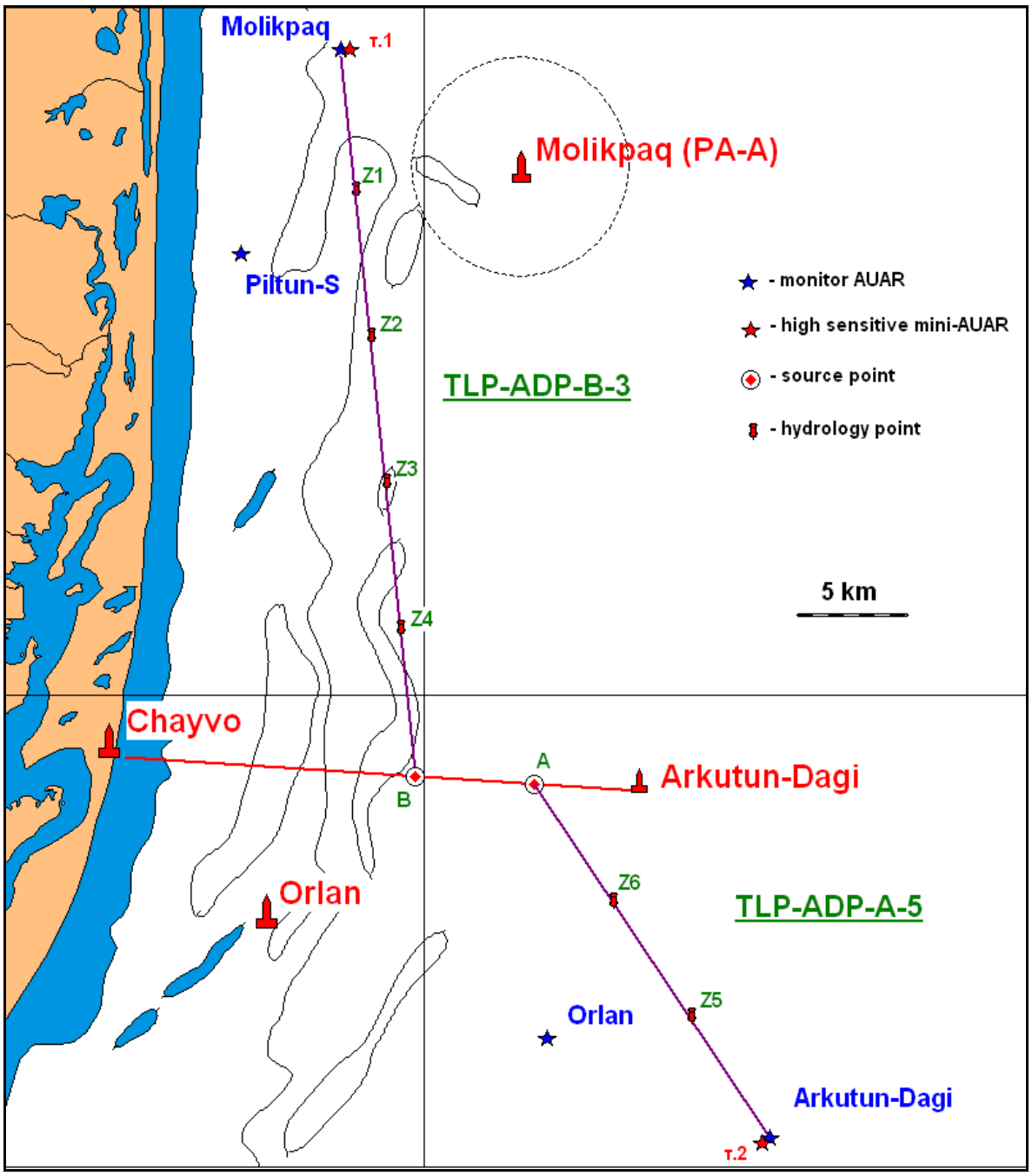

Figure 4.29 - Map of the study area showing the major facilities as well as the AUAR deployment locations for TLP-ADP-B-3 and TLP-ADP-A-5 along which frequency dependent TL studies were conducted on 21st August and 8th September, 2010.

The hydrological conditions along the profile were monitored at the source location and at intermediate locations during the acoustic measurements. Both an AUAR and mini-AUAR were deployed at the Molikpaq location, recording while signals were transmitted at the source location. The recording conditions along this profile were characterized by high ambient noise, probably due to the seismic survey being acquired in the vicinity of the offshore feeding area and thunderstorms. It was therefore difficult to identify and process signals from the *Akademik Oparin* in the acoustic records. It should also be noted that this profile runs through an area with complex bathymetry, especially bathymetric highs near the Molikpaq platform, which inhibit sound transmission (Figure 4.30).

Experimental TL profile TLP-ADP-A5 is 19.4 km long starting at location A along the future Arkutun-Dagi pipeline, and ending at the Arkutun-Dagi acoustic station at the northern edge of the offshore feeding area. The profile was acquired on 8th September 2010.

The hydrological conditions along the profile were monitored at the source location and at intermediate locations Z5 and Z6 during the acoustic measurements. Both an AUAR and mini-AUAR were deployed at the Arkutun-Dagi location, recording while signals were transmitted at the source location. Figure 4.31 shows the bathymetry and the spatial distribution of hydrology along the profile during the acoustic measurements. Figures 4.32 and 4.33 present the TL results obtained from the analysis of the data, acquired over the frequency range from 10 Hz to 15 kHz.

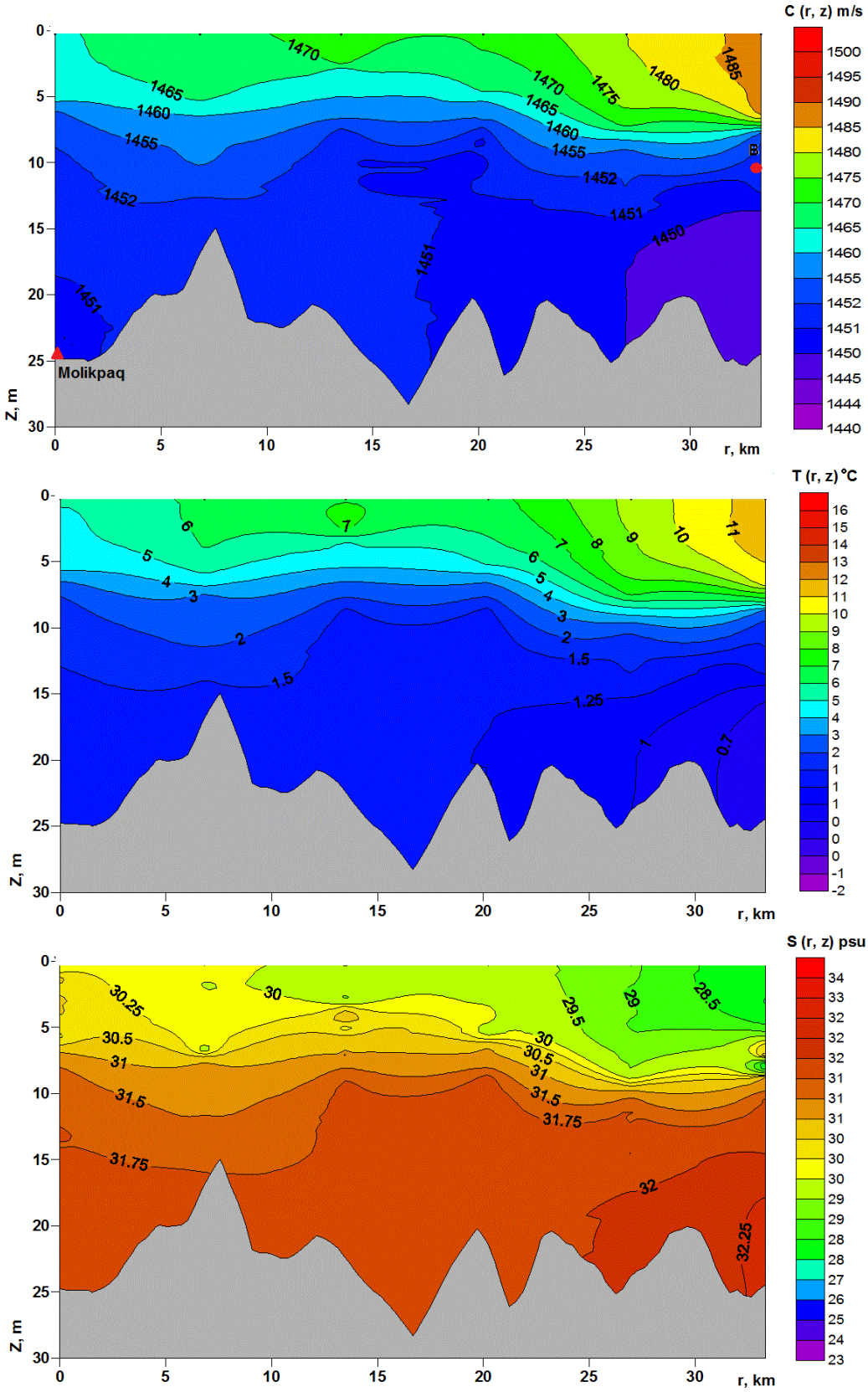

Figure 4.30 - TLP-ADP-B3: Bathymetry and hydrologic parameters (velocity *C(r,z)*, temperature *T(r,z)*, and salinity *S(r,z)* acquired on 21st August, 2010.

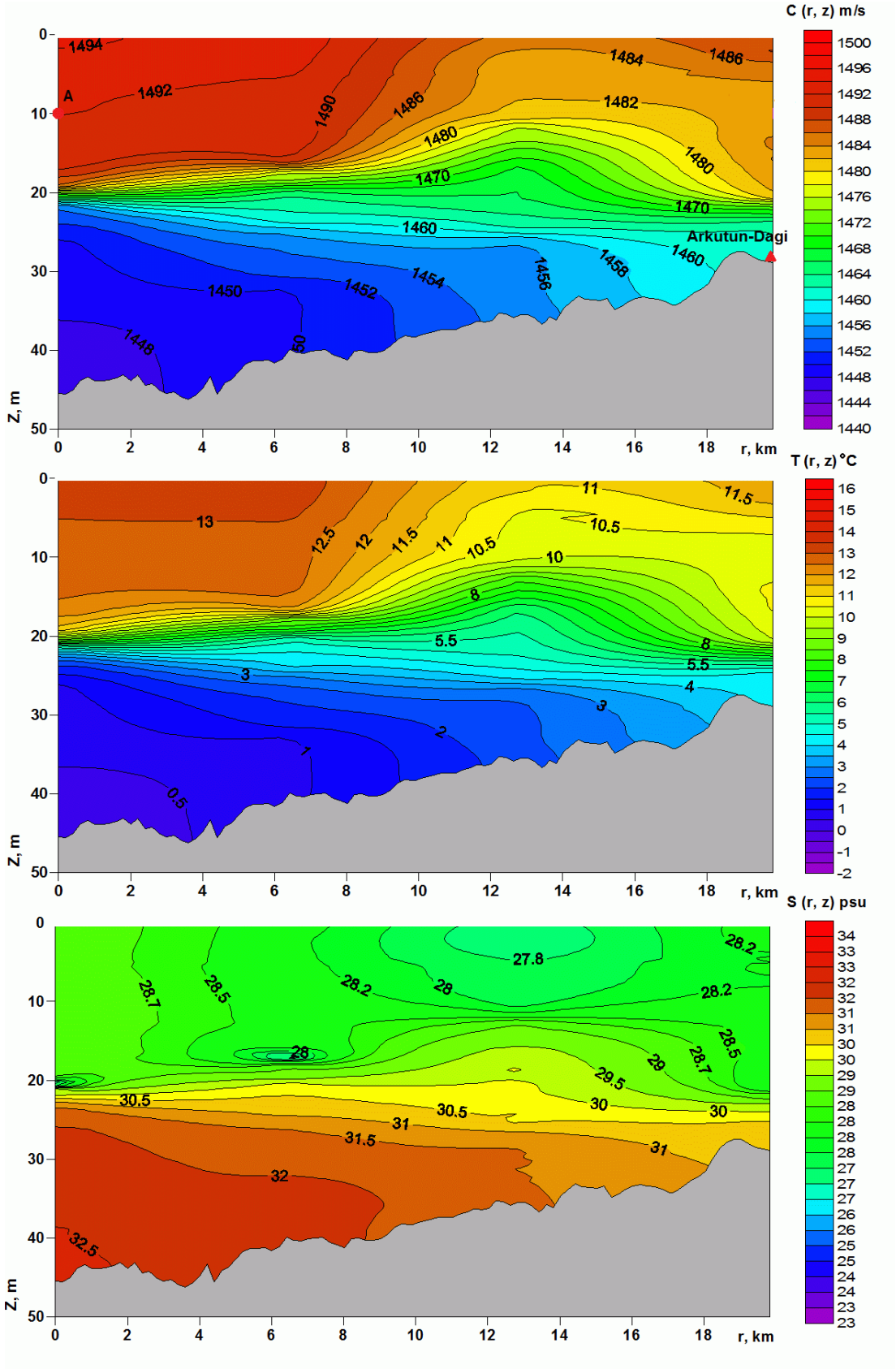

Figure 4.31 - TLP-ADP-A5: Bathymetry and hydrologic parameters (velocity *C(r,z)*, temperature *T(r,z)*, and salinity *S(r,z)* acquired on 9th September, 2010.

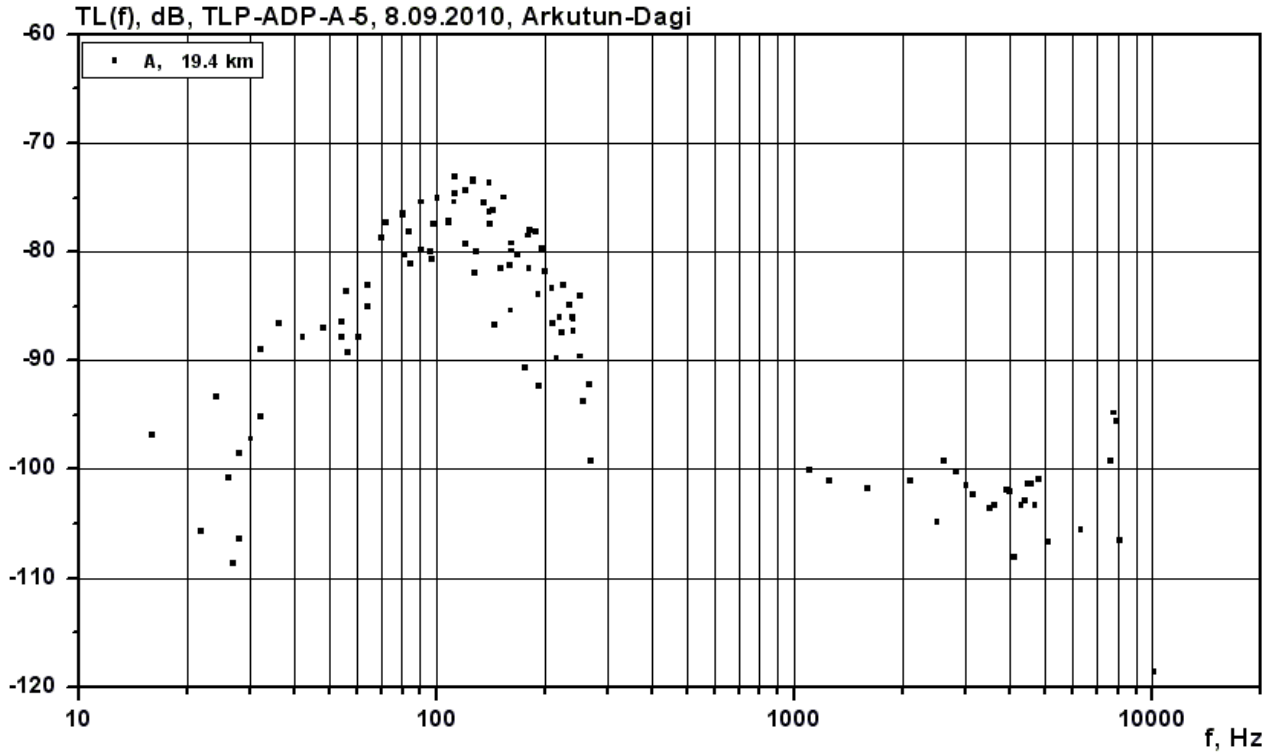

Figure 4.32 - TLP-ADP-A5: Frequency dependent TL plot showing data for source location A and the distance from the source locations to the Arkutun-Dagi location.

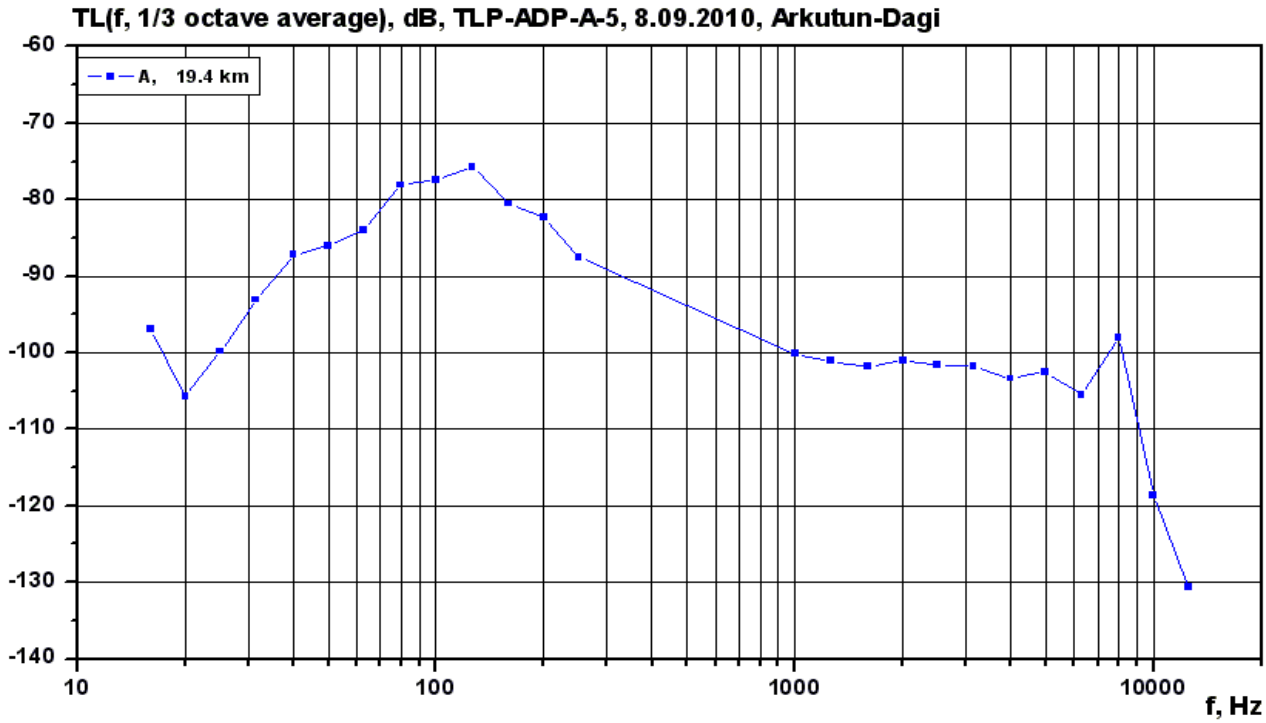

Figure 4.33 - TLP-22: One-third octave averaged frequency dependent TL plot showing the results for source location A and data in Figure 4.32.

5 Acoustic measurements of noise from the jet drive boat and Photo-ID zodiac

A satellite tagging program was conducted from the *Igor Maximov* in September 2010 using a jet-drive boat as the tagging vessel (Figure 5.1). At the request of the tagging team comparative field measurements of the noise generated by the jet-drive RHIB used by the satellite tagging team and the Photo-ID zodiac (Figure 5.2) used by the gray whale Photo-ID team based on the *Akademik Oparin* were acquired in the vicinity of the PA-B-20 station on 12th September, 2010.

Figure 5.1 – Picture of the jet-drive RHIB used by the satellite-tagging team.

Figure 5.3 gives a map of the area showing the location where the acoustic noise generated by the jet-drive boat and zodiac moving at a variety of speeds was measured.

The acoustic noise field in the frequency band from 2 Hz to 15 kHz was measured using two mini-AUARs: a high-sensitivity mini-AUAR (#14) (gain=38; sensitivity=48 mV/Pa; overdrive

sound level=127 dB re 1 μPa), and a low-sensitivity mini-AUAR (#23) (gain=2; sensitivity=9.8 mV/Pa; saturation level=166 dB re 1 μPa), installed at 20 m depth. Mini-AUAR#14 was 900 m east of mini-AUAR#23. An additional monitoring station, AUAR#21 (gain=8; sensitivity=50 mV/Pa; saturation level=140 dB re 1 μPa) was situated between the two mini-AUARs.

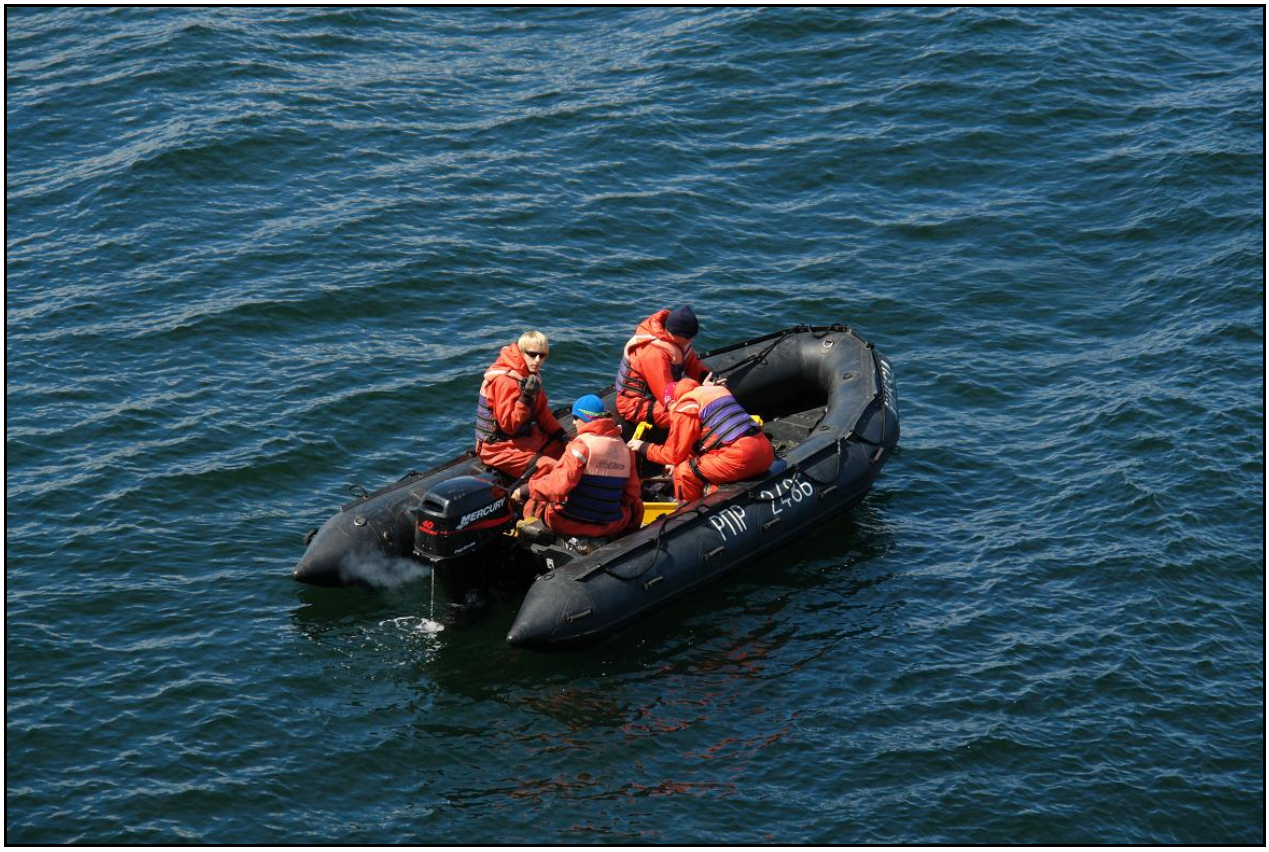

Figure 5.2 – Picture of zodiac used by the Photo-ID team.

The acoustic data were recorded by the mini-AUARs and AUAR in two stages:

1. From 11:55 am to 1:41 pm the jet-drive boat sailed a pre-arranged track at a number of pre-defined speeds.
2. From 2:23 pm to 4:13 pm the zodiac sailed the same route at the same pre-defined speeds.

During the experiments the *Igor Maximov* drifted southwards with its engine turned off more than 2 miles southwest of the experimental location. The *Akademik Oparin* drifted in the same direction more than 8 miles south of the experimental location with its engine idling.

Figures 5.4, 5.5, 5.10 and 5.11 display sonograms of the acoustic signals recorded by the mini-AUARs; these sonograms show that acoustic noise in the frequency range from 200 Hz to 2 kHz was approximately 10-20 dB higher during the jet-drive boat movements than during the zodiac

movements along the same track at the same speed.

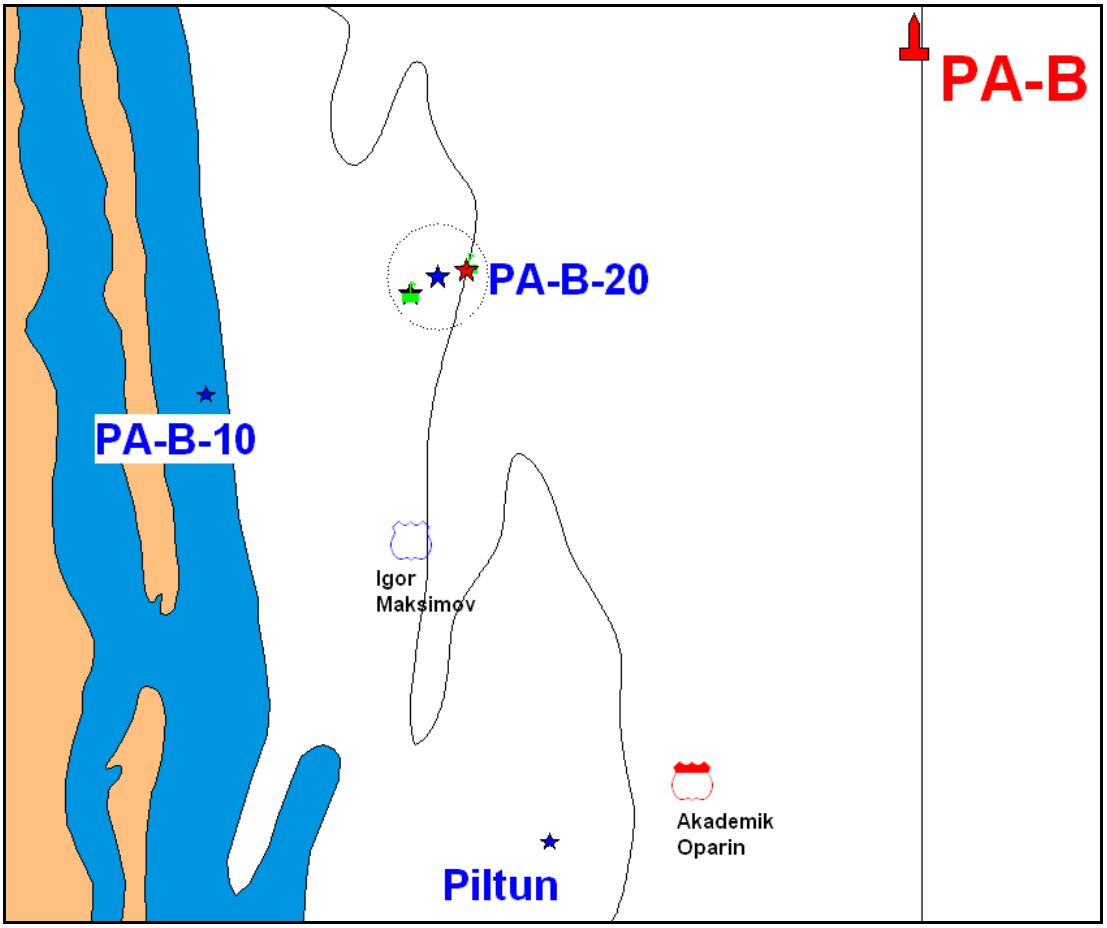

Figure 5.3 - Map of the study area with the locations where the acoustic output of the satellite tagging jet-drive boat and Photo-ID zodiac were measured.

The acoustic time series from mini-AUAR#14 indicates that clipping occurred in the analog channel when the jet-drive boat moved at a high speed and when the Photo-ID zodiac was less than 200 m away from the station. However, there was no clipping at speeds of < 2 knots. Figures 5.6 to 5.9 show the planned tracks of the jet-drive boat and Photo-ID zodiac for four different speeds:

For the jet-drive boat:

1. Sail consistently at 2 knots
2. Sail consistently at 6-7 knots
3. Sail consistently at 13-15 knots
4. Sail with an acceleration from 2 to 6 knots in 26 s near mini-AUAR#23 and AUAR#21.
5. Sail with an acceleration from 2.5 to 7 knots in 14 s near mini-AUAR#23 and AUAR#21.
6. Sail with an acceleration from 2 to 7 knots in 11 s near mini-AUAR#23 and AUAR#21.

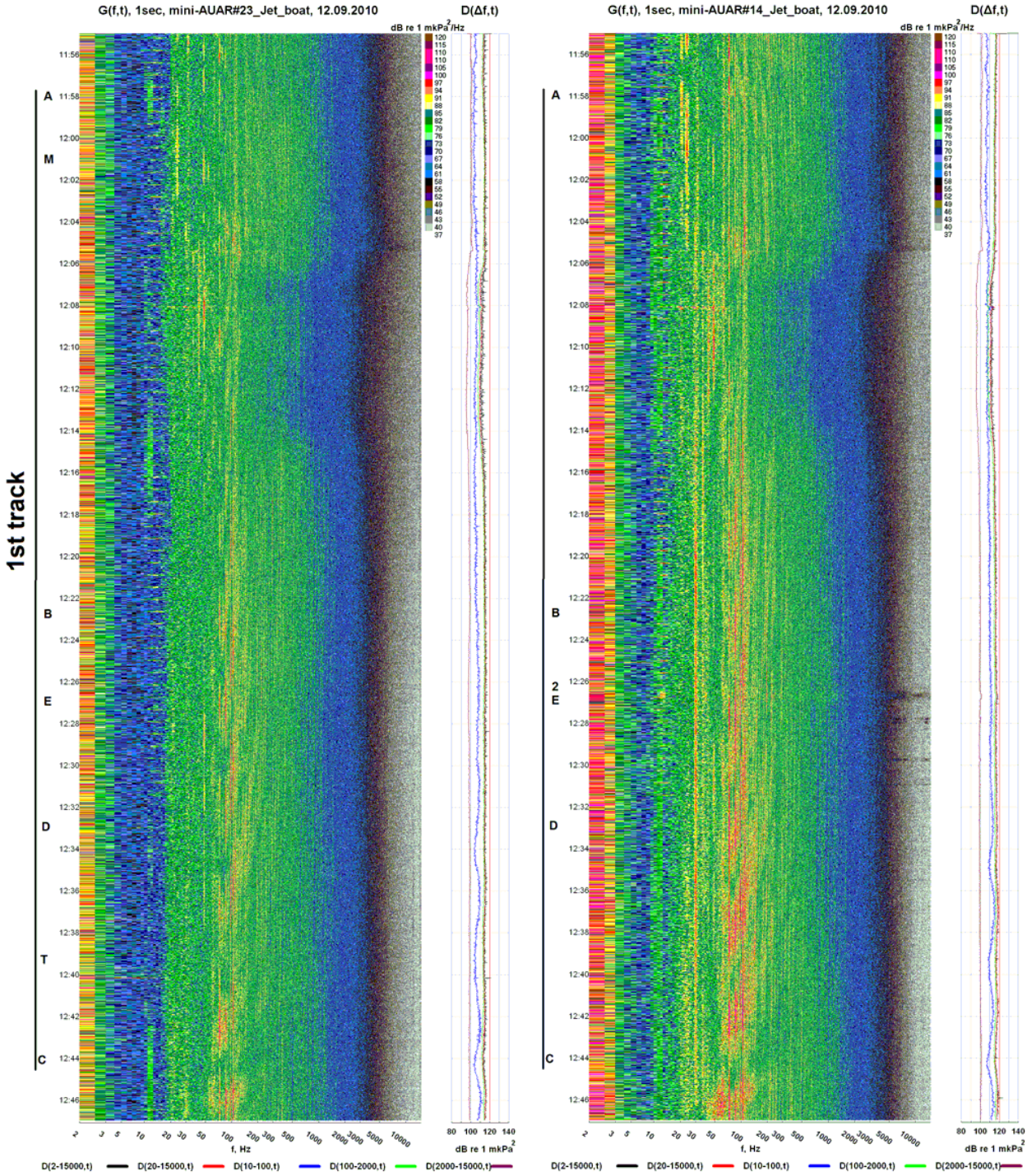

Figure 5.4 - Sonogram *G(f,t)* and of acoustic signals recorded by mini-AUAR#23 (left) and mini-AUAR#14 (right) when the jet-drive boat sailed the first track. The letters designate moments in time when the jet-drive boat passed the points shown in Figure 5.6.

For the Photo-ID zodiac:

1. Sail consistently at 2-3 knots
2. Sail consistently at 18-23 knots
3. Sail consistently at 6-15 knots
4. Sail with an acceleration from 2 to 14 knots in 30 s near mini-AUAR#23 and AUAR#21.
5. Sail with an acceleration from 2 to 17 knots in 9 s near mini-AUAR#23 and AUAR#21.

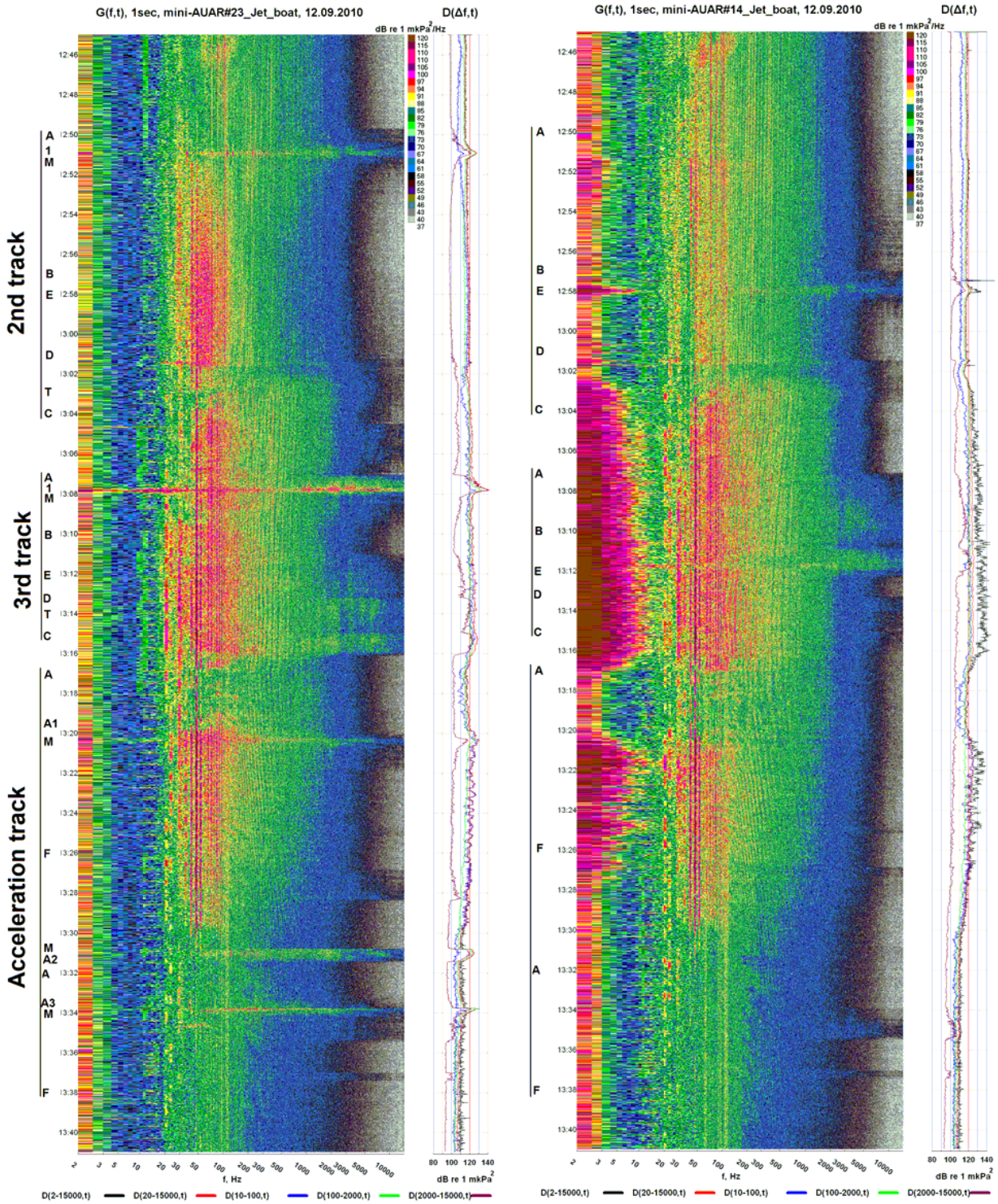

Figure 5.5 - Sonogram G(f,t) and of acoustic signals recorded by mini-AUAR#23 (left) and mini-AUAR#14 (right) when the jet-drive boat sailed the second and third tracks and the acceleration track. The letters designate moments in time when the jet-drive boat passed the points shown in Figure 5.6 and 5.7. The data recorded by mini-AUAR#14 is distorted due to clipping in its analog channel

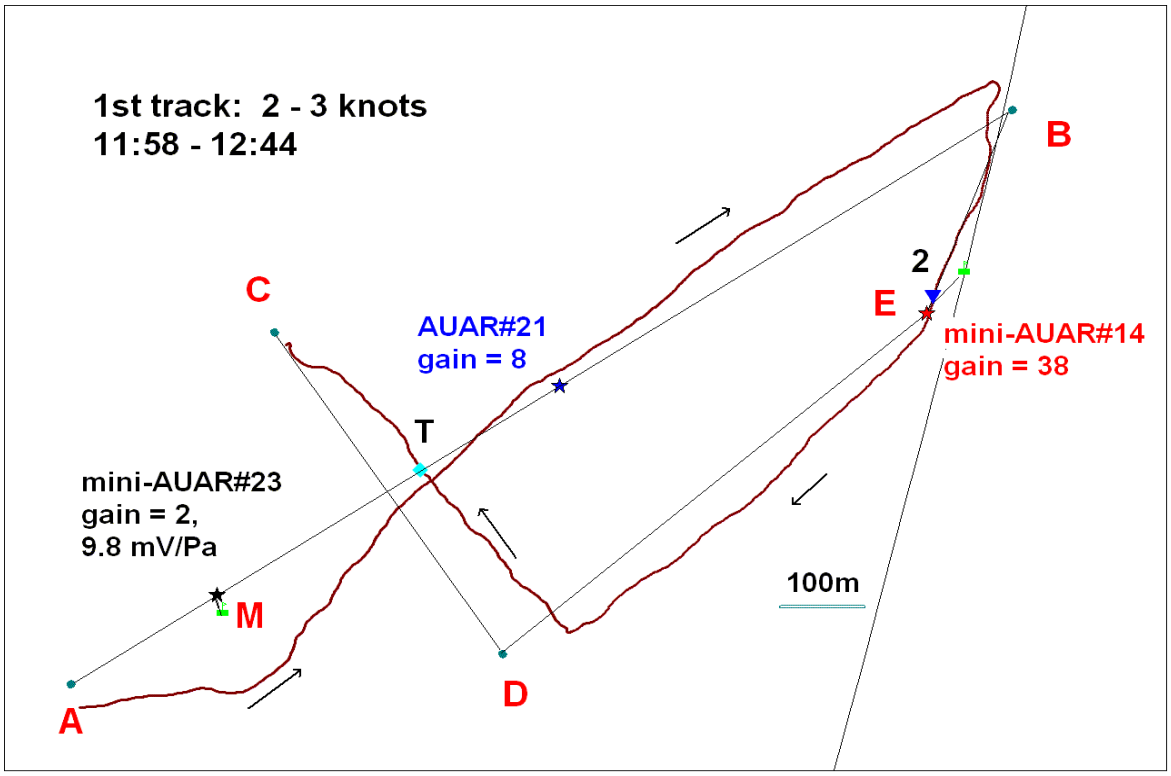

Figure 5.6(a) – First track of the jet-drive boat (uniform speed of 2-3 knots). Spectra are calculated for points 2 & T.

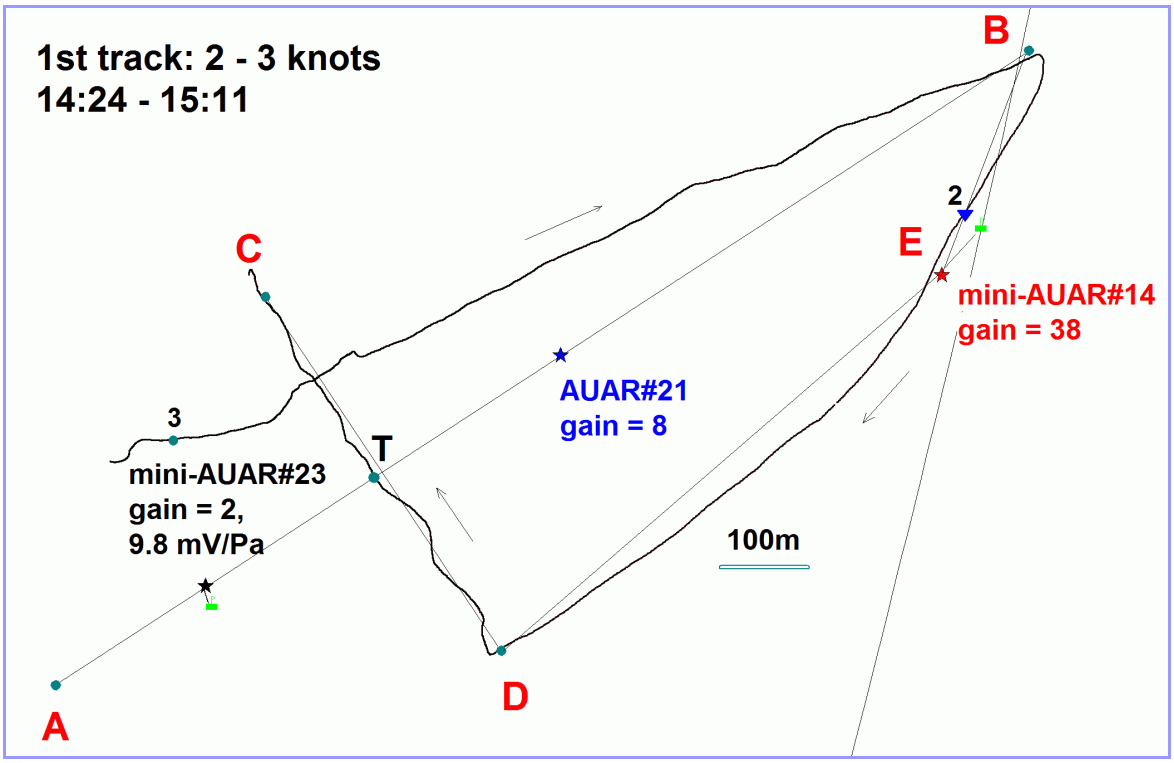

Figure 5.6(b) – First track of the Photo-ID zodiac (uniform speed of 2-3 knots). Spectra are calculated for points 2, 3 & T.

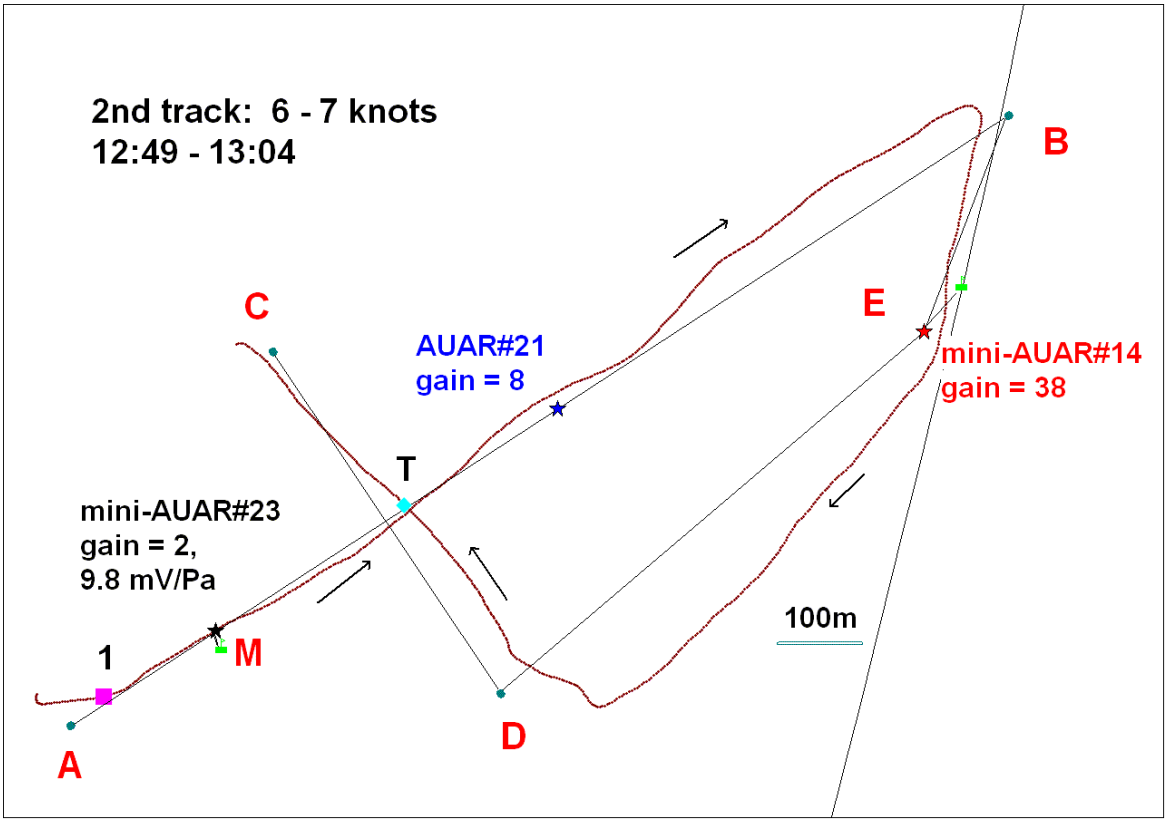

Figure 5.7(a) – Second track of the jet-drive boat (uniform speed of 6-7 knots). Spectra are calculated for points 1 & T.

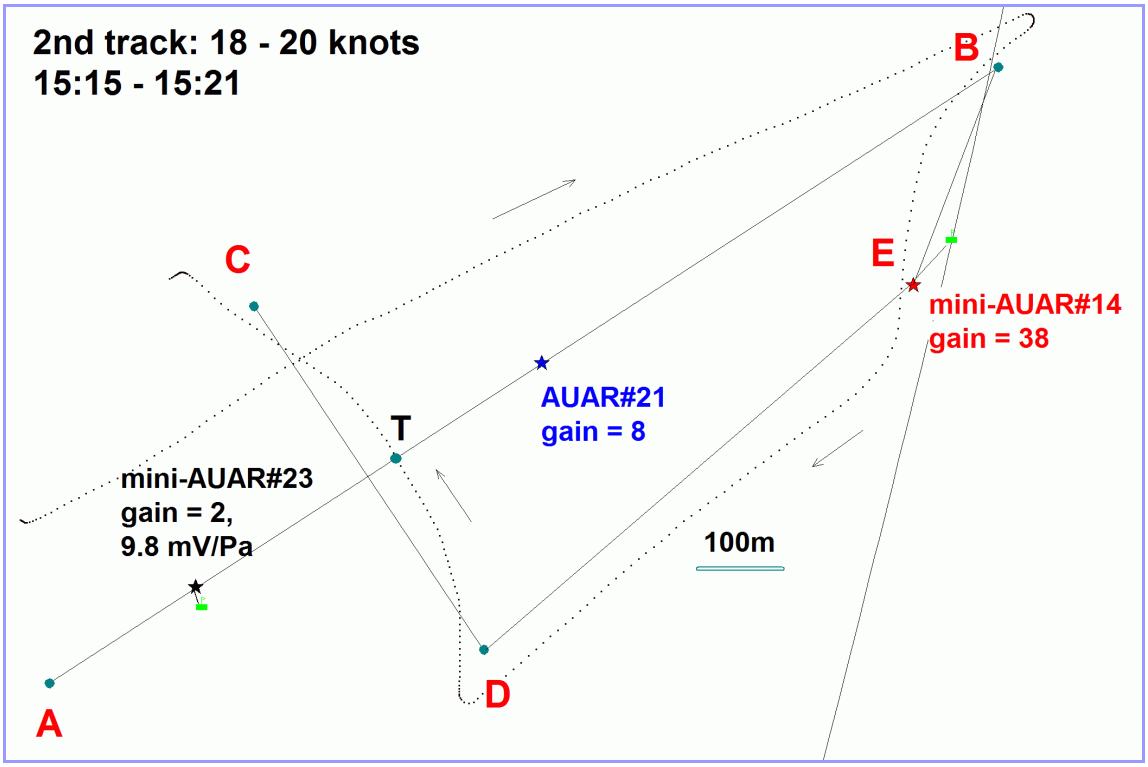

Figure 5.7(b) – Second track of the Photo-ID zodiac (uniform speed of 18-20 knots). Spectra are calculated for point T.

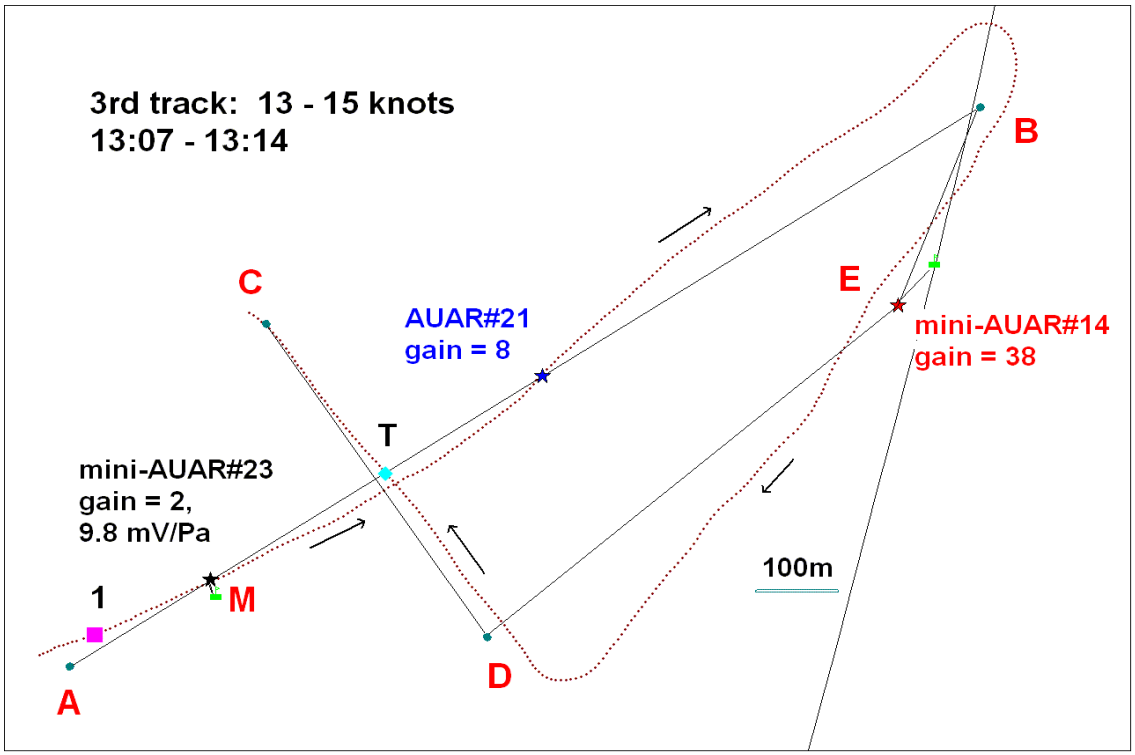

Figure 5.8(a) – Third track of the jet-drive boat (uniform speed of 13-15 knots). Spectra are calculated for points 1 & T.

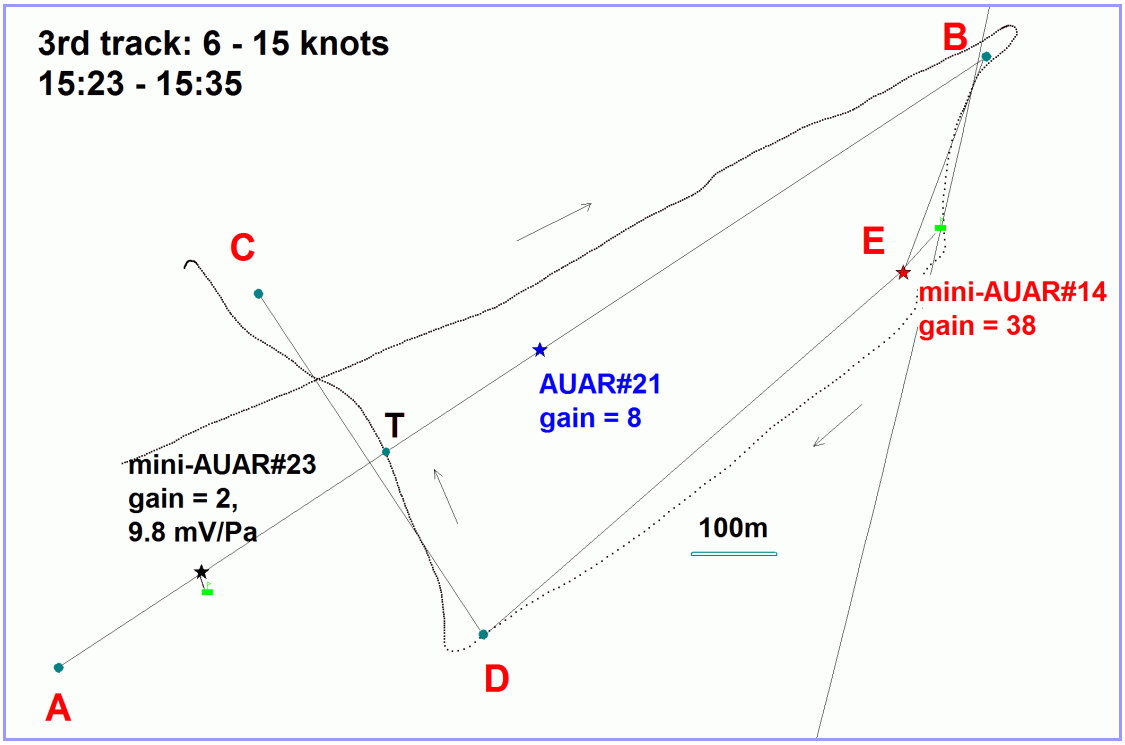

Figure 5.8(b) – Third track of the jet-drive boat and Photo-ID zodiac (uniform speed of 13-15 knots). Spectra are calculated for point T.

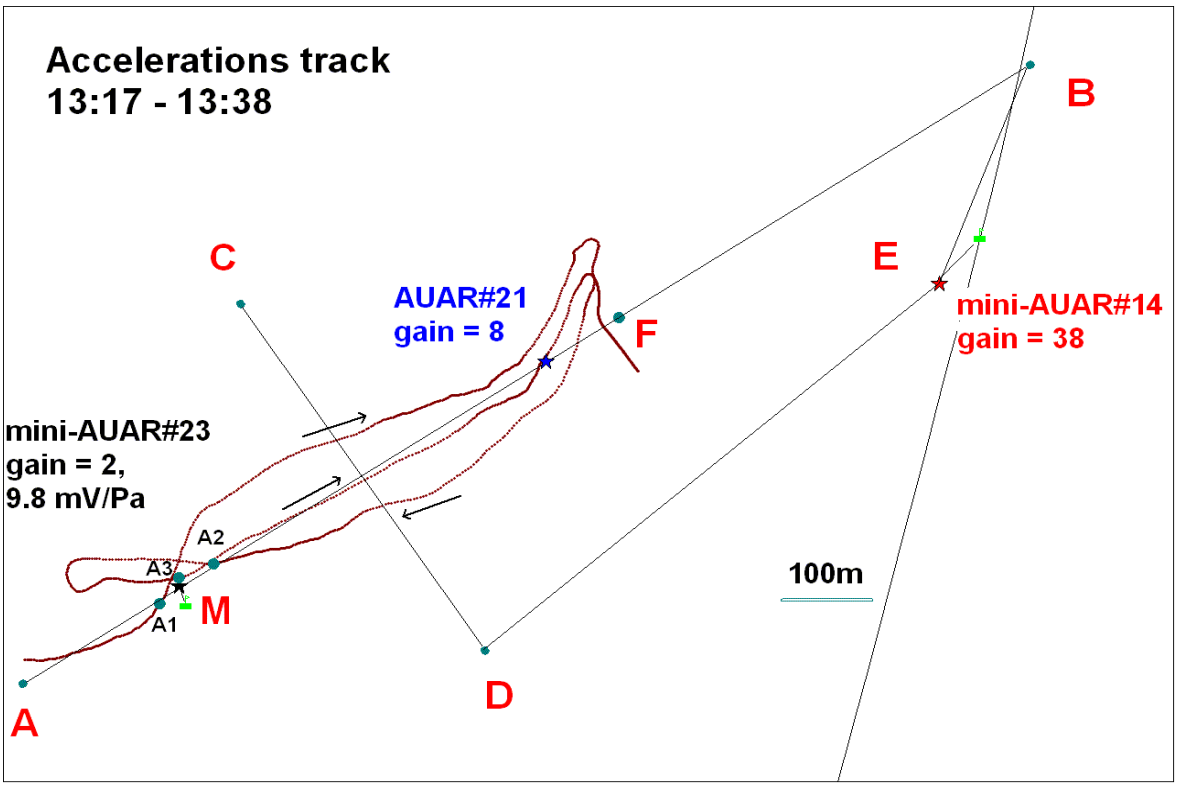

Figure 5.9(a) – Acceleration track of the jet-drive boat. Spectra are calculated for points A1, A2 and A3.

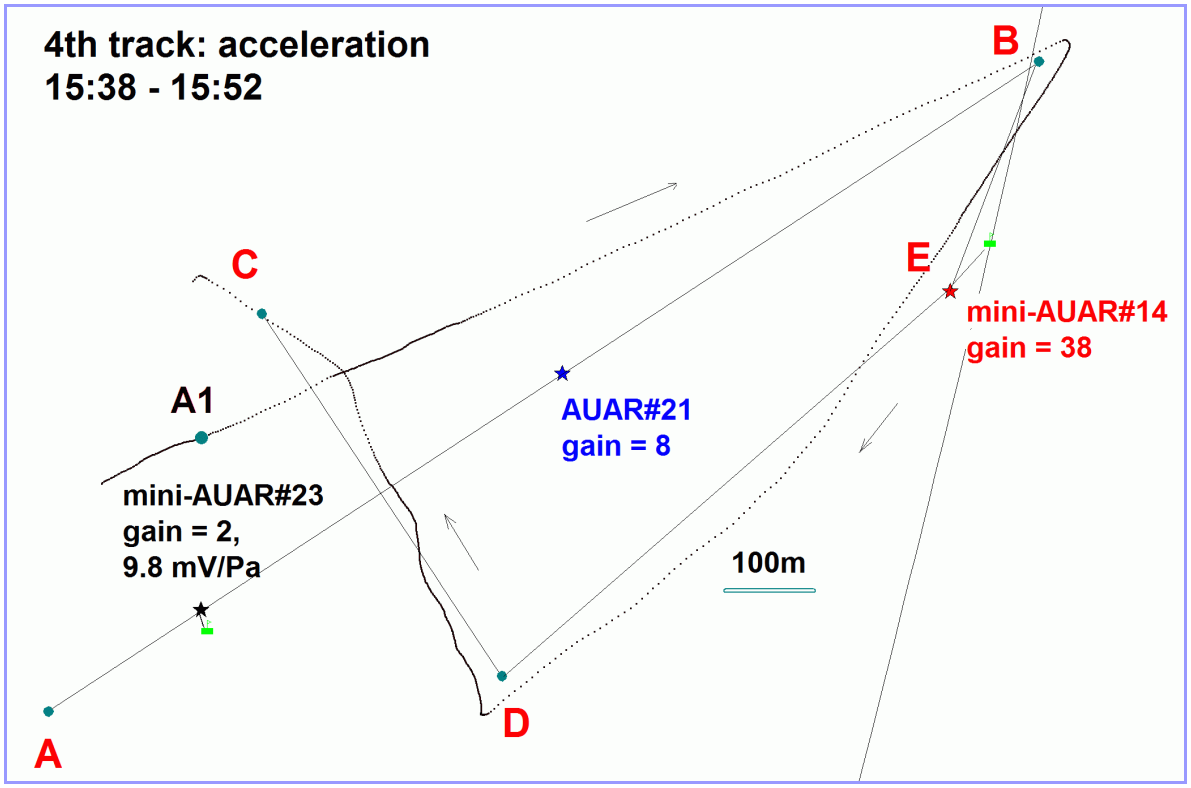

Figure 5.9(b) – Acceleration track of the Photo-ID zodiac. Spectra are calculated for point A1.

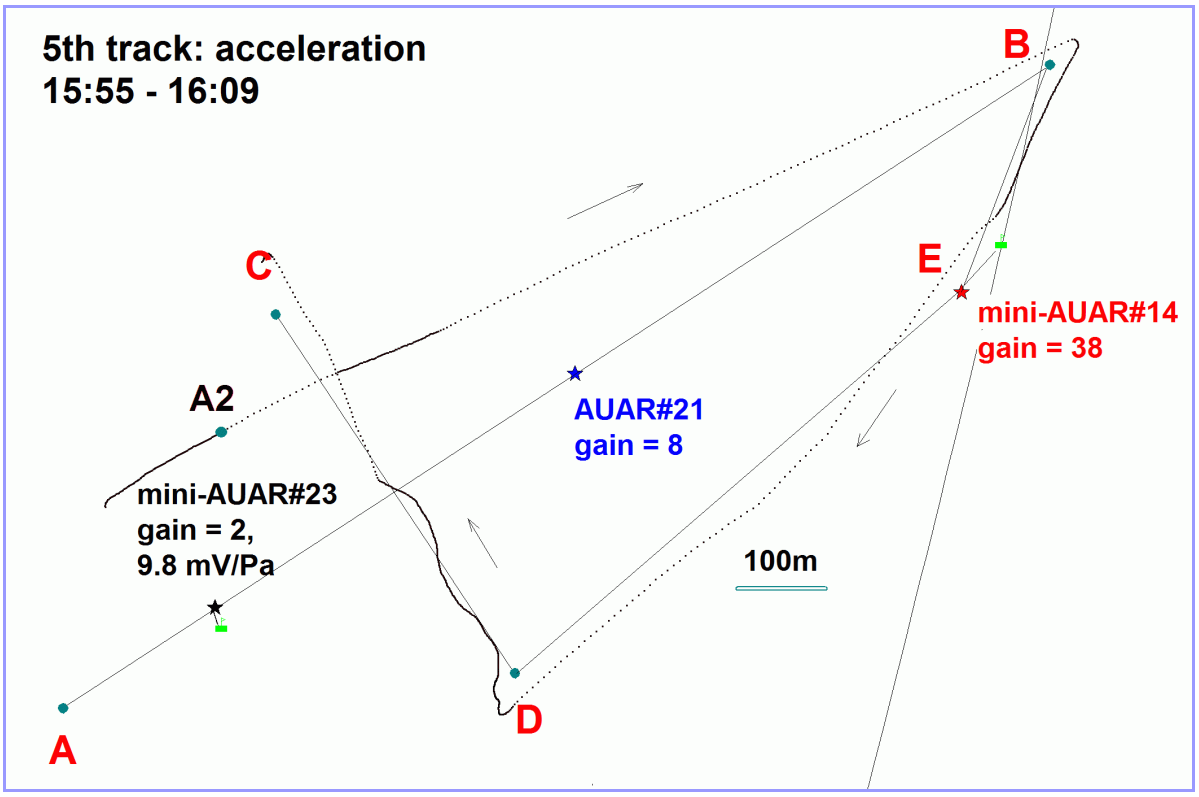

Figure 5.9(c) – Fifth acceleration track of the Photo-ID zodiac. Spectra are calculated for point A2.

Unfortunately, due to a navigation error, the starting point of all the Photo-ID zodiac tracks was shifted 200 m north of A, the planned location. Therefore, our ability to directly compare the noise characteristics of the jet-drive boat and Photo-ID zodiac is limited. Where possible similar ranges are selected for the analysis.

Figures 5.12 and 5.13 show power spectral density spectra *G(f)* calculated for the first track (uniform motion of the jet-drive boat and Photo-ID zodiac at 2 knots). The vessels sailed towards mini-AUAR#14 at a distance of 50 m (Figure 5.12) and moved perpendicular to the A-B line while mini-AUAR#23, which recorded the noise, was abeam the boat at a distance of 250-300 m on the port side (Figure 5.13). These spectra are 20 second spectral averages. It can be seen that the noise from the Photo-ID zodiac during this experiment is 5 to 10 dB lower than the noise from the jet-drive boat across the entire frequency range. The three narrow-band power peaks in the 100-200 Hz frequency range for the Zodiac spectrum are attributed to engine vibrations at low speeds.

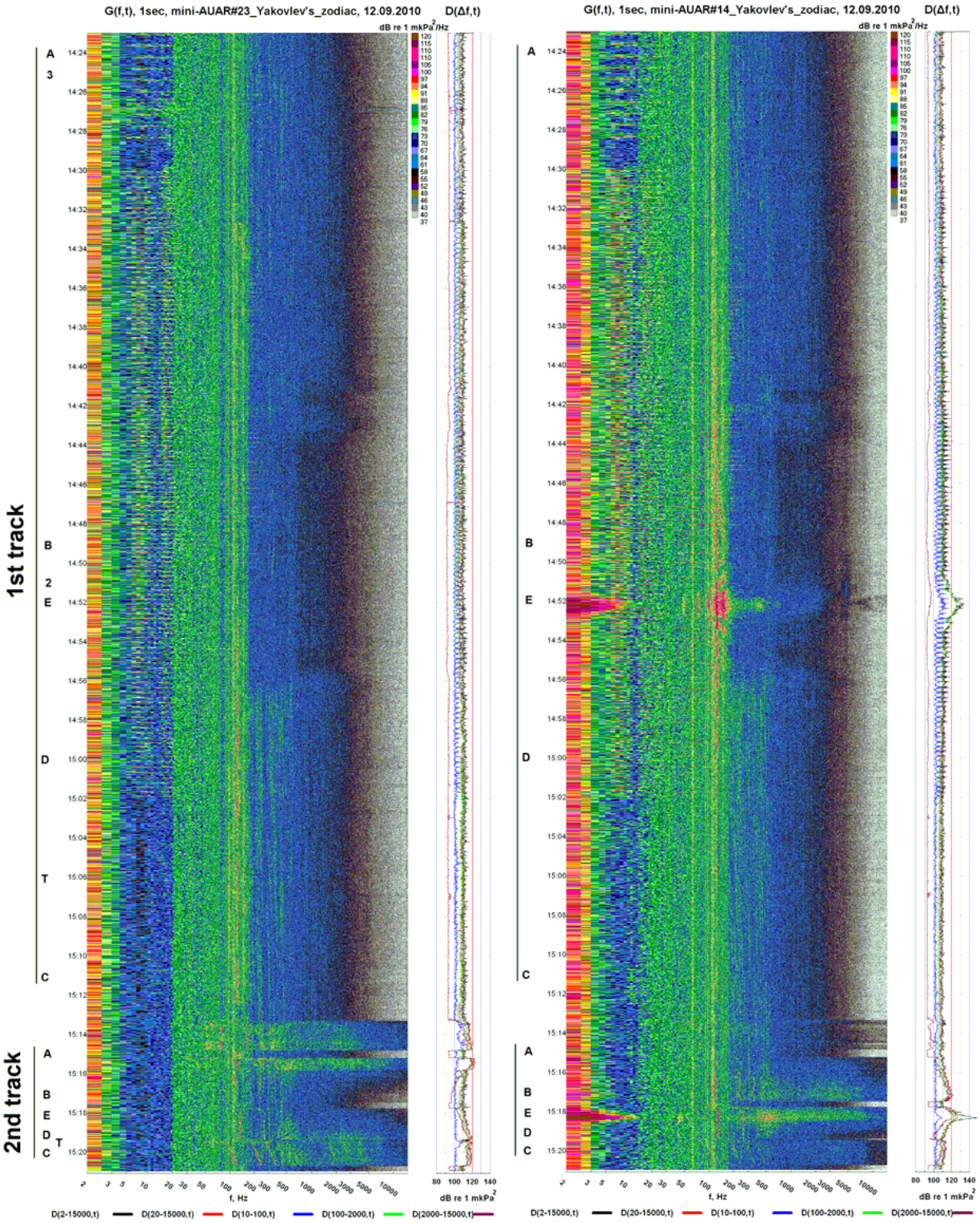

Figure 5.10 - Sonogram *G(f,t)* and of acoustic signals recorded by mini-AUAR#23 (left) and mini-AUAR#14 (right) when the Photo-ID zodiac sailed the first and second tracks. The letters designate moments in time when the jet-drive boat passed the points shown in Figure 5.6 and 5.7.

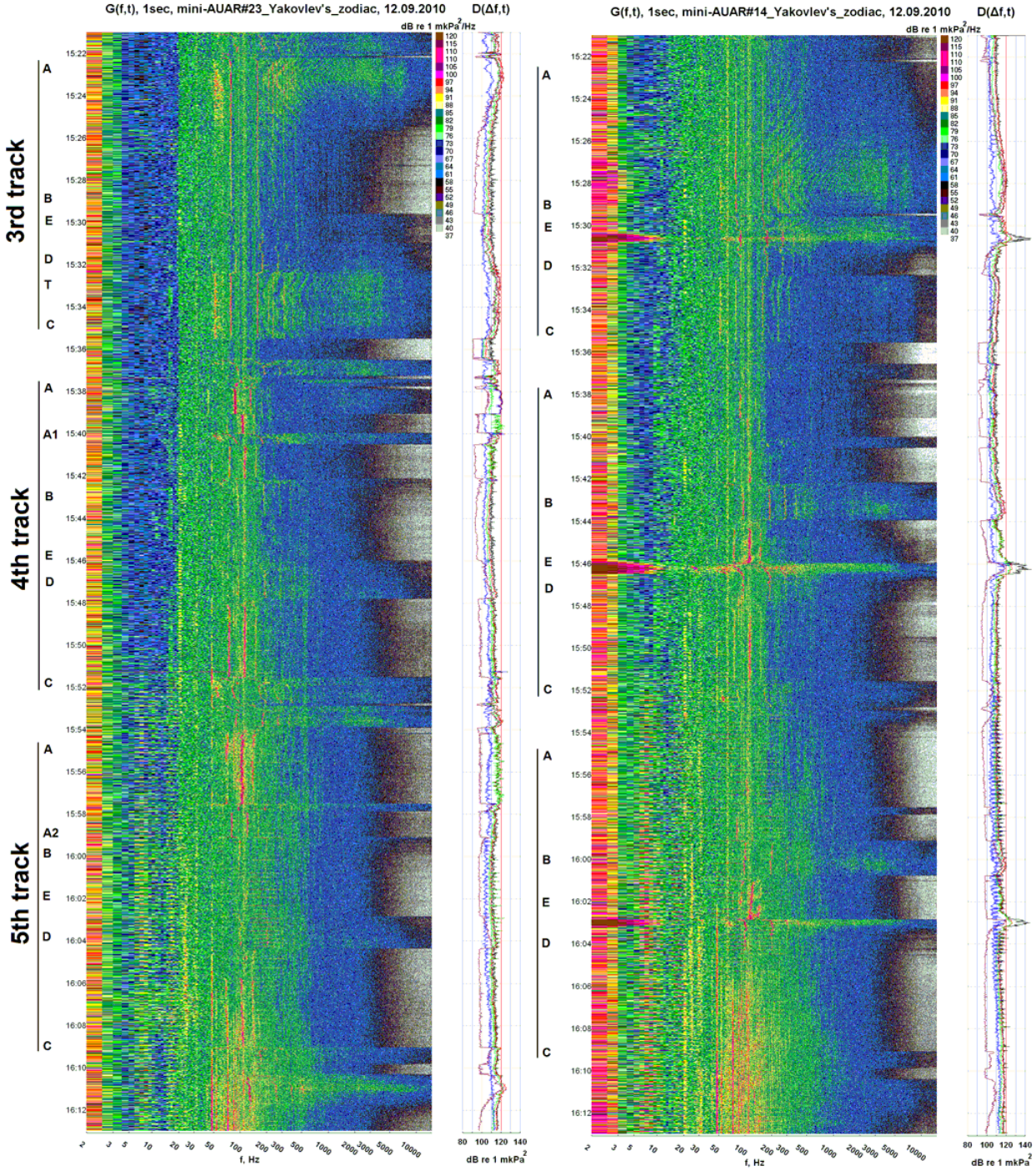

Figure 5.11 - Sonogram *G(f,t)* and of acoustic signals recorded by mini-AUAR#23 (left) and mini-AUAR#14 (right) when the Photo-ID zodiac sailed the third, fourth, and fifth tracks. The letters designate moments in time when the jet-drive boat passed the points shown in Figure 5.6 and 5.7.

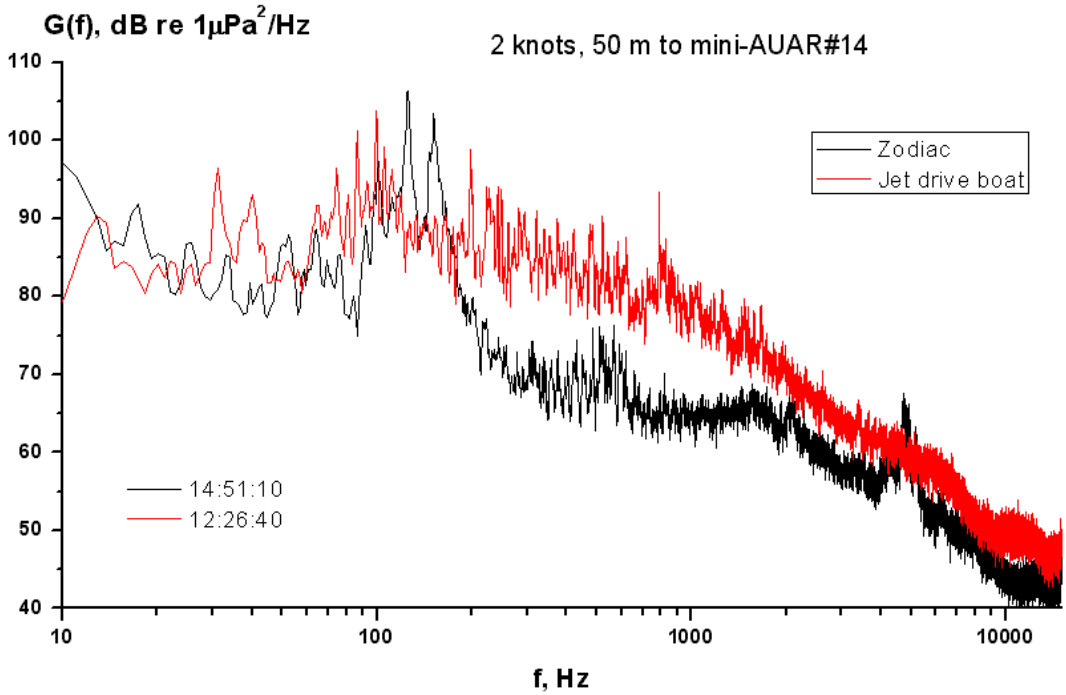

Fig[illegible] Photo-ID zodiac and the jet-drive boat sailed at 2 knots towards mini-AUAR#14 at a range of 50 m.

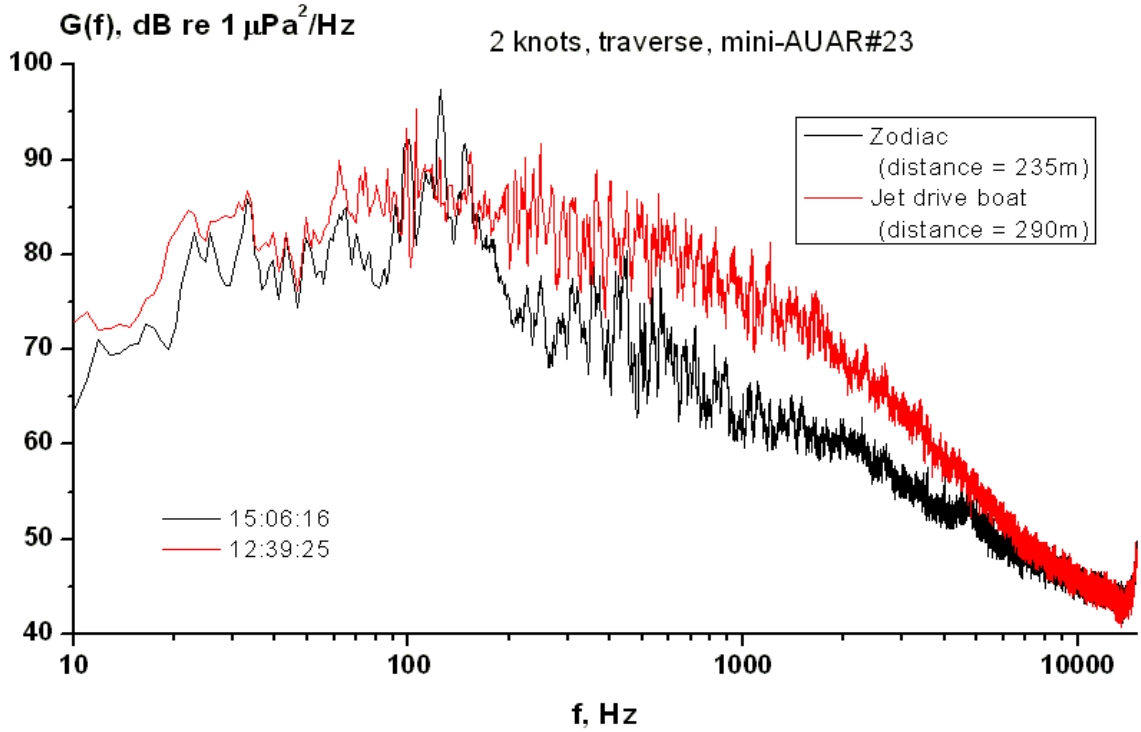

Figure 5.13 – Power spectral density levels *G(f)* of acoustic signals recorded when the Photo-ID zodiac and the jet-drive boat sailed perpendicular to the A-B line at 2 knots while mini-AUAR#23 located 250-300 m abeam recorded the data.

Figure 5.14 shows power spectral density spectra *G(f)* calculated for jet-drive boat when sailing towards mini AUAR#23. The spectra for uniform motion of the jet-drive boat at 6 and 15 knots were calculated with 20 and 10 second averaging, respectively. It can be seen that the power spectral density levels differ by approximately 5 dB in the 100-1000 Hz range and by 10-20 dB at frequencies above 1 kHz.

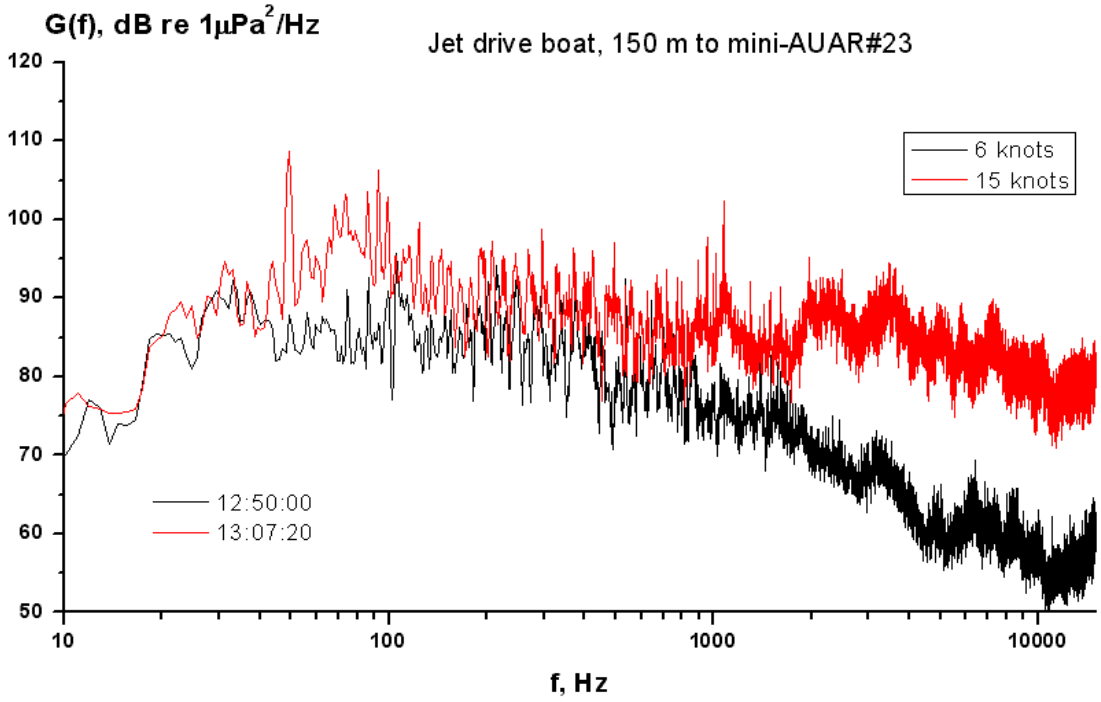

Figure 5.14 – Power spectral density levels *G(f)* of acoustic signals recorded when the Photo-ID zodiac and the jet-drive boat sailed towards mini-AUAR#23 at 2 different speeds.

Figure 5.15 compares the power spectral density levels for the noise generated by the jet-drive boat and Photo-ID zodiac sailing at a uniform speed of 15 knots while mini AUAR#23, which recorded the noise, was about 260 m abeam to the port side of the vessel. It can be seen that the jet-drive boat noise is 5-10 dB greater than the Photo-ID zodiac noise.

Figure 5.16 illustrates the differences in the power spectral density levels produced by the jet-drive boat moving at uniform speeds of 2, 6 and 15 knots. The jet-drive boat moved perpendicular to the A-B line, so mini AUAR#23, which recorded the noise, was 250-300 m abeam its portside. The power spectral density levels differ by approximately 5 dB in the 100-1000 Hz range and by 10-20 dB at frequencies above 1 kHz.

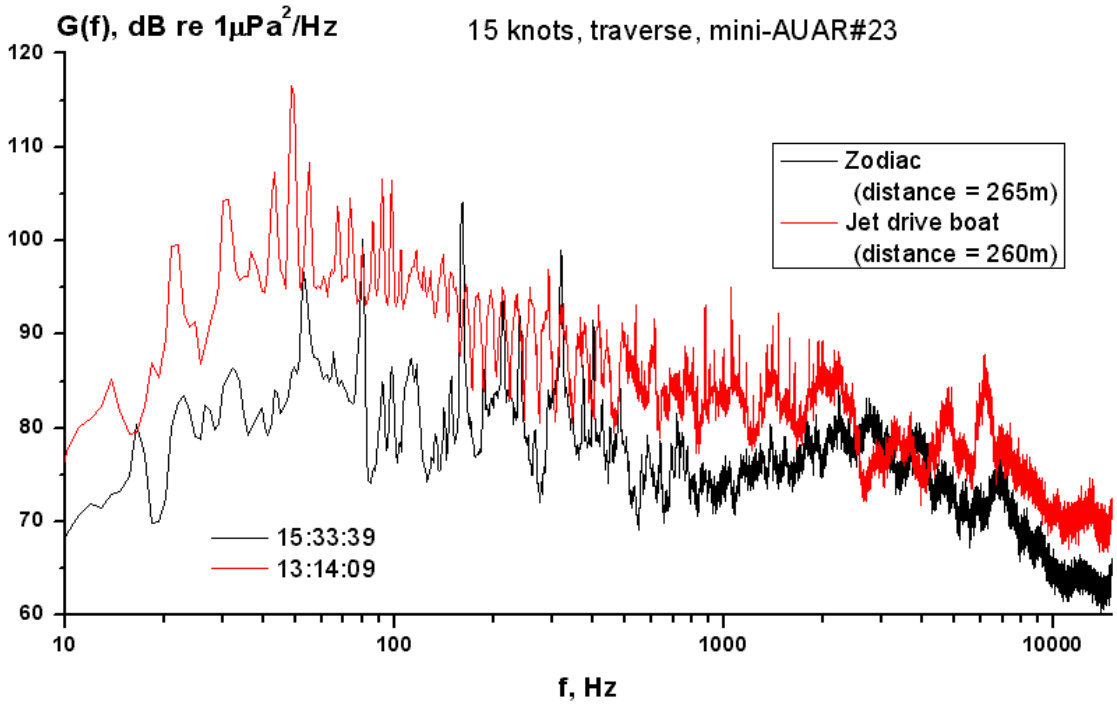

Figure 5.15 – Power spectral density levels *G(f)* of acoustic signals recorded when the Photo-ID zodiac and the jet-drive boat sailed at 15 knots while mini-AUAR#23 located 260 m abeam on the port side recorded the data.

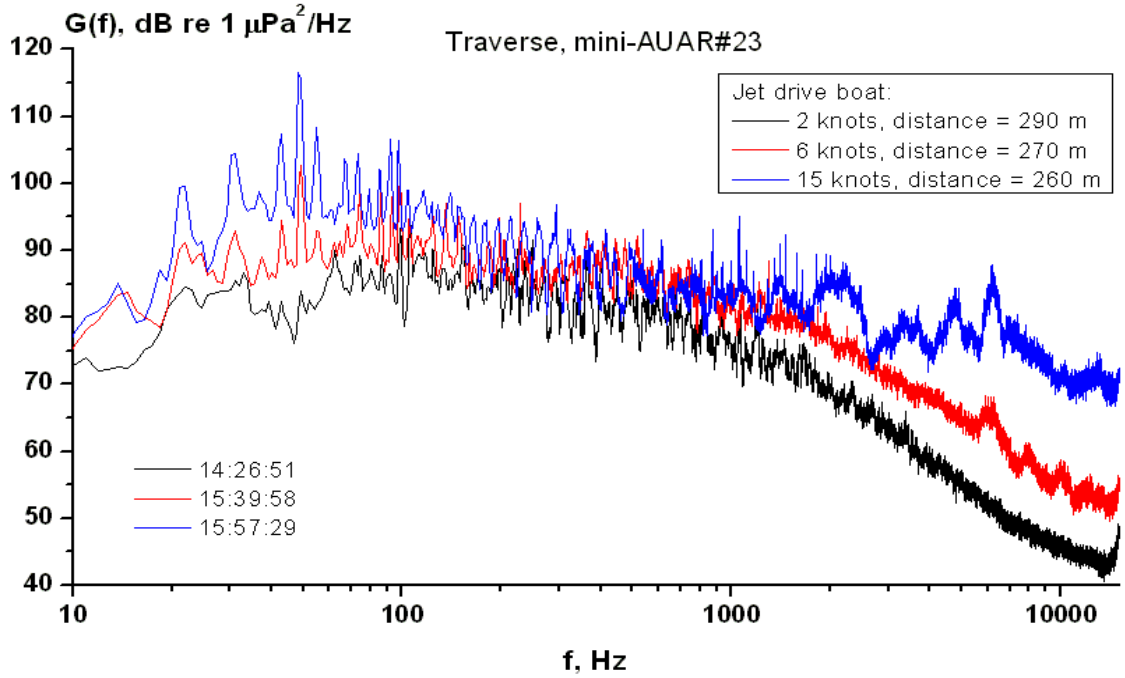

Figure 5.16 – Power spectral density levels *G(f)* of acoustic signals recorded when the jet-drive boat sailed at different speeds while mini-AUAR#23 located 250-300 m abeam on the port side recorded the data (spectra are for location T).

Figures 5.17 and 5.18 illustrate the variations in the power spectral density levels produced by the jet-drive boat and Photo-ID zodiac when accelerating at different rates.

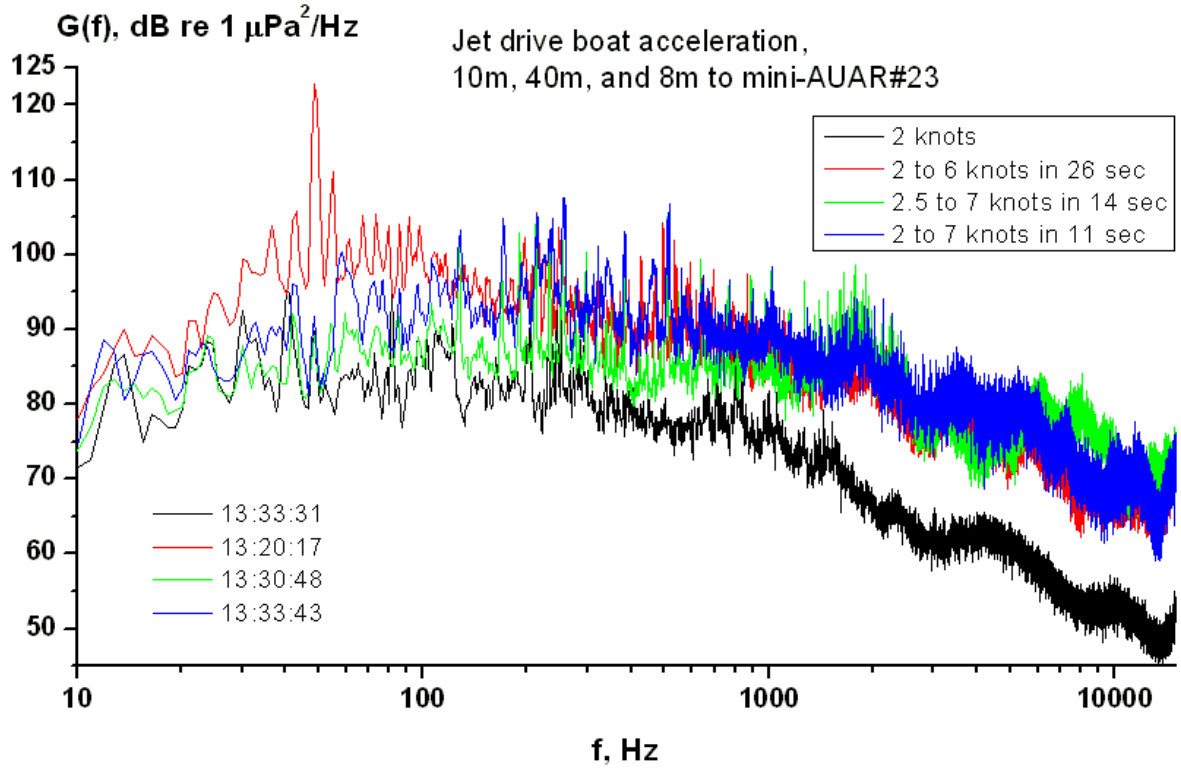

Figure 5.17 – Power spectral density levels *G(f)* of acoustic signals recorded when the jet-drive boat sailed at different acceleration rates. The spectrum for a uniform speed of 2 knots is provided for comparison.

Figure 5.17 shows the power spectral density levels for the jet-drive boat when sailing at different acceleration rates: 4 knots in 26 seconds, 5 knots in 14 seconds and 5 knots in 11 seconds. The spectral level of the jet-drive boat when sailing at a constant speed of 2 knots is also provided for comparison. It can be seen that accelerated motion increases the power spectral density level by 5-10 dB in for frequencies up to 1 kHz and by 10-20 dB for frequencies above 1 kHz, when compared to the power spectral density level for a jet-drive boat moving at 2 knots. Higher accelerations increase the sound level by 5 dB for frequencies under 1 kHz only. Analysis of the sound spectra for the different jet-drive boat acceleration modes does not allow us to make a specific recommendation on the optimum acceleration rate because all are virtually the same from a noise perspective, except for the low frequency (<100 Hz) part of the slow acceleration experiment.

Figure 5.18 shows the Photo-ID zodiac power spectral density levels when sailing at different acceleration rates: 11 knots in 31 seconds and 12 knots in 9 seconds. The spectral level of the Photo-ID zodiac when sailing at a constant speed of 2 knots is also provided for comparison. As with the jet-drive boat described above, accelerated motion of the Photo-ID zodiac increases the power spectral density level by 5-10 dB for frequencies up to 1 kHz and by 10-20 dB for frequencies above 1 kHz, when compared to the power spectral density level for a Photo-ID zodiac moving at 2 knots.

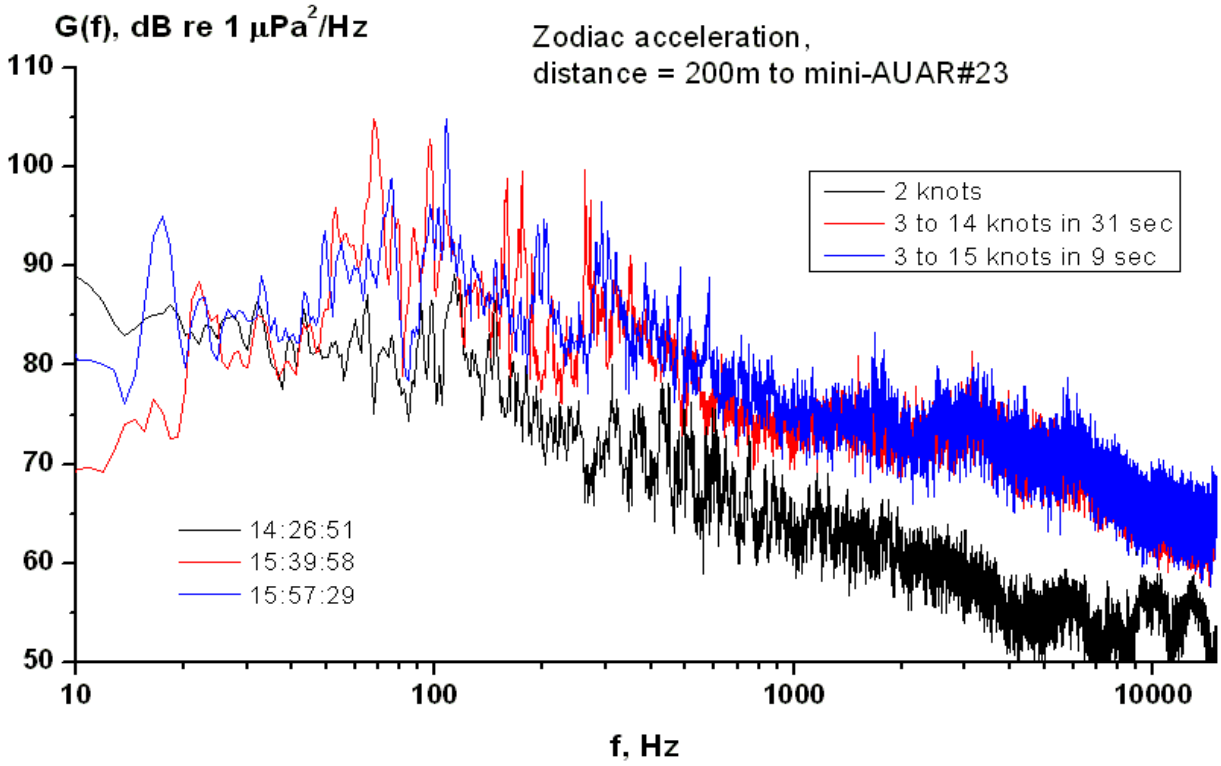

Figure 5.18 – Power spectral density levels *G(f)* of acoustic signals recorded when the Photo-ID zodiac sailed at different acceleration rates. The spectrum for a uniform speed of 2 knots is provided for comparison.

The following conclusions can be drawn from this study:

1. In virtually all transiting modes, the power spectral density level of the jet-drive boat is at least 5 dB greater than that of the Photo-ID zodiac.
2. For the acceleration modes, the power spectral density levels for frequencies above 1 kHz increase by 10-16 dB when compared to the power spectral density level for a constant speed of 2 knots. Both the jet-drive boat and the Photo-ID zodiac generally exhibit the same increase. These higher spectral levels may be caused by cavitation generated by accelerating propeller speed.
3. The Photo-ID zodiac generates less noise when rapidly accelerating up to 15 knots than the jet-drive boat at a constant speed of 15 knots.

6 Analysis of Bathymetric and Hydrologic Studies on the NE Sakhalin Shelf

The 2010 season saw a continuation of hydrological observations in the shallow-water Piltun and deep-water offshore NE Sakhalin gray whale feeding areas. The observations were conducted both over extended areal surveys as well as along individual transects semi-perpendicular to the shoreline. Observations along standard transects through the Piltun and offshore feeding areas were planned and conducted at approximately the same times each year in order to evaluate the intra-annual variability of hydrological characteristics and to compare the year to year differences. In order to evaluate the inter-annual variability of hydrological characteristics during the summer season, hydrological data at two representative locations was acquired repeatedly throughout the season (as in previous years).

This section presents the analysis of bathymetric and hydrological measurements performed during the 2010 field season. The hydrological work on the NE Sakhalin shelf was performed with the Valeport MIDAS-CTD+500 sonde, which is equipped with temperature, conductivity, pressure and sound velocity sensors[30]. The expedition acquired vertical hydrologic profiles at 372 stations in 2010. These included 168 in August and 204 in September. The location of these hydrological stations is shown in Figure 6.1.

The hydrologic observations were conducted in the Piltun and Offshore gray whale feeding areas and at almost every benthos sampling station (138 stations total); vertical hydrologic profiling was also performed at new gray whale feeding locations. Additionally, vertical hydrologic profiles were acquired in conjunction with phytoplankton sampling on long individual profiles. A total of 125 samples were taken at 35 stations from different depths. The results of these observations will be analyzed together with the Benthos Team after the benthic data has been analyzed at an onshore laboratory.

The areal hydrologic surveys and individual transects were acquired for differing summer and fall weather conditions. This data allowed the short-term variability of hydrological parameters to be evaluated.

[30] The sonde sensors were calibrated, see Appendix A for the calibration certificates.

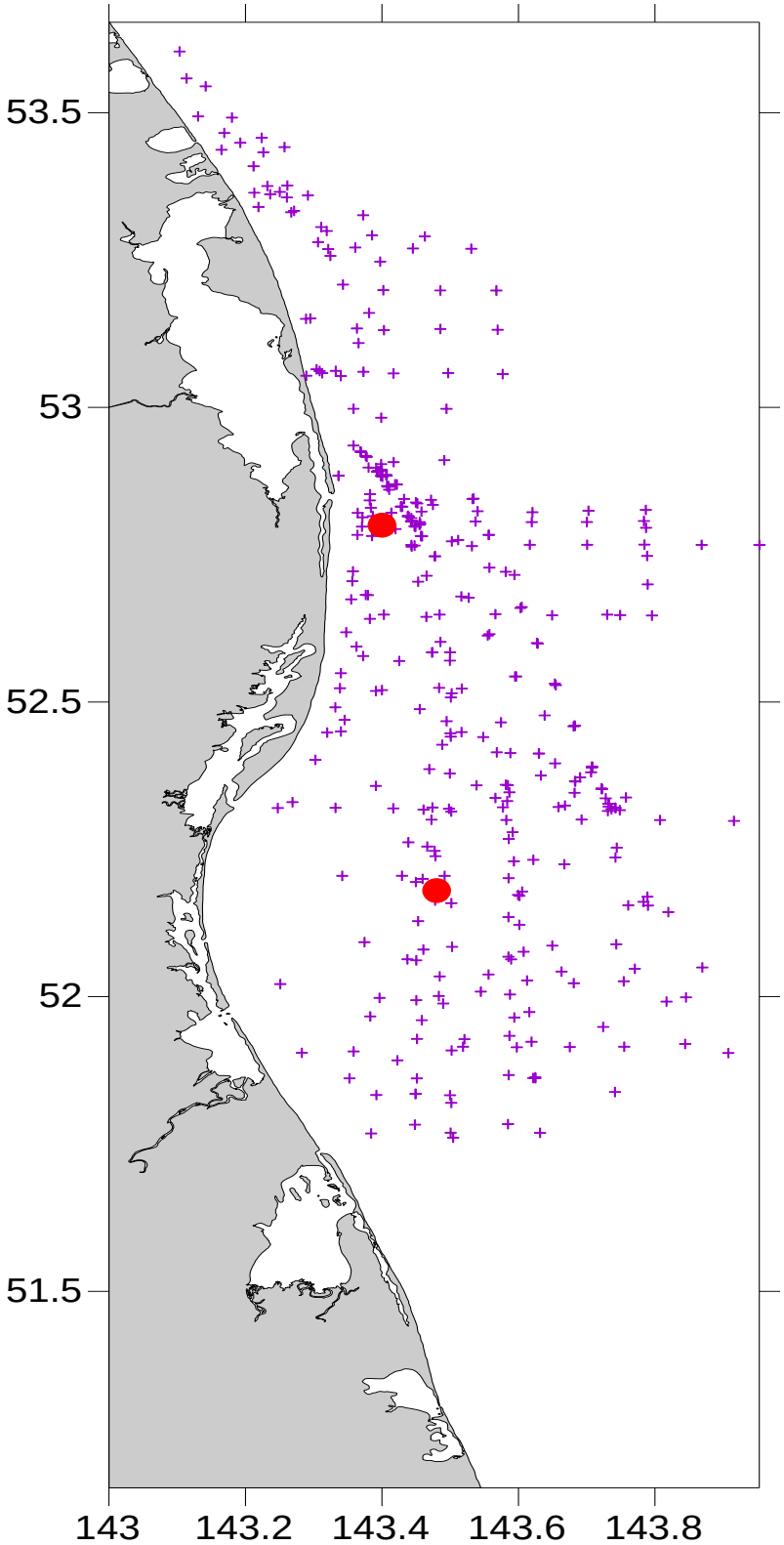

Figure 6.1 - Map of the NE Sakhalin Shelf showing the bathymetry of the study area and the locations where vertical hydrologic profiles were acquired as of September 2010. The red circles indicate multi-annual hydrological monitoring stations.

6.1 Meteorological conditions observed in the study area in 2010

Before proceeding to a direct analysis of the hydrological data, it is valuable to discuss the peculiarities of the weather observed over the Sea of Okhotsk in the summer of 2010. Firstly, the summer of 2010 was characterized by unusually calm and stable weather over the Sea of Okhotsk. The high pressure area above the Sea of Okhotsk produced a large number of clear and pleasant weather days in August and September. Southerly and southeasterly winds were rare in the Sea of Okhotsk when compared to previous years. Fog was relatively rare off the NE coast of Sakhalin Island, being recorded 4 times, but none was seen in the inshore area.

Table 6.1 summarizes the weather in the survey area as recorded in the log of the *Akademik Oparin.* Table 6.1 shows that there were 14 sunny days and 17 overcast and rainy days off the NE shore of Sakhalin Island in August 2010. In September, the number of sunny days increased to 17 and the total number of sunny and partially sunny days was 24.

Cyclones that occasionally appeared in the offshore area arrived from the west and crossed the northern sectors of the Sea of Okhotsk, bringing with them westerly and northerly winds. On 15th-16th August the southern sector of the Sea of Okhotsk was hit by a cyclone, forcing the vessel to take shelter in Severny Bay.

During the second half of September (20th-22nd September, 2010), a deep cyclone developed over the entire offshore area, but soon shifted to the east. When the cyclone passed the eastern coast of Sakhalin Island, 16-18 m/sec southerly winds were first observed, which were later replaced by easterly and northerly winds. Large swells were noted near the coast after the cyclone had passed. Another deep cyclone developed over Sakhalin Island on 28th September. It brought strong southerly and southwesterly winds of up to 30 m/sec. Passing Sakhalin Island, the cyclone caused blackouts in some areas and disrupted public utility services. This cyclone forced the *Akademik Oparin* to take shelter on the westward side of the northern end of Sakhalin Island. After it passed on 30th September, 2010, upwelling phenomena were observed in Severny Bay, which was the first case of upwelling recorded during that season.

Table 6.1: Weather Conditions in the Survey Area
Abbreviations: R – Rain; O – overcast; F – fog; C – clear

Day of month	August	September
1	**R**	**O**
2	**O**	**R-S**
3	**O**	**S**
4	**O**	**S**
5	**O**	**S**
6	**R**	**S**
7	**S**	**S-R**
8	**O-S**	**S**
9	**S**	**S**
10	**S-O**	**S-O**
11	**F**	**S**
12	**O**	**S**
13	**F**	**S**
14	**F**	**S**
15	**O**	**S**
16	**R**	**O-S**
17	**O**	**S**
18	**O-S**	**S**
19	**S**	**S**
20	**S-O**	**S-O**
21	**O-F**	**O-R**
22	**S**	**O**
23	**S**	**S**
24	**S**	**O-S**
25	**S**	**O**
26	**S**	**S**
27	**S**	**S**
28	**S**	**O-S**
29	**O**	**O-R**
30	**R**	**O**
31	**O**	

Amur River water was pushed only a short distance from shore and a dark band of this water set off the greenish cold water. On the eastern side of the island the strong southerly wind was unable to cause any upwelling on this day, and fog was absent.

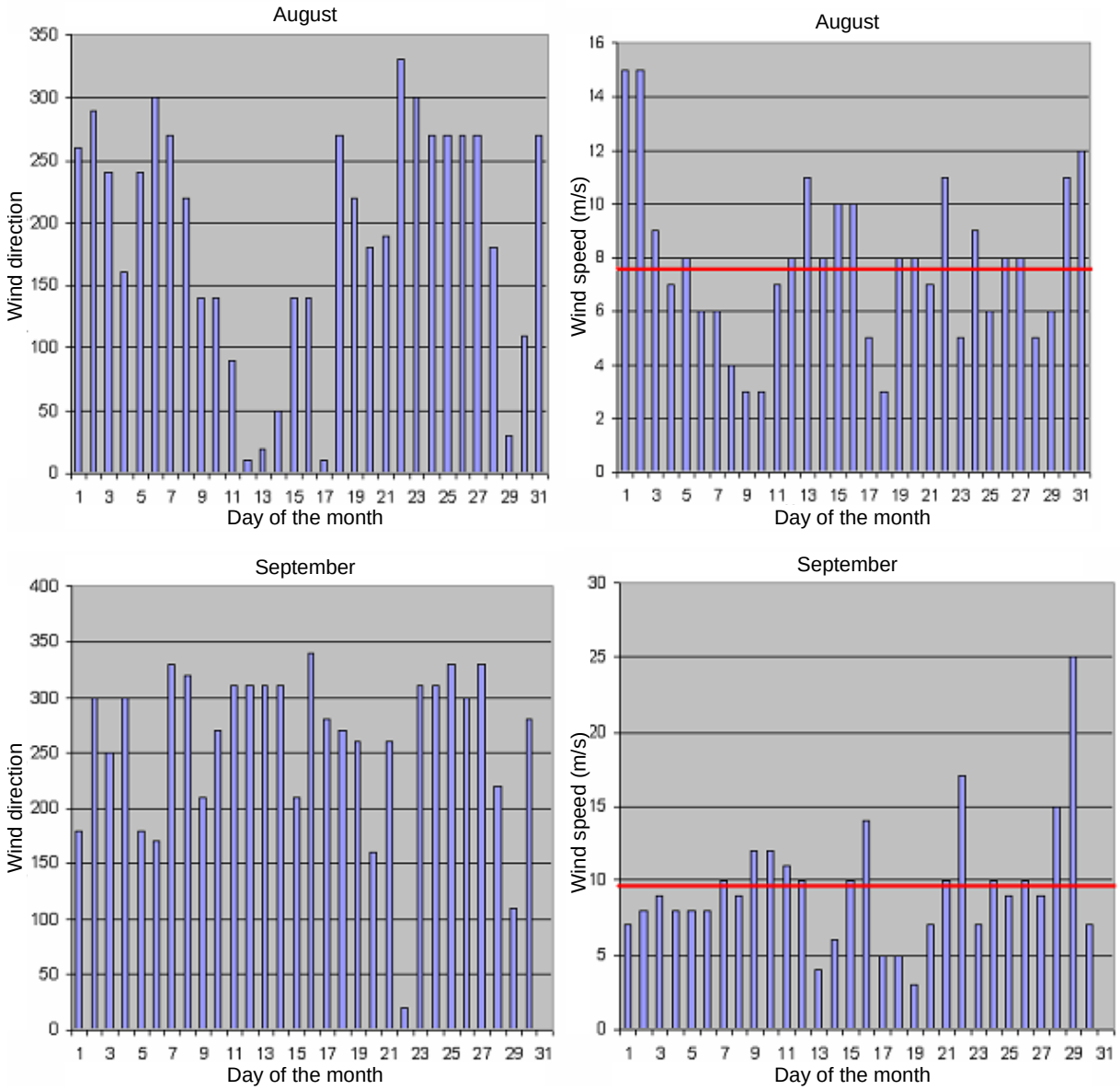

Figure 6.2 – Average daily wind directions and wind speeds for the summer months of 2010. The red line is the average for each month.

Figure 6.2 presents data on the speed and direction of winds during the summer period of 2010. The figure shows average daily wind speeds for the summer of 2010 (the data are averages for the period of observations – daylight hours). The plots show that westerly and northerly winds were predominant offshore NE Sakhalin in the summer of 2010. Southerly winds were rare compared to previous years. The red lines show the average wind speed for each month, the average wind speed for August was 7.8 m/s) or almost 2 m/s lower than during the same period in 2009 (Figure 6.3). Southerly winds with an average speed of 9.6 m/sec prevailed in August 2009.

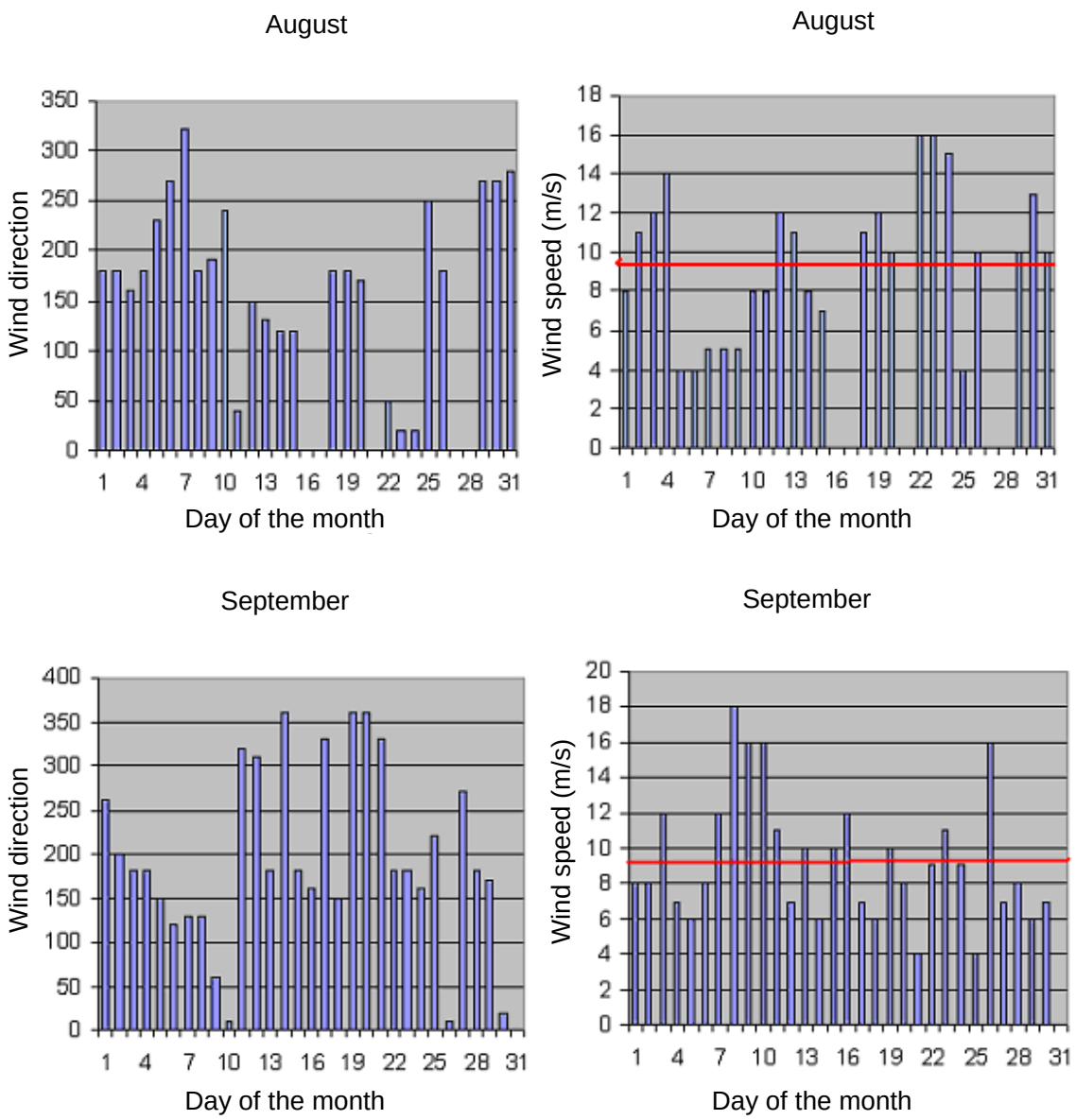

Figure 6.3 – Average daily wind directions and wind speeds for the summer months of 2009. The red line is the average for each month.

Northerly and northwesterly winds continued to play an important role in overall atmospheric circulation during September 2010 (Figure 6.2). The average wind speed in that month was 9.5 m/s, or very close to the 9.3 m/s observed the year before. Gale-force winds of up to 30 m/s encountered during the last third of the month were caused by a deep cyclone that passed across the central part of the Sea of Okhotsk.

Thus, the meteorological setting during the summer season of 2010 was characterized by sunny weather without fog. All unusual weather was associated with the prevailing westerly and

northerly winds that affected hydrological conditions offshore NE Sakhalin Island. These winds did not cause upwelling near the northeastern end of Sakhalin Island, i.e. did not push the fresh water away from the coast, which contributed to its accumulation.

6.2 Hydrological conditions observed over the study area in August 2010

Vertical hydrologic profiles were acquired at 168 stations in August 2010; making it possible to characterize in detail the hydrological conditions in the survey area. The results of these measurements were used to plot near-surface temperature and salinity maps (Figures 6.4).

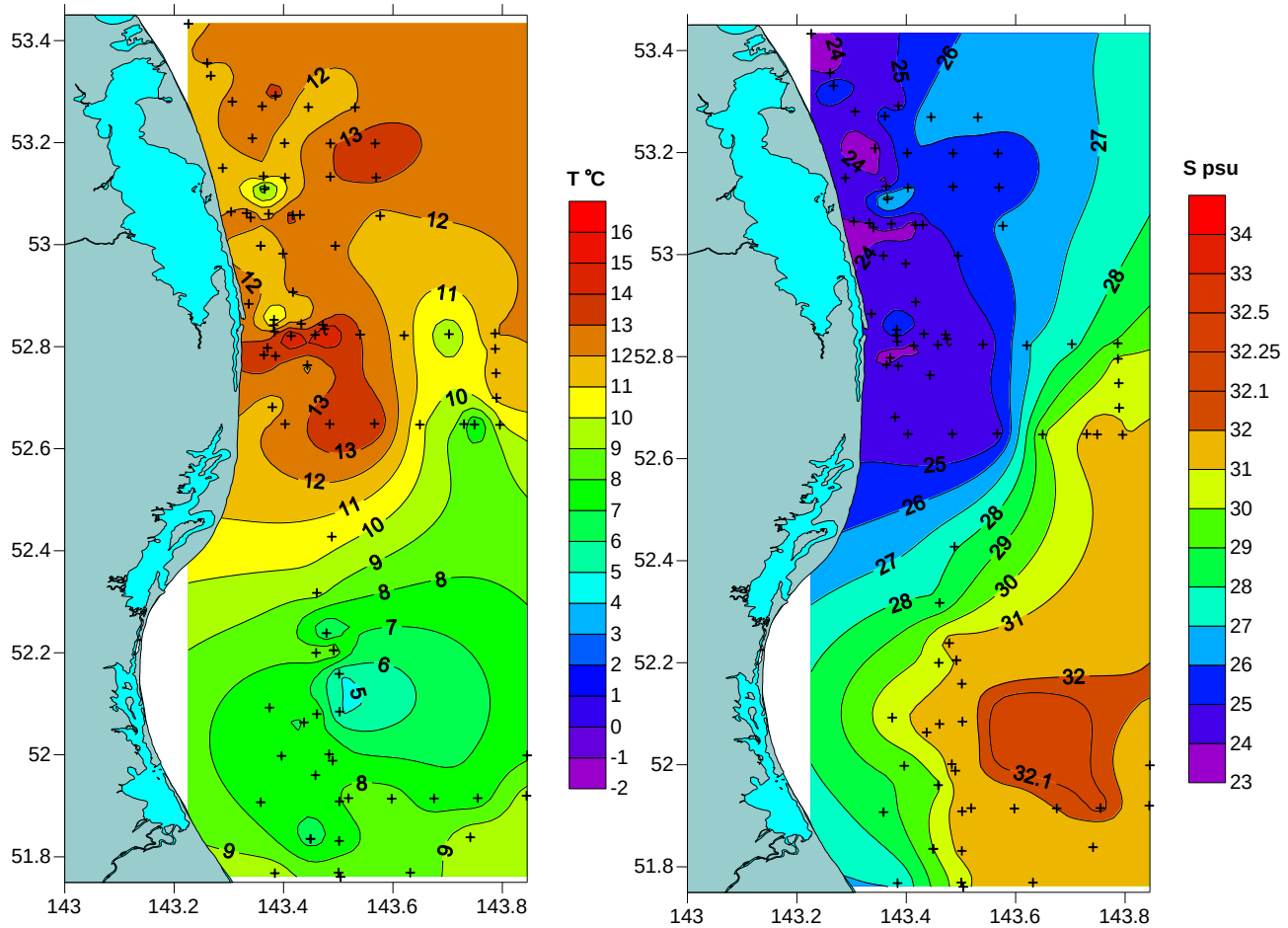

Figure 6.4 - Spatial distribution of water temperature and salinity near the sea surface in August 2010 (constructed from vertical hydrologic profiles acquired between 3rd and 10th August, 2010).

The absence of fresh water in the offshore feeding area in mid-August was noted. Warm water with a salinity less than 25 psu (practical salinity units) was concentrated in the area of Piltun Bay. The thermohaline front separating the Inshore and Offshore areas was located in the northern part of Chayvo Bay. Water temperatures recorded during August in the offshore area

were rather low at 7-8°C and the lowest temperature was 4.8°C. These temperatures were lower than the year before, even though August 2009 was the coldest month since 2005 in the offshore area. The surface water temperature in August 2009 was 7.69°C, which was the lowest temperature ever recorded by the program until 2010.

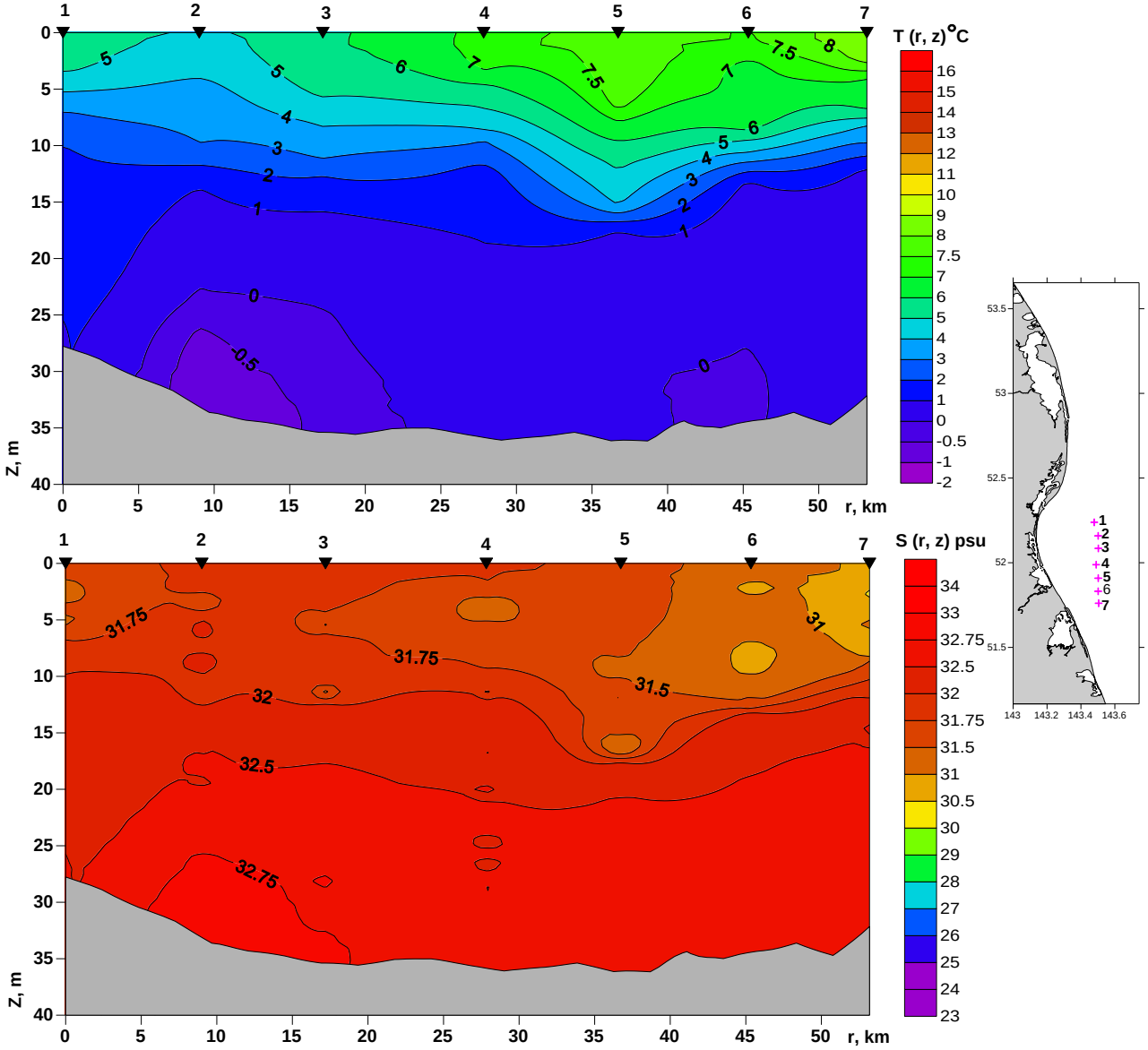

Figure 6.5 - Distribution of Temperature *T(r,z)* and salinity *S(r,z)* and the location of the sampling stations for a hydrologic transect in the offshore feeding area acquired on 3rd August 2010.

In August 2010 the surface water salinity in the offshore area was 32.10 psu, which was higher than in 2009, when the maximum salinity was 31.86 psu. The high near-surface water salinity indicates that the Amur River water did not affect the offshore area which only contained water from the Sea of Okhotsk in August 2010. This is confirmed by observation data from early

August (Figure 6.5). High salinities and relatively low temperatures can be seen throughout the entire water column in the offshore area. The only remarkable feature being that, contrary to what was expected in the Sea of Okhotsk, there was little water with temperatures below 0°C in the near- bottom layers.

At the same time, fresh (up to 23.83 psu) and warm (15.41°C) water was present in the inshore area of Piltun Bay in close proximity to the coastline (Figure 6.6). Note that water with temperatures below 0°C was seen far from the shallow inshore area.

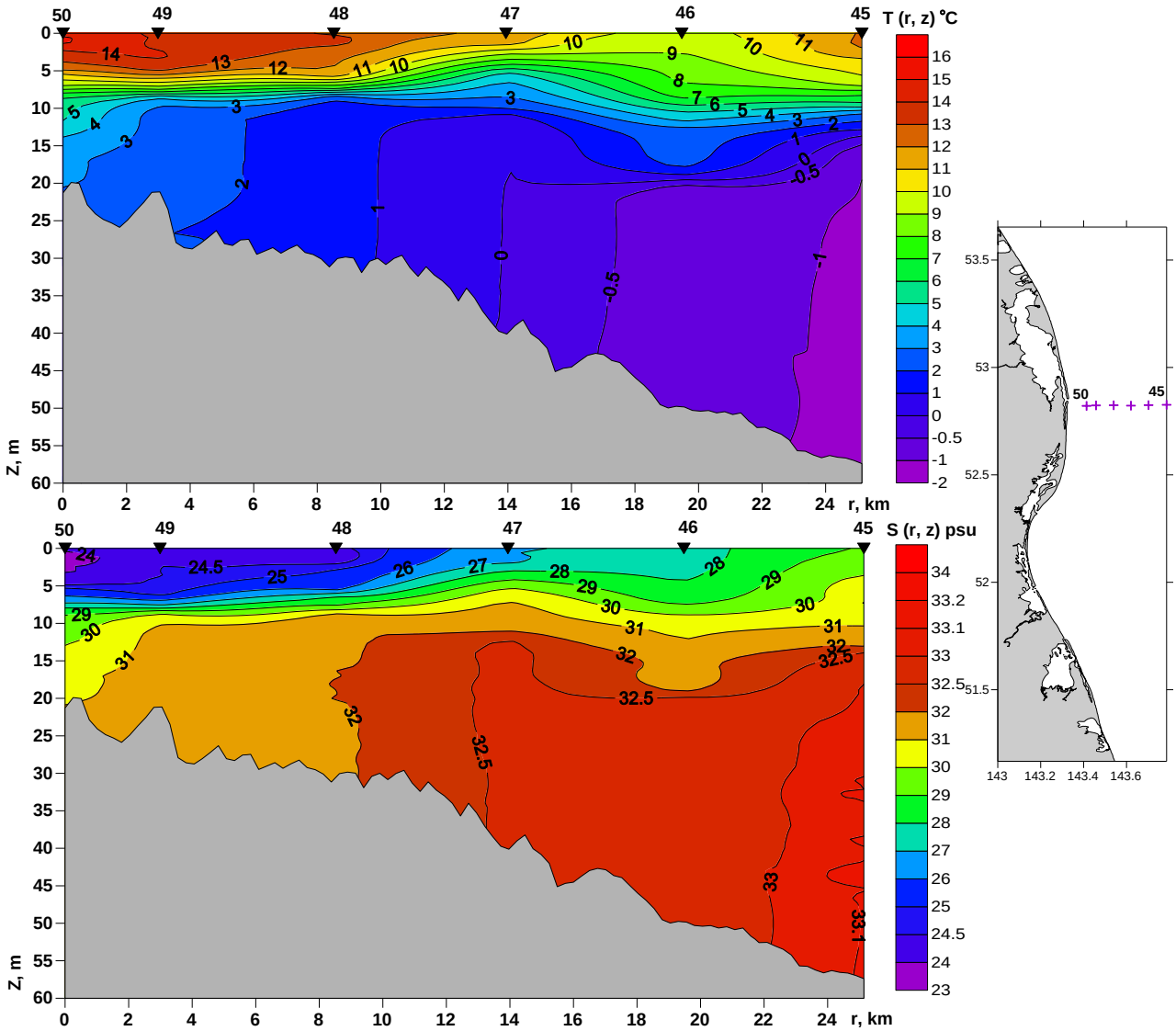

Figure 6.6 - Distribution of Temperature *T(r,z)* and salinity *S(r,z)* and the location of the sampling stations for a hydrologic transect near Piltun Bay acquired on 8th August, 2010.

The sea bottom temperature and salinity distributions (Figure 6.7) in these areas were generally

similar to the same distributions in previous years (Figure 6.8). The small volume of hydrological data acquired in the offshore area in 2010 does not permit a reasonable comparison with 2009.

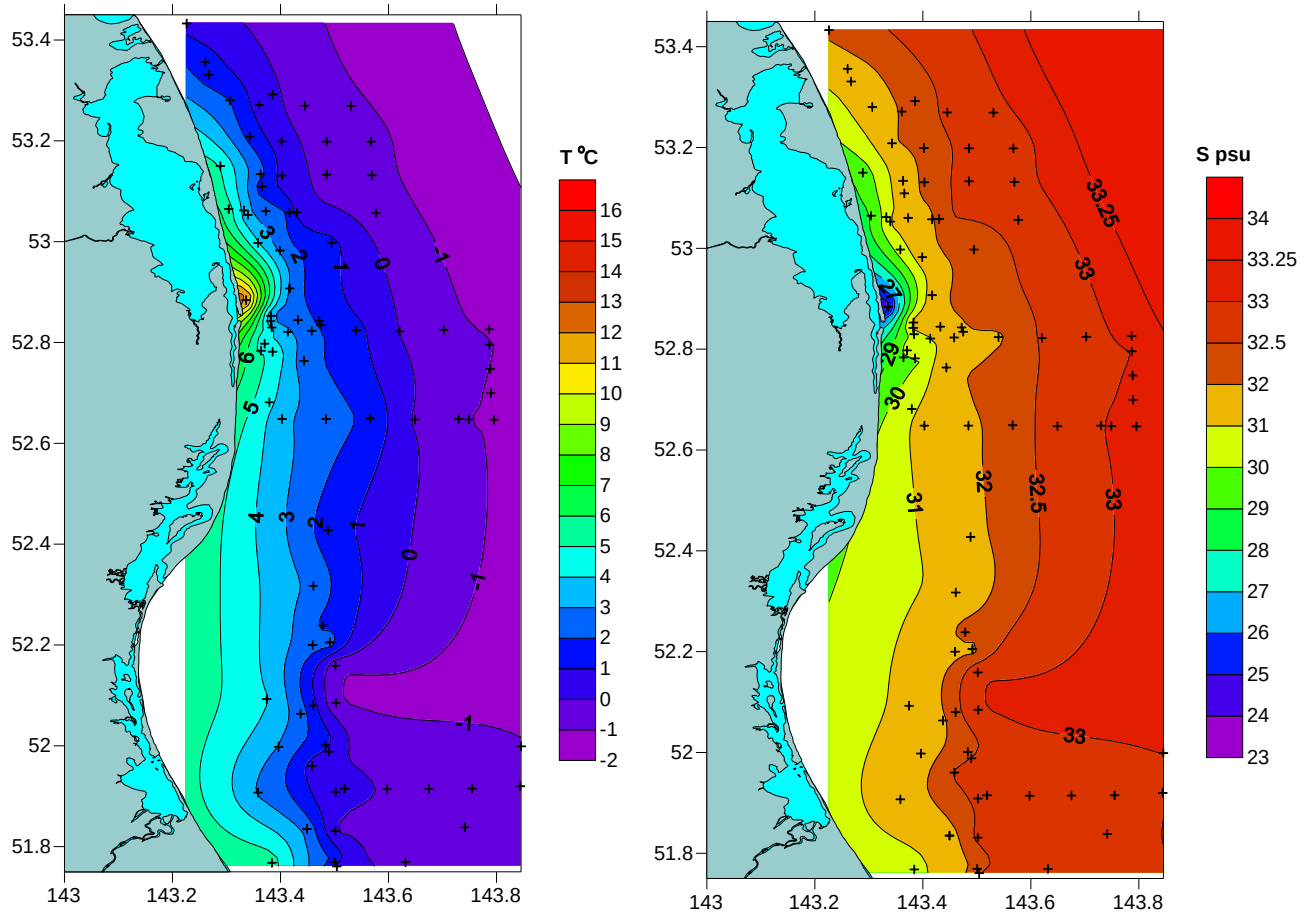

Figure 6.7 - Spatial distribution of water temperature and salinity near the sea floor in August 2010 (constructed from vertical hydrologic profiles acquired between 3rd and 10th August, 2010).

Hydrological conditions in the survey area began to change in late August. The long profile ran from the offshore feeding area towards Piltun Bay on 25th-26th August, 2010, showed that the hydrological characteristics of the offshore area had changed considerably since the beginning of August (Figure 6.9).

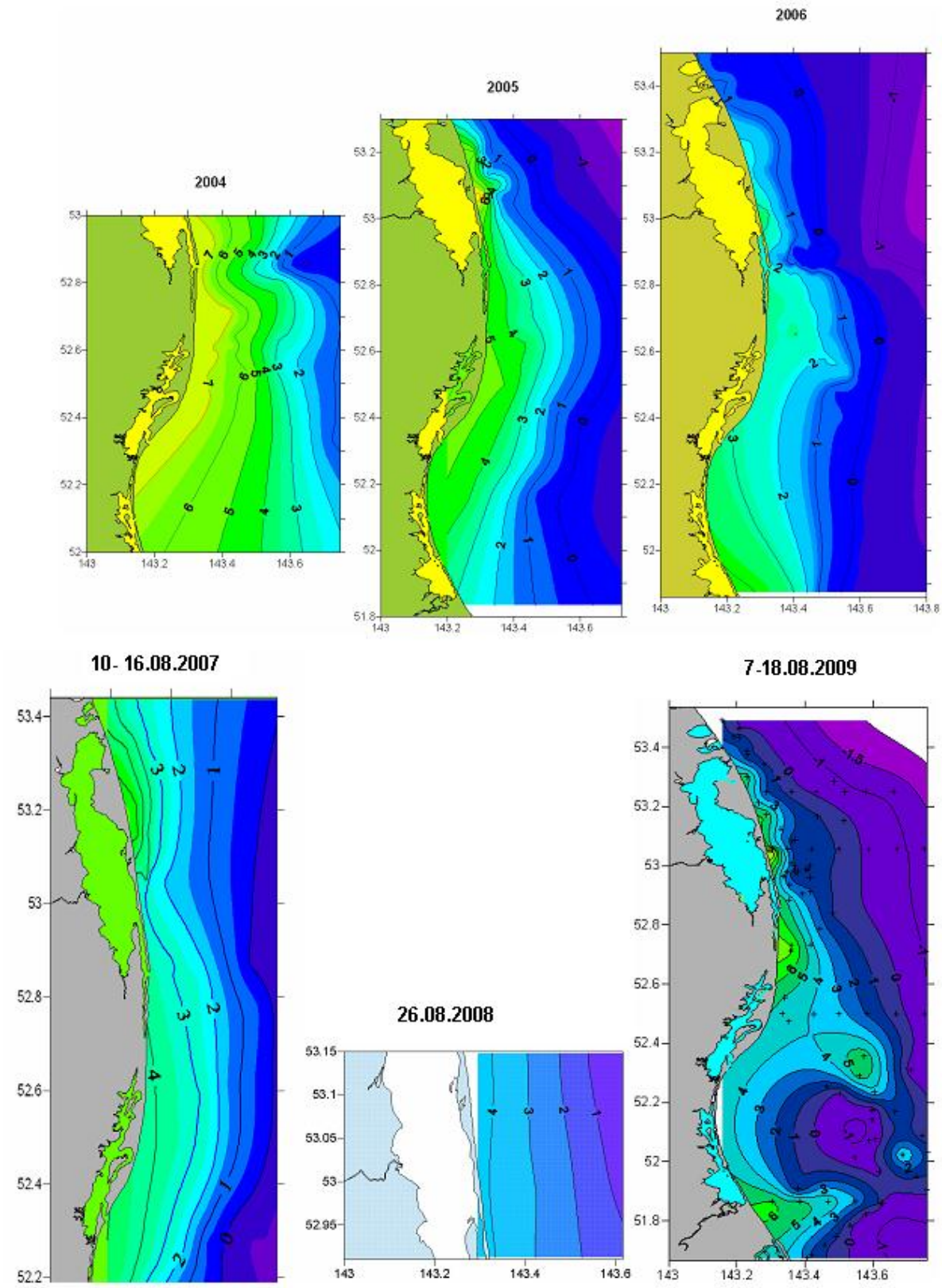

Figure 6.8 – Spatial distribution of water temperature near the sea floor in August 2004, 2005, 2006, 2007, 2008 and 2009.

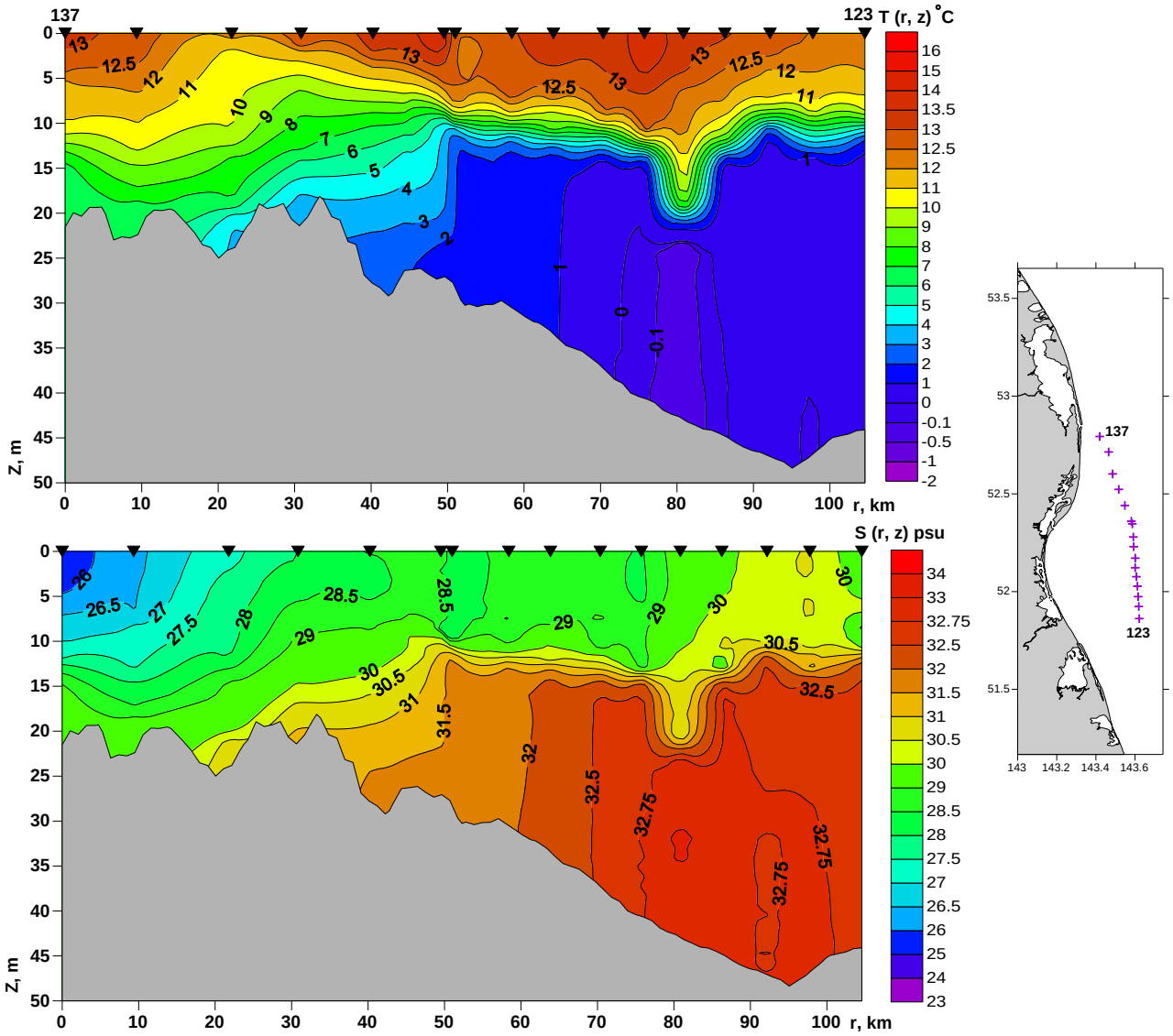

Figure 6.9 - Distribution of Temperature *T(r,z)* and salinity *S(r,z)* and the location of the sampling stations for a hydrologic transect adjacent to Chayvo Bay acquired on 25th-26th August, 2010.

This change in hydrological characteristics is largely attributable to the ingress of warm fresh water from the northern part of the inshore area. Surface water temperatures increased to 13.72°C while salinity decreased to 28.44 psu. This warm, fresh layer was more than 10 meters thick. The freshest water (salinity 25.71 psu) remained in the vicinity of Piltun Bay. The thermohaline front was also located at the same place in the northern part of the near-shore area just offshore of Chayvo Bay.

Fresh water continued to reach the offshore area until early September, as confirmed by the observations of 2nd September, 2010 (Figure 6.10). Note that the thermohaline front in the northern part of the near-shore area just offshore of Chayvo Bay, which apparently formed the

northern boundary of the fresh water lens, persisted up to that time.

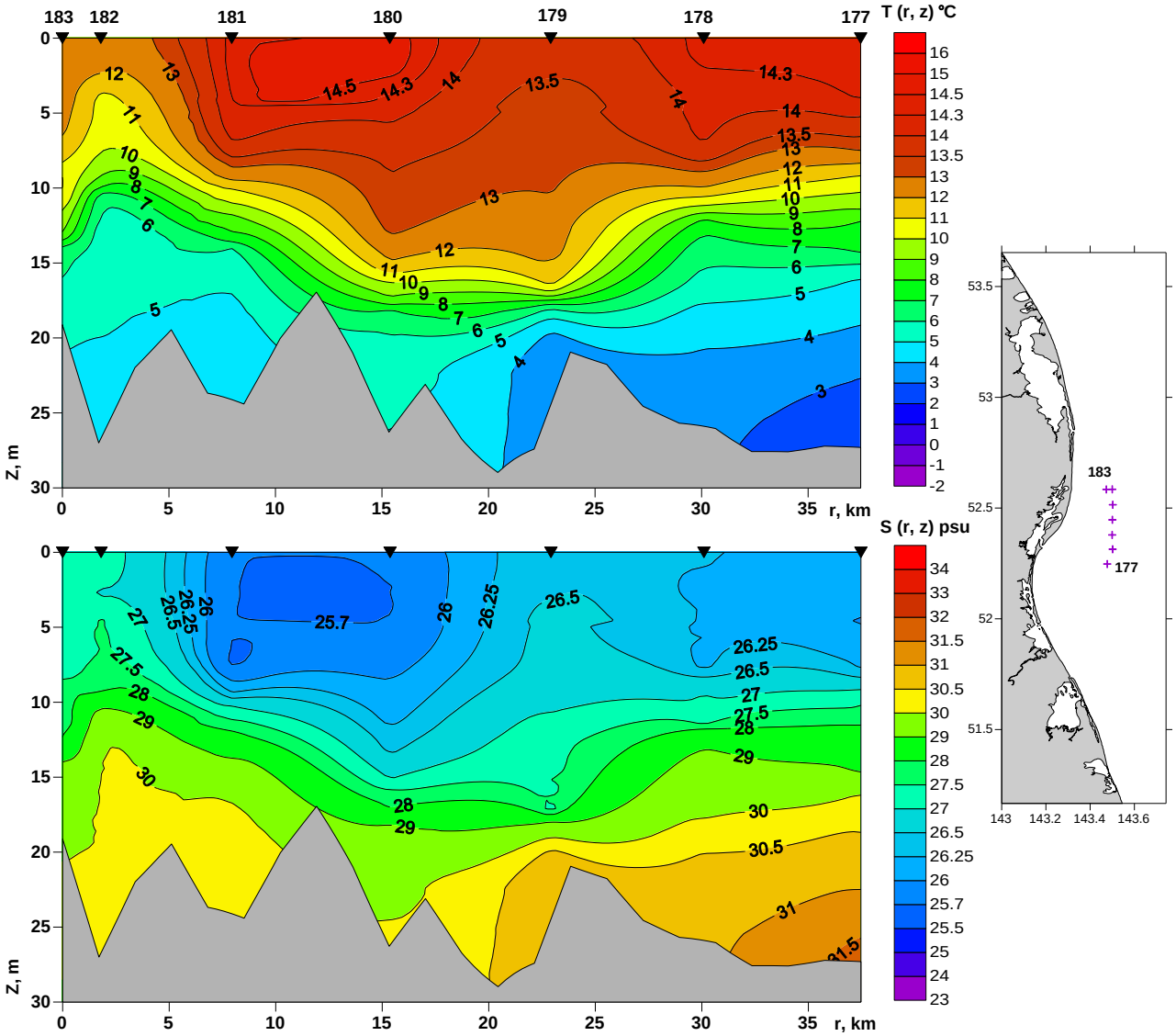

Figure 6.10 - Distribution of Temperature *T(r,z)* and salinity *S(r,z)* and the location of the sampling stations for a hydrologic transect adjacent to Chayvo Bay acquired on 2nd September, 2010.

It should also be noted that the thickness of the fresh water lens was 15 meters or greater. A fresh water layer this thick had not been observed there previously. Temperatures and salinities in the surface layer were considerably higher than for a similar lens observed in 2009 (Figure 6.11).

By mid-September 2010, the surface layer was characterized by high temperatures and low salinities throughout the offshore area (Figure 6.12). Comparison of Figures 6.12 and 6.13 suggests that a significantly greater volume of fresh water entered the offshore area in 2010

than in 2009.

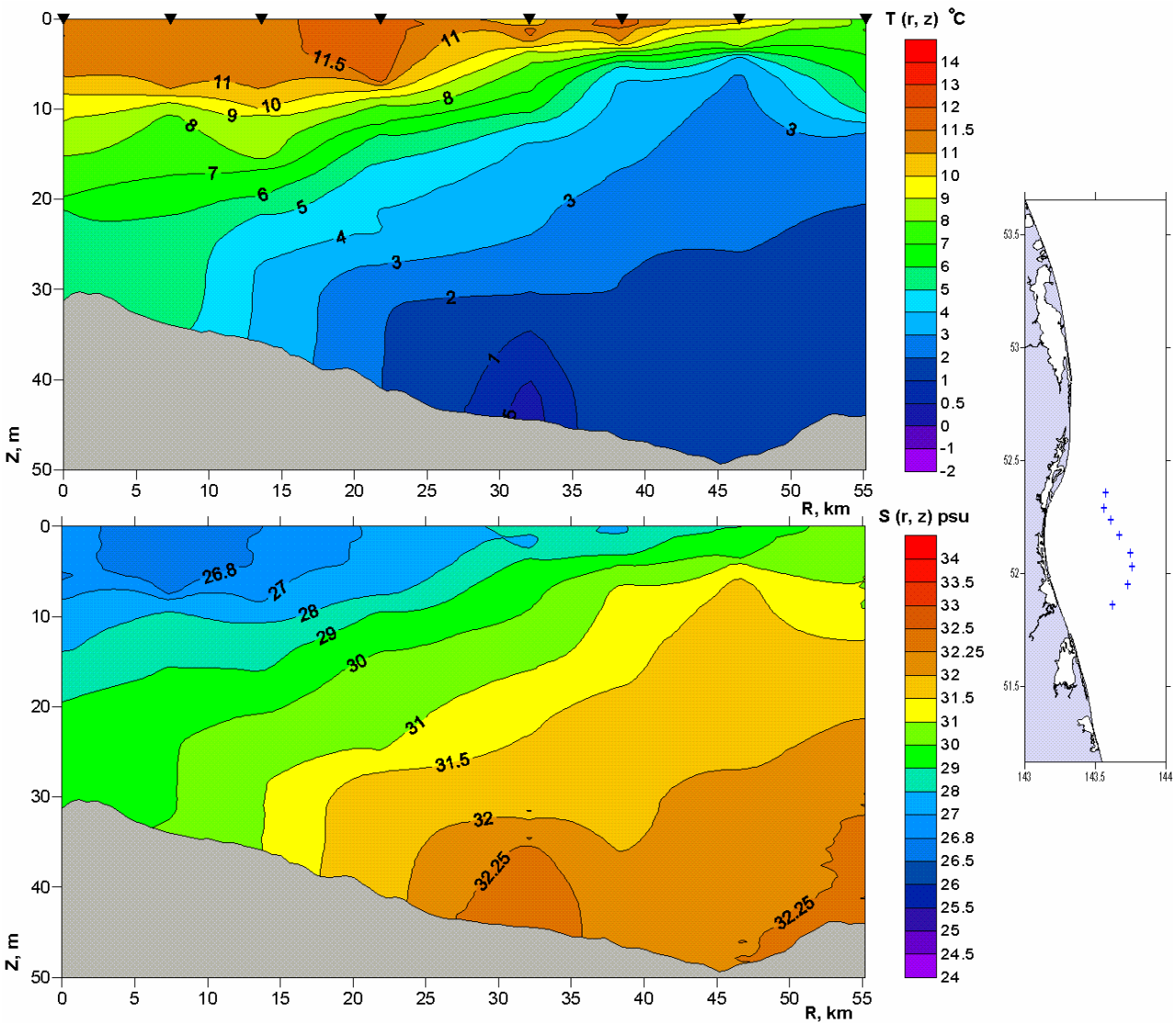

Figure 6.11 - Distribution of Temperature *T(r,z)* and salinity *S(r,z)* and the location of the sampling stations for a hydrologic transect adjacent to Chayvo Bay acquired on 6th September, 2009.

The hydrological survey conducted in September supports this conclusion. The hydrology data indicates that both the inshore and offshore areas were influenced by warm fresh water (Figure 6.13).

Very fresh water (23–25 psu) was only encountered close to shore in the inshore area. Salinity and temperature characteristics in the offshore portion of the inshore area are most likely different from those shown in Figure 6.13; although no field data are available to confirm this.

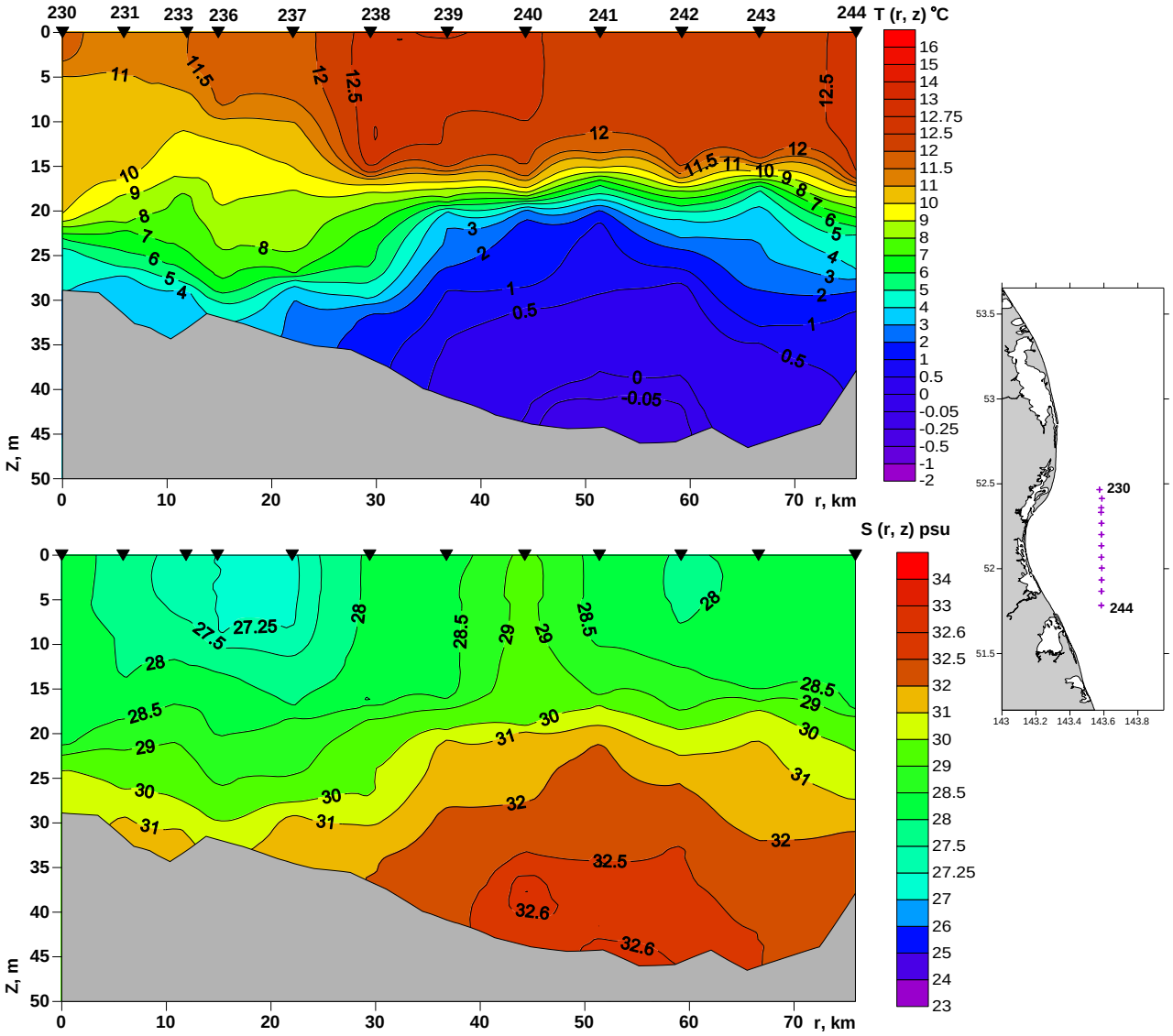

Figure 6.12 - Distribution of Temperature *T(r,z)* and salinity *S(r,z)* and the location of the sampling stations for a hydrologic transect in the offshore area acquired on 9th September, 2010.

Near-surface water salinity appears to be rather low in the offshore area, which is especially noticeable when compared with similar data for 2008 (Figure 6.14). The entire offshore area was filled with low-salinity water in 2010, indicating that Amur River water was present in large volumes. Note that the thermohaline front disappeared from the northern part of the near-shore area just offshore of Chayvo Bay. There was no trace of it in the southern part of the offshore area either. Apparently, it was located far to the south of the survey area. The temperature field was within 11–13°C and was relatively homogeneous along the entire coastline.

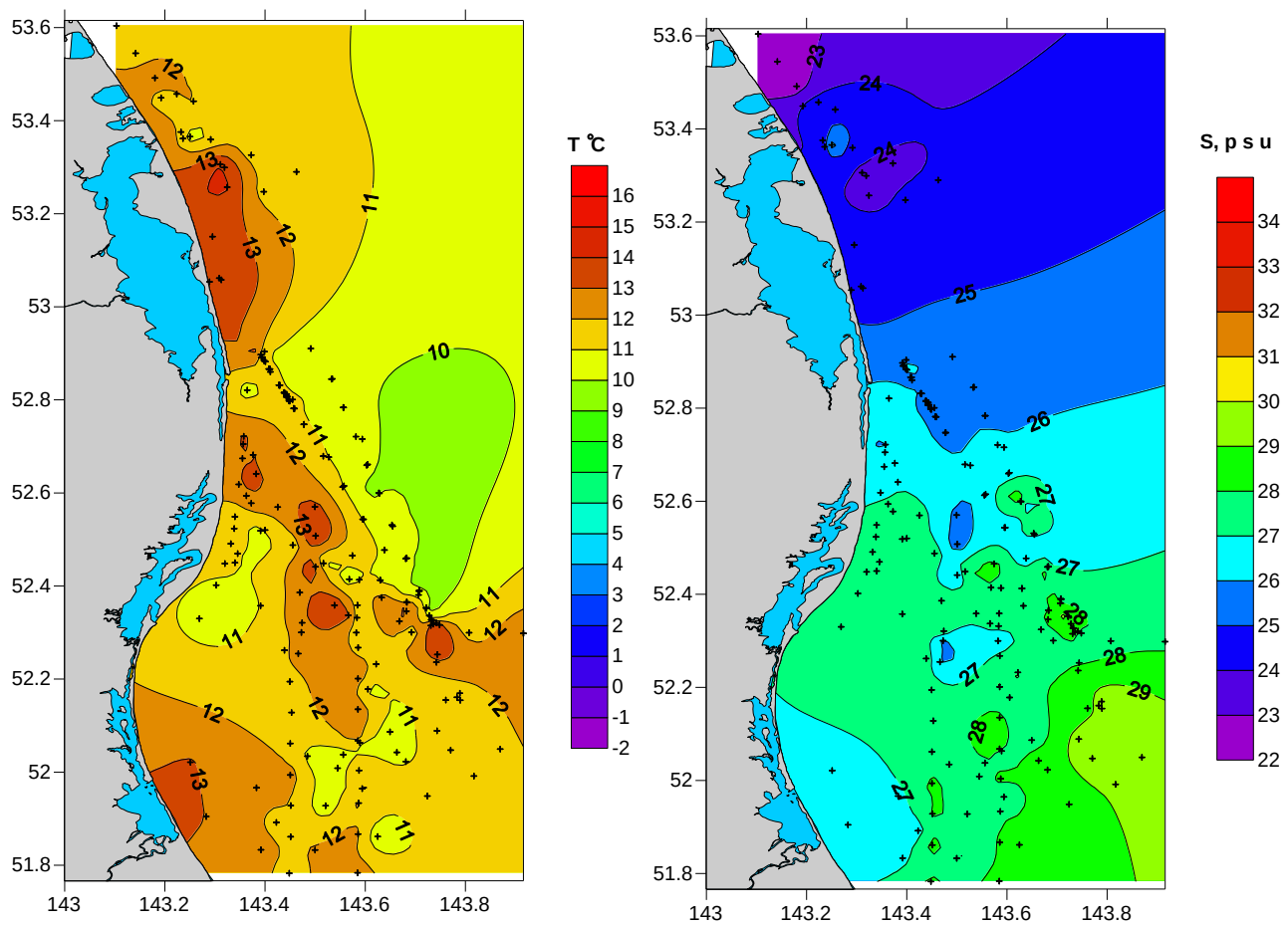

Figure 6.13 - Spatial distribution of near-surface water temperature and salinity in September 2010 (constructed from vertical hydrologic profiles acquired between 4th and 20th September, 2010).

It should be emphasized that the hydrologic survey was performed in good weather during the entire summer season and was completed before the arrival of the fall storm season on 21st September, 2010. An especially strong storm occurred at the end of September (29th-30th), although none of its after-effects were recorded.

Thus hydrologic conditions in the inshore and offshore areas were formed in the absence of intensive storm-wind mixing. As a consequence, only shallow inshore areas (Figure 6.15) were extensively warmed and freshened, not the deeper offshore area, as it was after a heavy fall storm in 2008 (Figure 6.16). The near sea-floor temperature and salinity distribution maps confirm the presence of a large volume of freshened water in the shallow zones of just offshore from the Piltun and Chayvo Bays.

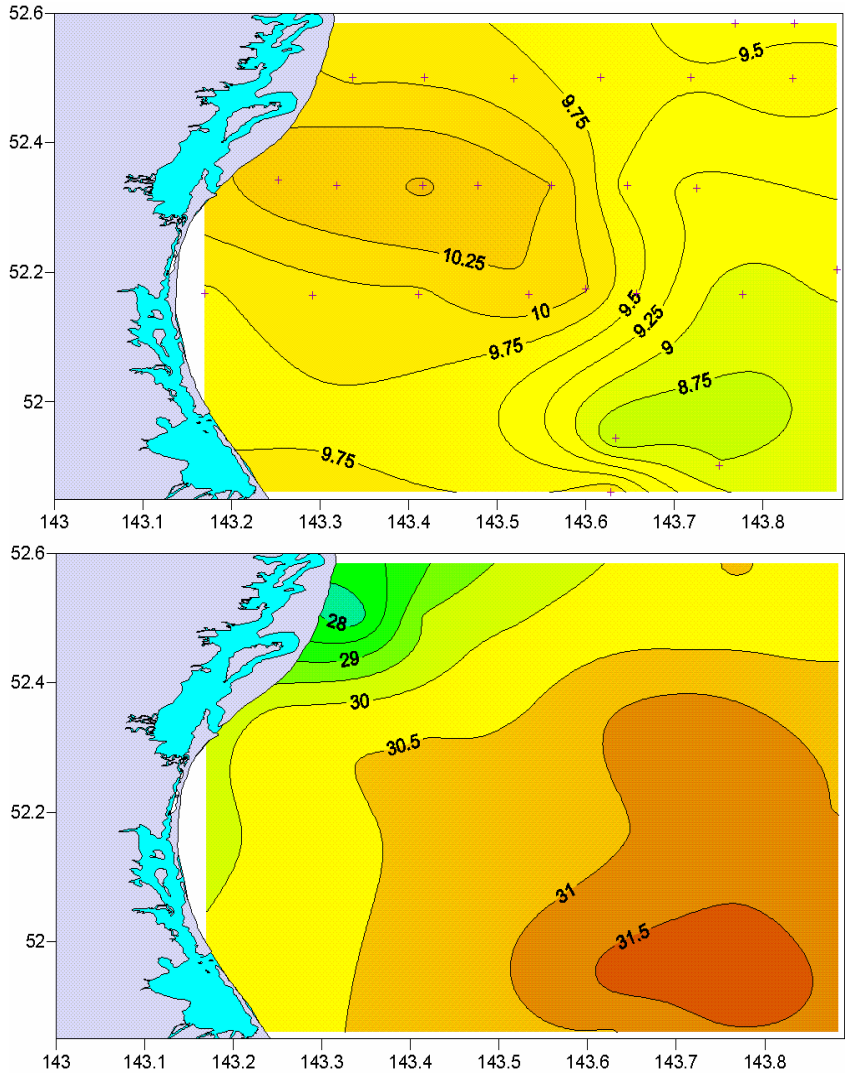

Figure 6.14 - Spatial distribution of near-surface water temperature and salinity for the southern section of the offshore area in September-October 2008 (constructed from vertical hydrologic profiles acquired between 28th September and 4th October, 2008).

A thermohaline front developed in the near sea-floor section of the waters adjacent to Piltun and Chayvo Bays in September 2010. This front divided the inshore waters into a warm and fresh shallow section and a deeper section with low temperatures and high salinities.

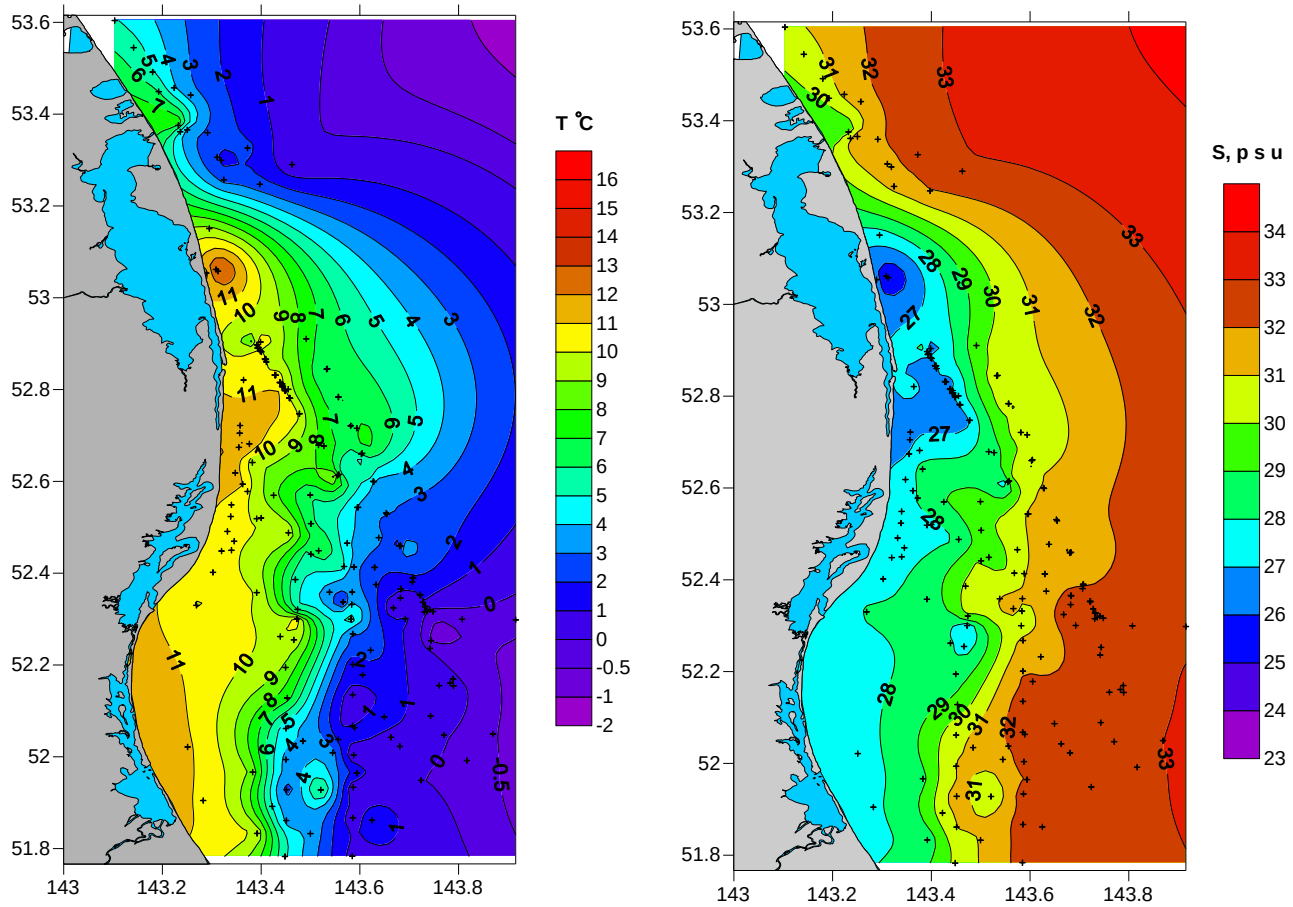

Figure 6.15 - Spatial distribution of near-surface water temperature and salinity during September, 2010 (constructed from vertical hydrologic profiles acquired between 4th and 20th September, 2010).

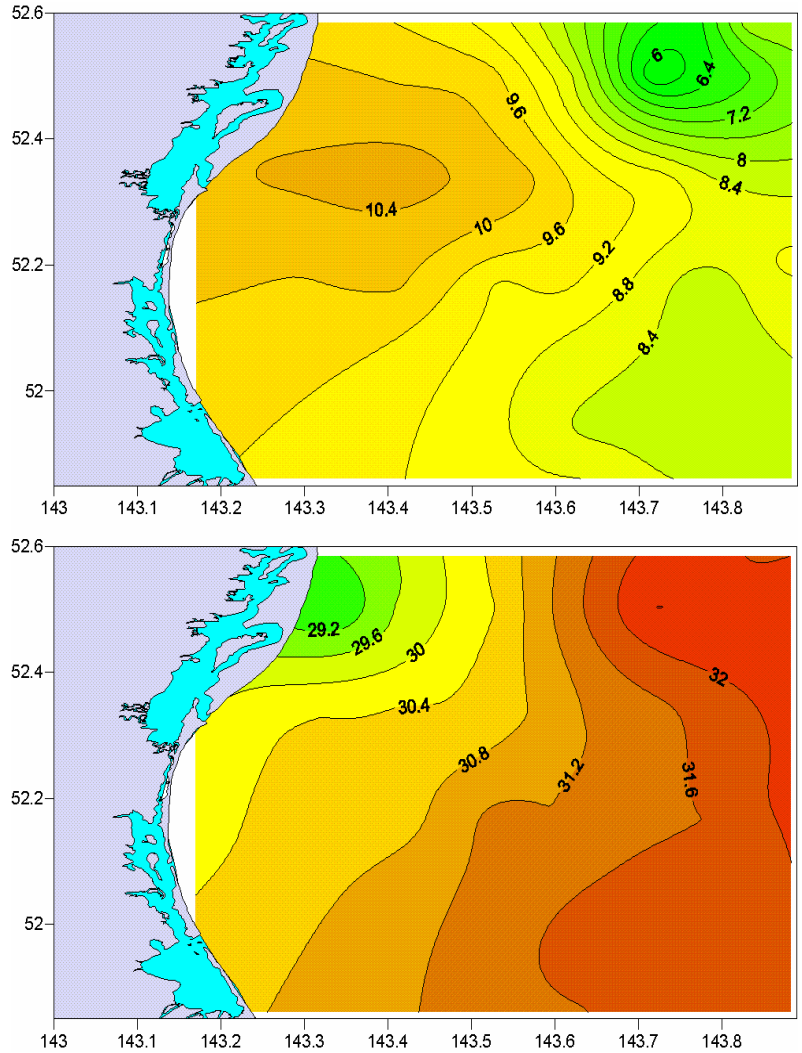

Figure 6.16 - Spatial distribution of near-surface water temperature and salinity for the offshore area in September-October 2008 (constructed from vertical hydrologic profiles acquired between 28th September and 4th October, 2008).

6.3 Monitoring the inter-annual variation of hydrology in the feeding areas

Hydrological observations to monitor the inter-annual variability of hydrological parameters in the Piltun and Offshore feeding areas were continued in 2010. Hydrological data were acquired at locations where data were acquired in previous years. The following section discusses the results of observations in both areas for August and September 2010.

Figures 6.17 and 6.18 are plots showing the vertical distribution of sea water temperature and salinity in the Piltun Bay area in August and September 2010. Analysis of this data indicates that the vertical distribution of water temperature and salinity is different than had been previously observed in the near-shore area just offshore of Piltun Bay during any previous

August; low near-surface salinity (24.29 psu) and near-surface temperature up to 14.10°C. This warm and fresh layer was 7 to 8 meters thick.

This was a very unusual situation and had never been observed before. It continued through the following weeks. The observations of September 2010 showed that the low-salinity water filled the near-shore area just offshore of Piltun Bay from the surface layer almost down to the bottom (Figure 6.18). The fact that this had not occurred previously indicates that the volume of fresh water was greater than normal in near-shore area just offshore of Piltun Bay.

It should be noted that fresh water continued to accumulate along the near-shore area just offshore of Piltun Bay until late August, and only began to accumulate in the near-shore area just offshore of Chayvo Bay after that. The fresh water accumulating and remaining in the inshore area probably accounts for the abnormally low salinity throughout the entire water column. The fact that the water did not move south along the coast from the mouth of Piltun Bay may be partially attributable to unusual atmospheric circulation in the summer of 2010. The absence of southerly and southeasterly winds in the coastal area and, as a consequence, the absence of upwelling, contributed to the accumulation of fresh water in the shallow near-shore area. It could also be attributed to a possible change in water circulation in the near-shore area just offshore of Chayvo Bay. The thermohaline front that was present in the northern part of the near-shore area just offshore of Chayvo Bay up to late August 2010 may have been caused by the stable upward movement of water from the bottom in that part of the near-shore area just offshore of Chayvo Bay.

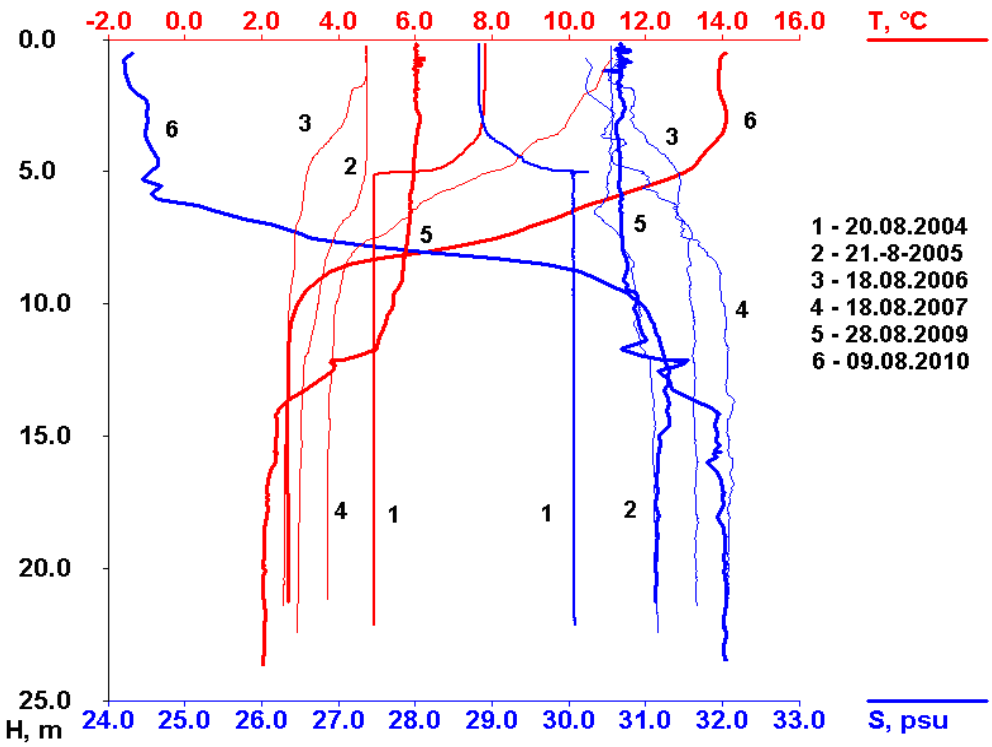

Figure 6.17 – Inter-annual water temperature and salinity variations in the waters adjacent to Piltun Bay for August.

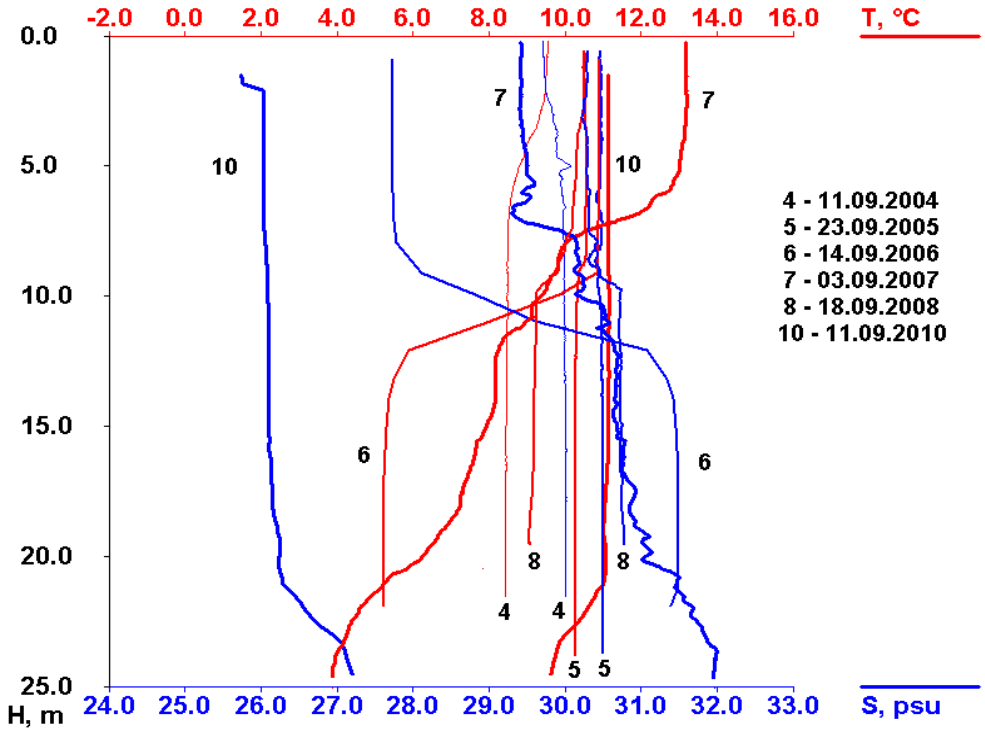

Figure 6.18 – Inter-annual water temperature and salinity variations in the waters adjacent to Piltun Bay for September.

The abnormal hydrologic situation that developed in the near-shore area just offshore of Piltun

Bay and persisted throughout the summer was bound to affect hydrologic conditions in the offshore Area. Only highly saline and cold water from the Sea of Okhotsk was present in the offshore area in early and mid August as a result of fresh water accumulation in the inshore area (Figure 6.4). Freshwater did not enter the offshore area until late August (Figure 6.19).

Water characteristics and volumes were typical for August and did not go beyond the values observed previously. Salinity was 28.88 psu and temperature was 13.98°C. However, an apparently significant ingress of Amur River water continued, because, unusually, the volume of fresh water was greater than normal in the offshore area the following month (Figure 6.20).

Such low near-surface salinity (27.64 psu) had not been observed there prior to 2010. Water temperature was 10.56°C, which was within the typical range for that area. Figure 6.20 shows that the freshening can reach depths of up to 28 meters. The low salinity forms a thick lens and is not the result of vertical mixing of the fresh surface layer. Water characteristics in the near sea-floor zone of the offshore area did not differ from the values typical for September. Water temperature and salinity were 1.68°C and 32.12 psu, respectively.

6.4 Possible explanation for the stationary fresh water lens off Piltun Bay in 2010

The unusual hydrological conditions experienced in the summer of 2010 off north eastern Sakhalin Island emerged at the very beginning of the summer season. This is confirmed by hydrological observations performed in June 2010.

The 2010 hydrologic observations in the Inshore and Offshore gray whale feeding areas were begun in June on the research vessel *Pavel Gordienko*. Between 6th June and 7th July 120 vertical hydrologic profiles were acquired. Figure 6.21 shows the locations of these hydrologic stations.

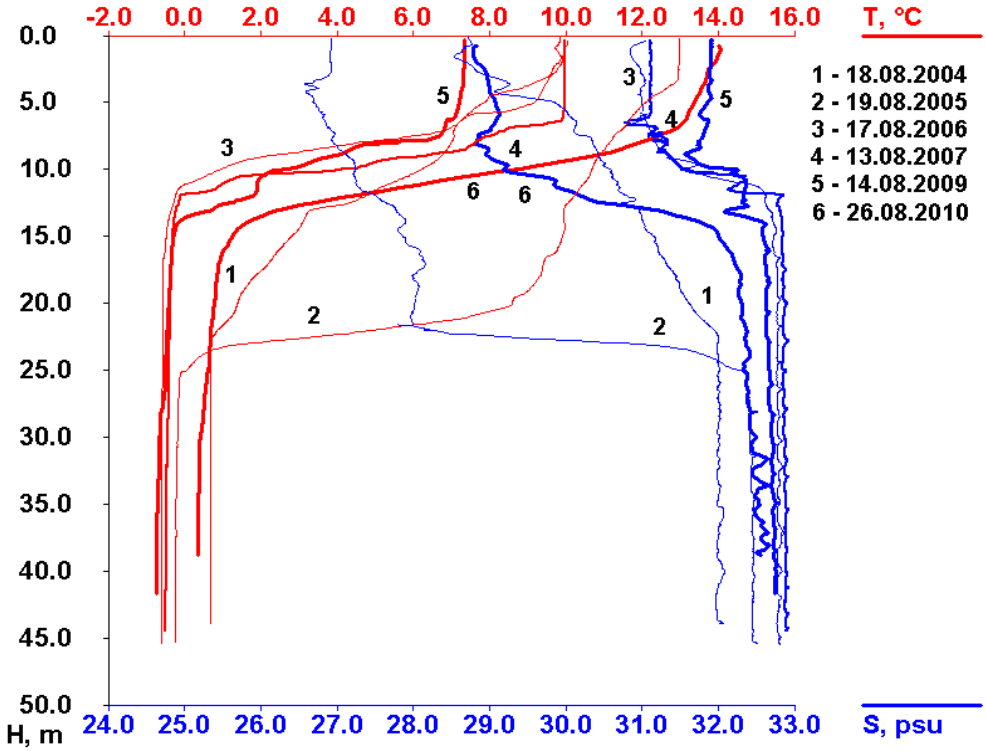

Figure 6.19 – Inter-annual water temperature and salinity variations in the offshore feeding area for August.

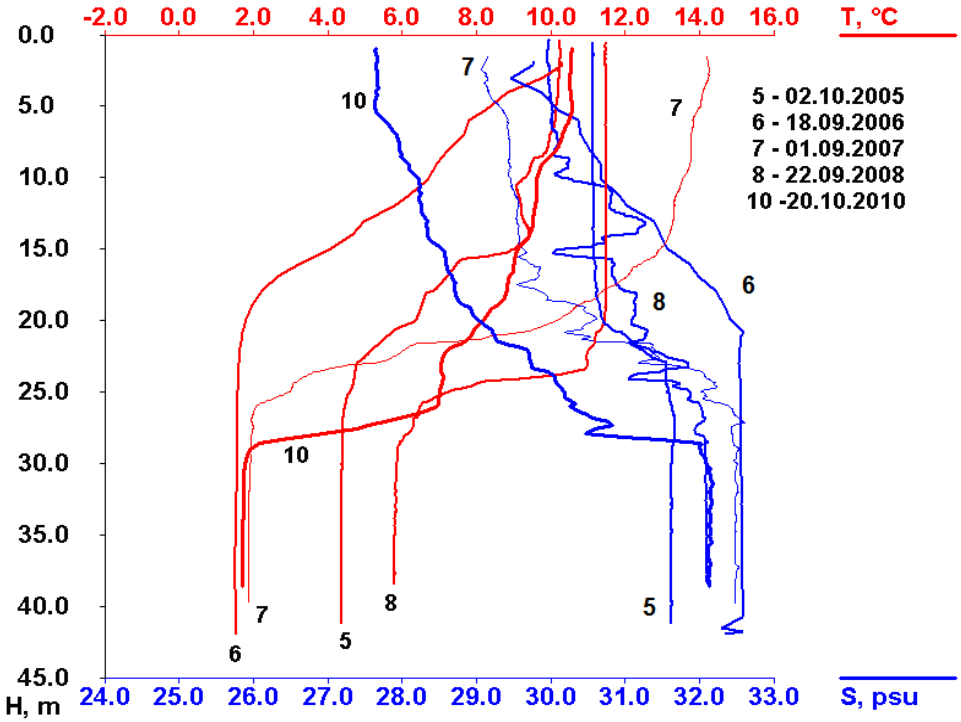

Figure 6.20 – Inter-annual water temperature and salinity variations in the offshore feeding area for September.

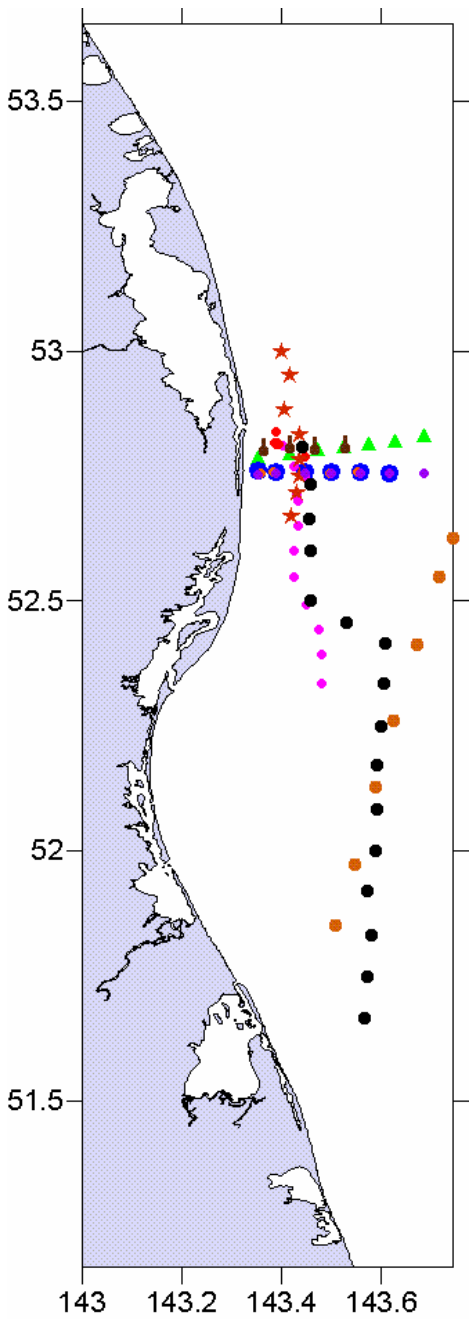

Figure 6.21 – Map of the survey area showing the hydrological station locations in June/early July 2010. Different symbols indicate profiles taken at different times.

These observations allowed the hydrologic conditions in both areas to be evaluated during the early summer of 2010.

Hydrologic observations in the summer of 2010 were begun on the 6th June on a profile running through the Offshore feeding area. This survey was used to evaluate the hydrologic conditions at the very beginning of the summer season (Figure 6.22).

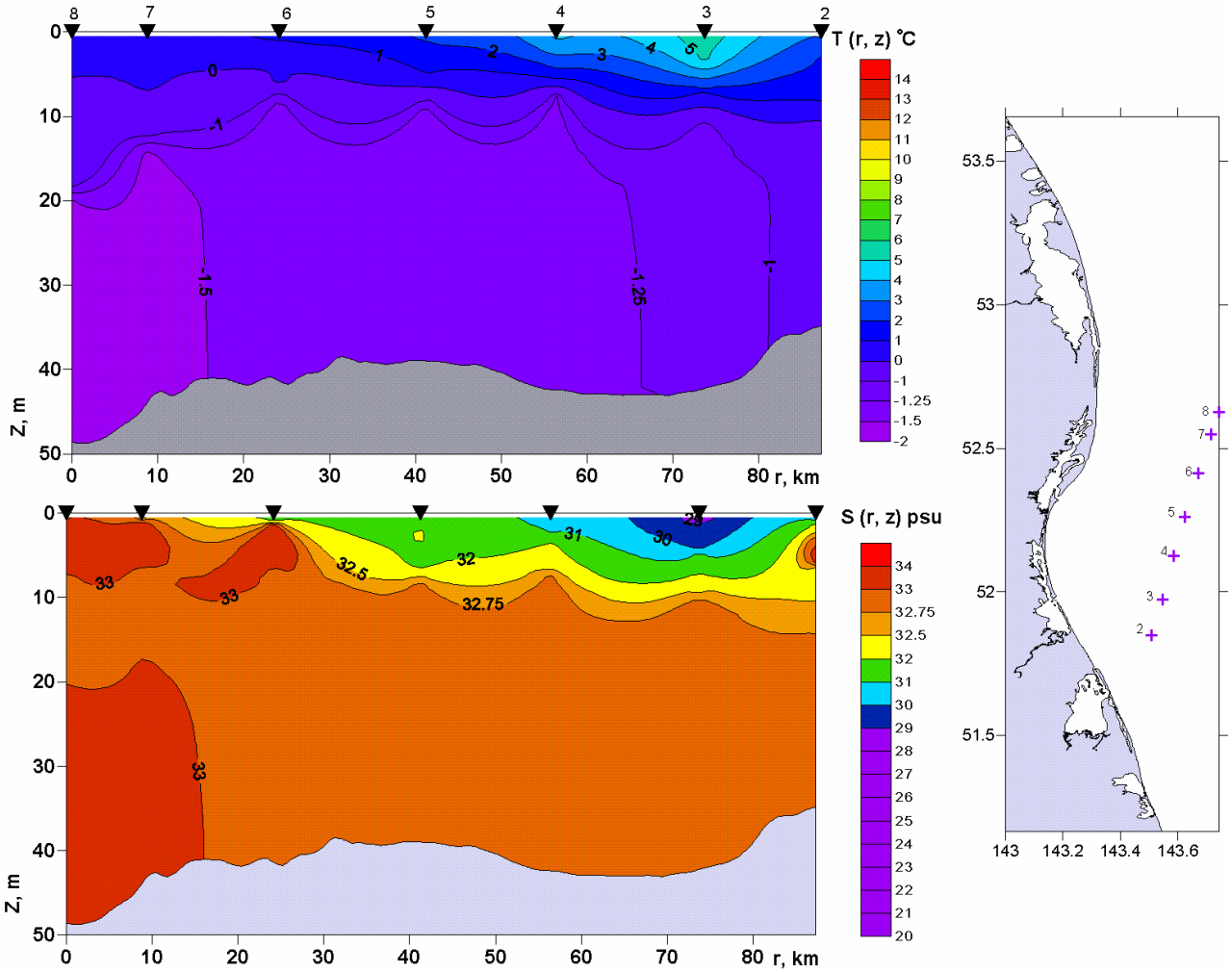

Figure 6.22 - Distribution of Temperature *T(r,z)* and salinity *S(r,z)* and the location of the sampling stations for a hydrologic transect in the offshore area acquired on 6th June, 2010.

The low absolute temperatures and high salinities on the surface marked the end of the winter season. Near-surface water temperatures below freezing (-0.09°C) and salinities of up to 32.93 psu were recorded at station 8 in the northern part of the profile. These values are typical for the beginning of spring. The low temperature of -1.55°C and high salinity of 33.03 psu at a depth of 20 m signify that these values are close to winter conditions.

An area of fresh (28.90 psu) and relatively warm (4.99°C) near-surface water in the southern part of the offshore area appears to be somewhat abnormal; the layer was less than 4 m thick. The low salinity suggests that this water might have flown in from the Amur River estuary. This early appearance of Amur River water in the offshore area was unexpected, since it was expected that fresh water would reach the offshore area later. It is difficult to estimate the length

of the lens along the coast. However, subsequent observations made in the inshore area on 12th June, 2010 confirmed the presence of warm and fresh water along the coast (Figure 6.24).

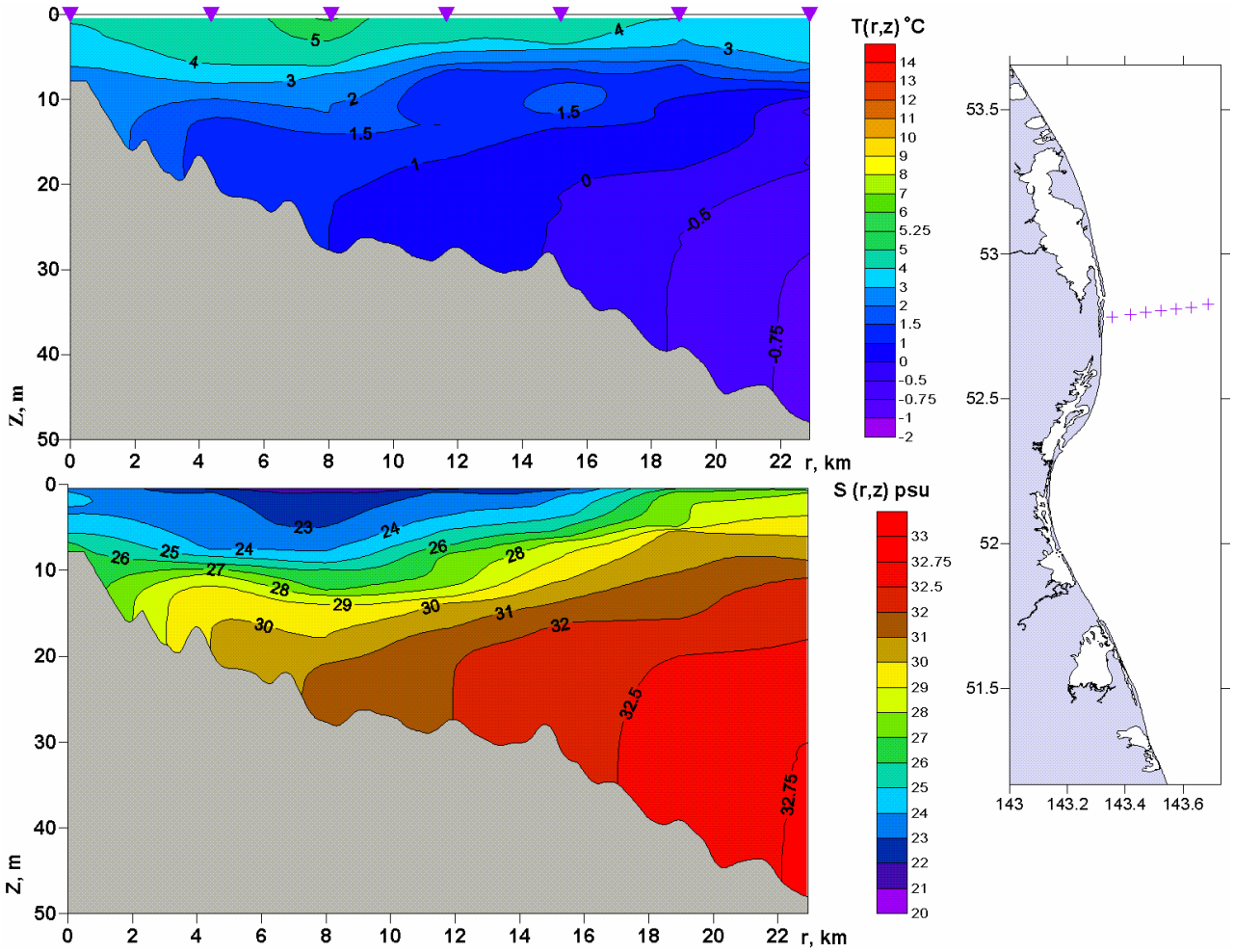

Figure 6.23 - Distribution of Temperature *T(r,z)* and salinity *S(r,z)* and the location of the sampling stations for a hydrologic transect in the area adjacent to Piltun Bay acquired on 12th June, 2010.

The core of this water was at some distance from the coast. Water salinity was 22.8 psu in the core and the fresh water reached a depth of 18 meters.

These data indicate that water from the Amur River estuary can reach the inshore and offshore gray whale feeding areas in early June. It is not known whether the two fresh water spots encountered at two relatively distant locations are parts of a single lens. They were probably different portions of the Amur River water reaching the area after the ice cover melted. Critically, this water began entering the northeastern shelf while the offshore water still had temperatures below 0°C.

Subsequent observations showed that these water patches were relatively small and passed by the survey area very quickly. This was confirmed by the survey of 18th June, 2010, during which no fresh water was recorded (Figure 6.24).

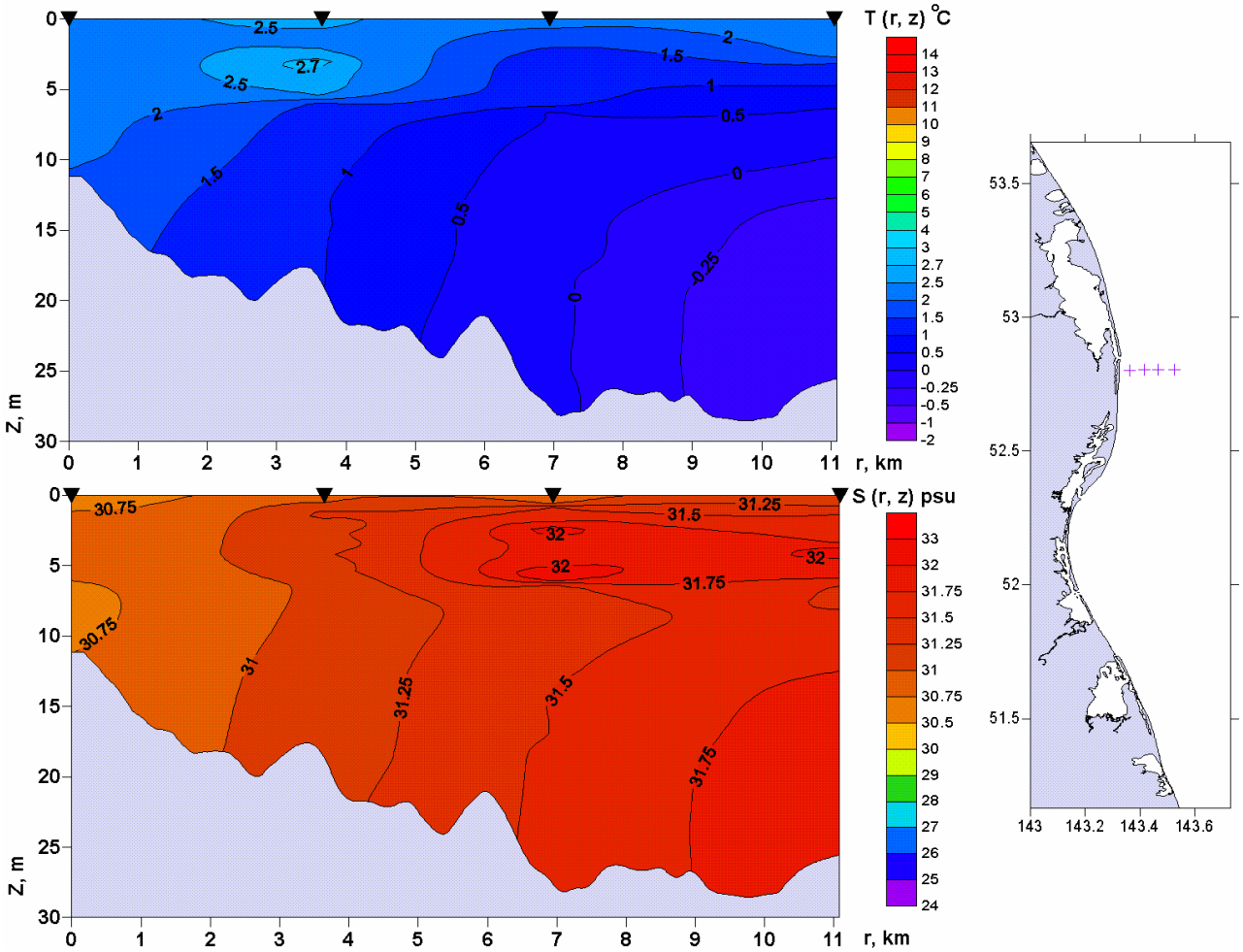

Figure 6.24 - Distribution of Temperature *T(r,z)* and salinity *S(r,z)* and the location of the sampling stations for a hydrologic transect in the area adjacent to Piltun Bay acquired on 18th June, 2010.

It should be noted that stable southerly and southeasterly winds at speeds of 7 to 8 m/s, lasting from 12th June through 24th June, 2010,. It is a reasonable assumption that these water characteristics were caused by upwelling, which was occurring at this time. However, the most probable assumption is that the upwelling took place at the same time or after one of the slugs of fresh water had passed the area. The subsequent observations of 22nd June, 2010 recorded another slug of Amur River water approaching the area. Its precursors, such as higher water temperatures and lower salinities, although not yet significant, were clearly evident against the surrounding water, indicating the future boundaries and core of the lens (Figure 6.25).

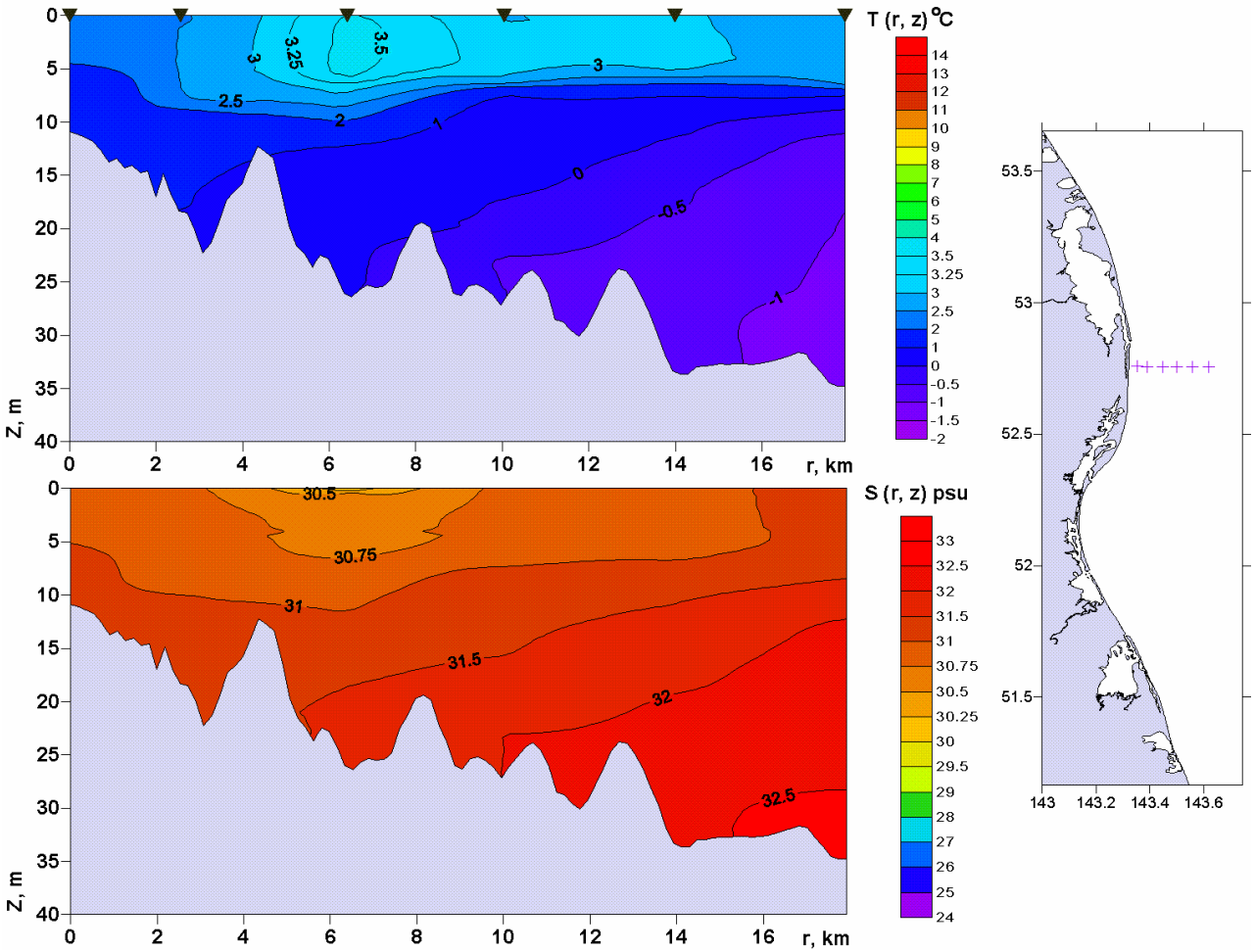

Figure 6.25 - Distribution of Temperature *T(r,z)* and salinity *S(r,z)* and the location of the sampling stations for a hydrologic transect in the area adjacent to Piltun Bay acquired on 22nd June, 2010.

Note that the slug of Amur River water had begun its approach before the wind changed its direction from southerly to northerly on 25th June, 2010. The lens was observed near the mouth of Piltun Bay on 26th June, 2010. Its boundary, marked by froth and dirty green color water, could clearly be seen against the clear and transparent cold water (Figure 6.26).

A thin layer of fresh, warm water (up to 27 psu and 8.24°C) approached from the North. Its core was in the top 2 m layer; however, it could be traced down to 5–6 m, as recorded by several vertical profiles acquired around the approaching front.

Another profile covering the northern part of the inshore area was acquired on the same day (26th June, 2010) to confirm the approach of the fresh water. The observations confirmed that a slug of fresh water was approaching the mouth of Piltun Bay (Figure 6.27). The head of the slug

with a salinity of up to 26.32 psu was thicker than the tail, where salinity was lower (up to 26.23 psu). This feature of the movement of the slug was later confirmed by other observations. The warm layer was 6-7 m thick and the water temperature at the slug surface was 7.74°C. The warm and fresh layer thinned towards the tail ('tail' is arbitrarily used for this section of the slug because its real boundaries are unknown).

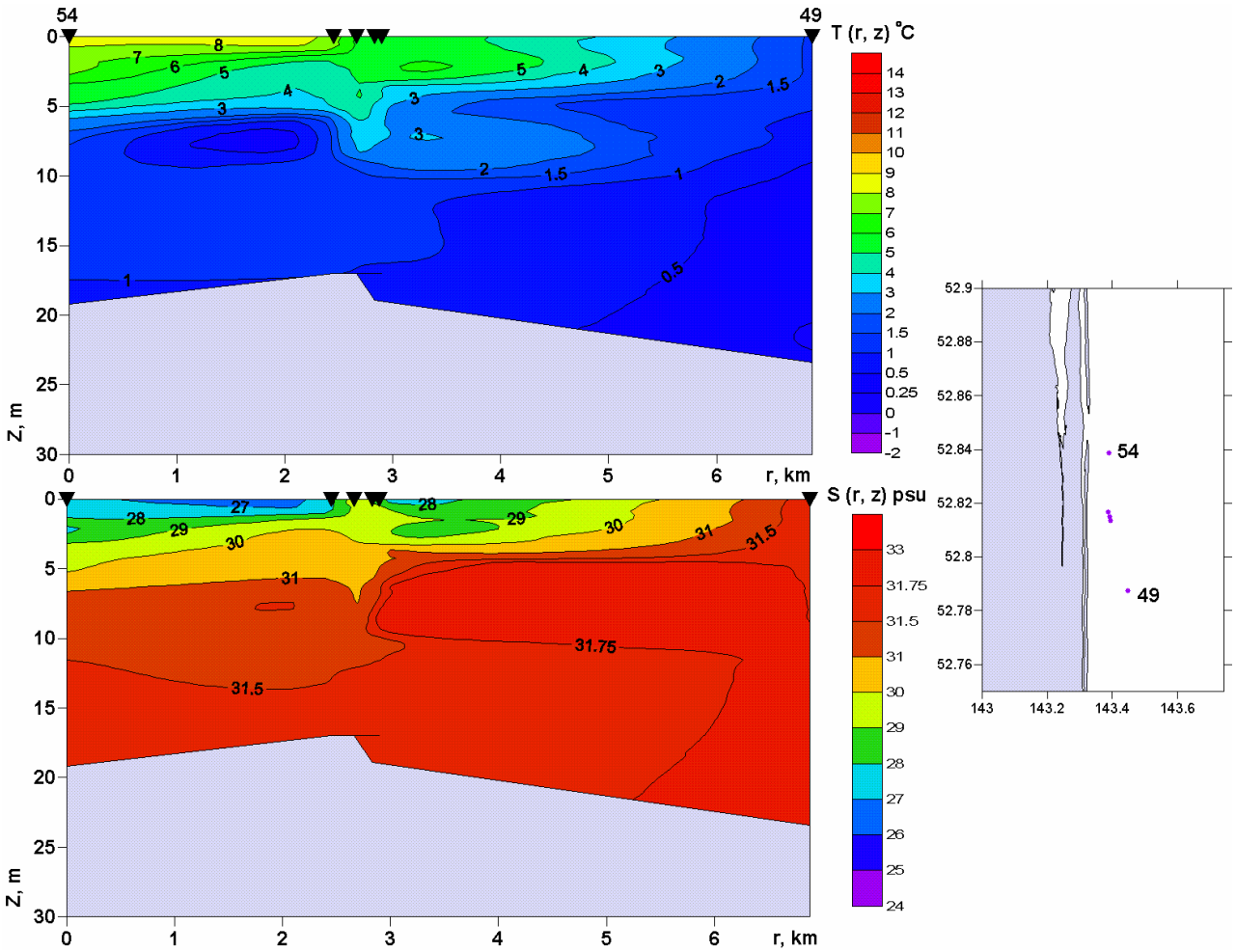

Figure 6.26 - Distribution of Temperature *T(r,z)* and salinity *S(r,z)* and the location of the sampling stations near the mouth of Piltun Bay acquired on 26th June, 2010, during the passing of the fresh water boundary.

A latitudinal profile was acquired on 27th June, 2010 to obtain better data on the approaching slug and its horizontal dimensions. This profile showed the eastern boundary of the slug and its core, which was near the coast (Figure 6.28). It was near the coast where fresher and relatively warm water occurred throughout the entire water depth. The maximum near-surface water temperature in that area reached 9.26°C while the salinity was 25.96 psu.

An attempt was made to identify the velocity of the fresh water slug moving along the coast. Observations were executed for this purpose southwards from the mouth of Piltun Bay on 28th June, 2010. These observations showed that the front of warm and freshened water had moved southwards from the mouth of Piltun Bay (Figure 6.29). The observations on this profile confirmed that the core of the slug had the maximum depth and extreme temperature and salinity values (Figure 6.29).

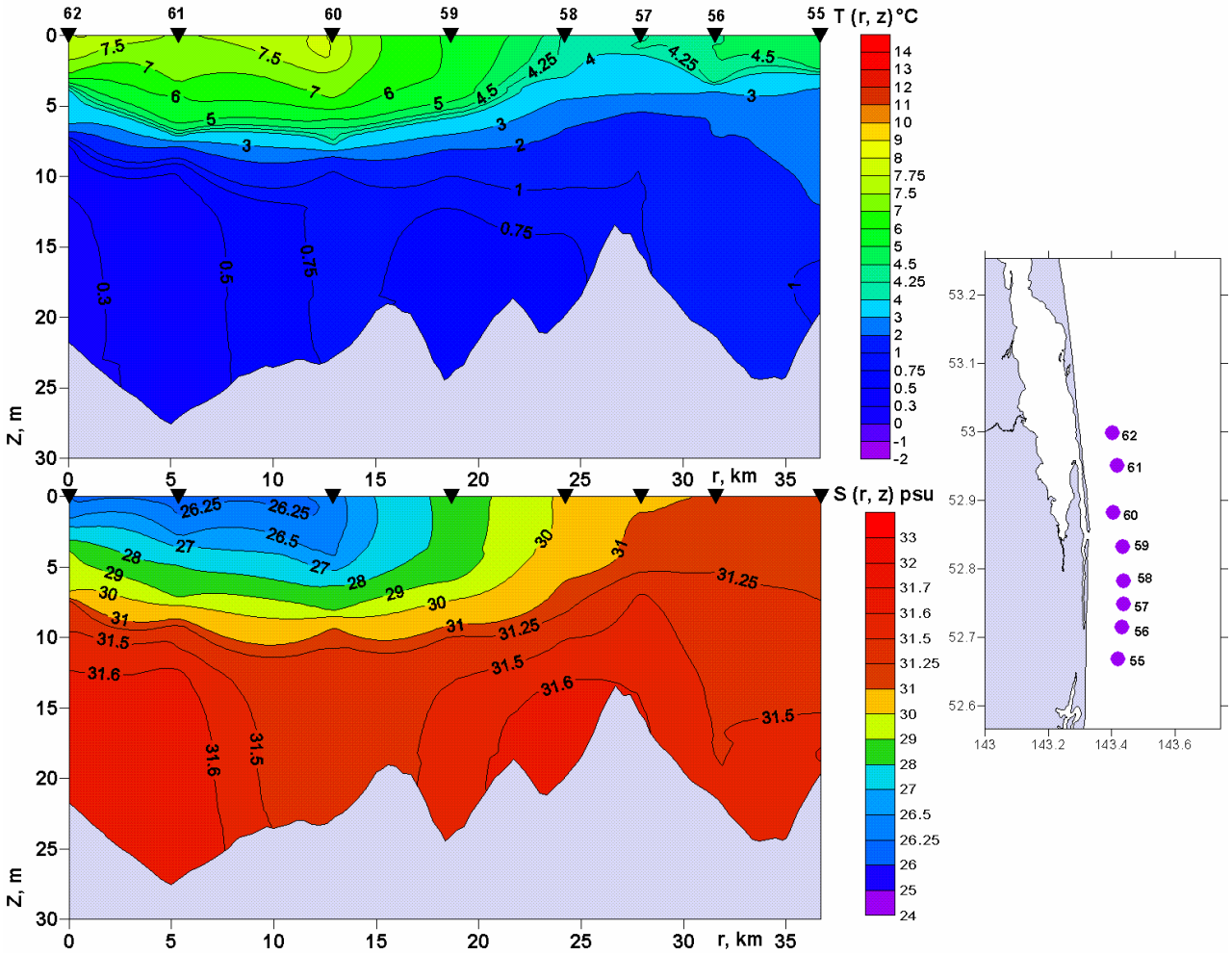

Figure 6.27 - Distribution of Temperature *T(r,z)* and salinity *S(r,z)* and the location of the sampling stations near Piltun Bay acquired on 26th June, 2010.

This can clearly be seen at measurement station 72 located near the fresh water front, which could be identified on the surface by the characteristic layer and water color. Another slug of fresh water with a salinity slightly above 26.88 psu could be distinguished downstream of the fresh water front towards the south.

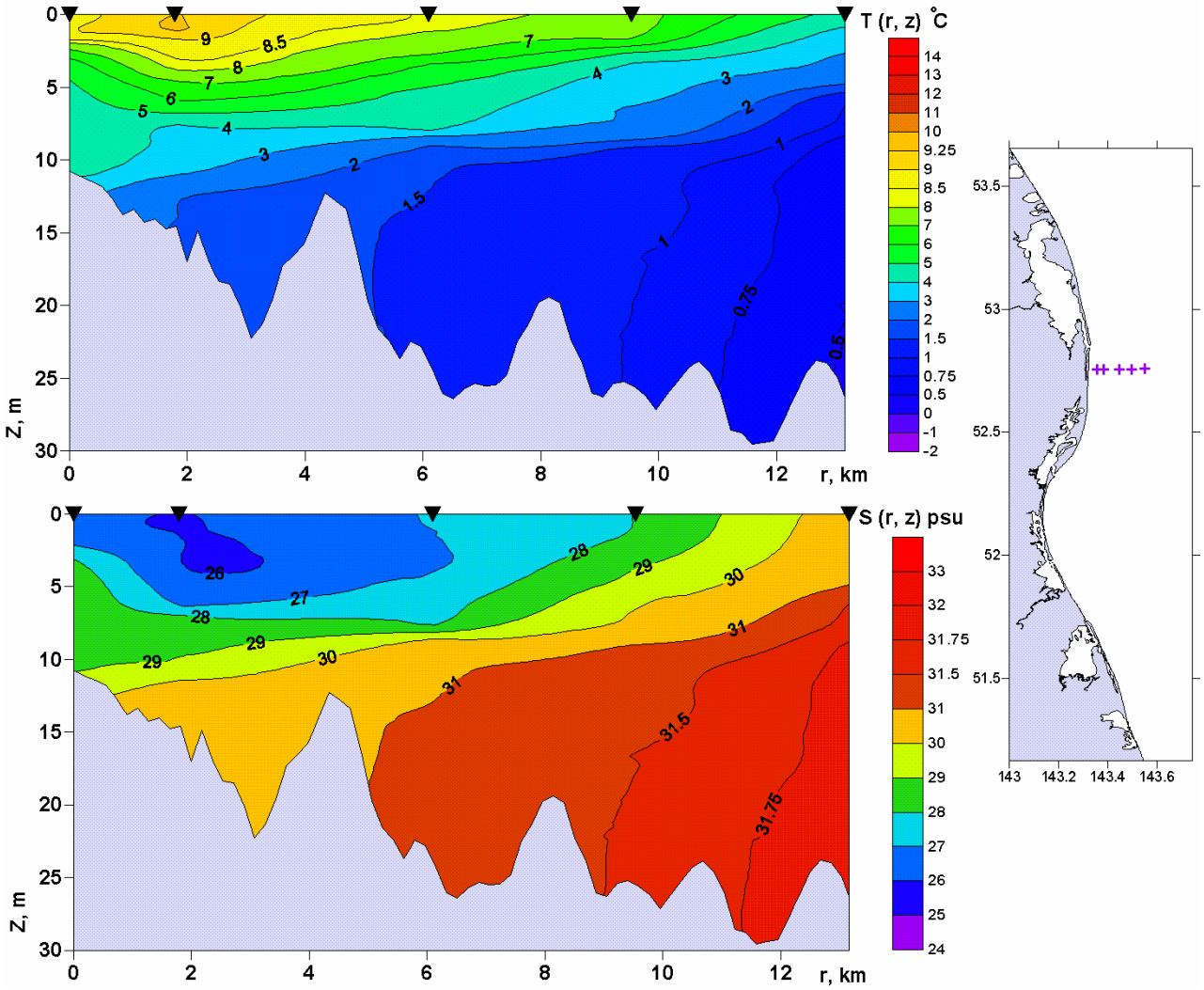

Figure 6.28 - Distribution of Temperature *T(r,z)* and salinity *S(r,z)* and the location of the sampling stations near Piltun Bay acquired on 27th June, 2010.

Water characteristics measured at station 79 are notable on this profile, since that station recorded the lowest surface water temperature of 3.06°C. The water temperature increases towards the south until it reaches 4.07°C at the southern-most station of this profile. A thermohaline front was formed upstream of Station 79, which separated the waters of the Amur River and the Sea of Okhotsk. It should be noted that the front was in the northern part of the near-shore area just offshore of Chayvo Bay.

The above description shows that a slug of freshened and warm water was identified on 26th June through 28th June, 2010, passing the mouth of Piltun Bay moving south. Within two days from the time it was identified on 26th June, 2010 it moved 40 km towards the south. Its average speed was therefore 20 cm/sec.

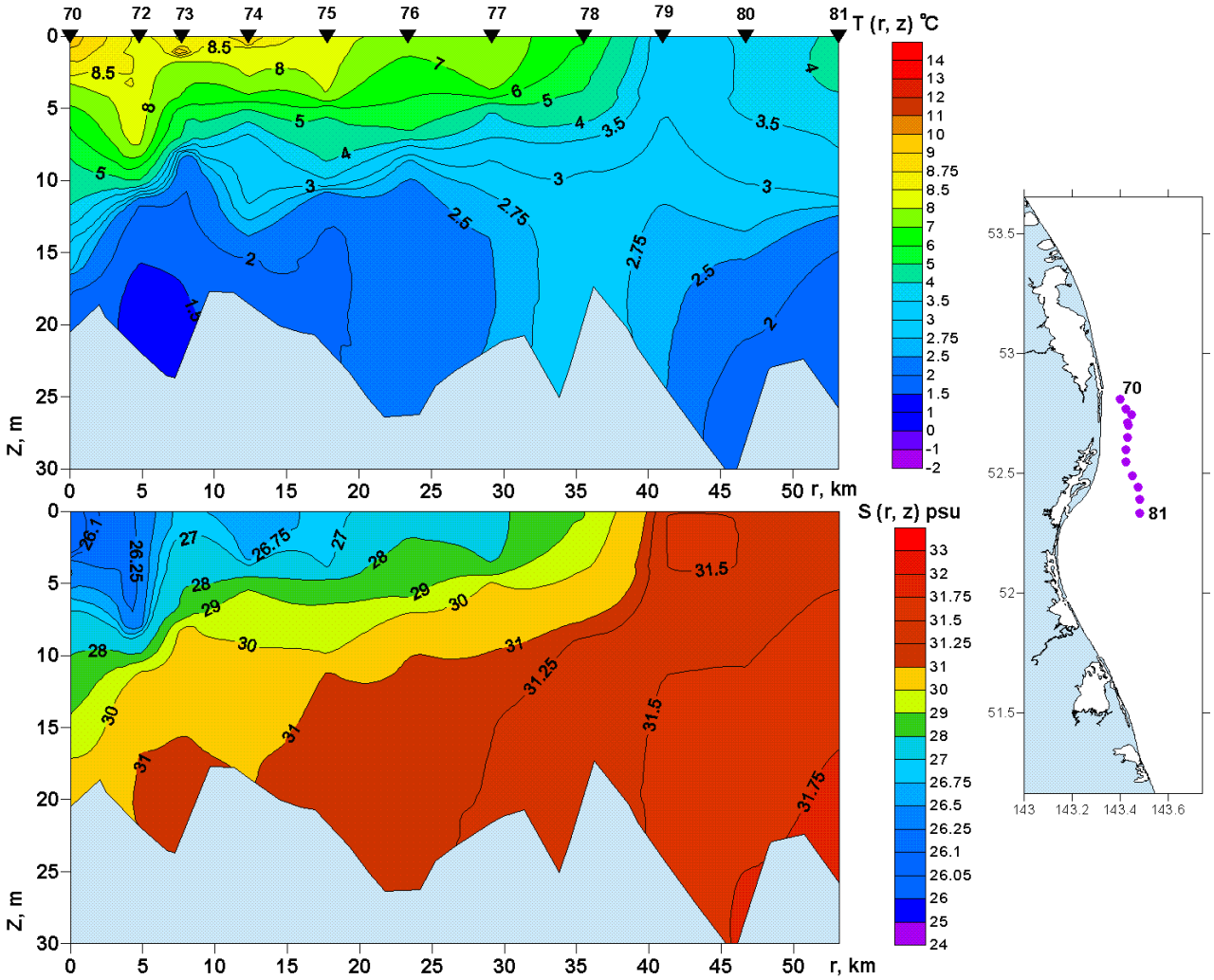

Figure 6.29 - Distribution of Temperature *T(r,z)* and salinity *S(r,z)* and the location of the sampling stations near Piltun Bay acquired on 28th June, 2010.

Another profile was acquired on 2nd July, 2010, running offshore from the coast. The measurements showed that the slug of freshened water remained in the Piltun feeding area (Figure 6.30). Compared to the previous similar survey of 27th June, 2010, the core of the slug had shifted offshore. A few days later, on 7th July, 2010, another long hydrological profile running through the Piltun and Offshore feeding areas was taken. That profile showed that the lens of freshened water was not far from the area where it was observed on 28th June, 2010 (Figure 6.31).

This indicated that the lens of fresh water remained near the area where it was first identified and had not moved farther towards the south (Figure 6.32). Figure 6.32 shows the location of the slug of freshened water boundary at different times. The observations of 7th July 2010

showed that the slug had even retreated slightly northward from the area where it was seen on 28th June, 2010. This shows that the slug of Amur River water stopped near Piltun Bay and its front was in the northern part of the near-shore area just offshore of Chayvo Bay at that time. It stopped moving farther south and impacted hydrologic conditions in the inshore area for that season.

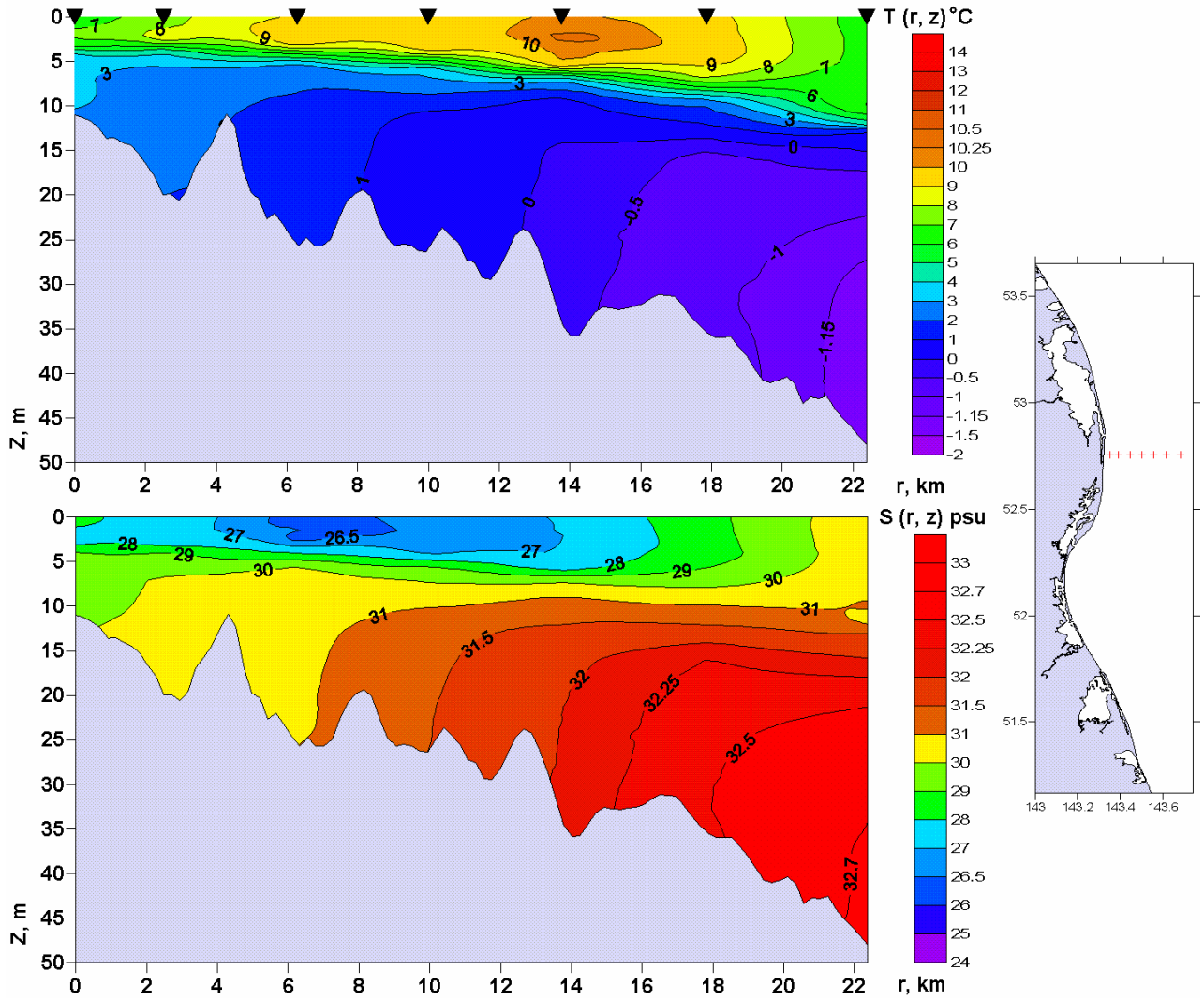

Figure 6.30 - Distribution of Temperature *T(r,z)* and salinity *S(r,z)* and the location of the sampling stations near Piltun Bay acquired on 2nd July, 2010.

Of all the stations on the long profile transecting both areas (Figure 6.31), the water characteristics near Station 108 are noteworthy. The thermohaline front facing that station is very distinct and remains in the northern part of the near-shore area just offshore of Chayvo Bay. The area of cold water on the surface at Station 108 resembles the conditions of 28th June, 2010 (Figure 6.29). It is possible that this is a constant feature of the water structure in that area

and is persistent over time.

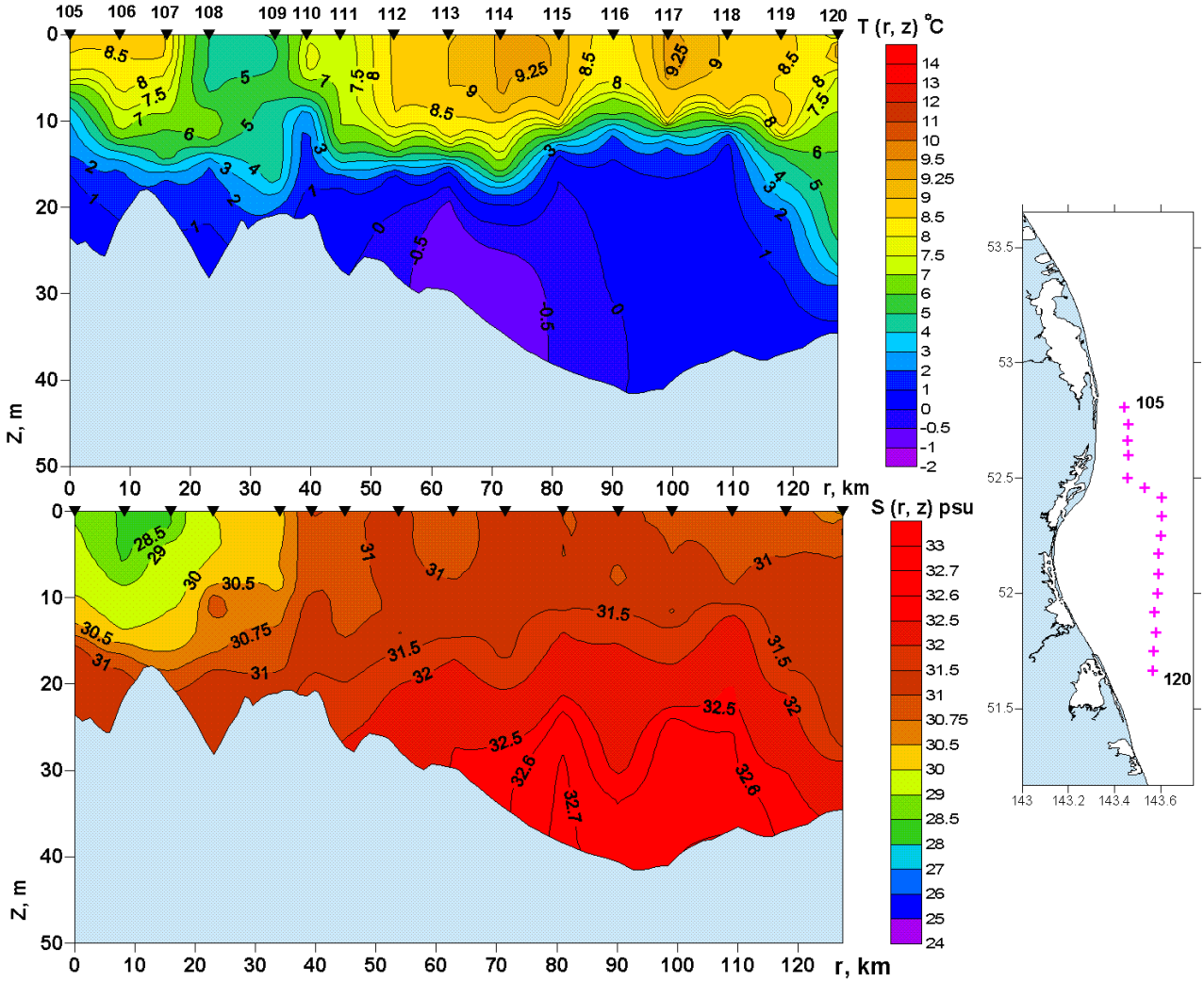

Figure 6.31 - Distribution of Temperature *T(r,z)* and salinity *S(r,z)* and the location of the sampling stations in the inshore and offshore areas acquired on 28th June, 2010.

The rise in iso-temperature contours towards the surface may signify upward movement of near-bottom water. The halt in the southward movement of the slug of warm, freshened water may be attributed to the upward movement of bottom water in the northern part of the near-shore area just offshore of Chayvo Bay. The longitudinal profiles (Figure 6.29 and Figure 6.31) suggest the same. A similar distribution of temperature contours in the northern part of the near-shore area just offshore of Chayvo Bay also occurs, but at a later time, late August (Figure 6.9), and early September (Figure 6.10) and, to some extent, mid September (Figure 6.12) of 2010. The stability of these dynamics over a long period of time could cause Amur River water to become stationary in the inshore area.

Additional information, especially, satellite surveys, are required to confirm this theory. Clear weather in the summer season must have enabled sufficient satellite coverage of the inshore area, and those data must also be analyzed.

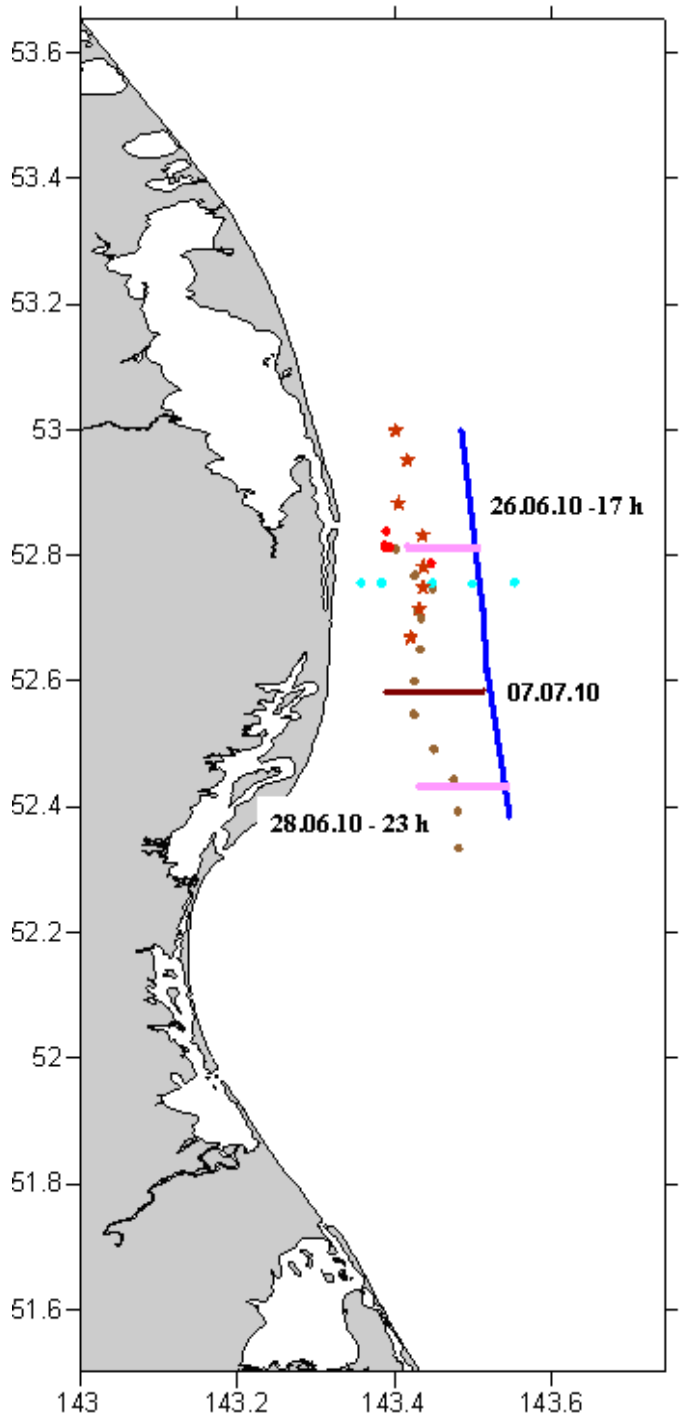

Figure 6.32 – Map of the survey area showing the boundaries of the fresher water and the hydrological station locations from 26th June to 7th July 2010. Different symbols indicate profiles taken at different times. The blue line represents the probable eastern boundary of the fresher water slug.

6.5 The effect of shallow bays on inshore hydrological conditions

It is believed that the numerous shallow bays located along the northeastern coast of Sakhalin Island significantly influence the hydrologic conditions in the inshore area and, consequently, the gray whale feeding base. No special studies have covered this issue or been referenced in previous reports. This section will present some external evidence of this influence to further define the issue.

The waters of these bays, rich in inorganic and organic material enter the inshore area. Satellite photos provide clear evidence of this process (Figure 6.33), two spots of turbid water out flowing from the Piltun and Chayvo Bays are clearly distinguishable on the photograph. This process is most pronounced in spring after the snowmelt and in summer during heavy rains.

This phenomenon is also observed during hydrologic surveys. It was first recorded on 26th June, 2010 not far from the mouth of Piltun Bay. Somewhat later, on 7th July, 2010, a patch of turbid water was identified south of the mouth of Piltun Bay. In August, a patch of turbid water was recorded twice in the mouth of Piltun Bay, on 4th and 23rd August, 2010. Figure 6.34 gives a panoramic photo of the patch. Hydrologic measurements were taken within and near this patch (Stations 8 and 9). Figure 6.35 gives the results of these measurements.

The plots show that water temperature in Piltun Bay is higher (10.51°C) than the background water temperature of 9.57 °C. Water salinity in the bay (25.09 psu) is lower than the background water salinity of 26.24 psu.

The bay water proved to be less saturated with oxygen than the background water. Moreover, at depths of 5-10 m, where the background water exhibited a maximum oversaturation of up to 120 percent, the oxygen saturation of the bay water was at a distinct minimum.

The temperature and salinity distribution suggests that the slug of the Piltun Bay water was about 5 m thick.

Figure 6.33 – Satellite images of the out flow of water from: (Top) Piltun Bay; and (Bottom) Chayvo Bay.

Figure 6.34 – Out flow of water from Piltun Bay on 4th August, 2010.

The turbidity levels of bay water were different from those of background water both near the surface and near the bottom. The turbidity level of the water moving out from the bays is apparently higher in spring than in summer. This can be attributed to the accumulation of organic matter in the bays in winter when drainage from minor rivers is small. In spring, however, the active discharge of water into the inshore area makes turbidity levels so high that the hydrologic sonde disappears from view after sinking only 40-50 cm below the water surface.

The volume and mineral content of the organic matter carried over from the bays changes by the end of summer, which also affects its appearance.

Field water turbidity measurements acquired in the summer of 2010 confirm the assumption that bay water turbidity is higher at the beginning of the summer season (Figure 6.37 and Figure 6.38). Near-surface and near-bottom water is more turbid in August (Figure 6.37) than in September (Figure 6.38).

Our observations show that bottom water is more turbid than near-surface water throughout the summer season. The high turbidity areas are generally confined to the areas around the mouths of Piltun and Chayvo Bays.

It is worth noting that high water turbidity can occur at a significant distance from the inshore area and also deep in the water column (Figure 6.39).

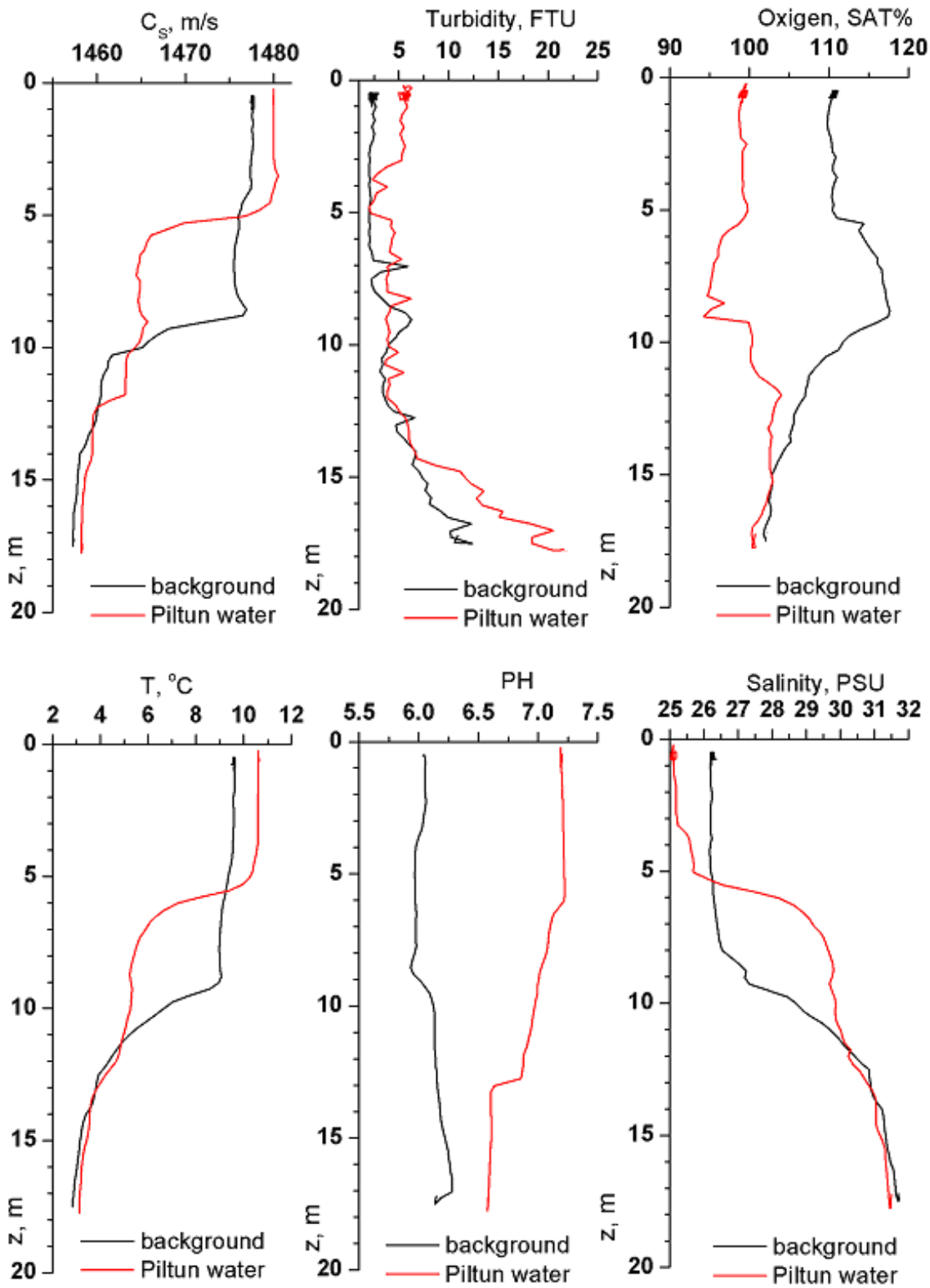

Figure 6.35 - Vertical distribution of sound velocity, turbidity, dissolved oxygen, temperature, pH and salinity in the patch of water outflowing from Piltun Bay, compared to background water.

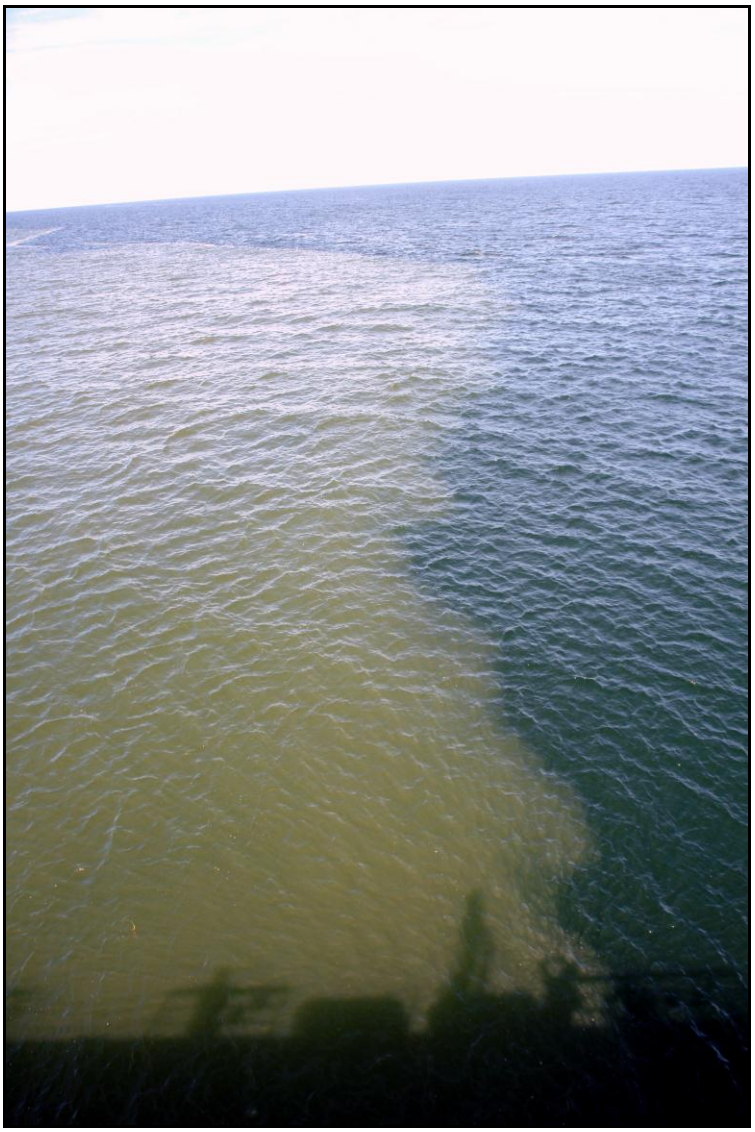

Figure 6.36 – Out flow of water from Piltun Bay in early September, 2010.

The high turbidity levels immediately below the surface at a distance from the inshore area are associated with the rapid development of phytoplankton which reaches its maximum concentrations at a depth of 10 m, rather than the carryover of turbid water from the bays. This is evidenced by the maximum oxygen saturation associated with the change in density between the two layers. The surface water layer is oversaturated with oxygen. Oxygen concentration is 145% at a depth of 7 m. Such concentrations of oxygen are typical for the phytoplankton blooming period.

The dissolved oxygen distribution in the inshore area indicates that this parameter is closely connected with the spatial distribution of temperature and salinity (Figure 6.40 and Figure 6.41).

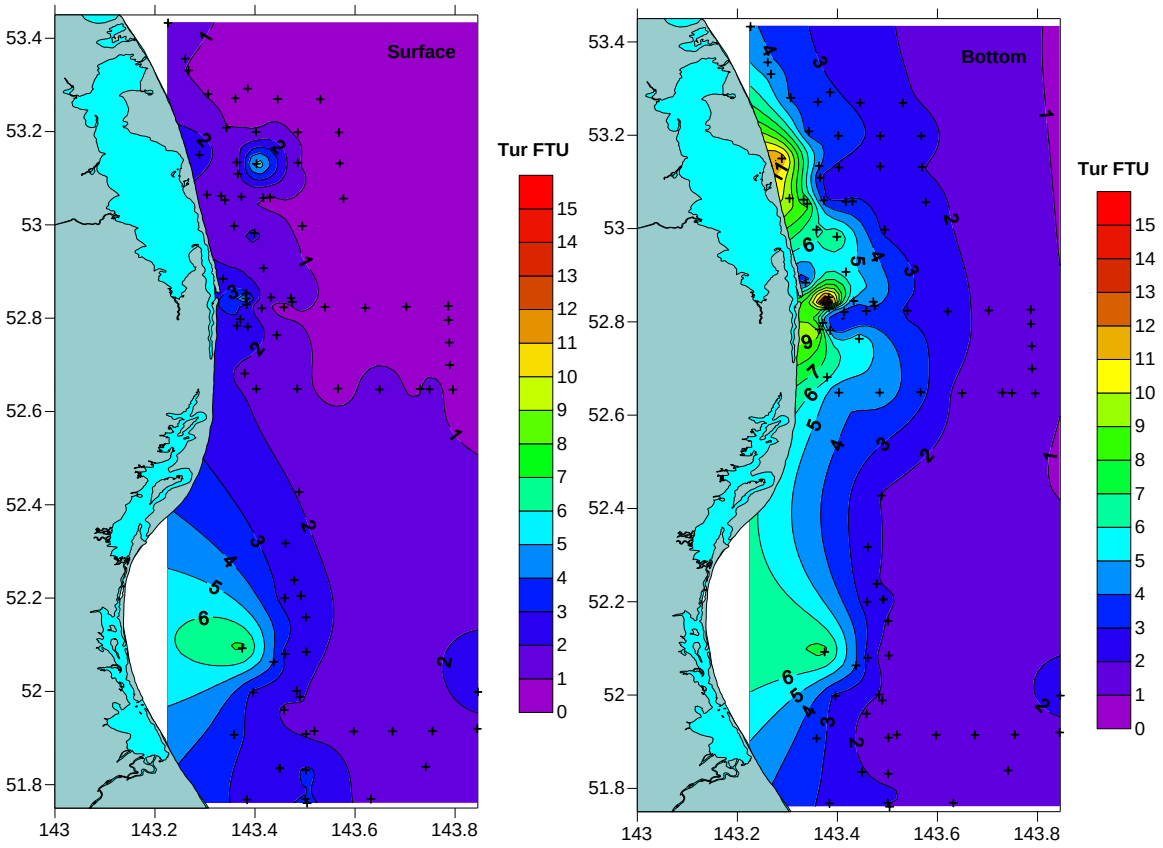

Figure 6.37 - Spatial distribution of turbidity in: (Left) near-surface and (Right) near-bottom water turbidity for August 2010.

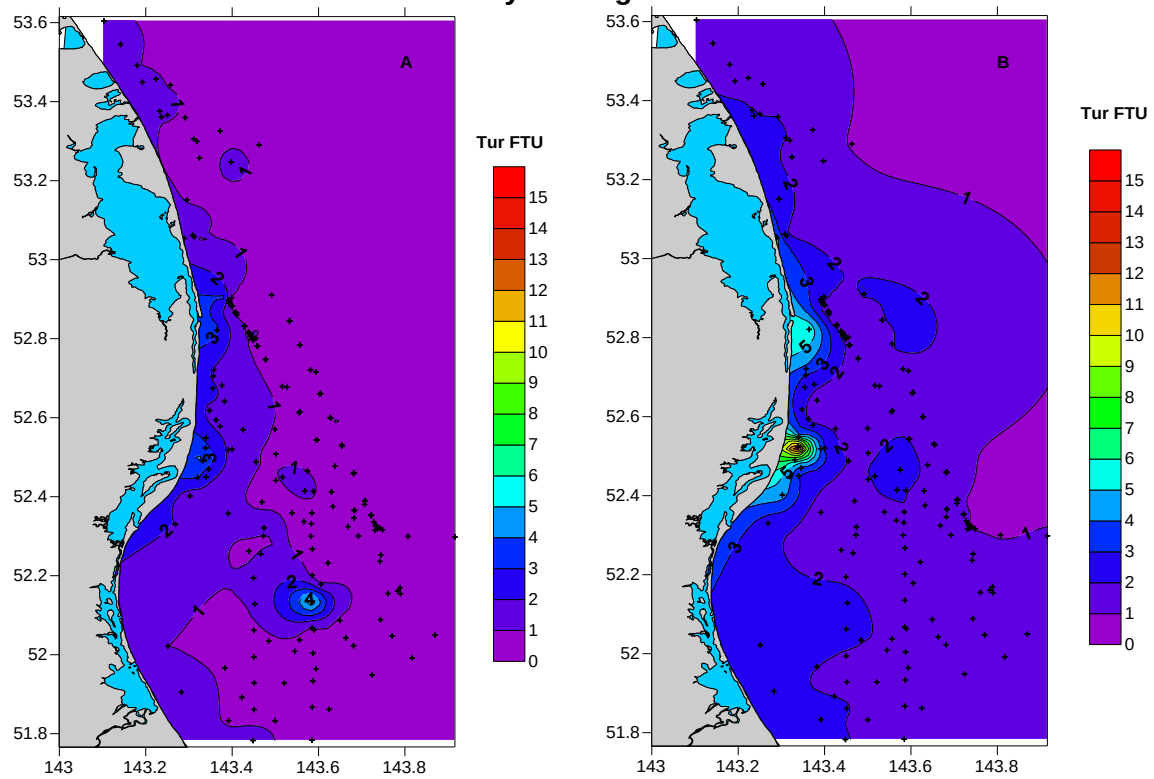

Figure 6.38 - Spatial distribution of turbidity in: (Left) near-surface and (Right) near-bottom water turbidity for September, 2010.

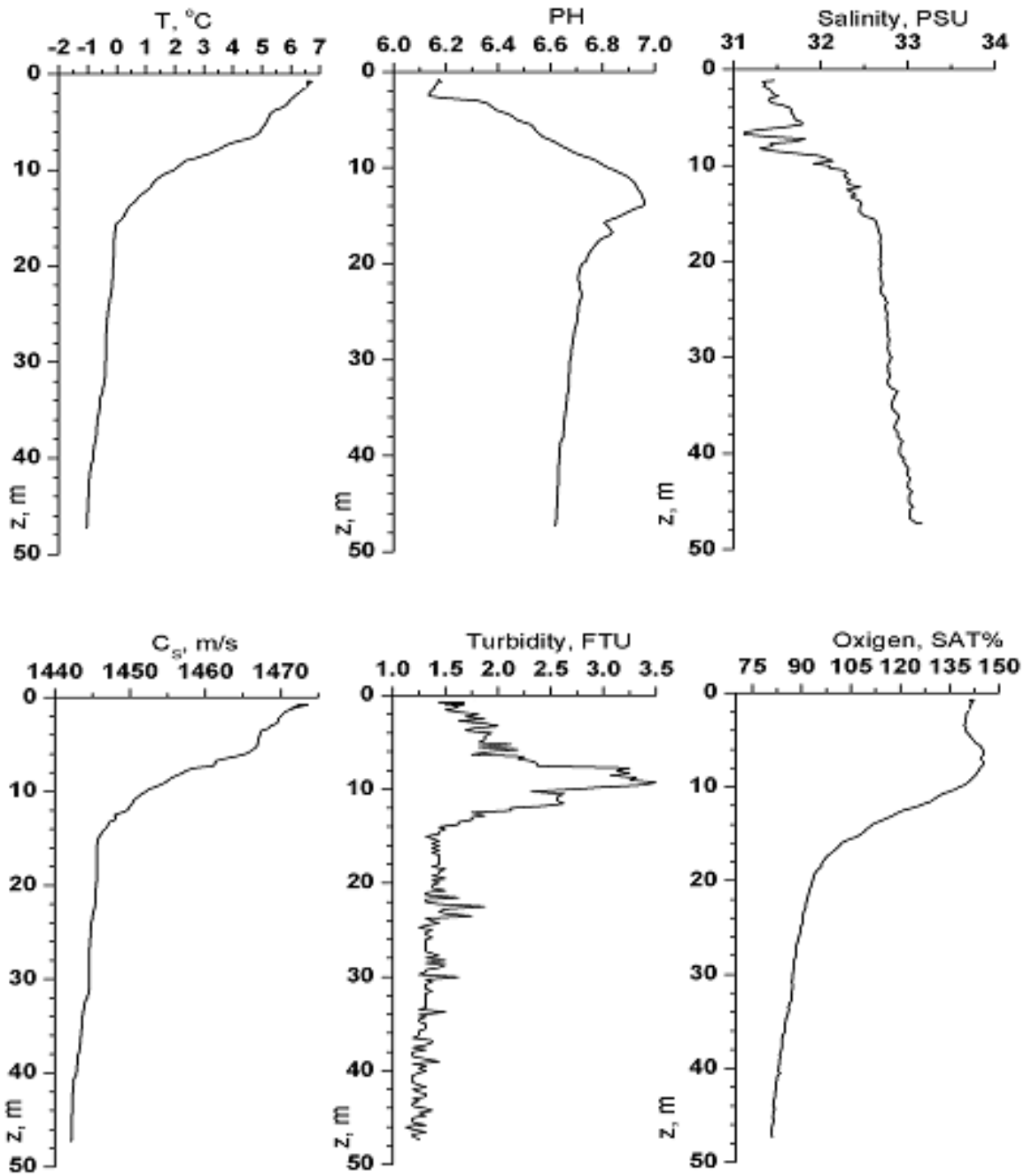

Figure 6.39 - Vertical distribution of sound velocity, turbidity, dissolved oxygen, temperature, pH and salinity in the offshore area on 5th August, 2010.

The high dissolved oxygen content (up to 13 mL/L) of the near-surface layer in the offshore area in August is attributable to the low surface water temperature in the area. Oxygen saturation is higher throughout the entire water column in August than in September.

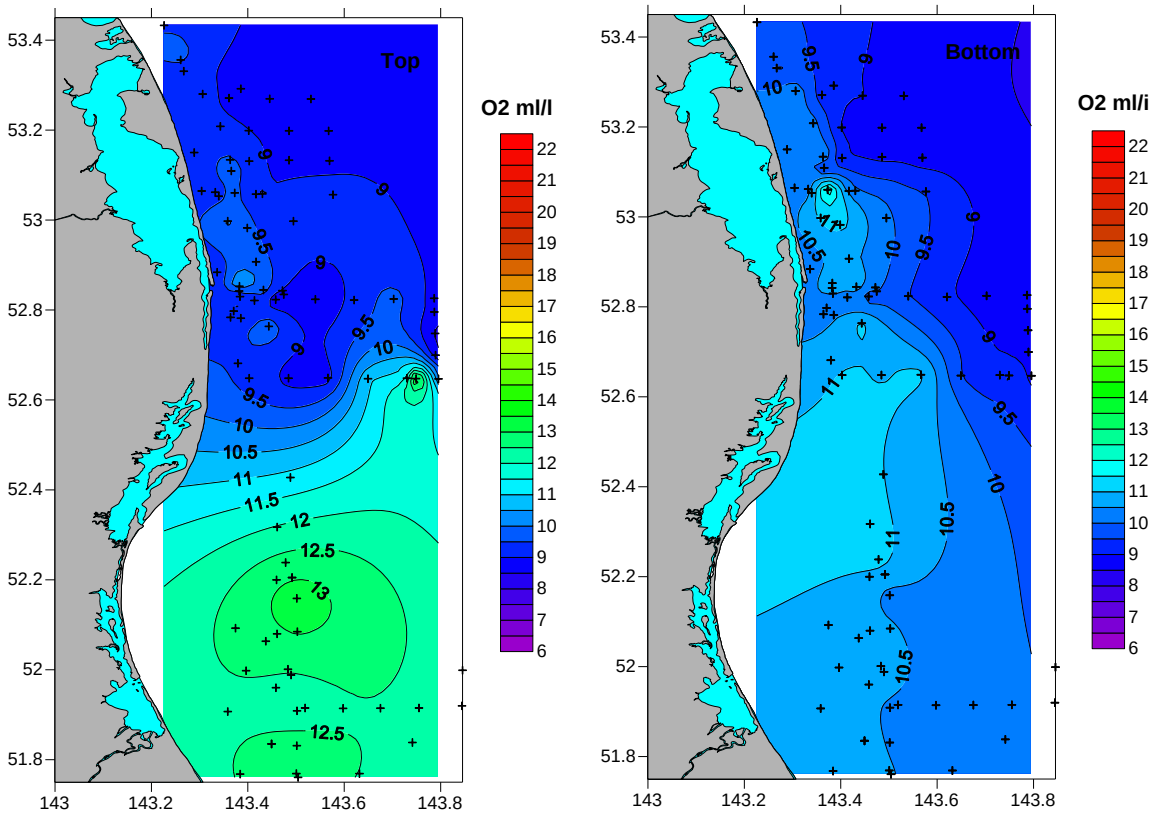

Figure 6.40 - Spatial distribution of dissolved oxygen (mL/L) in: (Left) near-surface and (Right) near-bottom for August 2010.

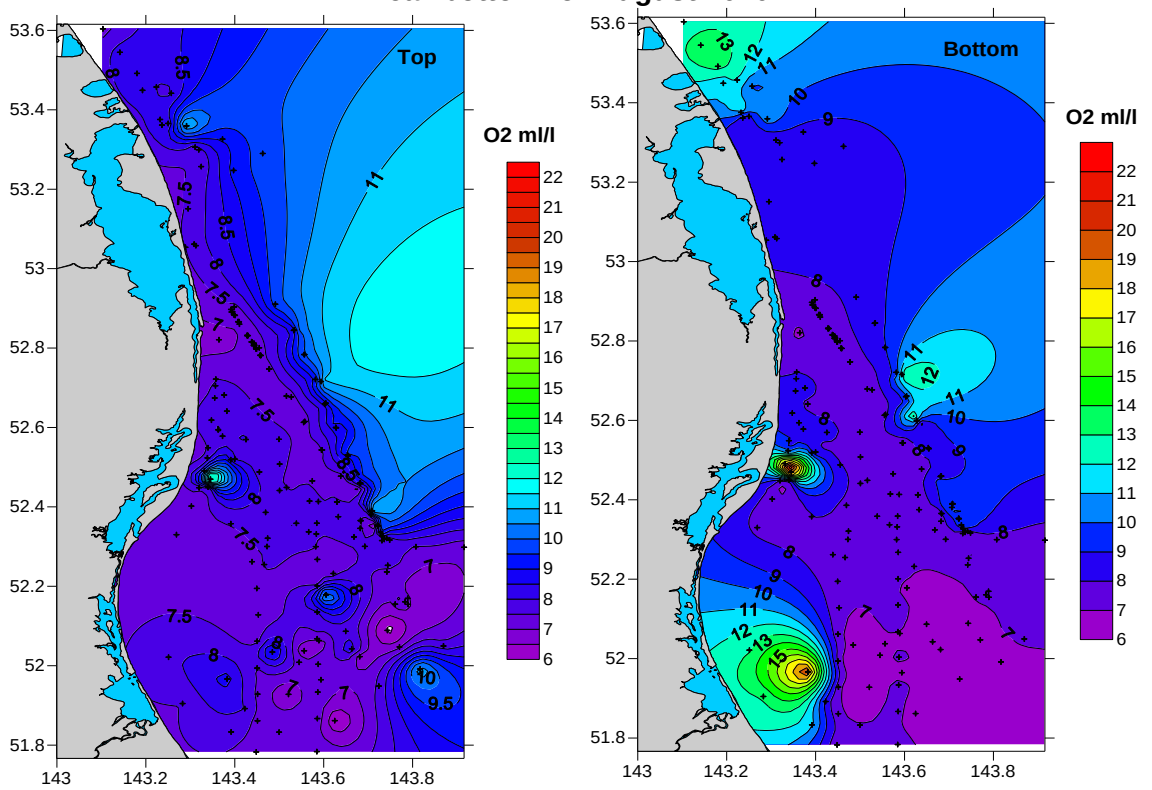

Figure 6.41 - Spatial distribution of dissolved oxygen (mL/L) in: (Left) near-surface and (Right) near-bottom for September, 2010.

Abnormal concentrations of dissolved oxygen in September are confined to the inshore area (Figure 6.41). Attempts to link this to the possible out flow of water from the adjacent bays have been unsuccessful: turbidity charts do not show any corresponding anomalies (Figure 6.37).

7 Main Results

1. Alkaline cell composite battery pack modules were successfully tested as power sources for AUARs and mini-AUARs in 2010. These battery pack modules operated effectively and ensured autonomous operation of the AUARs and mini AUARs for 52 days and 160 hours, respectively.
2. During the 2010 expedition all of the AUARs operated with continuous acoustic recording with no 20-minute gaps to write to disk.
3. Transmission loss studies were conducted in the frequency range from 15 Hz-15 kHz on 5 profiles; these are shown in Figure 4.1.
4. The AUARs designed and developed at POI recorded 18,721 hours (780 days) of acoustic data. Acoustic monitoring was conducted from 1st July to the 27th September 2010 (Table 1.3). All the data acquired in 2010 is displayed, as daily sonograms (2 Hz to 15 kHz, 48 1-second spectral averages) and plots of sound pressure level for five frequency bands (2 Hz - 15 kHz, 20 Hz - 15 kHz, 10 - 100 Hz, 100 - 2000 Hz, 2 - 15 kHz). These are on a DVD enclosed with the report.
5. A field experiment was conducted to compare the acoustic noise generated by the jet-drive boat used for satellite tagging of gray whales and the Photo-ID zodiac moving in a program of different modes.
6. The analog gain factors for many of the AUARs deployed in 2010 were decreased for AUARs deployed near areas where seismic exploration was expected. Thus, it was possible to to record accurately the impulsive signals generated by seismic exploration operations conducted near the study area by other companies.
7. Six thousand five hundred and sixty (6,560) km of bathymetry data and 372 vertical hydrologic profiles were acquired in 2010. All the bathymetric data acquired from 2004 to 2010 was tide-corrected, and, together with hydrology data is available on the DVD at the back of this report.
8. The hydrological surveys and individual transects allowed researchers to obtain data for different meteorological conditions within the summer season.

8 Conclusions

1. In 2010 when deploying AUARs at the annual monitoring locations, the gain factors for the AUAR analog channels were increased to take into account nearby seismic surveys. It was therefore possible to record accurately the impulsive signals generated by seismic exploration operations conducted near the study area by other companies. However, in a number of cases the seismic signals exceeded expected levels, which still resulted in clipping.
2. A Seismic survey began on 18th August, 2010 and continued sporadically beyond the end of the field season in the Sakhalin-5 Lebedinskoye area. A Seismic survey for the Sakhalin-3 Project was conducted to the east of the Offshore feeding area from 15th August 15 to 7th September, 2010.
3. During the seismic survey in the southern part of Sakhalin-5 Lebedinskoye area, the impulses recorded at the Odoptu-N-10 and Odoptu-N-20 stations had peak sound pressure levels exceeding the maximum value of 350 Pa or 170 dB re 1 μPa, measurable by an AUAR with a hydrophone sensitivity of 10 mV/Pa. The peak sound pressures in the recorded pulses reached 17 and 8 Pa at stations A10 and Odoptu-S-10, respectively, and the corresponding SPL_{rms} values were as high as 135 and 130 dB re 1 μPa.
4. During the seismic survey in the southern part of Sakhalin-3 area, the acoustic impulses recorded at the Arkutun-Dagi monitoring station had peak sound pressures as high as 170 dB re 1 μPa and SPL_{rms} values up to 160 dB re 1 μPa.
5. Statistical analysis of the 2010 acoustic measurements showed that anthropogenic noise was more than 6 dB lower in 2010 than in 2009 at the Molikpaq monitoring station.
6. When measuring transmission losses on TLP-22 for signals emitted at points J (26 km from PA-B-20), K (42 km), and P-Arkutun-Dagi (49 km) the *Smit Sibu* was in the immediate vicinity of the PA-B-20 and Piltun stations.
7. Analysis of the experimental acoustic data showed that in almost all motion modes, the power spectral density level of the jet-drive boat (Figure 5.1) is at least 5 dB higher than that of the Photo-ID zodiac.
8. In 2010, researchers measured hydrological data at 372 hydrological stations. These were used to analyze the spatial distribution and temporal variability of the hydrology. The following conclusions can be drawn from the analysis of the hydrological data:
   - The summer of 2010 was characterized by stable atmospheric conditions with rare fog

and clear weather that was conducive to local warming of the offshore waters.

- The effect of the southeasterly winds was too weak in 2010 to cause upwelling, which resulted in the accumulation of fresh water near the coast in the area of Piltun Bay. The salinity and temperature of the top layers reached 24.29 psu and 14.10°C, respectively, in August. The warm and fresh layer was 7 to 8 meters thick. The water salinity was about 26 psu throughout the entire depth of the inshore area in September.
- A thermohaline front was observed in the waters offshore the northern part of Chayvo Bay, which persisted until late August, restricting the fresh and warm water from the waters offshore the southern part of Chayvo Bay.
- No freshened water was present in the Offshore feeding area until late August. This suggests that Amur River water did not affect the Offshore area hydrology until early September.
- Amur River water began to actively ingress into the Offshore area in early September, which freshened the surface water layer down to a salinity of 27.64 psu. The hydrological conditions in the bottom layers were typical for that area.
- The high turbidity in the inshore area was caused by water outflow from Piltun and Chayvo Bays. Water turbidity was higher in spring than at the end of summer.
- The higher turbidity of the entire water column at the end of the summer was associated with a rapid growth of phytoplankton. The surface layer was oversaturated with oxygen at that time, with oxygen concentrations reaching 145% at 7 m depth.
- Dissolved oxygen distribution at the beginning of the summer season was relatively homogeneous throughout the water area. The fall outburst of phytoplankton caused an inhomogeneous spatial distribution of phytoplankton.

9 Future plans

1. The 2010 field tests showed that 400 Duracell batteries assembled in a battery pack module has sufficient power to continuously operate an AUAR for 56 days. It is planned to switch these modules over to allow up to 52 days of autonomous operation limited by hard drive capacity.
2. For longer operating times it is critical that there is a method for ensuring the AUARs are operating correctly. In 2011 POI will check the viability of an acoustic modem to transmit AUAR operating data.
3. During the multiyear western gray whale program, POI has gathered a large quantity of acoustic, hydrologic and bathymetric data. POI will continue establishing a database of field data and analysis results allowing easy access and reliable storage and backup.
4. The MIDAS-CTD+500 profiler may be equipped with a chlorophyll sensor to better map the phytoplankton sensor to increase the biological focus of the hydrological studies
5. The integration between the acoustic and hydrologic studies and other components of the western gray whale research program will continue in 2011. Two integrated programs will be conducted in 2011:
   - Measurements of oxygen distribution, pH, turbidity and direct measurements of phytoplankton concentrations will be used to evaluate phytoplankton species composition and productivity during its fall growth period when the phytoplankton concentration is at a maximum.
   - Investigation of the correlation between the spatial distribution and development of benthos and variations in the bathymetry and hydrology of the study area.

10 Acknowledgements

The authors would like to thank the V.I. Il`icev Pacific Oceanological Institute, FEB Academy of Sciences of Russia (POI), (Тихоокеанский океанологический институт им. В.И. Ильичева ДВО РАН) and its director, Academician V.A. Akulichev (академик Акуличев В.А.) for their assistance in performing this work.

The authors would also like to acknowledge the following personnel from POI, who while they did not contribute to the report, contributed significantly the field program and the analysis of the data acquired: T.Y. Antipenkova (Т.Я. Антипенкова) and P. Petrov (П. Петров). The authors wish to thank the crew of the *Akademik Oparin* and the head of the expedition Dr. A. Kalachev for their hospitality and assistance while conducting acoustic measurements on the NE Sakhalin shelf.

Finally the authors would like to express their gratitude to Dr. Sc. Yu. N. Morgunov (д.т.н. Моргунов Ю.Н.) (POI), Dr. Sc. V.G. Petnikov (д.ф-м.н Петников В.Г.) (Institute of general physics, RAS, Moscow), and Dr. H.R. Melton (ExxonMobil Upstream Research Co.) for reviewing this report.

Our special thanks go to the investment companies, their employees and consultants, without whom the present work could not have been conducted. These include:
Exxon Neftegas Ltd. - M.R. Jenkerson, H.R. Melton and E.N Kalinin.
Sakhalin Energy Investment Company Ltd. – D. Bell, Koen Broker and V.V. Efremov.
Oasis Limited. – L. Aerts.
LGL Sakhalin - I. Zhmaev.

11 Authors

The following members of staff from the V.I. Il`icev Pacific Oceanological Institute, Far East Branch, Academy of Sciences of Russia have contributed to the report:

Sc. S.V. Borisov (Борисов С.В.)

Research engineer D.G. Borovoy (Д.Г. Боровой)

Research engineer V. A. Gritsenko (Гриценко А.В.)

Dr. Sc. A.N. Rutenko (Рутенко А.Н.)

Dr. V.N. Sosnin (В.А. Соснин В.А.)

Sc. V.G. Ushipovsky (Ущиповский В.Г.)

12 Bibliography

1. Blokhin, S.A., S.B. Yazvenko, V.L. Vladimirov and S.I. Lagerev. (2002). Population Size, Distribution and Behavior of Gray Whale (*Eschrichtius robustus)* Based on Aerial Observations on the Northeast Shelf of Sakhalin Island in the Summer and Fall of 2001 // Report to the conference on Marine Mammals in Remote Regions of the Arctic, September 11–13, 2002, Lake Baikal, Russia.

   Блохин С.А., Язвенко С.Б., Владимиров В.Л., Лагерев С.И. (2002). Численность, распределение и характер поведения серого кита (*Eschrichtius robustus)* на основании авиационных наблюдений на северо-восточном шельфе острова Сахалин летом и осенью 2001 г. // Доклад на конференции Морские млекопитающие в удаленных районах Арктики, 11-13 сентября 2002 г., озеро Байкал, Россия.
2. Borisov, S.V., A.V. Gritsenko, M.R. Jenkerson, A.N. Rutenko and A,V. Hodzevich. (2002). Evaluating and Monitoring Acoustic Transmission from the Odoptu 3D seismic Survey 5 August - 9 September, 2001; Sakhalin, Russian Federation // Pacific Oceanological Institute (FEB RAS) report for Exxon Neftegas Ltd.

   Борисов С.В., Гриценко А.В., Дженкерсон М.Р., Рутенко А.Н., Ходзевич А.В. (2002). Оценка и наблюдение распространения акустических сигналов, при проведении трехмерной сейсморазведки в районе Одопту с 5 августа по 9 сентября 2001 г. на о.Сахалин, Россия // Отчет Тихоокеанского океанологического института ДВО РАН для компании Эксон Нефтегаз Лимитед.
3. Borisov, S.V., A.V. Gritsenko, A.N. Rutenko, and A.V. Hodzevich. (2003). Results of Acoustic Studies Within and Adjacent to the Piltun-Astokh License Area 1-6 August, 2001 and 17-24 September, 2001; Sakhalin, Russian Federation // Pacific Oceanological Institute (FEB RAS) report for Exxon Neftegas Ltd. and Sakhalin Energy Investment Co.

   Борисов С.В., Гриценко А.В., Рутенко А.Н., Ходзевич А.В. (2003). Результаты акустических исследований, проведенных с 1 по 16 августа 2001 г. и с 17 по 24 сентября 2001 г. в акватории Пильтунско-астохской лицензионной зоны, а также прилегающей к ней акватории на о.Сахалин, Россия / Отчет Тихоокеанского океанологического института ДВО РАН для компаний Эксон Нефтегаз Лимитед и Сахалин Энерджи Инвестмент Компани.
4. Borisov, S.V., A.V. Gritsenko, M.V. Kruglov, R.A. Korotchenko, and A.N. Rutenko. (2003). Results of Acoustic Studies between Molikpaq and Piltun and Near Chayvo Bay, 12

September to 23 September, 2002; Sakhalin, Russian Federation // Pacific Oceanological Institute (FEB RAS) report for Exxon Neftegas Ltd. and Sakhalin Energy Investment Co.

Борисов С.В., Гриценко А.В., Круглов М.В., Коротченко Р.А., Рутенко А.Н. (2003). Результаты акустических исследований, проведенных с 12 по 23 сентября 2002 г. на акваториях между платформой Моликпак и заливом Пильтун, и прилегающей к заливу Чайво, на о.Сахалин, Россия / Отчет Тихоокеанского океанологического института ДВО РАН, г. Владивосток, для компаний Эксон Нефтегаз Лимитед и Сахалин Энерджи Инвестмент Компании .

5. Borisov, S.V., A.V. Gritsenko, and A.N. Rutenko. (2004). Acoustic Studies on the North East Sakhalin Shelf, Volume 1: Equipment, Methodology and Data; 15 August to 20 September, 2003; Sakhalin, Russian Federation // Pacific Oceanological Institute (FEB RAS) report for Exxon Neftegas Ltd. and Sakhalin Energy Investment Co.

   Борисов С.В., Гриценко А.В., Рутенко А.Н. (2004). Результаты акустических исследований, проведенных с 15 августа по 20 сентября 2003 г. на северо-восточном шельфе о. Сахалин, Россия. Том 1: «Оборудование, методика и данные» / Отчет Тихоокеанского океанологического института ДВО РАН, г. Владивосток, для компаний Эксон Нефтегаз Лимитед и Сахалин Энерджи Инвестмент Компании.

6. Borisov, S.V., A.V. Gritsenko, A.V. Dmitrieva, A.A. Karnauhov, M.V. Kruglov and A.N. Rutenko. (2005). Acoustic Studies on the North East Sakhalin Shelf, Volume 1: Equipment, Methodology and Data; 30 July to 7 October, 2004; Sakhalin, Russian Federation // Pacific Oceanological Institute (FEB RAS) report for Exxon Neftegas Ltd. and Sakhalin Energy Investment Co.

   Борисов С.В., Гриценко А.В., Дмитриева А.В., Карнаухов А.А., Круглов М.В., Рутенко А.Н. (2005). Результаты гидро-акустических исследований, проведенных с 30 июля по 07 октября 2004 г. на северо-восточном шельфе о. Сахалин, Россия. Том 1: «Оборудование, методика и данные» / Отчет Тихоокеанского океанологического института ДВО РАН, г. Владивосток, для компаний Эксон Нефтегаз Лимитед и Сахалин Энерджи Инвестмент Компании.

7. Borisov, S.V., A.V. Gritsenko, R.A. Korotchenko, D.G. Kovzel, M.V. Kruglov, A.N. Rutenko and A.A. Solovyev. (2006). Acoustic Studies on the North East Sakhalin Shelf, Volume 2: Equipment, Calibration and Methodology; 7 July to 7 October, 2005; Sakhalin, Russian Federation // Pacific Oceanological Institute (FEB RAS) report for Exxon Neftegas Ltd. and Sakhalin Energy Investment Co.

Борисов С.В., Гриценко А.В., Коротченко Р.А., Ковзель Д.Г., Круглов М.В., Рутенко А.Н., Соловьев А.А. (2006). Гидроакустические есследования, проведенные с 07 июля по 07 октября 2005 г. на северо-восточно шельфе о,Сахалин, Россия. Том 2: «Обороудование, калибровка и методика» / Отчет Тихоокеанского океанологического института ДВО РАН для компаний Эксон Нефтегаз Лимитед и Сахалин Энерджи Инвестмент Компани.

8. Borisov, S.V., A.V. Gritsenko, D.G. Kovzel, M.V. Kruglov, A.N. Rutenko, A.A. Solovyev, V.G. Ushipovsky and F.F. Khrapchenkov. (2007). Acoustic and Hydrographic Studies on the North East Sakhalin Shelf, 15 June to 5 October, 2006; Sakhalin, Russian Federation // Pacific Oceanological Institute (FEB RAS) report for Exxon Neftegas Ltd. and Sakhalin Energy Investment Co.

   Борисов С.В., Гриценко А.В., Ковзель Д.Г., Круглов М.В., Рутенко А.Н., Соловьев А.А, Ущиповский В.Г., Храпченков Ф.Ф. (2007). Акустико-гидрофизические исследования на северо-восточном шельфе о. Сахалин с 15 июня по 05 октября 2006 г.; о. Сахалин, Российская Федерация. / Отчет Тихоокеанского океанологического института ДВО РАН для компаний Эксон Нефтегаз Лимитед и Сахалин Энерджи Инвестмент Компани.

9. Borisov, S.V., A.V. Gritsenko, D.G. Kovzel, R.A. Korotchenko, M.V. Kruglov, A.N. Rutenko, A.A. Solovyev, V.A. Sosnin, V.G. Ushipovsky and F.F. Khrapchenkov. (2008). Acoustic and Hydrographic Studies on the North East Sakhalin Shelf, 22nd June to 15th September, 2007; Sakhalin, Russian Federation // Pacific Oceanological Institute (FEB RAS) report for Exxon Neftegas Ltd. and Sakhalin Energy Investment Co.

   Борисов С.В., Гриценко А.В., Ковзель Д.Г., Коротченко Р.А., Круглов М.В., Рутенко А.Н., Соловьев А.А, Соснин В.А., Ущиповский В.Г., Храпченков Ф.Ф. (2008). Акустико-гидрофизические исследования на северо-восточном шельфе о. Сахалин с 22 июня по 15 сентября 2007 г.; о. Сахалин, Российская Федерация. / Отчет Тихоокеанского океанологического института ДВО РАН для компаний Эксон Нефтегаз Лимитед и Сахалин Энерджи Инвестмент Компани.

10. Borisov S.V., D.G. Kovzel, A.N. Rutenko, V.G. Ushchipovsky. (2008). A self-contained hydro-acoustic station with radio channel for acoustic measurements on the shelf // Instrumental and Experimental Techniques. 2008. Vol. 51. №5. pp. 132-137.

    Борисов С.В., Ковзель Д.Г., Рутенко А.Н., Ущиповский В.Г. (2008). Автономная гидроакустическая станция с радиоканалом для акустических измерений на шельфе // Приборы и техника эксперимента. 2008. №5. С. 132-137.

11. Borisov, S.V., D.G. Kovzel, R.A. Korotchenko, A.N. Rutenko, T.V. Saltanova, V.A. Sosnin, and V.G. Ushipovsky. (2009). Acoustic and Hydrographic Studies on the North East Sakhalin Shelf, 25th June to 10th October, 2008; Sakhalin, Russian Federation // Pacific Oceanological Institute (FEB RAS) report for Exxon Neftegas Ltd. and Sakhalin Energy Investment Co.

    Борисов С.В., Ковзель Д.Г., Коротченко Р.А., Рутенко А.Н.,Салтанова В.А., Соснин В.А., Ущиповский В.Г., (2009). Акустико-гидрофизические исследования на северо-восточном шельфе о. Сахалин с 25 июня по 10 октября 2008 г.; о. Сахалин, Российская Федерация. / Отчет Тихоокеанского океанологического института ДВО РАН для компаний Эксон Нефтегаз Лимитед и Сахалин Энерджи Инвестмент Компани.

12. Brekhovskikh, L.M. and Yu.P. Lysanov. (2003). Fundamentals of Ocean Acoustics, 3rd ed. (Modern Acoustics and Signal Processing). AIP Press, Springer-Verlag.

13. Brovko, P.F. and Y.A. Mikishin. (1999). Modern tendencies in the development of the North East Sakhalin coasts // FERHRI Special Issue # 2, Vladivostok, Dalnauka, pp. 193-203.

    Бровко П.Ф., Микишин Ю.А. (1999) Современные тенденции развития берегов северо-восточного Сахалина // Гидрометеорологические и экологические условия дальневосточных морей: оценка воздействия на морскую среду. Владивосток, с. 193-203. (Тематический выпуск № 2).

14. Buckland, S.T., D.R. Anderson, K.P. Burnham, J.L. Laake, D.L. Borchers and L. Thomas. (2001). Introduction to Distance Sampling. Oxford University Press. New York.

15. Fadeev, V.I. (2010). Benthos studies in the feeding grounds of the Okhotsk-Korean gray whale population in 2009. // Institute of Marine Biology (FEB RAS), Vladivostok, Russia. Research report for Exxon Neftegas Ltd., Yuzhno-Sakhalinsk, Russia and Sakhalin Energy Investment Co., Yuzhno-Sakhalinsk, Russia.

    Фадеев В.И. (2010). Состояние бентоса и кормовой базы в районах питания охотско-корейской популяции серого кита в 2009 году. // Отчет о научно-исследовательской работе Института биологии моря ДВО РАН для компаний Сахалин Энерджи. Южно-Сахалинск, Россия и Эксон Нефтегаз. Южно-Сахалинск, Россия.

16. Gershanovich, D.E. and A.M. Muromtsev. (1982). Oceanological principles of the biological productivity of the world's oceans // Gidrometeoizdat, 320 pp.

    Гершанович Д.Е., Муромцев А.М. (1982). Океанологические основы биологической продуктивности Мирового океана. // Гидрометеоиздат. 320 с.

17. Hooge, P.N. and B. Eichenlaub. (1997). Animal movement extension to arcview. Ver. 1.1.

Alaska Science Center - Biological Science Office // U.S. Geological Survey, Anchorage, AK, USA.

18. Karnauhov, A.A., M.V. Kruglov and A.N. Rutenko. (2005). Acoustic Studies on the North East Sakhalin Shelf, Volume 2: Analysis, Conclusions and Recommendations; 30 July to 7 October, 2004; Sakhalin, Russian Federation // Pacific Oceanological Institute (FEB RAS) report for Exxon Neftegas Ltd. and Sakhalin Energy Investment Co.

    Карнаухов А.А., Круглов М.В., Рутенко А.Н. (2005). Результаты гидроакустических исследований, проведенных с 30 по 07 октября 2004 г. на северо-восточном шельфе о. Сахалин,Россия. Том 2: «Оборудование методика и данные» / Отчет Тихоокеанского океанологического института ДВО РАН, г. Владивосток, для компаний Эксон Нефтегаз Лимитед и Сахалин Энерджи Инвестмент Компании.

19. Knudsen, V.O., R.S. Alford and J.W. Emling. (1948). Underwater ambient noise // J. Mar. Res. Vol. 7. № 3, pp. 410-429.

20. Krasavtsev, V.B., K.L. Puzankov and G.V. Shevchenko. (2000). Wind driven upwelling formation on the northeast shelf of Sakhalin Island. // DVNIGMI special issue No. 3, Vladivostok, Dalnauka, pp. 106–120.

    Красавцев В. Б., Пузанков К. Л., Шевченко Г. В. (2000). Формирование апвеллинга на северо-восточном шельфе острова Сахалин под воздействием ветра. // Тематический вып. ДВНИИГМИ № 3. Владивосток: Дальнаука, С. 106-120.

21. Kruglov, M.V., and A.N. Rutenko. (2003). Transmission Loss Studies on the North East Sakhalin Shelf 2001 and 2002; Sakhalin, Russian Federation // Pacific Oceanological Institute (FEB RAS) report for Exxon Neftegas Ltd. and Sakhalin Energy Investment Co.

    Круглов М.В., Рутенко А.Н. (2003). Исследования потерь акустических шумов, проведенные в 2001, 2002 гг. На северо-восточном шельфе о.Сахалин, Россия / Отчет Тихоокеанского океанологического института ДВО РАН для компаний Эксон Нефтегаз Лимитед и Сахалин Энерджи Инвестмент Компани.

22. Kruglov, M.V., and A.N. Rutenko. (2004). Acoustic Studies on the North East Sakhalin Shelf, Volume 2: Analysis, Conclusions and Recommendations; 15 August to 20 September, 2003; Sakhalin, Russian Federation // Pacific Oceanological Institute (FEB RAS) report for Exxon Neftegas Ltd. and Sakhalin Energy Investment Co.

    Круглов М.В., Рутенко А.Н. (2004) Результаты акустических исследований, проведенных с 15 по 20 сентября 2003 г. на северо-восточном шельфе о.Сахалин, Россия. Том 2: «Анализ, выводы и рекомендации» / Отчет Тихоокеанского

океанологического института ДВО РАН для компаний Эксон Нефтегаз Лимитед и Сахалин Энерджи Инвестмент Компани.

23. Kruglov, M.V., A.N. Rutenko and F.F. Khrapchenkov. (2006). Acoustic Studies on the North East Sakhalin Shelf, Volume 3: Analysis, Conclusions and Recommendations; 7 July to 7 October, 2005; Sakhalin, Russian Federation // Pacific Oceanological Institute (FEB RAS) report for Exxon Neftegas Ltd. and Sakhalin Energy Investment Co.

    Круглов М.В., Рутенко А.Н., Храпченков Ф.Ф. (2006). Гидроакустические исследования, проведенные с 07 июля по 07 октября 2005 г. на северо-восточном шельфе о.Сахалин. Том 3: «Анализ, выводы, рекомендации». / Отчет Тихоокеанского океанологического института ДВО РАН для компаний Эксон Нефтегаз Лимитед и Сахалин Энерджи Инвестмент Компани.

24. Kruglov, M.V., A.N. Rutenko and R. Racca. (2006). Estimating anthropogenic sound levels at the boundaries of gray whale feeding areas during construction and production activities on the northeastern shelf of Sakhalin Island // Ocean Acoustics / Proceedings of the 11th L. M. Brekhovskikh Conference. M.: GEOS. pp. 340-343.

    Круглов М.В., Рутенко А.Н., Расчет уровней акустических шумов на границах районов кормления серых китов во время проведения строительных работ на северо-восточном шельфе о. Сахалин (2006).// Акустика океана/ Доклады на 11-ой школе-семинаре Л.М. Бреховских/ М.. ГЕОС. С. 340-343.

25. Malme, C.I., P.W. Smith Jr. and P.R. Miles. (1986). Study of the effects of offshore geophysical acoustic survey operations on important commercial fisheries in California. BBN Rep. 6125; OCS Study MMS 86-0032. Rep. from BBN Labs Inc., Cambridge, MA, for Battelle Labs, Ventura, CA, and U.S. Minerals Manage. Serv., Los Angeles, CA. 106 p.

26. Miller, J.F. and S.N. Wolf. (1980). Modal acoustic transmission loss (MOATL): A transmission loss computer program using a normal mode model of acoustic field in the ocean // Naval research laboratory, Washington.

27. Perlov, A.S. and M.K. Maminov. (2002). Population size, distribution and behavior of gray whales (*Eschrichtius robustus)* in the coastal waters of northeast Sakhalin in 2002 (Vessel Observations) // Pacific Oceanological Institute (FEB RAS), Vladivostok, report for Exxon Neftegas Ltd. and Sakhalin Energy Investment Co.

    Перлов А.С., Маминов М.К. (2002) Численность, распределение и характер поведения серого кита (*Eschrichtius robustus)* в прибрежных водах северо-восточного Сахалина в 2002 г. (судовые наблюдения) // Отчет Тихоокеанского научно-исследовательского

рыбохозяйственного центра, г. Владивосток, для компаний Эксон Нефтегаз Лимитед и Сахалин Энерджи Инвестмент Компании ЛТД.

28. Pishchalnik, V.M. and V.S. Arkhipkin. (1999). Seasonal variations in the circulation of waters on the Sakhalin shelf of the Sea of Okhotsk // Hydrometeorological and Ecological Conditions of Far Eastern Seas: Assessment of Impact on Marine Environment, DVNIGMI special issue No. 2, Vladivostok, Dalnauka, pp. 193-95.

    Пищальник В.М., Архипкин В.С. (1999). Сезонные вариации циркуляции вод на охотоморском шельфе острова Сахалин. // Гидрометеорологические и экологические условия Дальневосточных морей: Оценка воздействия на морскую среду. Тематический выпуск № 2. – Владивосток. Дальнаука, С. 84-95.

29. Rexstad, E. and D. Borchers. (2006). Memorandum: Western gray whale detection function and gradient // University of St. Andrews. Scotland.

30. Richardson, W.J., C.R. Greene, C.I. Malme and D.H. Thomson. (1995). Marine mammals and noise. Academic Press Limited. 576 p.

31. Rutenko, A.N. (2006). Acoustic Studies on the North East Sakhalin Shelf, Volume 1: Objectives and Data; 7 July to 7 October, 2005; Sakhalin, Russian Federation // Pacific Oceanological Institute (FEB RAS) report for Exxon Neftegas Ltd. and Sakhalin Energy Investment Co.

    Рутенко А.Н. (2006) Гидроакустические исследования, проведенные с 07 июля по 07 октября 2005 г. на северо-восточном шельфе о.Сахалин, Россия. Том 1: «Цели и полученные данные». / Отчет Тихоокеанского океанологического института ДВО РАН для компаний Эксон Нефтегаз Лимитед и Сахалин Энерджи Инвестмент Компани.

32. Rutenko, A.N. (2006). Effect produced on sound propagation by an internal temperature front moving over the shelf // Acoustical Physics, Vol. 52, No. 5, pp, 613-617.

    Рутенко А.Н. (2006) Влияние движущегося по шельфу внутреннего температурного фронта на распространение звука // Акустический журнал Том. 52, № 5, С. 710-715.

33. Rutenko A.N., F.F. Khrapchenkov, and V.A. Sosnin. (2009). Near-shore upwelling on the Sakhalin shelf // Russian Meteorology and Hydrology. 2009. Vol. 34. №2. pp. 93-99.

    Рутенко А.Н., Храпченков Ф.Ф., Соснин В.А. (2009). Прибрежный апвеллинг на шельфе о. Сахалин // Метеорология и гидрология. 2009. №2. С.44-53.

34. Rutenko A.N., Gritsenko V.A. (2010) Monitoring of anthropogenic acoustic noise on the Sakhalin shelf // Acoustic journal. №1, pp. 77-81

    Рутенко А.Н., Гриценко В.А. (2010) Мониторинг антропогенных акустических шумов на

шельфе о. Сахалин // Акустический журнал. №1. С. 77-81.

35. Thomas, L., J.L. Laake, S. Strindberg, F.F.C. Marques, S.T. Buckland, D.L. Borchers, D.R. Anderson, K.P. Burnham, S.L. Hedley, J.H. Pollard and J.R. B. Bishop. (2004). Distance 4.2. Research Unit for Wildlife Population Assessment, University of St. Andrews, UK. http://www.ruwpa.st-and.ac.uk/distance/
36. Thomas, L., Laake, J.L., Strindberg, S., Marques, F.F.C., Buckland, S.T., Borchers, D.L., Anderson, D.R., Burnham, K.P., Hedley, S.L., Pollard, J.H., Bishop, J.R.B. and Marques, T.A. 2006. Distance 5.0. Release 1. Research Unit for Wildlife Population Assessment, University of St. Andrews, UK. http://www.ruwpa.st-and.ac.uk/distance/.
37. Yakovlev, Yu.M. (2003). Photo-identification of the Okhotsk-Korean gray whale population *(Eschrichtius Robustus)* в 2002. // Report for Exxon Neftegas Ltd. and Sakhalin Energy Investment Co.

    Яковлев Ю.М. (2003). Фотоидентификация корейско-охотской популяции серого кита *(Eschrichtius Robustus)* в 2002 г. // Отчет для Эксон Нефтегаз и Сахалин Энерджи Инвестмент Компании.
38. Zhabin, I.A., L.N. Propp, T.I. Volkova and P.Ya. Tishchenko. (2005). Variability of hydrochemical and hydrologic parameters near the mouth of the Amur River // *Okeanologiya*, Vol. 45, No. 5, pp. 703-709.

    Жабин И.А., Пропп Л.Н., Волкова Т.И., Тищенко П.Я. (2005). Изменчивость гидрохимических и гидрологических параметров вблизи устья реки Амур.// Океанология, том 45, № 5, с. 703-709.
39. Marine Hydrometeorology and Hydrochemistry. Volume 9. Sea of Okhotsk. Edition 1. Hydrometeorological Conditions. St. Petersburg, Gidrometeoizdat, 1998, 342 p.

    Гидрометеорология и гидрохимия морей. Том 9. Охотское море. Выпуск 1. Гидрометеорологические условия. – С-Пб., Гидрометеоиздат, 1998, 342 с.

August	Lunskoye	OFA	Orlan	Arkutun-Dagi	Piltun-S	Piltun	PA-B-10	PA-B-20	Odoptu-PA-B	Odoptu-S-10	Odoptu-S-20	Odoptu-N-10	Odoptu-N-20	Control	Molikpaq	BEH-Odoptu	BEH-North
#	1	2	3	4	5	6	7	8	9	10	11	12	13	14	15	A9	A10
1	✓	✓		✓													
2	✓	✓	✓	✓													
3	✓	✓	✓	✓													
4	✓	✓	✓	✓													
5	✓	✓	✓	✓											✓		
6	✓	✓	✓	✓				✓	✓				✓	✓	✓		✓
7	✓	✓	✓	✓			✓	✓	✓	✓	✓	✓	✓	✓	✓		✓
8	✓	✓	✓	✓	✓		✓	✓	✓	✓	✓	✓	✓	✓	✓		✓
9	✓	✓	✓	✓	✓	✓	✓	✓	✓	✓	✓	✓	✓	✓	✓		✓
10	✓	✓	✓	✓	✓	✓	✓	✓	✓	✓	✓	✓	✓	✓	✓		✓
11	✓	✓	✓	✓	✓	✓	✓	✓	✓	✓	✓	✓	✓	✓	✓		✓
12	✓	✓	✓	✓	✓	✓	✓	✓	✓	✓	✓	✓	✓	✓	✓		✓
13	✓	✓	✓	✓	✓	✓	✓	✓	✓	✓	✓	✓	✓	✓	✓		✓
14	✓	✓	✓	✓	✓	✓	✓	✓	✓	✓	✓	✓	✓	✓	✓		✓
15	✓	✓	✓	✓	✓	✓	✓	✓		✓	✓	✓	✓	✓	✓		✓
16	✓	✓	✓	✓	✓	✓	✓	✓		✓	✓	✓	✓	✓	✓		✓
17	✓	✓	✓	✓	✓	✓	✓	✓		✓	✓	✓	✓	✓	✓		✓
18	✓	✓	✓	✓	✓	✓	✓	✓		✓	✓	✓	✓	✓	✓		✓
19	✓	✓	✓	✓	✓	✓	✓	✓		✓	✓	✓	✓	✓	✓		✓
20	✓	✓	✓	✓	✓	✓	✓	✓		✓	✓	✓	✓	✓	✓		✓
21	✓	✓	✓	✓	✓	✓	✓	✓		✓	✓	✓	✓	✓	✓		✓
22	✓	✓	✓	✓	✓	✓	✓	✓		✓	✓	✓	✓	✓	✓		✓
23	✓	✓	✓	✓	✓	✓	✓	✓		✓	✓	✓	✓	✓	✓		✓
24	✓	✓	✓	✓	✓	✓	✓	✓		✓	✓	✓	✓	✓	✓		✓
25	✓	✓	✓	✓	✓	✓	✓	✓		✓	✓	✓	✓	✓	✓		✓
26	✓	✓	✓	✓	✓	✓	✓	✓		✓	✓	✓	✓	✓	✓		✓
27	✓	✓	✓	✓	✓	✓	✓	✓		✓	✓	✓	✓	✓	✓		✓
28	✓	✓	✓	✓	✓	✓	✓	✓		✓	✓	✓	✓	✓	✓		✓
29	✓	✓	✓	✓	✓	✓	✓	✓		✓	✓	✓	✓	✓	✓		✓
30	✓	✓	✓	✓	✓	✓	✓	✓		✓	✓	✓	✓	✓	✓		✓
31	✓	✓	✓	✓	✓	✓	✓	✓		✓	✓	✓	✓	✓	✓		✓

September	Lunskoye	OFA	Orlan	Arkutun-Dagi	Piltun-S	Piltun	PA-B-10	PA-B-20	Odoptu-PA-B	Odoptu-S-10	Odoptu-S-20	Odoptu-N-10	Odoptu-N-20	Control	Molikpaq	BEH-Odoptu	BEH-North
#	1	2	3	4	5	6	7	8	9	10	11	12	13	14	15	A9	A10
1	✓	✓	✓	✓	✓	✓	✓	✓		✓	✓	✓	✓	✓	✓		✓
2	✓	✓	✓	✓	✓	✓	✓	✓		✓	✓	✓	✓	✓	✓		✓
3	✓	✓	✓	✓	✓	✓	✓	✓		✓	✓	✓	✓	✓	✓		✓
4	✓	✓	✓	✓		✓	✓	✓	✓	✓	✓	✓	✓	✓	✓		✓
5	✓	✓	✓	✓	✓	✓	✓	✓	✓	✓	✓	✓	✓	✓	✓		✓
6	✓	✓	✓	✓	✓	✓	✓	✓	✓	✓	✓	✓	✓	✓	✓		✓
7	✓	✓	✓	✓	✓	✓	✓	✓	✓	✓	✓	✓	✓	✓	✓		✓
8	✓	✓	✓	✓	✓	✓	✓	✓	✓	✓	✓	✓	✓	✓	✓		✓
9	✓	✓	✓	✓	✓	✓	✓	✓	✓	✓	✓	✓	✓	✓	✓		✓
10	✓	✓	✓	✓	✓	✓	✓	✓	✓	✓	✓	✓	✓	✓	✓		✓
11	✓	✓	✓	✓	✓	✓	✓	✓	✓	✓	✓	✓	✓	✓	✓		✓
12	✓	✓	✓	✓	✓	✓	✓	✓	✓	✓	✓	✓	✓	✓	✓		✓
13	✓	✓	✓	✓	✓	✓	✓	✓	✓	✓	✓	✓	✓	✓	✓		✓
14	✓	✓	✓	✓	✓	✓	✓	✓	✓	✓	✓	✓	✓	✓	✓		✓
15	✓	✓	✓	✓	✓	✓	✓	✓	✓	✓	✓	✓	✓	✓	✓		✓
16	✓	✓	✓	✓	✓	✓	✓	✓	✓	✓	✓	✓	✓	✓	✓		✓
17	✓	✓	✓	✓	✓	✓	✓	✓	✓	✓	✓	✓	✓	✓	✓		✓
18	✓	✓	✓	✓	✓	✓	✓	✓	✓	✓	✓	✓	✓	✓	✓		✓
19	✓	✓	✓	✓	✓	✓	✓	✓	✓	✓	✓	✓	✓	✓	✓		✓
20	✓	✓	✓	✓	✓	✓	✓	✓	✓	✓	✓	✓	✓	✓	✓		✓
21	✓	✓	✓	✓	✓	✓	✓	✓	✓	✓	✓	✓	✓	✓	✓		✓
22				✓	✓	✓	✓	✓	✓	✓	✓	✓	✓	✓	✓		✓
23				✓	✓	✓	✓	✓	✓	✓	✓	✓	✓	✓	✓		✓
24				✓	✓	✓	✓	✓	✓	✓	✓	✓	✓	✓	✓		✓
25				✓	✓	✓	✓		✓			✓	✓	✓			✓
26									✓			✓	✓	✓			✓
27									✓			✓	✓	✓			✓
28																	
29																	
30																	

Hydrophones:

1. Certificate # 5/32-008-07	Hydrophone # GI-50 № 25	Type GI-50 (GI-50)
	Hydrophone # GI-50 № 28	Type GI-50 (GI-50)
	Hydrophone # GI-50 № 26	Type GI-50 (GI-50)
	Hydrophone # GI-50 № 29	Type GI-50 (GI-50)
2. Certificate # 5/32-009-07	Hydrophone # GI-50 № 41	Type GI-50 (GI-50)
	Hydrophone # GI-50 № 43	Type GI-50 (GI-50)
	Hydrophone # GI-50 № 44	Type GI-50 (GI-50)
	Hydrophone # GI-50 № 45	Type GI-50 (GI-50)
3. Certificate # 5/32-010-07	Hydrophone # GI-50 № 32	Type GI-50 (GI-50)
	Hydrophone # GI-50 № 34	Type GI-50 (GI-50)
4. Certificate # 5/24-006-06	Hydrophone # GI-50 №009	Type GI-50 (GI-50)
	Hydrophone # GI-50 №011	Type GI-50 (GI-50)
	Hydrophone # GI-50 №014	Type GI-50 (GI-50)
	Hydrophone # GI-50 №016	Type GI-50 (GI-50)
	Hydrophone # GI-50 №019	Type GI-50 (GI-50)
5. Certificate # 5/24-004-05	Hydrophone # GI-50 №004	Type GI-50 (GI-50)
	Hydrophone # GI-50 №006	Type GI-50 (GI-50)
	Hydrophone # GI-50 №018	Type GI-50 (GI-50)
	Hydrophone # GI-50 №010	Type GI-50 (GI-50)
6. Certificate # 5/24-005-05	Hydrophone # GI-50 №007	Type GI-50 (GI-50)
	Hydrophone # GI-50 №017	Type GI-50 (GI-50)
	Hydrophone # GI-50 №023	Type GI-50 (GI-50)
7. Certificate # 5/32-002-08	Hydrophone # GI-50 №030	Type GI-50 (GI-50)
8. Certificate # 5/32-003-08	Hydrophone # GI-50 №042	Type GI-50 (GI-50)

Midas STD+ hydrologic sonde:

1. Warranty statement.		
2. Calibration Certificate	SN #32358	
3. Instrument Test Certificate		
4. Sound Velocity Sensor Calibration record	SN # 48894	Type 100 mm
5. Conductivity Sensor Calibration record	SN #48949	Type 65R
6. Pressure Sensor Calibration record	SN # 48907	Type Keller PAA 10LX
7. Temperature Sensor Calibration record	SN # 2964	Type PRT
8. Turbidity Sensor Calibration record	SN # 12422	Type Seapoint
9. Oxygen Sensor Calibration record	SN # 48950	Type Oxyguard
10. pH Sensor Calibration record	SN # 52052	Type Russell

Copies of these calibration certificates are in the file 'Calibration certificates (Appendix B)' on the DVD at the back of this report.

In these analyses, cumulative probability contours are used to visualize areas with the greatest likelihood of encountering gray whales, and examine shifts in the 'centers of activity' of gray whales over time[32]. Probability contours of 50% and 95% are generated to visualize the distribution of gray whales. The 50% contour represents the area within which 50% of the whales sighted are expected to be found. In 2003, the probability contours were estimated from 2003 and 2004 aerial survey data that took the survey effort into account[33] using a conventional kernel density method[34]. This kernel density method employed a square-gridding process, which is robust for small sample sizes unless the variances of the north-south and east-west components of the distribution are very different, which is the case for the Piltun feeding area.

For the Piltun feeding area the distribution of whale sightings is oriented parallel to the coast with significantly greater variance in the along-shore direction than in the perpendicular-to-shore direction. For this reason, in 2004, a grid was constructed for the Piltun feeding area that was oriented along-shore and with an along-shore grid cell dimension greater than the perpendicular-to-shore dimension, (i.e. each cell was 4 km by 0.5 km). Density was then computed for each cell as the number of whales divided by the cumulative area surveyed within the cell. The same methodology was employed for the offshore feeding area except that, in this case, the conventional assumptions about distribution were satisfied and a grid of 1 km by 1 km cells was employed.

There was substantial variation among the 2003, 2004, 2005 and 2006 estimates of the western gray whale core areas. Consequently, this analysis was updated in 2007 using all available systematic survey data. These included data from the 2001 to 2005 aerial surveys, 2002 to 2006 vessel-based surveys, 2001 to 2006 shore-based behavior scan surveys, and the 2004 to 2006 shore-based vehicle scan surveys.

Because there are significant differences in these survey methods, it is necessary to calibrate the observations or bring them to a common standard, before performing density calculations.

---

[31] This section is based on work performed by LGL Limited (Robin Tamasi, Peter Wainwright, Judy Muir, Sergei Yazvenko, Sonya Meier, and Steve Johnson).

[32] Probability contours were computed independently for the Piltun and offshore feeding areas.

[33] Density is the number of whales per unit area, multiple surveys over a grid cell can result in larger densities within that cell if the survey effort is not taken into account.

[34] The kernel density contours were mapped using the ArcView© 3.1 extension Animal Movement v2.04 [Hooge et. al., 1997]. Kernel density contours are an estimator that assesses an animal's probability of occurrence at each point in space based on a

This was achieved by using Distance analysis [Buckland et. al. 2001] to correct for differences in the ability to detect whales, and by applying an additional correction for the probability that some whales were underwater during the survey. Details of the density calculations are as follows:

- Distance 4.2 software [Thomas et. al. 2004] was used to compute sightability functions and Effective Strip Width (ESW) for the aerial survey data set. Distance 5.0 software [Thomas et. al. 2006] was used to compute a sightability function and Effective Strip Width (ESW) for the vessel survey data. There are issues with using standard Distance analysis methodology to develop sightability functions for the shore-based surveys. In particular, the assumption that the observation stations are located randomly with respect to the whale distribution is violated because whale density is correlated with water depth. This confounds sightability functions because the variability in detections with distance may be due to effects of both changing density and sightability. The shore-based detection function was determined instead based on an analysis conducted by the University of St. Andrews that used simultaneous shore-based and ship-based sightings to estimate parameters of a shore-based detection function (Rexstad and Borchers 2006). This analysis showed that the shore-based detection function is flat (i.e. the detection probability does not decrease with increasing distance from the observation station) for up to 0.1 reticle radial distance (range 4.5 to 10.8 km) from each shore station, to a maximum of 8 km distance.
- Two grids were produced: one for the Piltun feeding area and one for the offshore feeding area.
- The Piltun feeding area grid consisted of a grid of cells oriented north/south with cell dimensions of 4-km alongshore by ½-km perpendicular to shore with an average area of 2.03 km² (standard deviation = 0.02 km²).
- The Offshore feeding area grid consisted of a grid of cells oriented north/south with cell dimensions of 1-km alongshore by 1-km perpendicular to shore with a cell area of 1.0 km² (standard deviation = 0.02 km²).
- ArcGIS v9.0 (ESRI 2005) geographic information system (GIS) software was used to construct buffers around each aerial survey transect(s) flown (1 km wide for surveys at 300m altitude and 1½ km wide for surveys at 500 m altitude) and each vessel survey transect (4.5 km wide) to represent the surveyed swathes. For shore-based stations, buffers with radius equal to 0.1 reticle radial distance (range 4.5 to 10.8 km) from each shore station, to a maximum of 8 km distance were constructed to represent the area surveyed by each station.
- These resulting buffers were then overlaid on the grid and the area of the cell within the buffer ($Area_i$) was computed. Where less than 10% of the cell area fell within the buffer it was considered inappropriate to estimate density for that cell because survey coverage was not sufficient to provide a reliable estimate of density.
- The number of whales within the buffer within each grid cell was then computed. First, the number of whales for each sighting was inflated for aerial and vessel surveys using the appropriate sightability function to compensate for the lower probability of sighting whales at greater distances from the observer.
- Next, the inflated whale sightings were overlaid on the result of the grid/buffer overlay. This

---

utilization distribution. It is a non-parametric estimator that has no underlying assumptions of how animals use space.

resulted in an estimate of the number of whales within the surveyed area of each grid cell ($Count_i$). Finally, density was estimated for each grid cell as the number of whales per unit area adjusted by the probability that whales were underwater during the period of the survey ($g(0)$):

$$Density = \frac{\left[\frac{Count_i}{Area_i}\right]}{g(0)} \qquad \text{(C.1)}$$

g(0) was estimated separately for each survey type and year based on 2001-2006 western gray whale surface-respiration-dive cycle behavior data, the field of view, and the aircraft or vessel speed or the rate of scanning at shore-based observation stations.

- A weighted average of the density estimates from individual surveys was then computed to obtain an overall average estimated density for each grid cell. The weightings were based on the area of the grid cell that was sampled by the individual survey.

Kernel probability densities were then computed for the Piltun and offshore feeding areas separately as follows:

- The total of the densities of all cells in the feeding area grid was computed.
- The cell data were then sorted by density in ascending order.
- *Cumulative densities* were computed for each cell by summing the densities of all preceding cells in the sorted cell density list, i.e., summing all cells with lower estimated gray whale densities.
- Kernel probability densities were then calculated for each cell by dividing the *cumulative density* of the cell by the total of the feeding area grid densities, expressed as a percentage.
- Finally, the ArcGIS Spatial Analyst extension inverse distance weighting (IDW) method with a distance threshold of 3-km was used to compute 25%, 50%, 75% and 95% probability contours for the feeding area grid. These contours were then used in combination with the kernel probability density grid cells to manually delineate smoothed 50% and 95% probability contours for the feeding area.

At the start of the 2010 expedition a cross-calibration of the seventeen AUARs and five mini-AUARs used during the 2010 field program was conducted on the *Akademik Oparin*. The purpose of these calibrations was to confirm the absolute calibration[35] of all the recording systems by comparing the acoustic spectra of synchronously measured signals. All AUARs were calibrated by comparing the synchronous spectra of broadband and tonal signals generated by the *Akademik Oparin* and the HF broadband sound transducer. All spectra were corrected for amplitude and frequency (using the instrument response of each system determined by instrument tests in the laboratory), so the absolute acoustic level of the signal was calculated for the specified frequencies.

The field cross-calibration was conducted by tying a number of hydrophones together in a bundle, and deploying them from the *Akademik Oparin* at a depth of 10-15 m while it was drifting in 20-30 m of water. The hydrophones were divided into groups (Figure D.1) due to the large number of hydrophones being calibrated. One mini-AUAR (No. 24) was used as a control for all the groups. The AUARs on the *Akademik Oparin* synchronously recorded the signals from these hydrophones. The purpose was to simultaneously record the same signal on all the units, allowing the relative calibrations of the AUARs to be confirmed. Data were recorded using the operational configurations for the equipment. The methodology described by Borisov [Borisov et. al., 2006, 2007] was used to calculate the relative error for each AUAR. The results from these measurements are given in Figures D.2 to D.8 and Tables D.1 to D.7.

[35] These cross-calibrations allowed the amplitude response (with frequency) of the analog circuits of the AUARs and sonobuoys to be compared with the laboratory measurements. They also allowed the manufacturer's hydrophone calibrations to be confirmed.

Figure D.1 – Cross-calibration of the AUARs and sonobuoys on the *Akademik Oparin.*

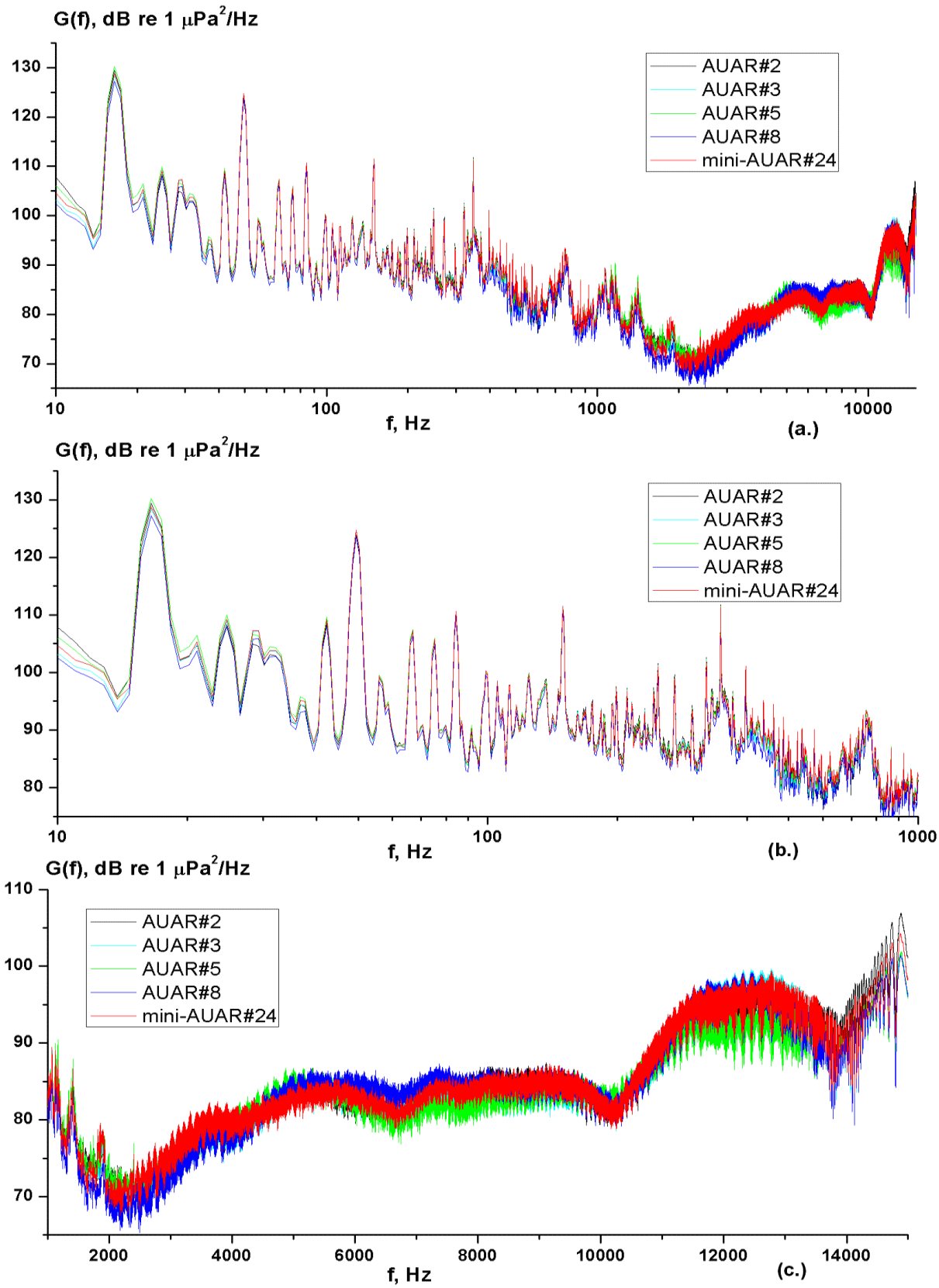

Figure D.2 - Spectra of acoustic signals synchronously measured by AUARs No. 2, 3, 5, 8, and the reference mini-AUAR No. 24 (after instrument response [amplitude-frequency] correction). (a) 10 Hz-15 kHz; (b) 10 Hz-1 kHz; (c) 1-15 kHz.

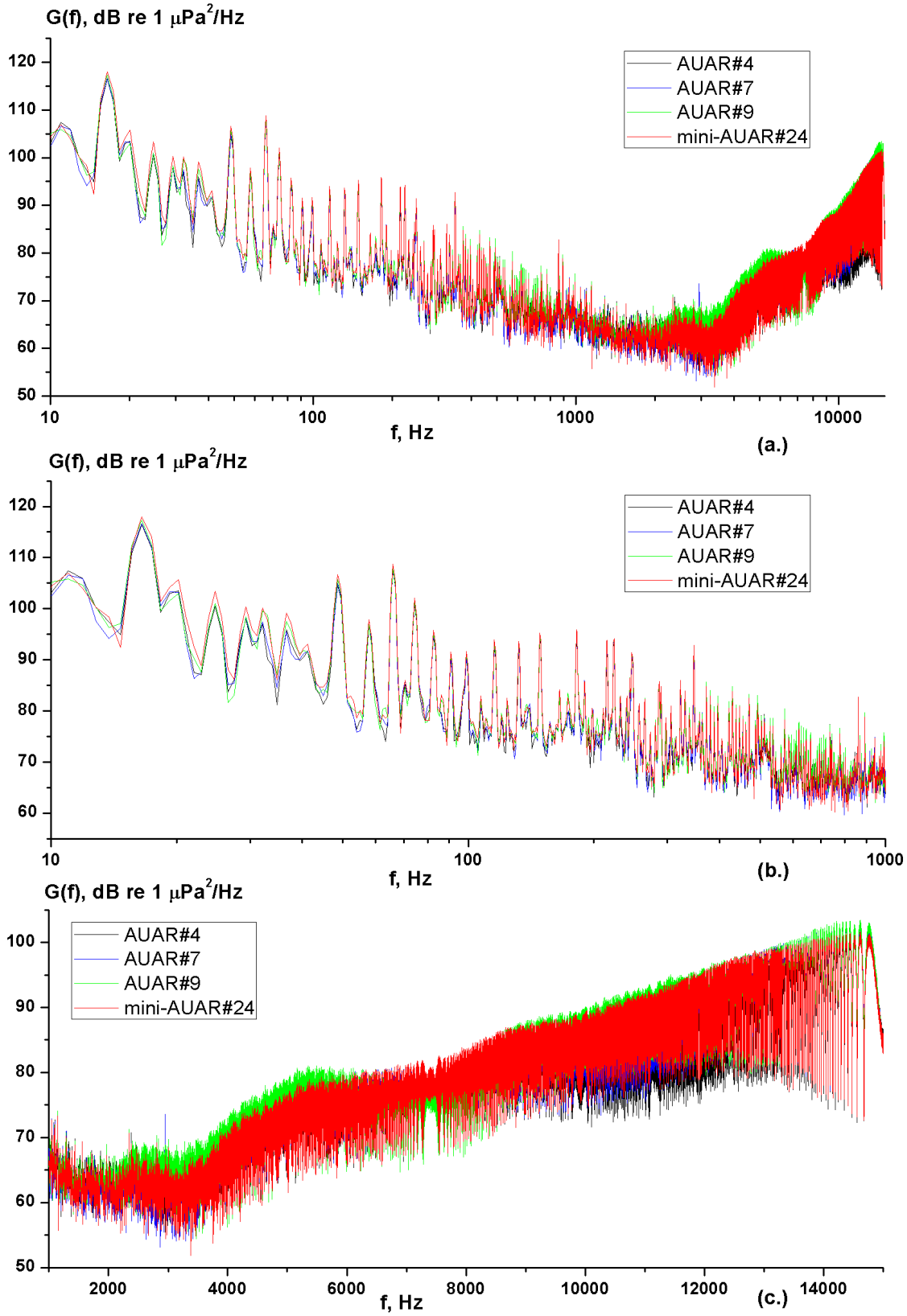

Figure D.3 - Spectra of acoustic signals synchronously measured by AUAR No. 4, 7, 9, and the reference mini-AUAR No. 24 (after instrument response [amplitude-frequency] correction).

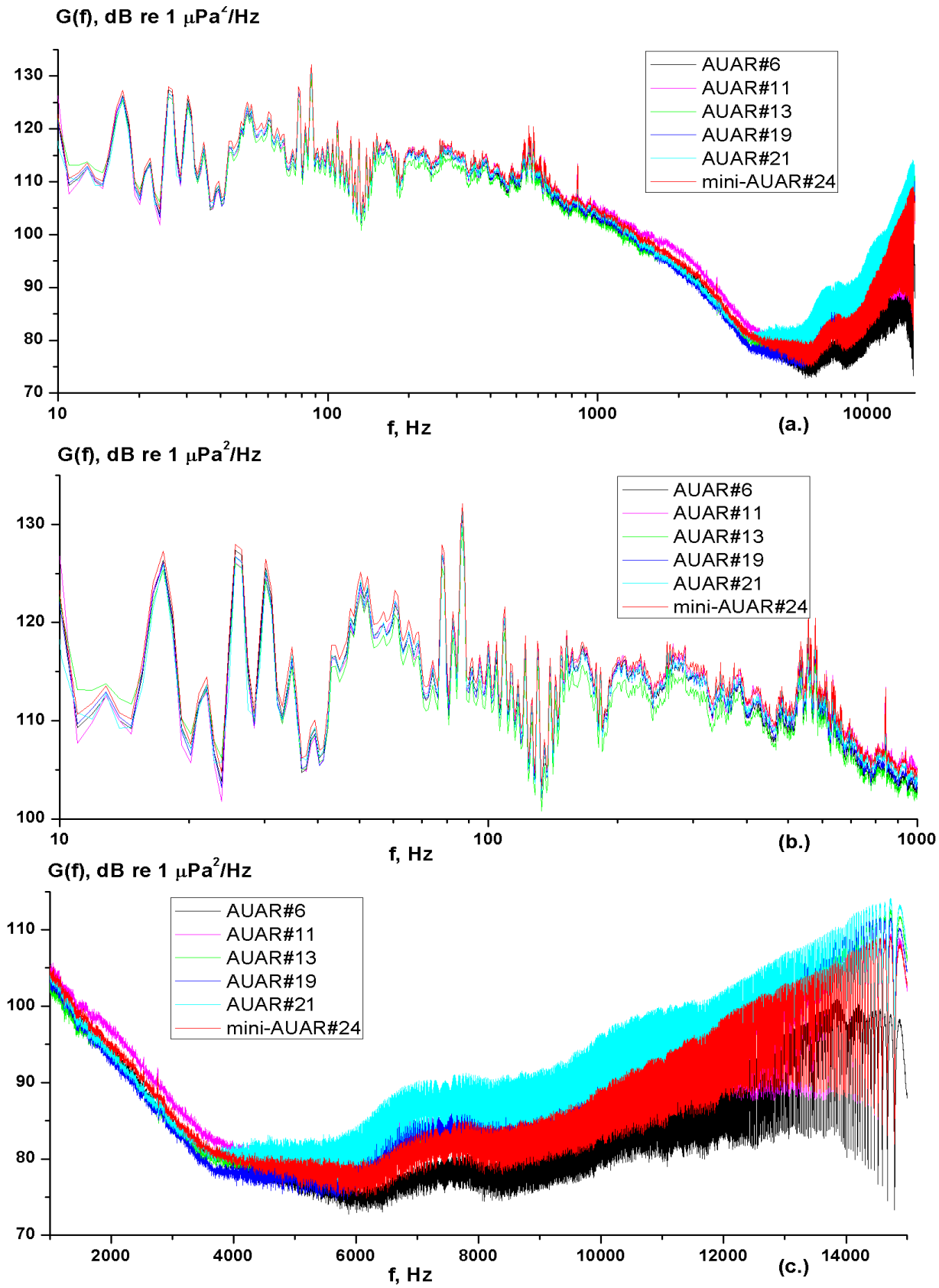

Figure D.4 - Spectra of acoustic signals synchronously measured by AUARs No. 6, 11, 13, 19, and 21, and the reference mini-AUAR No. 24 (after instrument response [amplitude-frequency] correction). (a) 10 Hz-15 kHz; (b) 10 Hz-1 kHz; (c) 1-15 kHz.

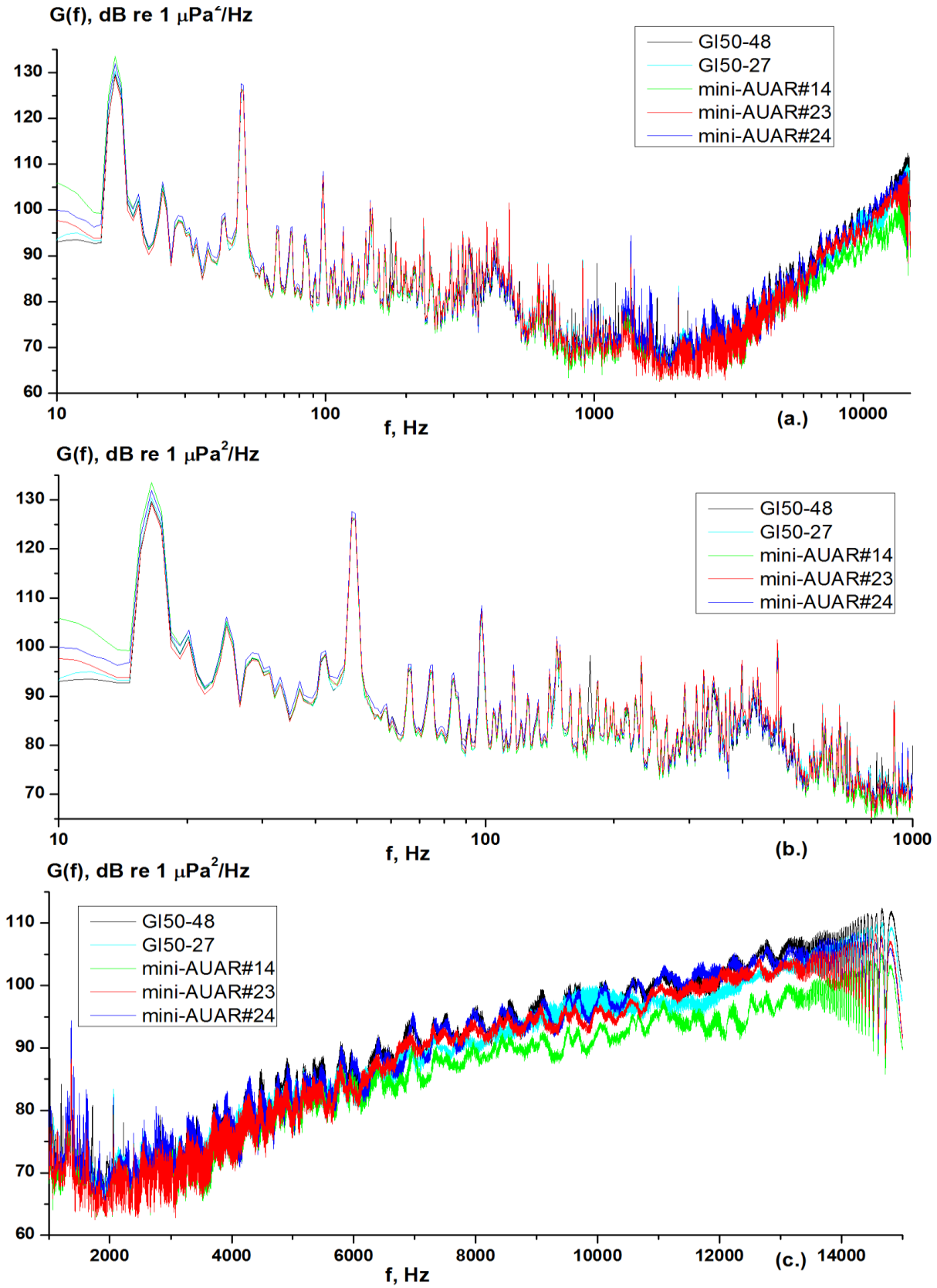

Figure D.5 - Spectra of acoustic signals synchronously measured by mini-AUARs No. 14 and 23, transducer reference hydrophones GI50-48 and GI50-27 and the reference mini-AUAR No. 24 (after instrument response [amplitude-frequency] correction). (a) 10 Hz-15 kHz; (b) 10 Hz-1 kHz; (c) 1-15 kHz.

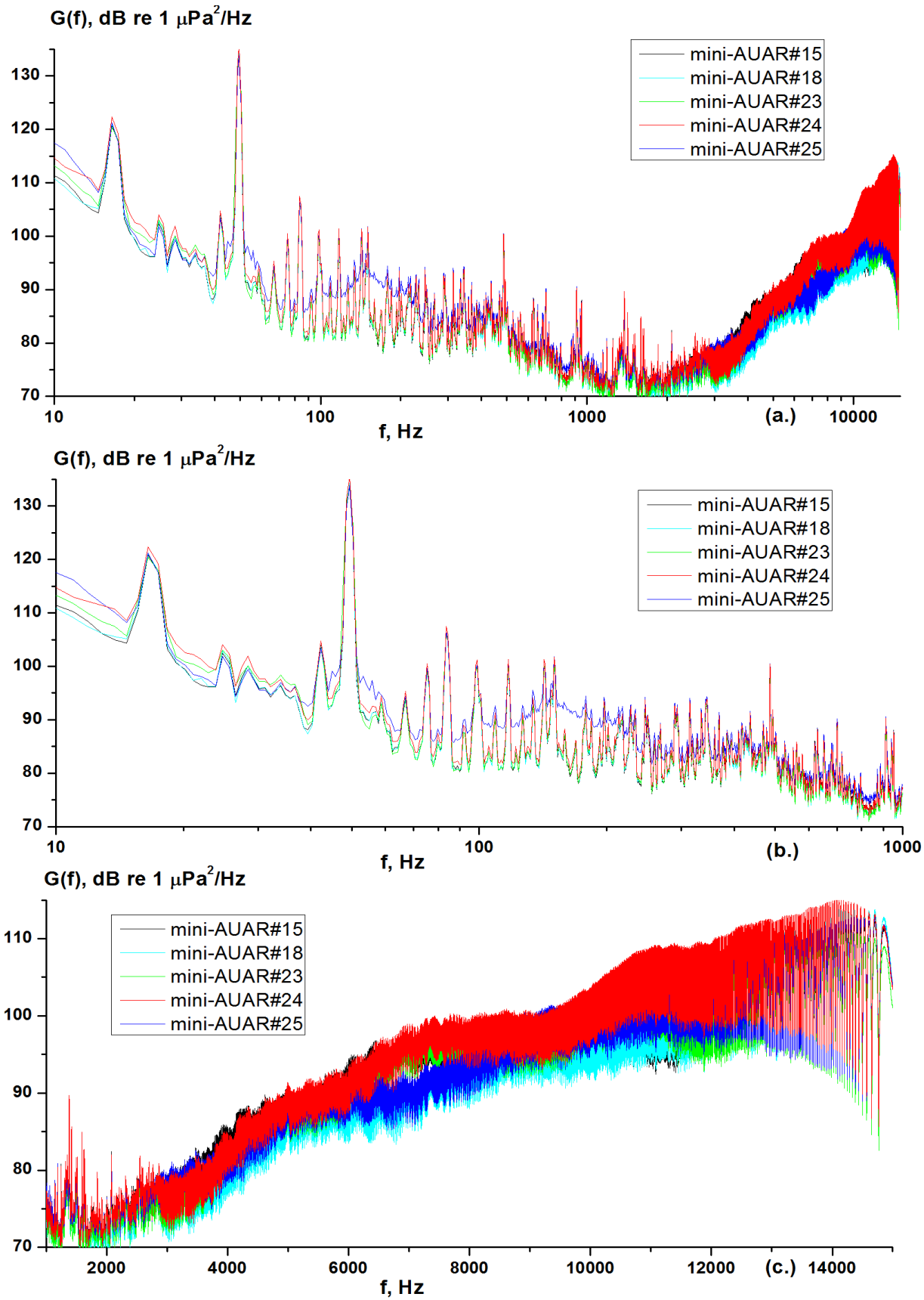

Figure D.6 - Spectra of acoustic signals synchronously measured by mini-AUARs No. 15, 18, 23 and 25, and the reference mini-AUAR No. 24 (after instrument response [amplitude-frequency] correction). (a) 10 Hz-15 kHz; (b) 10 Hz-1 kHz; (c) 1-15 kHz.

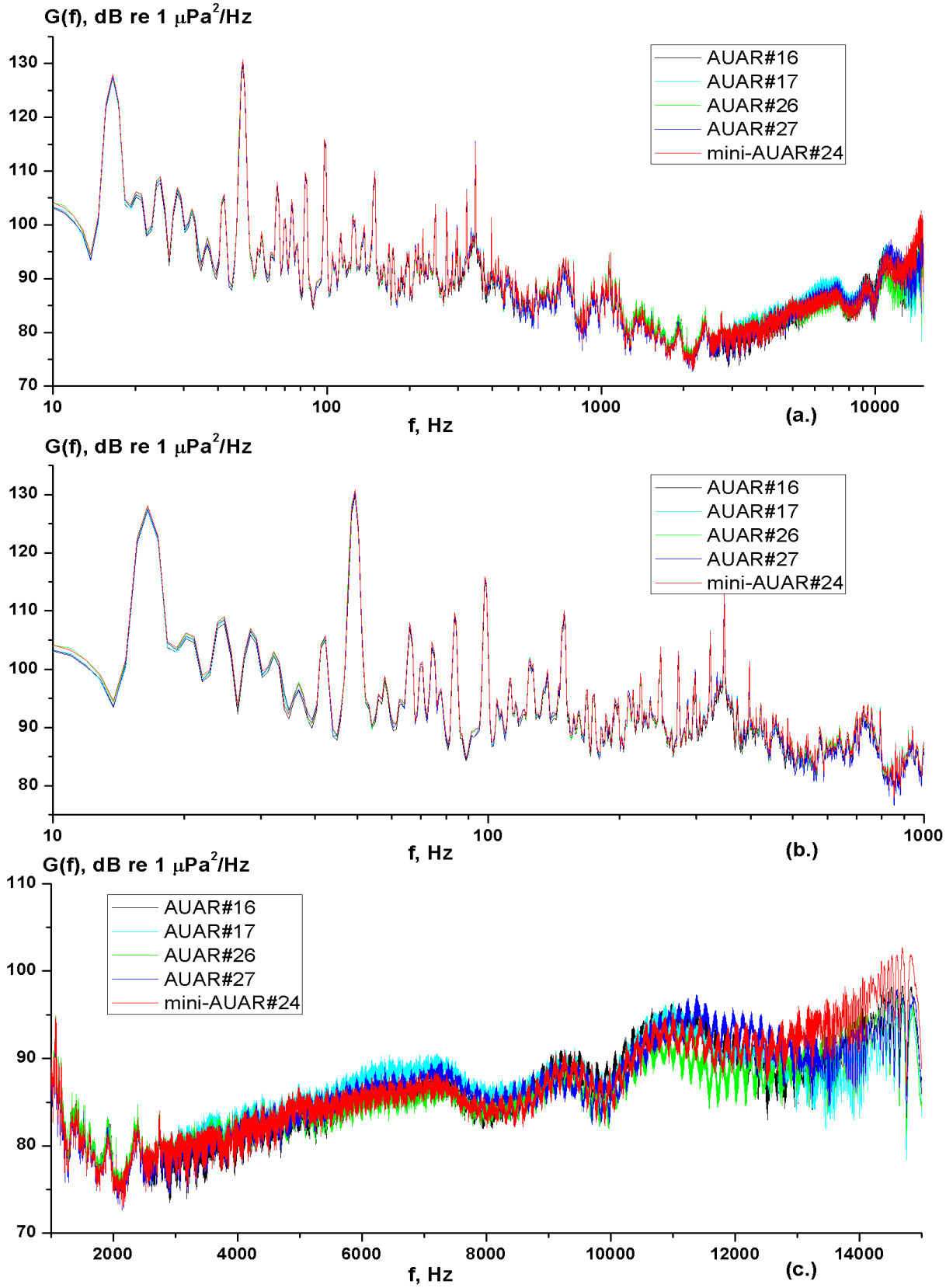

Figure D.7 - Spectra of acoustic signals synchronously measured by AUARs No. 16, 17, 26 and 27, and the reference mini-AUAR No. 24 (after instrument response [amplitude-frequency] correction).

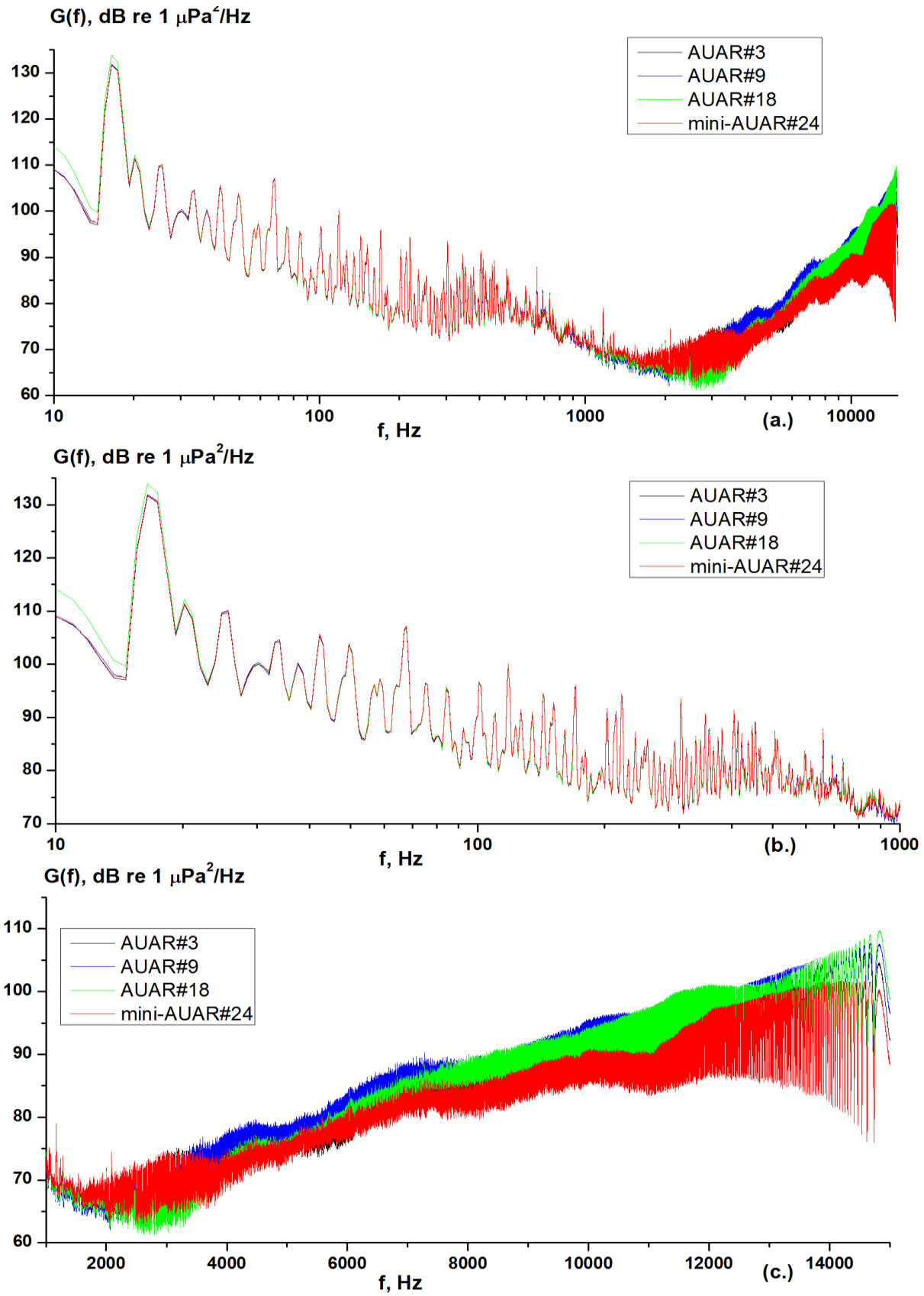

Figure D.8 - Spectra of acoustic signals synchronously measured by AUARs No. 3, 9 and 18, and the reference mini-AUAR No. 24 (after instrument response [amplitude-frequency] correction).

Table D.1 - Cross-calibration - statistical relative error analysis in the frequency bands 10-1000 Hz, 10 Hz to 15 kHz for AUARs No. 4, 7, 9 and the reference (mini-AUAR No. 24)

AUAR #	$D(\Delta f_1)$ [dB] f_1 = 10-1000	$\sigma(\Delta f_1)$ [dB] f_1 = 10-1000	$D(\Delta f_2)$ [dB] f_2 =10Hz-15 kHz	$\sigma(\Delta f_2)$ [dB] f_2 =10Hz-15 kHz
Reference	122.3	0.9	130.0	0.5
4	120.8	0.6	127.7	1.8
7	120.9	0.5	130.0	0.5
9	121.5	0.1	130.4	0.9
Mean	***121.4***		***129.5***	

Table D.2 - Cross-calibration - statistical relative error analysis in the frequency bands 10-1000 Hz, 10-15 kHz for AUARs No. 2, 3, 5, 8, and the reference (mini-AUAR No. 24).

AUAR #	$D(\Delta f_1)$ [dB] f_1 =10-1000 Hz	$\sigma(\Delta f_1)$ [dB] f_1 =10-1000 Hz	$D(\Delta f_2)$ [dB] f_2 =10Hz-15 kHz	$\sigma(\Delta f_2)$ [dB] f_2 =10Hz-15 kHz
Reference	133.0	0.1	135.0	0.2
2	133.2	0.3	134.9	0.1
3	132.8	0.1	134.9	0.1
5	133.9	1.0	135.0	0.2
8	131.7	1.2	134.2	0.6
Mean	***132.9***		***134.8***	

Table D.3 - Cross-calibration - statistical relative error analysis in the frequency bands 10-1000 Hz, 10-15 kHz for AUARs No. 16, 17, 26, 27, and the reference (mini-AUAR No. 24)

AUAR #	$D(\Delta f_1)$ [dB] f_1 = 10-1000	$\sigma(\Delta f_1)$ [dB] f_1 = 10-1000	$D(\Delta f_2)$ [dB] f_2 =10Hz-15 kHz	$\sigma(\Delta f_2)$ [dB] f_2 =10Hz-15 kHz
Reference	135.4	0.3	136.5	0.4
16	134.5	0.6	135.7	0.4
17	135.1	0.0	136.2	0.1
26	135.4	0.3	136.1	0.0
27	134.9	0.2	136.1	0.4
Mean	***135.1***		***136.1***	

Table D.4 - Cross-calibration - statistical relative error analysis in the frequency bands 10-1000 Hz, 10-15 kHz for AUARs No. 6, 11, 13, 19, 21 and the reference (mini-AUAR No. 24).

AUAR #	$D(\Delta f_1)$ [dB] f_1 = 10-1000	$\sigma(\Delta f_1)$ [dB] f_1 = 10-1000	$D(\Delta f_2)$ [dB] f_2 =10Hz-15 kHz	$\sigma(\Delta f_2)$ [dB] f_2 =10Hz-15 kHz
Reference	145.4	1.1	145.8	0.8
6	144.2	0.2	144.4	0.6
11	145.3	1.0	145.8	0.8
13	143.0	1.3	143.8	1.2
19	144.1	0.3	144.9	0.1
21	144.1	0.3	145.2	0.2
Mean	***144.4***		***145.0***	

Table D.5 - Cross-calibration - statistical relative error analysis in the frequency bands 10-1000 Hz, 10-15 kHz for mini-AUARs No. 15, 18, 23, 25 and the reference (mini-AUAR No. 24)

AUAR #	$D(\Delta f_1)$ [dB] f_1 = 10-1000	$\sigma(\Delta f_1)$ [dB] f_1 = 10-1000	$D(\Delta f_2)$ [dB] f_2 =10Hz-15 kHz	$\sigma(\Delta f_2)$ [dB] f_2 =10Hz-15 kHz
Reference	137.6	1.1	145.2	2.2
15 (mini)	136.2	0.3	142.2	0.8
18 (mini)	136.3	0.2	142.3	0.7
23 (mini)	136.3	0.2	142.4	0.6
25 (mini)	136.0	0.5	143.1	0.1
Mean	***136.5***		***143.0***	

Table D.6 - Cross-calibration - statistical relative error analysis in the frequency bands 10-1000 Hz, 10-15 kHz for AUARs No. 14, 23, transducer reference hydrophones GI50-48 and GI50-27 and the reference (mini-AUAR No. 24).

AUAR #	$D(\Delta f_1)$ [dB] f_1 = 10-1000	$\sigma(\Delta f_1)$ [dB] f_1 = 10-1000	$D(\Delta f_2)$ [dB] f_2 =10Hz-15 kHz	$\sigma(\Delta f_2)$ [dB] f_2 =10Hz-15 kHz
Reference	135.3	0.8	140.1	0.7
GI50-48	133.4	1.1	140.6	1.2
GI50-27	133.9	0.5	138.9	0.4
14	136.1	1.6	137.8	1.6
23	133.2	1.3	139.0	0.4
Mean	***134.5***		***139.4***	

Table D.7 - Cross-calibration - statistical relative error analysis in the frequency bands 10-1000 Hz, 10-15 kHz for AUARs No. 3, 9, 18 and the reference (mini-AUAR No. 24).

AUAR #	$D(\Delta f_1)$ [dB] f_1 = 10-1000	$\sigma(\Delta f_1)$ [dB] f_1 = 10-1000	$D(\Delta f_2)$ [dB] f_2 =10Hz-15 kHz	$\sigma(\Delta f_2)$ [dB] f_2 =10Hz-15 kHz
Reference	134.9	0.3	136.3	1
3	134.6	0.7	136.8	0.5
9	134.8	0.4	137.5	0.2
18	136.7	1.4	138.7	1.4
Mean	***135.3***		***137.3***	

Tables D.1 to D.7 give an analysis of sound pressure levels for the two frequency bands (10 Hz to 1 kHz and 10 Hz to 15 kHz) and the calibration error from the mean for the two frequency bands. As can be seen the maximum absolute error for any AUAR, mini-AUAR or transducer hydrophone from the mean is 1.6 dB in the frequency band from 10 to 1000 Hz and less than 2.2 dB between 10 Hz and 15 kHz[36]. This is within the expected relative error limits for the equipment and the absolute calibration of the data were therefore confirmed.

[36] The highest error (2.2 dB) were received at high frequencies. These signals are measured approximately synchronously by the AUAR. Also certain field inaccuracies are present in the cross-calibration measurements; the acoustic measurements are not synchronous, spatial interference due to the different position of the hydrophones in the bundle and possible masking, these errors are not large enough to invalidate the results).